AGING AND CREEP OF NON-PLASTIC SILTY SAND

A thesis submitted in partial fulfillment of the requirement for the
Degree of Doctor of Philosophy
in the
Department of Civil and Natural Resources Engineering

Muhamad Yusa

University of Canterbury
Christchurch, New Zealand

August 2015

Abstract

Soil aging refers to the increase in strength and stiffness that is exhibited over time after it is disturbed. It is common in granular soils, such as sands, occurring over periods from hours to years. There have been relatively numerous laboratory studies on sand aging phenomena. However the majority of these studies were conducted on relatively clean sand (fines content <5%) and were performed under isotropic condition. In nature, granular soils with fines content > 5% are not uncommon.

This research is an attempt to gain further insight and understanding of mechanical aging on silty sand by conducting laboratory studies mostly under K_0 condition, which better reflects the field condition, at both macro-scale (triaxial test) and micro-scale (fabric test). As many factors (e.g. plasticity of fines, fines content, grain size composition, angularity and shape) affect silty sand behaviour and not all those factors could be investigated during the study period, this study focused on mechanical aging of non-plastic silty sand with 15% fines content.

Triaxial tests have been conducted in this study in order to observe creep behavior under different density, initial fabric, and consolidation stress paths (K_0 and isotropic). The tests were conducted at low effective confining stress stresses i.e. σ'_3= 30 – 120 kPa as this is relevant to many geotechnical aging problems (e.g. time effects on freshly deposited or disturbed soils such as in the case of hydraulic fills, mine tailings, and post-liquefaction state of soil behaviour following earthquakes). Creep induced aging effects on undrained shear behaviour at small-strain (<0.1% of shear strain), were investigated, as this strain range is most common in geotechnical structures under gravity-induced working loads. Aging effects on one way cyclic behaviour were also studied. Some new key findings from these tests are as follows: (1) Creep following K_0 consolidation indicated that the soil tends to expand radially over time, resulting

in a tendency of increasing horizontal stress with time even at low stress. (2) Following K_0 consolidation, density appears to have more significant effect on creep compared to initial shear stress ratio and mean effective stress; as demonstrated by loose samples (low stress ratio and mean effectives stress) which exhibited greater creep compared to those of dense sample (higher stress ratio and mean effective stress) (3) For loose soils, there is a trade-off between high confining stresses driving aging and collapsing pore space. Generally higher confining stress was found to increase creep tendency thus enhancing aging, however there was also found to be a certain confining pressure where the aging effects became less due to local structure collapse. (4) Initial fabric plays an important role on creep development, thus aging. For instance, dense dry pluviated samples developed larger axial strain over time but also gained less increase in stiffness compared to dense moist tamped samples. This suggests the importance of specimen preparation for laboratory testing that replicates the field scenarios e.g. natural deposition and associated fabric; (5) Dense K_0 consolidated samples produce more increase in stiffness with time than corresponding isotropically consolidated samples. Hence, as the K_0 condition generally reflects the level-ground free field stress condition better, it is important to test under K_0 if the degree of stiffness gain is important; (6) The number of cycles to trigger cyclic softening and liquefaction for one way cyclic loading increases with the aging duration. In addition there is tendency that the aging effect is more pronounced at lower cyclic stress ratios.

Fabric tests under K_0 consolidation with similar variables as the triaxial tests were also performed. Some new insights and contributions have been obtained as follows: (1) Moist tamped samples, have particles that are more clustered together and structured than dry pluviated samples; (2) In terms of particle orientation, a change in the degree of orientation for both sand particles and ‘fines’ under constant loading was observed with time. The dominant (i.e. most) rotated particles (sand or “fines’) depends on the initial fabric and density; (3) Over time, under constant loading, growth of micro voids was observed for

dense samples while those of loose samples contracted; (4) A new parameter, variance to mean void ratio of void distance, was introduced as a measure of the degree of interlocking during aging. The variance to mean ratio of void distance for moist tamped samples tends to decrease whereas those of dry pluviated samples tends to increase with time. An increase in variance and variance to mean ratio for dry pluviated samples indicates that particles are more clustered together with time; (5) Original work on spatial void distance for the numerical analysis of creep induced aging based on Kang et al. (2012) was conducted (note: the model's boundary condition allows lateral expansion, which is not the same as the fabric tests conducted). The analysis showed that mean void size in dense soil tends to increase with time under constant load while for loose sample it tends to decrease. However the particles also clustered together more – increasing structure. (6)

A microstructural study of "undisturbed samples", obtained by gel-push sampling, of clean sand (fines content = 4%) and silty sand (fines content = 30%), was conducted to investigate anisotropy of natural fabric of granular soils. The results show that dry pluviation reflects the field condition more, in terms of natural deposition, than moist tamping. In addition, spatial void distance qualitatively indicated the undisturbed samples are relatively "very young", even in terms of engineering time, as indicated by similar variance to mean ratio and kurtosis with those of 1 hour and 1 week reconstituted samples.

This research has shown that there was a relation between changes in the microstructure over time and changes in macro mechanical properties of non-plastic silty sand. Further improvement in theoretical modeling (e.g. numerical modeling of creep on polydisperse granular material) and experimental aspects (e.g. examining different grain size composition and angularity, different fines content, the influence of the shape of sand and fines and use of the photo-elastic method) will allow a better understanding of the sand aging phenomenon in silty sand.

Acknowledgements

All praise and thank belong to the Allah, Lord of all universe.

Firstly, I would like to thank Prof. Misko Cubrinovski and Dr. Elisabeth Bowman. Their advise, expertise and continuous support have been invaluable. I would like to express my sincere gratitude to Dr. Elisabeth Bowman for introducing me to the topic and for being patient in guiding and encouraging me throughout of the course of my Phd research. I would like also to say my sincere gratitude to Prof. Misko Cubrinovski who has opened the way for the funding during my study.

I am also indebted to Sean Rees who have taught and helped me regarding the use GDS Triaxial. Many thank for Siale Faitatonu who helped to order the required materials for my experimental test. I am obliged also to say thank you to others technician, in particular John Koolos, who spent his skill and time developing the local data logging systems and fixing all the mechanical and electrical problems; Rob spiers and Kevin Stobbs who taught me how to grind and polish the sample; Mike Flaws, who helped me with the scanning electron microscope. Many thanks also to all departmental staffs who have been very supportive. I wish to extend my thanks to other students of geotechnical group: Jawad, Merrick, Catherine, Kelly who have made my Phd experience more enjoyable. I am grateful to Directorate of Higher Education of Indonesia and EQC Capability Funding Research Project who funded my study.

Finally and foremost, I must express million thanks to my wife Evelyn, my daughter Shavina Alifia whose love always accompany me throughout my winding Phd journey. To my beloved parents, without whom I would not be who and where I am today. Thank you Mom and Dad, for your continuous

love, moral support to keep me going and for all your sincere pray during night prayer.

CONTENT

LIST OF FIGURES

LIST OF TABLES

1 Introduction

1.1 Background

Time has known to affect the behavior of soils. Over geological time, soils can turn into rock (e.g. sand into sandstone), and rock weather to form soils. It has been observed that over a shorter period, e.g. weeks, months, and years, soils properties and behavior can also change. Some laboratory studies (Howie *et al.*, 2002) have even shown that the time effect in the range of minutes could also be significant.

Generally, time has been widely recognized to have a pronounced effect on clay. Gradual and measurable changes in clay properties over time are usually related to its low permeability allowing slow pore water dissipation, and to its chemical nature. However, in the last fifty years it has been revealed that generally sands, after some disturbance, exhibit time dependent behavior regardless of their near-instantaneous pore water dissipation and chemically hard inert properties. The majority of this evidence comes from the increase in penetration resistance in hydraulically placed fills and freshly disturbed deposits after ground improvement, such as via explosive blasting and dynamic deep compaction (e.g. Ashford *et al.*, 2004; Debats & Sims, 1997; Mitchell & Solymar, 1984; Saftner, 2009), This phenomenon usually is referred as *sand aging*. Another phenomenon related to *sand aging* is the increase in pile capacity of driven piles over sands.(e.g. Astedt *et al.*, 1992; Bullock *et al.*, 2005; Ng *et al.*, 2010).

An example of sand aging is illustrated in the Jacksonville Power Plant project at Florida (Schmertmann, 1991; Schmertmann *et al.*, 1986b). The power plant was to be built in a low-lying, naturally filled-in, former estuary consisting of very loose to dense silty sand about 10 meters in thickness. Ground improvement by dynamic deep compaction (DDC) was performed to provide a suitable foundation to support the extremely heavy loading in the power block

area. Quality control cone penetration tests (CPT) were performed before and after the treatment. Typical CPT profiles taken before and after densification indicate a significant increase i.e. about 35% in penetration resistance in 40 days (Figure 1-1). The ordinates in the figure represent the ratio of q_c at time t to that immediately after deep dynamic compaction (Mitchell, 2008). The figure clearly shows that time has considerable effects on mechanical properties of the soil.

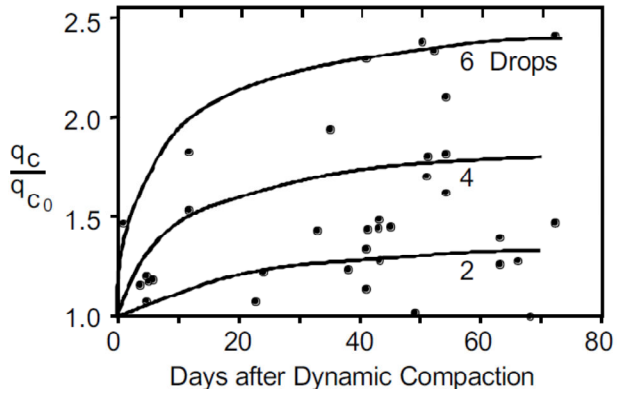

Figure 1-1 Normalized increase in cone penetration resistance with time after deep dynamic compaction on 10 m sand with layer of silty sand (After Schmertmann, 1991)

Following numerous field observations, there has been relatively many laboratory studies on *sand aging* (e.g. Afifi & Woods, 1971; Al-Sanad & Ismael, 1996; Bowman & Soga, 2003; Wang & Tsui, 2009). The majority of these laboratory studies were performed on clean sand. Regardless of the practical significance as exemplified in the figure above, few reported laboratory studies have attempted to understand aging and creep on *silty sand* i.e. their mechanism and their effects on undrained behavior particularly at small strain range (less than 0.1%). This is relevant due to the fact that natural sand deposits, hydraulic fills and tailing sands usually contain various amounts of fines. Additionally, strain ranges under working loads for most geotechnical structures such as tunnels, foundations and retaining walls are in the small range from 0.005-0.5% (Mair, 1993), for which time may have beneficial effects.

1.2 Aim and Objectives

The aim of this research is to provide a direct link between changes in the macro-mechanical undrained behavior of silty sand and its microstructural change with time. The main objective is to investigate the relationship between creep and aging of silty sand in order to shed some light on the aging mechanism particularly under low effective stresses. Based on the aim several objectives were defined as follows:

- To observe creep following K_0 and isotropic consolidation in specimens with different density, aging time and fabric.
- To investigate effects of creep induced aging of silty sand under undrained condition at small strain range. The tests mainly consist of monotonic undrained tests and one way cyclic undrained tests following K_0 or isotropic consolidation.
- To examine the change in microstructure during aging of silty sand.
- To directly observe and quantify the microstructure of silty sand for 'undisturbed' samples and reconstituted ones.

1.3 Limitation

As many other factors (e.g. plasticity of fines, fines content, grain size composition, angularity and shape) could affect silty sand behavior (Carraro & Salgado, 2004) and not all those factors could be investigated during the study period, this study focused only on aging of non-plastic silty sand with 15% fine content.

1.4 Thesis Organization

This thesis is organized as follows:

Chapter 2 reviews past and recent research on sand aging from field tests, laboratory tests and numerical micro-mechanical modelling. This chapter also explains small strain behavior of granular soils.

Chapter 3 describes material and some experimental aspects of this study related to both triaxial and fabric tests. For the triaxial tests, this chapter explains the development of small strain measurements to the existing apparatus, whilst for the fabric study this chapter presents the adopted system procedure for direct observation of silty sand microstructure.

Chapter 4 is the first chapter on the triaxial test series. It presents the observation of strain development during aging with different variables such as density, aging time, consolidation stress path and inherent fabric.

Chapter 5 is the second part that discusses the triaxial tests performed in this study to investigate the effects of creep and aging on undrained behavior particularly in the small strain range. The majority of stress paths are monotonic undrained compression tests under K_0 consolidation. The K_0 consolidation was chosen as representative of the in-situ condition for level ground in a free field. The stress path was chosen to simulate effects of time on freshly deposited or disturbed granular soils (e.g. hydraulic sand fill, mine tailings, and sandy soil following an earthquake) at shallow depth. Test variables are similar to those investigated in Chapter 4. A few tests were also performed using one-way cyclic loading to consider effects of creep on cyclic behavior relevant for natural slopes, embankments and quay wall backfills.

Chapter 6 focuses on the microstructure changes occurring during aging under K_0 condition. In this study the sample was loaded one dimensionally in the axial direction for various aging times under low effective stress. The sample

microstructure was preserved by introducing very low viscous epoxy resin into the specimen and then cutting, grinding, and polishing of the specimen for observation under high resolution scanning electron microscope (SEM) via back scattered electron detector. Apparent particle orientation and mean free path between particles were used as parameters to quantify the microstructure changes. In addition, observation of undisturbed granular soils recovered by gel-push sampling is also described.

Chapter 7 presents the conclusions of this research. Recommendations for future research also are given.

1.5 Terminology

In this study, the following terms or phrases are often used:

Sand aging: Apparent time dependent increase in stiffness and strength of granular materials.

Creep: continuous deformation of soils under constant stress where particle rearrangement and internal inter-particle stress changes and redistribution among groups of particles occur (including asperities damage and particle breakage)

Aging mechanism: Mechanism(s) underlying the *sand aging*. Hypothesized mechanism includes mechanical and chemical aging. Although some evidence now favours mechanical mechanism (Mitchell, 2008), particularly in engineering time (e.g. days, months and years), no conclusions have been set thus further study is required to understand the mechanism.

Fines: particles smaller than 75 μm in diameter

Silty sand : according to the Unified Soil Classification System, USCS, (ASTM D 2487), silty sand are either soils that contain at least 50% of particles smaller than 4.75 mm and more than 12% either low plasticity or non-plastic fines.

Small strain: strain less than 0.1%

2 Aging and Creep of Granular Soil

2.1 Introduction

Sand aging can be considered over two time scales, geological and engineering scales respectively. The former considers the aging effect over the age of the deposit since its deposition, and could be in the range of hundreds to thousands of years or more. The latter are the changes associated with time over a shorter period after disturbance of the ground in the range of minutes and days to years, which is the interest of this study.

The first section of this chapter will illustrate aging effects both from field observations and laboratory studies.The following section of this chapter will summarize previous studies of sand aging based on soil types, different theories underlying the phenomenon and last section of this chapter will discuss observation of creep from triaxial test and numerical modelling perspective.

2.2 Aging of Granular Materials

2.2.1 Sand aging previous studies based on soil types

There have been many reported field and laboratory studies related to sand aging. Table 2-1and Table 2-2 present previous studies on sand aging and their soil types from field and laboratory tests, respectively. It can be seen from Table 2-1 that most of the field studies of sand aging involve clean sand with few field studies involving silty sand. Likewise Table 2-2 shows that sand aging studies from laboratory testing were mainly performed on clean sand. Table 2-2 also reveal that most laboratory tests particularly from triaxial tests are under drained condition. Limited studies investigate aging effect on monotonic and one way cyclic undrained behavior.

Table 2-1 Field sand aging studies and soil types (Modified from Baxter (1999) and Saftner (2009))

Reference	Cu	Cc	D_{10}	D_{50}	Description/USCS	Dr(%)	Location
Denisov *et al.* (1963)	-	-	-	-	fine to medium clean sand	NA	Volga river
Hryciw (1986)	1.6	1.11	0.075	0.12	SP	40-50	Harriet's Bluff
Mitchell (1986)	2.94	0.94	0.31	1	SP	40-70	Jebba Dam
Schmertmann (1986a)	-	-	-	0.25	Very loose to dense silty sand.	20-60	St. John River
Petraborg (1987)	<6	-	-	-	FC<11%, sub rounded beach sand	60	Bay farm Island
Dumas & Beaton (1988)	3.06	-	-	0.79	medium to coarse clean sand	NA	Pointe Noire Harbour
Handford (1988)	2.3	1.17	0.09	0.16	Tailing sand/SP	40-60	Fort Mac Murray
Brown (1989)	0.3	-	-	-	Alluvial sand	40-45	Gray Beverages
Roger *et al.* (1990)	2.67	1.04	0.14	0.33	clean sea sand (FC<8%) / SP	60	Beaufort Sea
Thomann (1990)	2.42	1.04	0.11	0.2	SP		Douglas Laeke
(Charlie *et al.*, 1992a)	4.17-5.75	-	-	2.1-2.3	medium to fine sand and gravelly sand	70-85	South Plate River
Human (1992)	-	-	-	-	fine silty sand	NA	Bay farm Island
Gohl *et al.* (1994)	-	-	-	-	fill overlying loose sand	NA	Kelowna
AGRA (1995)	1.9-4.5	-	-	0.3-1.5	Loose river sand	40	Sept. Iles, Quebec
Ng *et al.* (1996)	4.5	-	-	0.8	Hydraulic sand fill (fines<12%)	30-40	Chep Lap Kok Airport
Howie and Amini (2004)	1.88	-	0.16	0.271	-	-	Fraser River
Ashford *et al.* (2004))	-	-	-	0.25	Clean fine sand /SP	20-70	Treasure Island
Holzer & Youd (2007)	-	-	-	0.091	SM	-	Wildlife site
Rollins a& Anderson (2008)	2.35	1.51	0.085	0.19	SP	-	Massey Tunnel
Safner (2009)	1.78	-	0.18	0.32	Loose sand / SP	40	Griffin
Narsilio *et al.* (2009)	1.47	-	-	0.21	Loose fine sand/ SP	38-44	South Carolina

Note: Cu=coefficient of uniformity; Cc=Coefficient of gradation; D_{10}=diameter associated with 10% pass; D_{50}= mean diameter; Dr=Relative density

Table 2-2 Sand aging from laboratory studies and their soil types (Modified from Saftner, 2009)

Reference	D_{10}	D_{50}	Cu	Cc	USCS	Sand	Note
Afifi and Woods (1971)	1.6	1.2	0.27	0.41	SP	Ottawa	Resonant columnt
Seed ((1979)	-	0.41	1.4	-	-	Monterey	Undrained cyclic two ways
Daramola (1980)	-	-	-	-	-	Ham River	Drained direct shear
Ishihara (1985)	-	0.3	2.5	-	-	-	Undrained cyclic two ways
Hryciw (1986)	1.5	1.03	0.15	0.2	SP	Evanston Beach	Mini cone penetration
Mejia et al.(1988)	1.5	-	-	0.4	-	Ottawa C-109	Oedometer
Thomann and Hryciw (1992)	1.89	-	0.07	-	-	Ottawa 100-200	Resonant columnt
Miller (1994)	2	-	-	0.3		Holliston	Direct simple shear
Joshi *et al.* (1995)	2.39	1.12	0.12	0.45	SP	River	Mini cone penetration
Lade & Liu (1998)	-1	-1	-	-	SP	Antelope Valley	Drained triaxial
Baxter (2004)	1.93	1.04	-	0.5	SP	Density	Mini cone penetration
Shozen (2001)	0.16	0.271	1.88		SP	Fraser River	Drained triaxial
Bowman (2002)	-	-	0.12	0.15	SP	Leighton Buzzard	Drained triaxial
Bowman (2002)	-	-	0.18	0.24	SP	Montepellier	Drained triaxial
Lam (2003)	0.16	0.271	1.88		SP	Fraser River	Drained triaxial
LeClerc(2008)	1.28	1.08	0.4	0.5	SP	Ottawa	Triaxial
(Lade *et al.*, 2009)	-1	-1	0.15	NA	SP	Crushed coral	Drained triaxial
Wang and Tsui (2009)	-	-	0.65	0.85	SP	Ottawa 20-30	Resonant column
Wang and Tsui (2009)	-	-	0.16	0.22	SP	Toyoura	Resonant column
Wang and Tsui (2009)	-	-	-	-	-	Toyoura+15%dry kaoline	Resonant column
Gao et al. (2011)					SP	Toyoura &Leighton Buzzard	Bender element
Wang & Gao (2014)	-	-	0.12	0.15	-	Leighton Buzzard	Oedometer

2.2.2 Aging effects

2.2.2.1 Effects of aging on penetration resistance

There have been numerous examples of aging since Mitchell (1986) documented the increase in cone penetration resistance after vibro-compaction and explosive blasting during the development of Jebba Hydroelectric Dam Project at Nigeria. Table 2-3 shows some examples of aging effect on the penetration resistance from different studies. Mitchell (2008) compiled penetration resistance data after ground improvement from a number of cases and noted a marked difference in the rate of increase in cone tip resistance, q_c, with time (Figure 2-1). There have been also some cases where q_c has decreased shortly after blast induced densification and then increased with time (e.g. Mitchell & Solymar, 1984) or never reached the pre-densification value (e.g. Thomann, 1990).

2.2.2.2 Aging effects on axial pile capacity

There are many field studies indicating that load bearing capacity of piles driven into sands may increase significantly over months, long after pore water pressures have dissipated, a phenomenon referred to as pile setup. The magnitude of increase in the axial capacity is variable, as can be seen Figure 2-2 with most of it due to increase in the shaft resistance rather than the tip resistance (Jardine *et al.*, 2006).

Bowman and Soga (2005) hypothesized that there is an increase in radial stress (i.e. horizontal effective stress) around the pile shaft after installation. After the process of driving the piles into sands, they proposed that displacement pile setup or restrained dilation occurs with time. With the presence of a pile in the ground, sand particles adjacent to the pile shaft tend to rearrange (i.e. creep) relative to the pile shaft. This process causes redistribution of the loads imposed on individual sand particles. In this process, dense sand around the pile initially tends to contract, and with time, it dilates under constrained lateral deformation.

Table 2-3 Examples of sand aging on cone penetration test from ground improvement cases (modified after Baxter, 1999)

Reference	D_{50} (mm)	Cu	Dr %	σ'_v (kPa)	Densification	Measured Time Period (days)	Improvement with Time	Soil description/ Note
Schmertmann et al. (1986)	0.25	NA	40-70	0-100	Dynamic deep Compaction	80	As much as 240% increase in qc .	Very loose to dense silty sand.
Handford (1988)	0.16	2.3	40-60	50	Blasting	45	30-50% increase in qc	Tailing sand
Troncoso (1990)	0.12	6	NA	50-100	Earthquake	1460	As much as 50% increase in SPT value	silty sand
Charlie et al. (1992)	2.1-2.3	4.17-5.75	70-85	30-90	Blasting	126	About 15% increase in qc	medium to fine sand and gravelly sand;dense to very dense;
AGRA (1995)	0.3-1.5	1.9-4.5	40	0-200	Blasting	30	200-300% increase in qc after 12 days; no further increase after 30 days	Loose river sand
Ng(1996); Covil et al.(1997)	0.8	4.5	30-40	100	Vibro-compaction	42	Average 35 % increase in qc	Hydraulic sand fill (fines<12%)
Ashford (2004)	0.25	NA	20-70	36	Blasting	294	qc between 2 and 5 m depth tip had increased to twice the pre-blast value and 2.5 times the value two days after the second blast.	Clean fine sand to silty sand
Safner(2009)	0.32	1.78	40	46	Blasting	671	43% increase in qc	Loose sand
Narsillo et.al (2009)	0.21	1.47	38-44	112	Blasting	1292	Limited increase in qc during first year, clear increase 2 years after	Loose fine sand

Note: D_{50} = diameter correspondent to 50%pass in particle size distribution; Cu= coefficient of uniformity; Dr=relative density; σ'_v=effective vertical stress

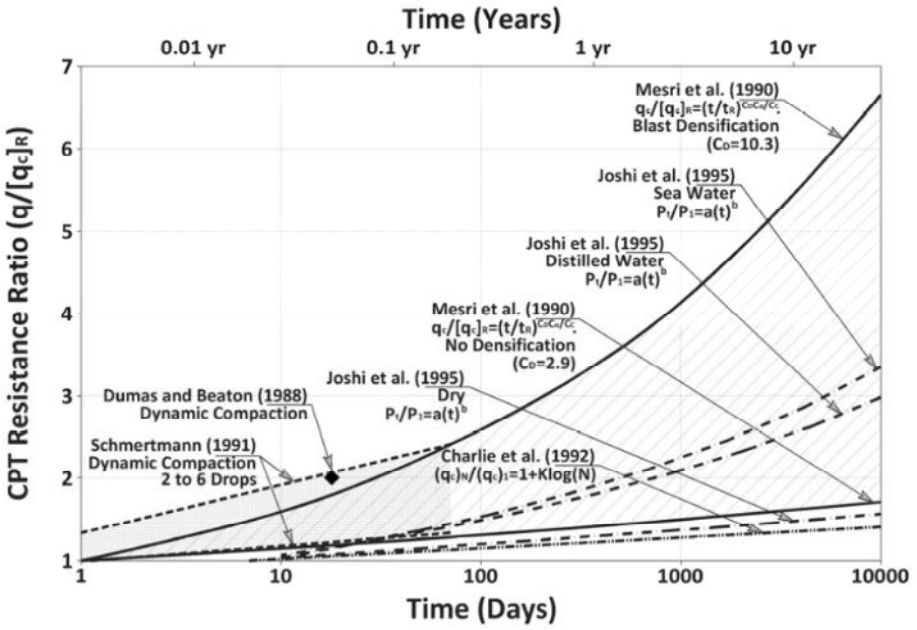

Figure 2-1 Rate of cone penetration resistance as result of sand aging (Mitchell, 2008)

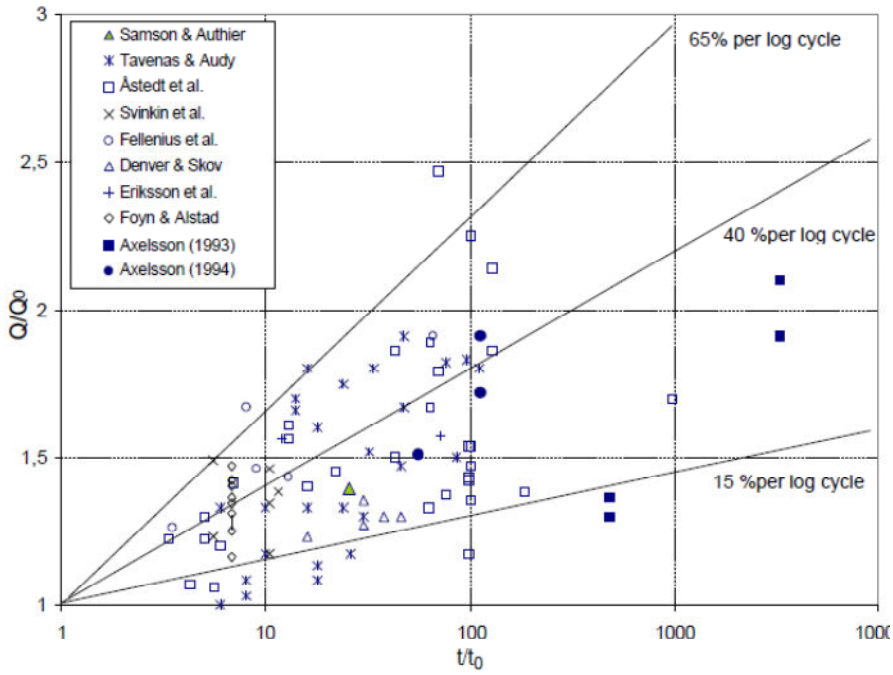

Figure 2-2 Increase in axial pile capacity with time for driven piles in sand (Axelsson, 2000)

2.2.2.3 Aging effects on small-strain properties

Afifi and Woods (1971), based on resonant column tests on Ottawa clean sand, silt and clay, showed that the small strain shear modulus increased linearly with the logarithm of time. This can be expressed by the following expression

$$\frac{G_{\max}(t)}{G_{\max}(t_p)} = 1 + N_G \log(\frac{t}{t_p}) \qquad \textbf{Eq. 2-1}$$

Where t_p is the time to the end of primary compression, t is any time greater than t_p, G max (t) is G_{max} at time t, $G_{max}(t_p)$ is G_{max} at time t_p. The reference time, t_p, was taken as 1000 minutes. N_G is a coefficient that can be back calculated from monitoring the increase in stiffness with time. N_G values were found to be between 1 and 12% with a typical value of 2%. Based on bender element tests on Evanston beach sand, Baxter and Mitchell (2004) found N_G values less than 4% and showed that N_G was influenced by sand type, pore-fluid and density, but did not find any obvious effect from temperature.

Howie *et al.* (2002) and Lam (2003) studied the effect of aging periods of up to 10,000 minutes on the stress-strain response of *very loose clean Fraser River sand* (mean diameter, D_{50}=0.27 mm and coefficient of uniformity, C_u= 1.9). The average mineral composition is 40% of quart, quartzite and chert, 11% feldspar, 45% unstable rock fragment, 4% miscellaneous detritus (Garrison *et al.*, 1969). A period of aging resulted in a much stiffer (small strain stiffness Young Modulus, E) response during the initial portion of the stress-strain curve (Figure 2-3) but the effect of aging tended to disappear at larger strains. The result suggests that aging increases initial (small strains) stiffness but has little effect on larger strain properties, including shear strength. It also revealed that contractive volumetric strain decreased with aging time.

Wang and Tsui (2008) investigated density effect on the aging behavior *of rounded Ottawa sands* and *sub angular Toyoura sands* using resonant column tests. The results on Ottawa sand demonstrated that medium-dense samples had the highest aging rate, as determined by shear modulus increase, followed by the dense and loose samples (Figure 2-4). The trend did not apply to Toyoura sand which suggests that the effect of packing density on the aging behavior of sand indeed varies with the characteristic/type of sand. Using bender elements in a true triaxial apparatus, the authors also demonstrated that aging is not isotropic by nature. The increase in shear wave velocities in different polarization planes varied under an isotropic stress state.

Wang and Tsui (2009) investigated the effect of fines (dry kaolinite powder) on aging behavior of the same materials. The period of aging was two days. It was revealed that sand containing fines has a greater shear-modulus increase than the clean sand does, which can be attributed to the more significant creep and aging rate made by the kaolinite (Figure 2-5). The sample with 15% kaolinite had a higher modulus increase than the sample with 3% kaolinite in the early aging period, but the two modulus growth curves came close to each other at the end of the test. This suggests that the contact properties vary from time to time and so do the associated aging effects.

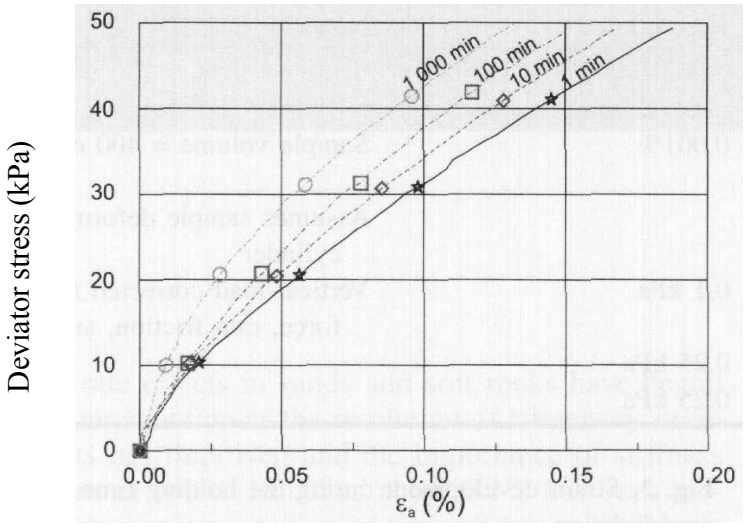

Figure 2-3 Aging effects on small stress-strain response (Howie et al., 2002)

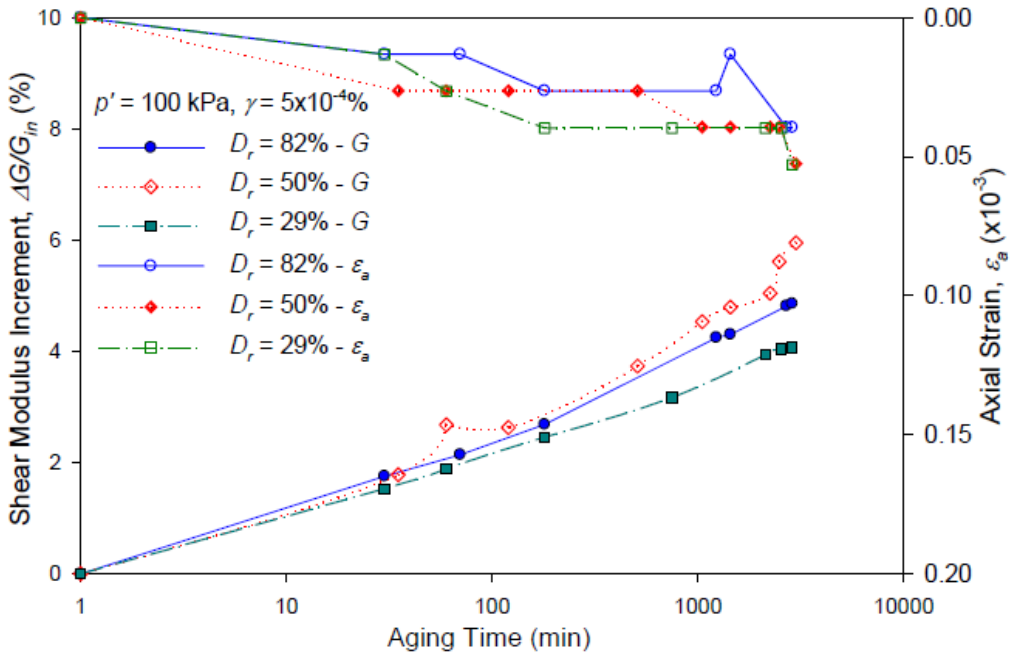

Figure 2-4 Variations in the small-strain shear-modulus increment and the axial strain in Ottawa sand samples with different relative densities (Wang & Tsui, 2008)

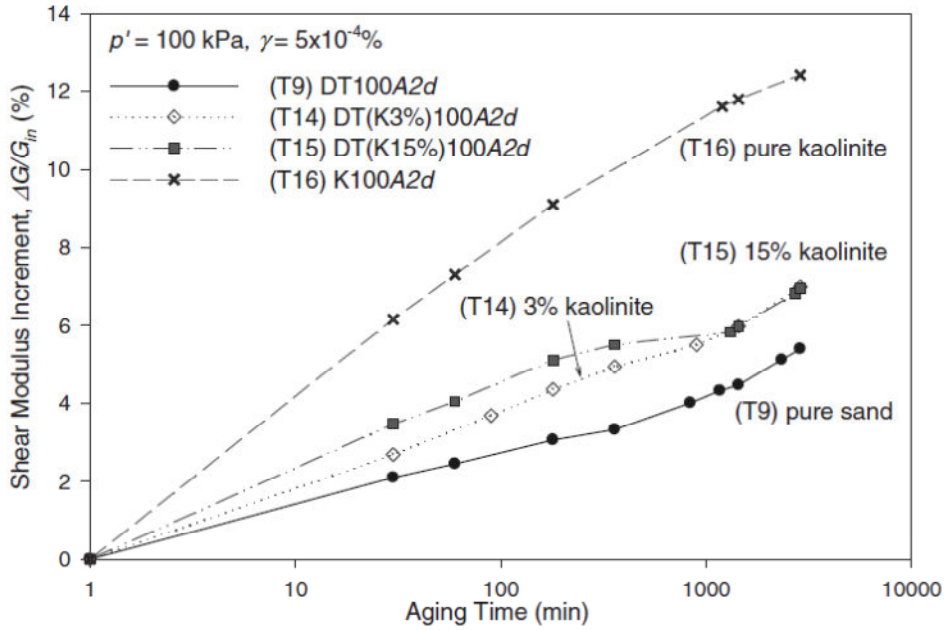

Figure 2-5 Effect of fines on aging behavior (Wang & Tsui, 2009)

The aging effect on the stiffness anisotropy of *Toyoura sand and Leighton Buzzard sand* were investigated by Gao *et al.* (2011) using bender elements in a true triaxial apparatus. The results suggest that during aging, changes in the

micromechanical properties, e.g., the contact normals and normal contact forces; continue with the same tendency that has already been established before the initiation of aging.

Howie and Amini (2004) investigated the time effect on the shear wave velocity thus small strain stiffness using seismic cone testing (SCPT). A seismic cone was pushed to a depth in medium fine sand to silty sand and the shear wave velocity was measured at different wait times after stoppage. The cone pushing disturbed a zone around the cone and set the aging time to zero for this zone. Aging stiffened up the disturbed zone with time which could be detected by seismic tests, Figure 2-6. As can be seen in the figure the aging rate is higher in the first 10 minutes (about 5% increases in Vs), and then becomes smaller (about 2.5% over 50 minutes). This is similar to the laboratory observations which show that aging rate is decreasing with time. The faster arrival of shear waves was attributed to the effects of aging of the soil in the disturbed zone around the cone. The advantage of this test is that it clearly shows the time effect and it is not affected by site variability since the tests at different times are carried out without changing the location. Moreover, no disturbance was imposed to the ground after the start of the aging process. Seismic tests impose very small shear strains on the soil and hence their aging effect would be negligible. Therefore, any change to the soil response with time could be directly attributed to the changes of soil properties with time.

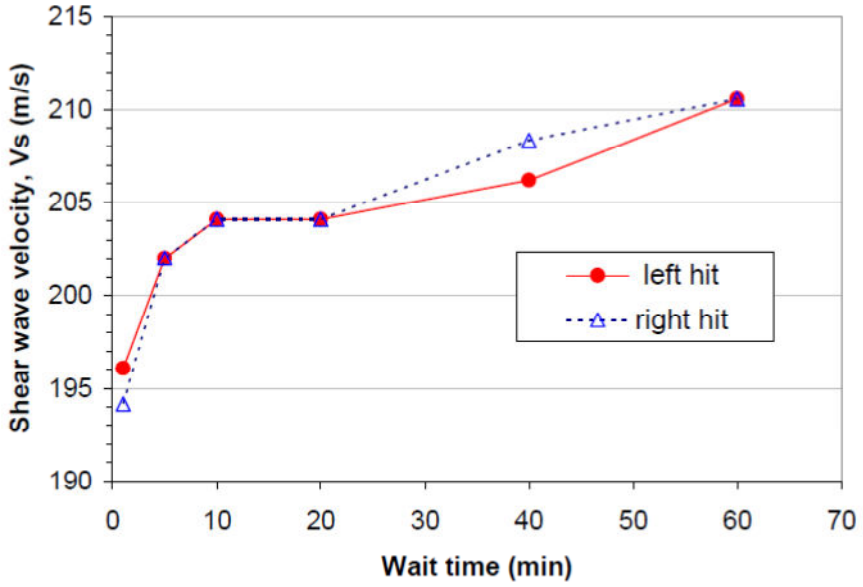

Figure 2-6 Aging effect to shear wave velocity from seismic cone Penetration test (Howie & Amini, 2004)

2.2.2.4 Aging effects on static shear strength and compressibility

Al-Sanad and Ismael (1996) investigated the effects of aging on strength (direct shear test) and compressibility of Khaldiya Gatch sand. The sand *is a fine-to-medium, calcareous silty sand* and can be classified as SM (low plasticity silty sand) according to the Unified Soil Classification System. The sand has a natural moisture content of 1.9%, a specific gravity of 2.67, and the amount of fines passing a No. 200 sieve is 17.5%. It is well graded, with a coefficient of uniformity (Cu) of 6, mean diameter (D_{50}) of 0.33 mm, minimum dry density 1449 kg/m^3, maximum dry density from modified Proctor (at optimum water content 10.3%) of 2068 kg/m^3. Chemical analyses indicate that quartz is the principal component of the particles. However, calcium carbonate, calcium magnesium carbonate (dolomite), and gypsum represent nearly 20% of the total composition.

Direct shear test results indicated that the friction angle of the specimens increased with time (Figure 2-7 left) as they aged under vertical stress. The increase in strength is about 10% over 6 months. In their research, specimens were built at a relative density of 60% and then aged under very low vertical stress of 2 kPa up to 6

months. The increase in strength over time appears to be in contradiction with Howie's *et al*. (2002) and Lam's (2003) observation, who suggested that aging has little effects on large strain properties such as strength. This may be due to the present of calcium carbonate, dolomite and gypsum which may act as cementing agents. Cementation is likely when carbonate is present (Mitchell, 2008). It is likely that the aging mechanism (see 2.2.3) in Al Sanad and Ismael's study is a combination of mechanical and chemical (see 2.2.3). Whereas aging mechanism in Howie's et al. and Lam's studies is mainly mechanical due to lack of cementing agents.

Consolidation tests were carried out on compacted sand at zero time (immediately after preparation) and at 3 months. Samples tested after 3 months were kept under a constant normal pressure of 40 kPa during the aging period. All specimens, 75 mm in diameter and 20 mm thick, were prepared at a relative density of 60% and saturated with water for 2 hours before the tests. The compressibility coefficient Cc decreased slightly from 0.23 to 0.20 for the aged samples over the 3-month period (Figure 2-7 right).

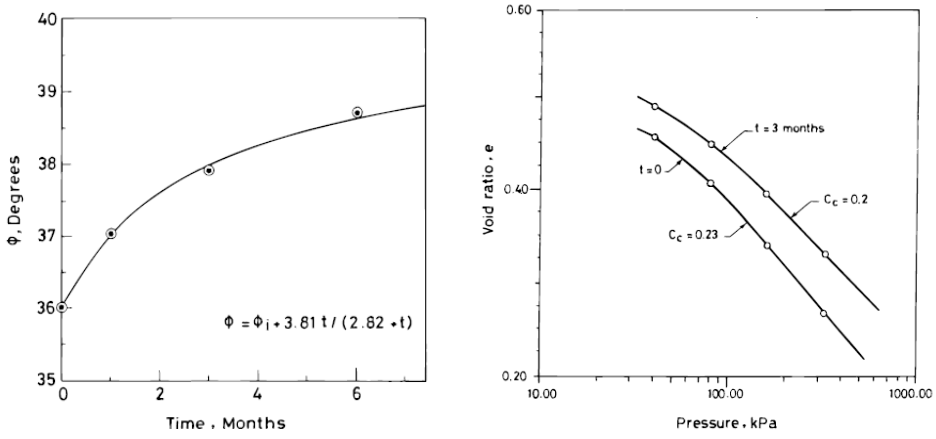

Figure 2-7 Aging effect on angle of friction and compressibility (Al-Sanad & Ismael, 1996)

2.2.2.5 Aging effects on cyclic strength and liquefaction resistance

Seed (1979) conducted cyclic triaxial tests on Monterey sand of about 50% relative density and found an increase in liquefaction resistance of 12% and 25%

for sands aged for 10 and 100 days, respectively. He also compared the resistance to liquefaction of some undisturbed and reconstituted samples which are plotted in the same figure. He concluded that the liquefaction resistance of natural deposits might be as high as 75% greater than that of freshly reconstituted samples in the lab.

Troncoso *et al.* (1988) investigated the effect of aging of tailing materials, by conducting a series of cyclic triaxial tests on undisturbed silty sands. The samples were recovered from two tailing dams at El Cobre in Chile. The sands are well graded with mean diameter of 0.12 mm and average fine content about 25%. Figure 2-8 shows that the sand with an age of one, 5, and 30.5 years of deposition possesses about 2.0 times, 2.4 times and times 3.5 times higher resistance to cyclic stress application, respectively, as compared to the freshly reconstituted sample using water pluviation.

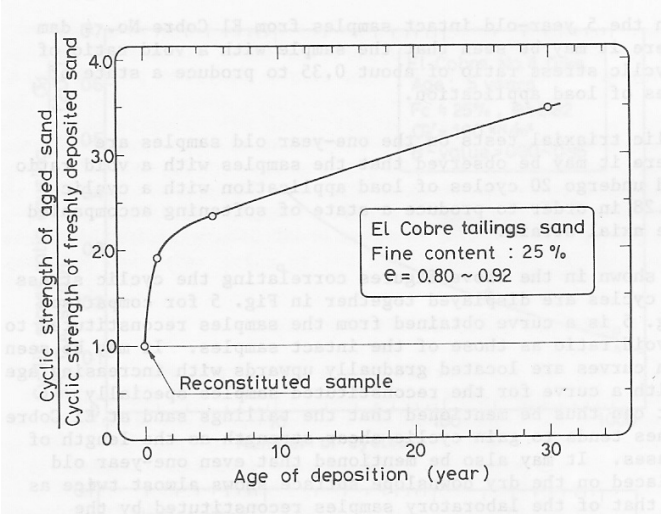

Figure 2-8 Aging effect on cyclic strength of silty sand (Troncoso et al. 1990)

2.2.2.6 Aging effects on horizontal stress

An experiment using a rigid retaining wall was conducted Terzaghi (1934) to measure the lateral earth pressure of dry Plum Island sand. After the sand was deposited, an increase in horizontal stress (σ'_h) was observed over a period of 17

hours as shown in Figure 2-9 (from point d to point e), although the position of the wall did not change.

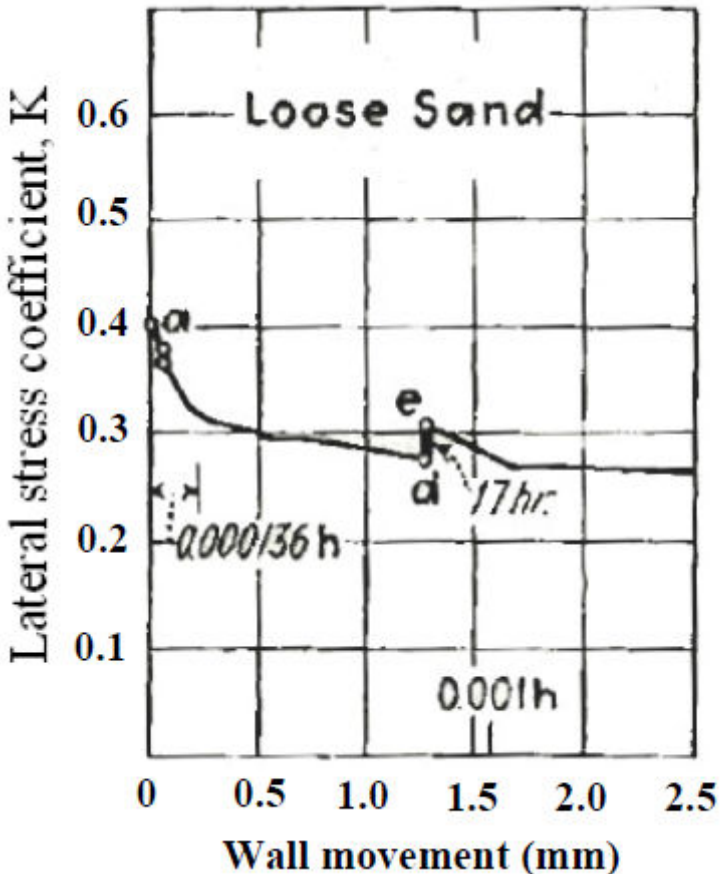

Figure 2-9 Aging effects to lateral stress in retaining wall (Terzaghi, 1934)

Continuous rearrangement of individual particles after deposition was believed by Terzaghi (1934) as the cause of the time-dependent increase in σ'_h in sand. The rearrangement, under constant pressure, results in the movement of the individual sand grains into more stable positions. This is turn reduces the frictional (shear) stress at contacts of sand grains.

Jirathanathaworn (2009) designed a system using photo-elasticity to measure changes in horizontal stress during aging of glass rods, representing a 2-dimensional (2-D) soil assembly. As depicted in Figure 2-10, during sustained load, the horizontal stress increases with time. Time-dependent surface settlement was observed to depend on the magnitude of the applied vertical

stress, particle shape, and particle surface roughness. Time-dependent surface settlement and particle re-arrangement occur more rapidly at higher vertical stresses. Assemblies of cylindrical particles showed more surface settlement than those of angular prism particles under the same applied stress. Surface settlement for assemblies of smooth cylinders was higher than those for assemblies of rough cylinders.

Horizontal stress increases during aging also observed following explosive blasting at the Griffin's sand and gravel quarry, Indiana USA (Saftner, 2011a). The soil layers consisted of a loose sand layer (poorly graded sand, SP, with coefficient of uniformity, Cu of 1.78 ; mean grain size diameter, D_{50} of 0.32 mm) and gravelly sand layer (classified as poorly graded sand with gravel, SP with >15% of gravel; Cu=2.42; D_{50}=0.8 mm). Horizontal stress was measured using flat dilatometer through horizontal stress index, K_D. Typical results from the flat dilatometer test are shown by Figure 2-11. There was an initial decrease in K_D following the blast and an increase between one week and one month. Measurements taken after one month do not show time-dependent behavior. In the loose sand layer, K_D was greater than pre-blast values, but other layers to not recover to pre-blast values.

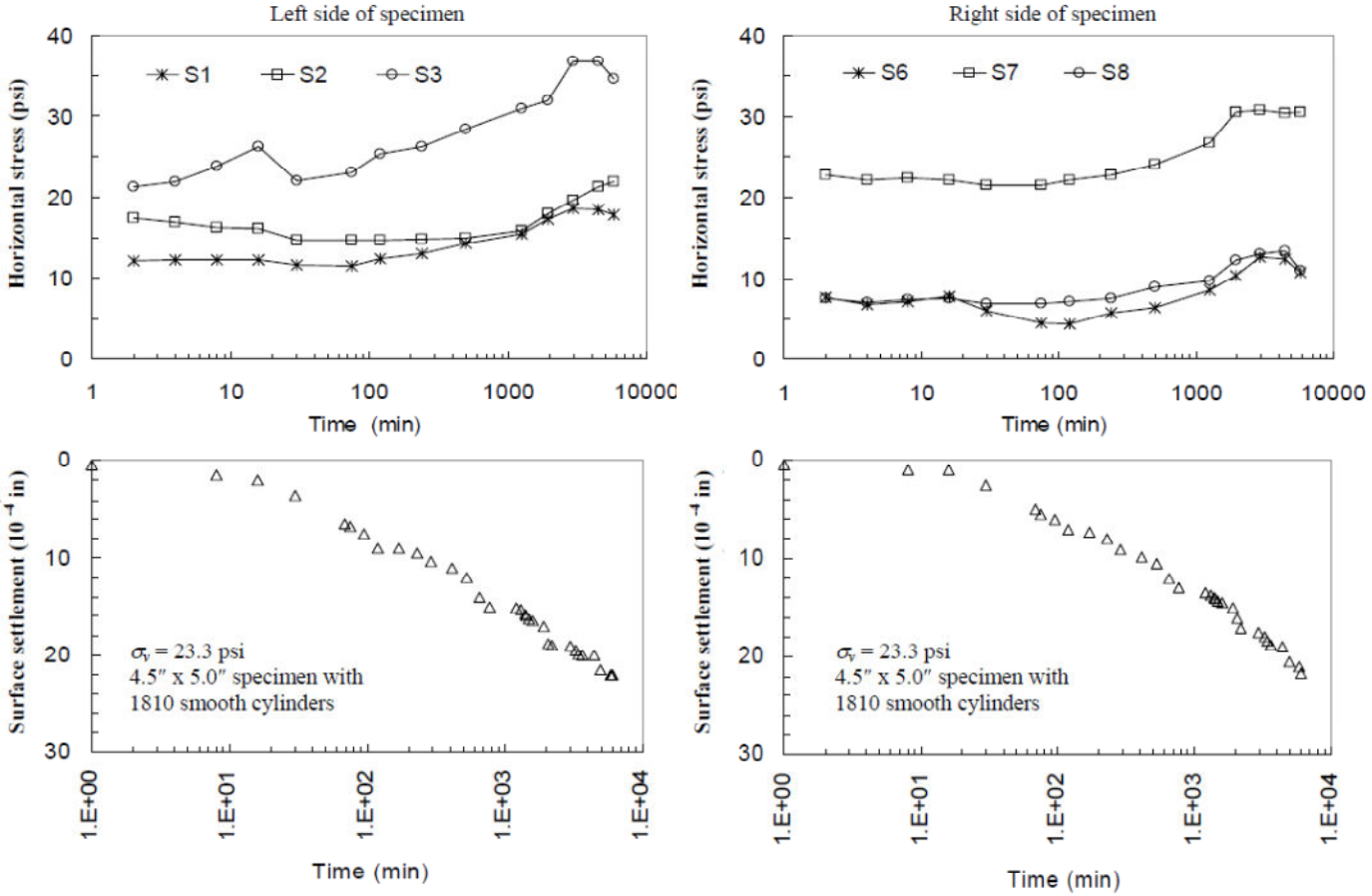

Figure 2-10 Horizontal stress and surface settlement during sustained vertical load (Jirathanathaworn, 2009)

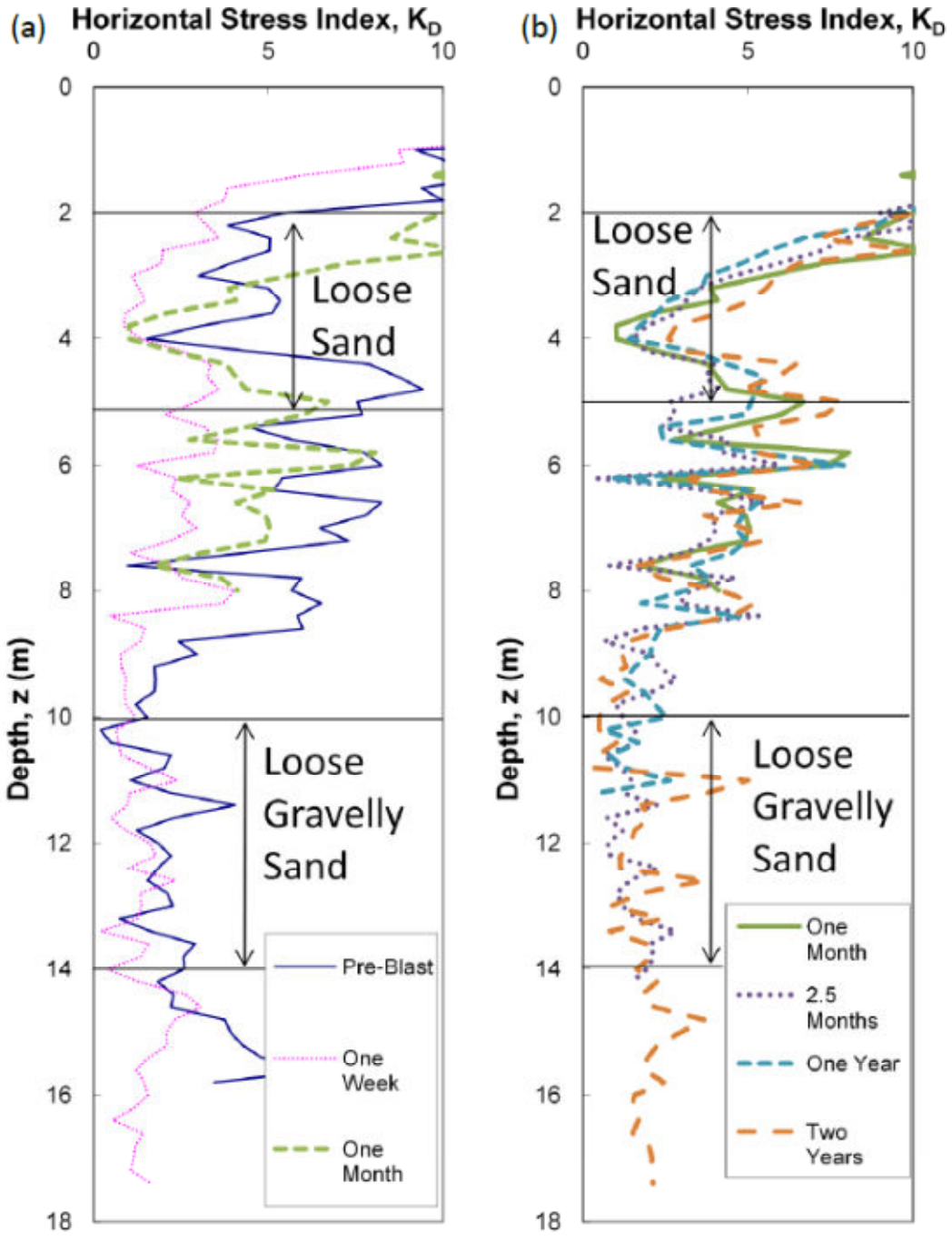

Figure 2-11(a) Horizontal stress index versus time up to one month (b) Horizontal stress index one month to two years (Saftner, 2011b)

2.2.3 Aging Mechanism

Four primary mechanisms have previously been proposed for aging: a mechanical mechanism, a chemical mechanism, a dissolving bubble mechanism, and a biological mechanism. The mechanical mechanism is the most widely accepted one (Mitchell, 2008). However, under the right circumstances; each of these mechanisms could affect sand aging behavior. This section summarizes aging mechanisms from previous research.

2.2.3.1 Mechanical aging mechanism

In general, the deformation of sandy soil is induced at micro scale by contact deformation, grain sliding and rolling, and grain crushing. The contributions of these factors are different at different stress levels (Mitchell and Soga, 2005). At very low stress levels, the contact deformation is a dominant contributor overall to the deformation of soil. The soil behaves elastically and the deformation is reversible. At low stress levels, grain sliding and rolling dominate the deformation behavior, while grain crushing dominates the deformation of the soil at high stress levels. In the latter two conditions, soil deforms elasto-plastically and most of the deformation of the soil is irreversible. This study will focus on creep behavior of silty sand at effective vertical stress between 30 to 300 kPa which is relevant for most of the geotechnical problems.

Mechanical aging is considered as a creep process due to particle rearrangement of granular assemblies. Under constant loading, particles rearrange into more stable position, results in a greater macro-interlocking of particles and micro-interlocking of surface roughness, and consequently, greater frictional resistance compared to that before the aging process. This is eventually manifested in time-dependent increase in strength and stiffness of sand (Bowman & Soga, 2003; Jirathanathaworn, 2009; Mesri *et al.*, 1990; Schmertmann, 1991; Terzaghi, 1934).

Schmertmann (1991) explained that particle reorientation causes time-dependent mechanical processes in aged sands. Despite the fact that the reorientation does not cause significant increase in density, the process results in stress redistribution (i.e., stress relaxation) at contacts of sand particles. The stress redistribution reduces frictional (shearing) stresses and likely increases the micro-interlocking at the associated particle contacts. Similar explanation also suggested by Mesri *et al.* (1990).

Direct observation that sand particles rotate and displace overtime during aging was provided by Bowman and Soga (2003). Very low viscosity epoxy resin was injected into air pluviated dense sand samples under K_0 condition. Initially after the application of loading, sand particles oriented perpendicular to major principal direction, and then with time they rotated in space. In addition the particles clustered together forming stronger force chains. Bowman and Soga's hypothesis was supported by photo-elastic experiment using glass rods (Jirathanathaworn, 2009). At a microscopic level, based on numerical results, Kuhn and Mitchell (1993) proposed that particles translate (or slide) with time. Another explanation was proposed by Bowman and Soga (2003), based on fabric test, where particles rotate (or roll) overtime.

2.2.3.2 Chemical aging mechanism

Mitchell and Solymar (1984) initially postulated a chemical aging mechanism in order to explain time-dependent increases in cone penetration resistance in sands at the Jebba dam's project. Dissolution of silica at particle contact was deemed as the cause of time-dependent chemical process mechanism. When the solution reaches the equilibrium, dissolved silica begins to precipitate, and chemical cement bonding is produced at grain contacts, thereby ultimately increasing strength and stiffness of sands (De Boer, 1977; Sheldon & Wheeler, 2003; Sheldon *et al.*, 2003; Weyl, 1959).

Cementation at grain contacts due to precipitation of dissolved silica was believed as the cause of the increase in penetration resistance by Mitchell and

Solymar (1984). They argued that the required time for reaching equilibrium of silica (within weeks to months) is consistent with the time period of the observed increases in cone penetration resistance at the Jebba dam site. Cementation of precipitated silica causes a cohesive bond in sands, thereby improving shearing resistance of sands (Barton, 1993; Dittes & Labuz, 2002; Hryciw, 1986; Joshi *et al.*, 1995; Sheldon & Wheeler, 2003; Sheldon *et al.*, 2003; Weyl, 1959).

The process of silica dissolution between two sand (quartz) grains under sustained normal stress is illustrated by Figure 2-13. Stress at contact points accelerates localized dissolution of silica from the two particles. The load, in terms of normal stress, is transferred to the contact of the two particles. The surface of the particles is then coated by the dissolved silica which moves away from the contact area toward the pore fluid. Precipitated silica around the edges of the sand grains eventually cements the grains together as shown in Figure 2-14.

It should be noted, Mitchell (2008) reported that the rate of silica precipitation is approximately 0.00005kg quartz per kg of sand per year, a very small amount. The rate is unlikely to cause significant strength gain in an engineering time scale. Mitchell (2008) also stated that cementation is more likely when carbonate or alumina or iron is present, particularly in evaporated deposits. This may help at explaining some gain in strength of silty sand in 2.2.2.4.

2.2.3.3 Blast gas aging mechanism

During the detonation of buried charges, blast gases are produced and. trapped underground. Hryciw (1986) believed that some of these gas bubbles entrapped underground may have diameters larger than the diameters of sand grains.

Immediately after blasting, the large gas bubbles impede the settlement of sand particles, thereby creating particle arches as shown in Figure 2-15. Over

time under constant stress, the trapped gas bubbles dissolve, and/or escape to the ground surface. The disappearance of the gas bubbles may cause some individual sand particles to rearrange into a more stable configuration. Another possibility is that the trapped gas bubbles may inhibit pore fluid flow, and thus prolong the dissipation of excess pore water pressures (Dowding & Hryciw, 1986; Hryciw, 1986; Mesri *et al.*, 1990).

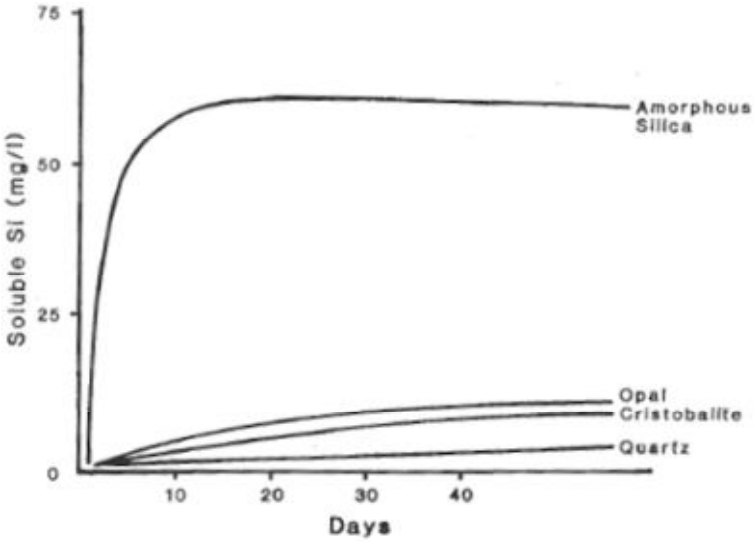

Figure 2-12 Dissolution rate of silica as a function of time (Wilding *et al.*, 1977)

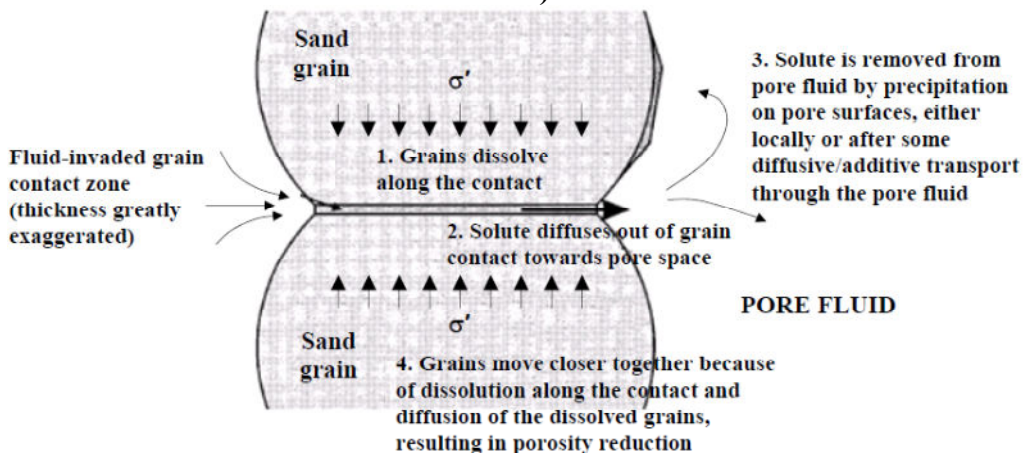

Figure 2-13 Silica dissolution and precipitation under contact stress (After Sheldon et al., 2003)

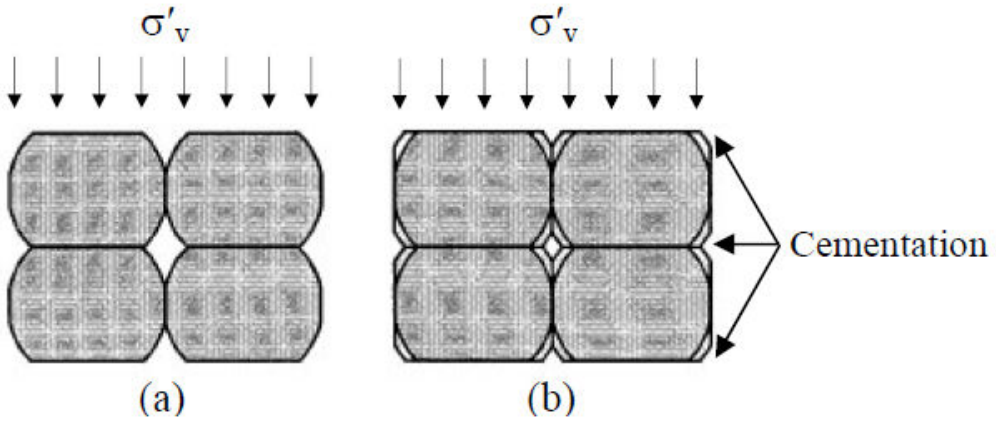

Figure 2-14 Grains under constant pressure: (a) initial state (b) precipitated silica around grains providing cementation between grains (after Sheldon et al., 2003)

Support for the hypothesis is provided by Leclerc (2008) who investigated effects of gas dissipation on aging in triaxial tests. The samples were Ottawa sand with 50% and 80% relative density, respectively, whilst the gasses were air and CO_2. Air was used to simulate conditions following vibro-compaction and CO_2 to simulate post-blast conditions. The results showed that the sample with 80% relative density did not age very much, while the 50% relative density samples showed a considerable increase in strength and stiffness. The behavior of the 50% relative density samples aged two weeks are similar to Dr=80% samples. The study revealed that the type of gas did not influence aging effects. Despite this, the work shows that gas dissipation can contribute to aging.

2.2.3.4 Biological aging mechanism

Recent researches in biology, e.g. Dejong *et al.* (2006), have shown that microbiology can have significant effects on strength and stiffness of sands. Dejong *et al.* found that Bacillus pasteurii produced calcite (i.e., calcium carbonate), which creates a cement bonding at the sand particle contacts. An increase in small-strain modulus over time was observed as the bacteria activities produce calcite. Isotropically consolidated undrained compression tests also showed that there was increase in the cohesion values. Scanning electron

micrographs along with x-ray compositional mapping revealed that the cement bonding at particle contacts was calcite. A similar observation was found by Joshi et al. (1995).

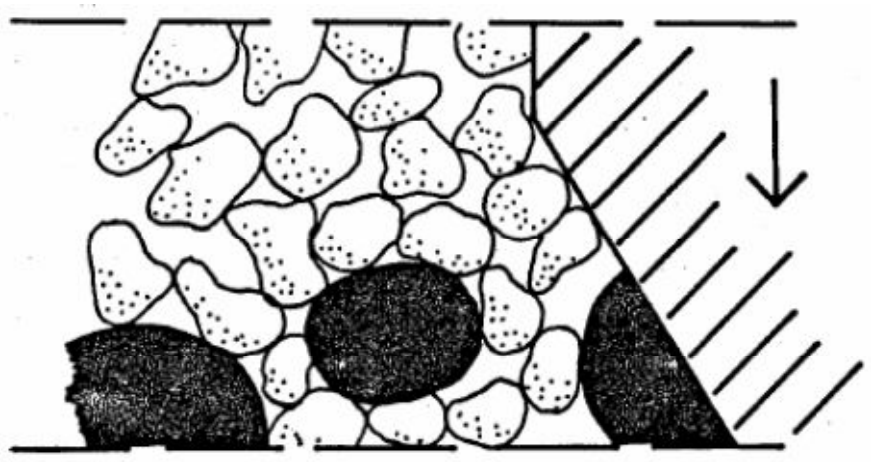

Figure 2-15 Blast-gas bubble producing arching of particles and loose sand pockets (adapted from Hryciw, 1986)

2.3 Creep

2.3.1 General

Soil exhibits creep behavior, in which the deformation of soil develops with time under constant mean effective stress. Creep can occur under anisotropic or isotropic condition. Creep under anisotropic condition (shear creep) exhibit initial shear stress due to the difference between major principal stress and minor principal stress, called stress ratio (R). While creep under isotropic condition practically exhibit no shear stress or very small shear stress as stress ratio equal to one.

Figure 2-16 illustrates the definition of shear creep (Augustesen *et al.*, 2004). When a soil is sheared up to point A (Figure 2-16 (a)), a creep process is commenced when the stress is kept constant (Figure 2-16 (b)). As the time passes, the strain is gradually increasing from A to B (Figure 2-16 (c)).Shear

creep can be classified into three stages: primary creep, secondary creep and tertiary creep (Augustesen *et al.*, 2004; Wang *et al.*, 2014). Primary creep is characterized by decreasing shear strain rate with time. A constant, minimum strain rate defines secondary creep. Tertiary creep is characterized by increasing shear strain rate. Figure 2-17 visualizes the three categories of shear creep.

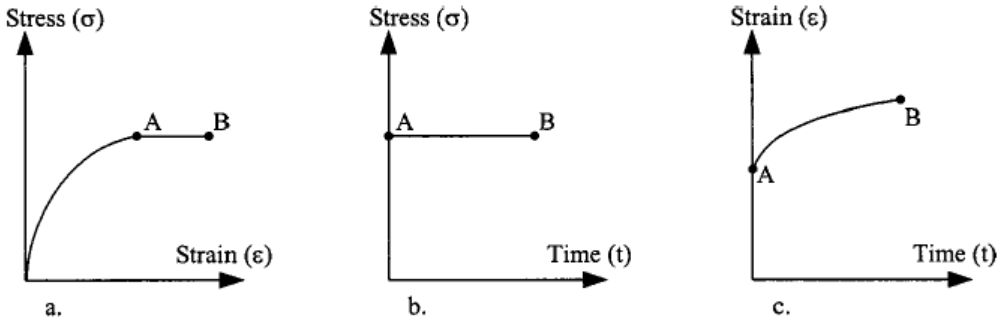

Figure 2-16 Definition of creep (Augustesen *et al.*, 2004)

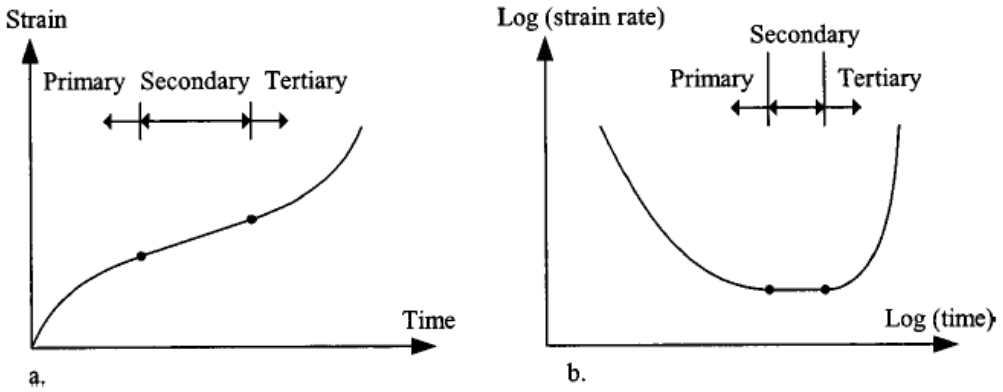

Figure 2-17 Creep classification (Augustesen *et al.*, 2004)

Most of the previous studies on creep induced aging effects on stiffness have been carried out under isotropic condition (Howie *et al.*, 2002). Previous studies also reported that creep under isotropic condition tends to be less than that under anisotropic condition(e.g. Lam, 2003; Shozen, 2001). Despite the fact that previous creep studies have been performed both under anisotropic and isotropic condition, to the author knowledge there has been very limited creep studies, if none, following K_0 condition.

2.3.2 Observation of Creep from Experimental Tests

This sub-section explains observations of creep from laboratory tests i.e. triaxial tests and oedometer.

The dependency of the creep behavior on the applied stress level is an important issue for the triaxial creep behavior of sand. For loose sand, the creep rate increases with the deviatoric stress in triaxial creep tests (di Prisco & Imposimato, 1996). For dense sand, the dependency is more complicated than that for loose sand. In one dimensional creep tests of sand at low stress levels, it was found that the creep rate of sand increases with the stress level (Mejia *et al.*, 1988; Zhang *et al.*, 2006) and the angularity of sand grains (Mejia *et al.*, 1988). At high stress levels, the creep deformation of sand is accompanied with grain crushing and the amount of crushed grains increases with time (Leung et al., 1996).

Based on observation from oedometer and triaxial tests, Tatsuoka *et al.* (2000) categorized post creep of soils (aging behavior) behavior into three types (Figure 2-18):

- Type 1, aging without structuration: The stress–strain relationship after aging rejoins the original primary loading relationship without exhibiting overshooting (B to C)

- Type 2, temporary structuration effects: The stress–strain relationship after aging rejoins the original primary loading relationship after having exhibited a temporary overshooting (B to D). It appears this type of behavior corresponds to the observed behavior of sand.

- Type 3, persistent structuration effects: The stress–strain relationship after aging does not rejoin the original primary loading relationship. There is a persistent overshooting with noticeably larger peak strength than that obtained by the original primary loading (B to E).

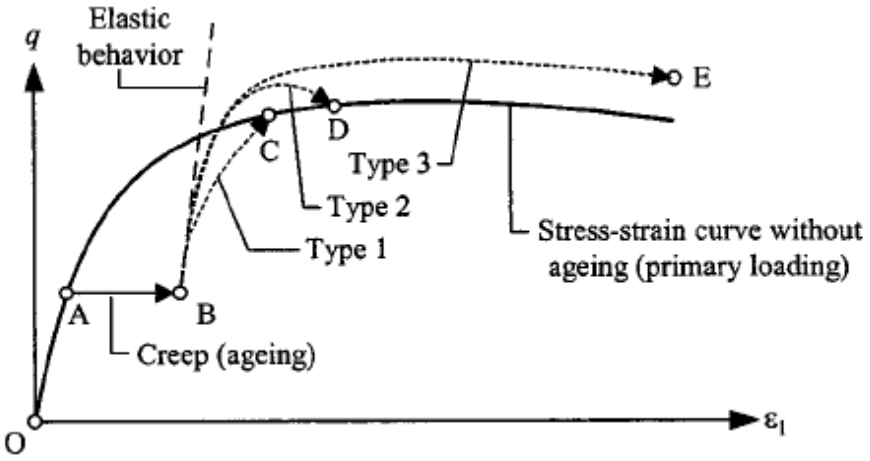

Figure 2-18 Typical post-aging stress-strain relationship (Tatsuoka *et al.*, 2000)

2.3.3 Creep Induced Aging Observed in Numerical Simulations

Creep causes change in the microstructure of sandy soil that changes the macro-mechanical behavior of the soil. Direct examinations of microstructure change during creep have been very limited (e.g. Bowman and Soga, 2002) with most of the observation coming indirectly from numerical modelling as described below.

2.3.3.1 Change of distribution of particle contact during creep

Suarez et al. (2009a) performed 2D and 3D discrete element model simulations on aging of granular material using OVAL software written by Dr Matthew Kuhn of the University of Portland. The numerical simulation results show a small increase in the small strain stiffness and dilatancy of the material. The increases in stiffness and dilatancy occurred with void ratio slightly decreased by 0.7% in 2D and 0.2% in 3D simulations. Figure 2-19 also shows an increase of about 30% in the number of inter-particle contacts and the development of stronger force chains during aging. These inter-particle effects might account for the changes in soil properties observed after aging. Translations of particles observed less than 50μm in 2D arrangement compared

to less than 30μm in 3D arrangement. In addition, particle rotation of less than 0.5^0 was observed. As the model was not calibrated and the aging mechanism was artificially induced, the magnitudes of change reported above only illustrate the general behavior. The authors also used X-ray computed tomography (e.g. Vlahinić *et al.*, 2014) and image analysis to detect any possible rearrangement of air pluviated sand (diameter 0.85-2mm) subjected to constant effective stress (62 kPa for 7 days) and restrained lateral strain (K_0 condition). However they did not find any conclusive particle rearrangement. One possible explanation is because the ratio of the diameter of specimen container (1 cm) to the ratio of the sand grains is smaller than the desired to prevent boundary effects. In addition, the authors stated that the sand grain diameters were selected due to better image quality at that ranges. This implies one limitation, to some degree, of X-ray computed tomography used in their study.

Discrete element simulation was also performed by Wang et.al (2008) using Particle Flow Code (PFC) and PFC3D (Itasca Consulting Group, Inc., Minn). They conducted three biaxial tests each on dense and loose samples: a sample with no aging, a sample aged until there was a 1.7% decrease in porosity due to creep, and a fresh sample with the aged sample's porosity. Following isotropic confinement at 400 kPa, creep stage under isotropic condition was performed under the same stress. They found higher strength and stiffness in aged samples than fresh samples. Contact stresses had a smaller standard deviation in aged samples, suggesting that aging redistributes contact stresses.

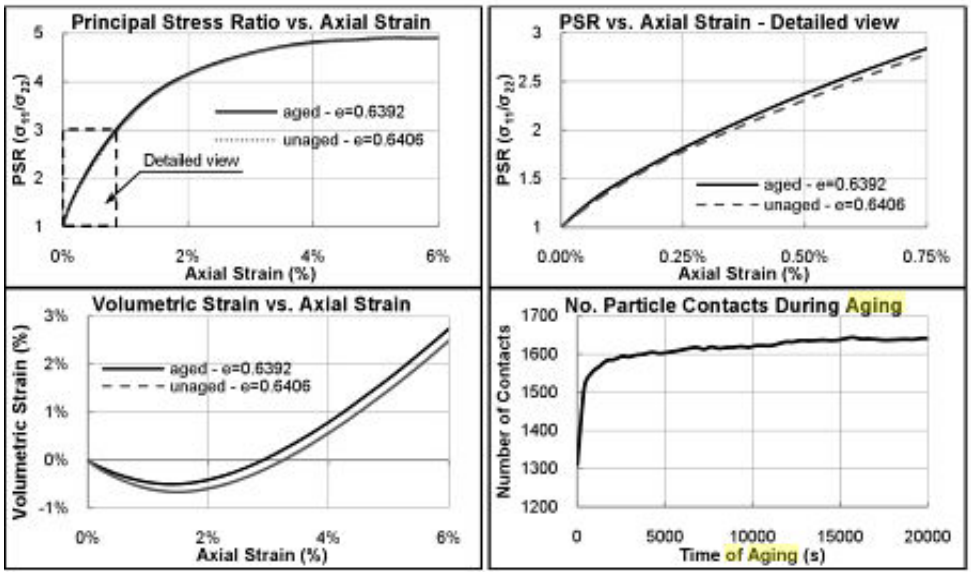

Figure 2-19 Aging modelling (Suarez et al, 2009)

2.3.3.2 Evolution of pore space during creep

Kang et al (2012) examined the evolution of pore space in dense sand and loose samples during biaxial creep. The irregularly shaped pore geometry in the soil packing was quantified using with a best fit ellipse.

Particle Flow Code (PFC) was used to simulate four different creep tests at different deviatoric stresses, q: two loose samples i.e. sample A ($R=\sigma_1'/\sigma_3' \approx 1.84$) and B ($R \approx 1.97$) and two dense samples i.e. sample C ($R \approx 0.9$) and D ($R \approx 2.47$). The simulation reasonably reproduces laboratory observations from triaxial creep tests (e.g. Lade & Liu, 1998; Mejia *et al.*, 1988; Murayama *et al.*, 1984). Creep causes more contraction in loose samples and less dilation in dense samples when compared with the response of the sample without creep. Moreover, the creep rate continuously decreases with time and increases with increasing deviatoric stress applied during creep, unless creep rupture occurs.

Figure 2-20 presents the pore size distribution curves (loose sample A and dense sample D) at a selected axial strain region. The equivalent diameter of pores that are enclosed by unique numbers of enclosing particles N corresponds to each hill of curves denoted by the vertical solid lines. As creep proceeds, the

pore volume of N=3 and 4 cases increase whereas those of N>5 decrease. As the strain increases, the inset pictures in Figure 2-20(a) shows that the equivalent diameter gradually decreases, whilst the average coordination number increases (Figure 2-21). This suggests that the pores enclosed by a large number of particles begin to collapse forming the small pores. In contrast, the pore spaces of the dense sample D merge so the equivalent diameter increases as axial strain increases (Figure 2-20(b)). This observation corresponds to the dilation response of dense samples and decrease in the average coordination number (Figure 2-21).

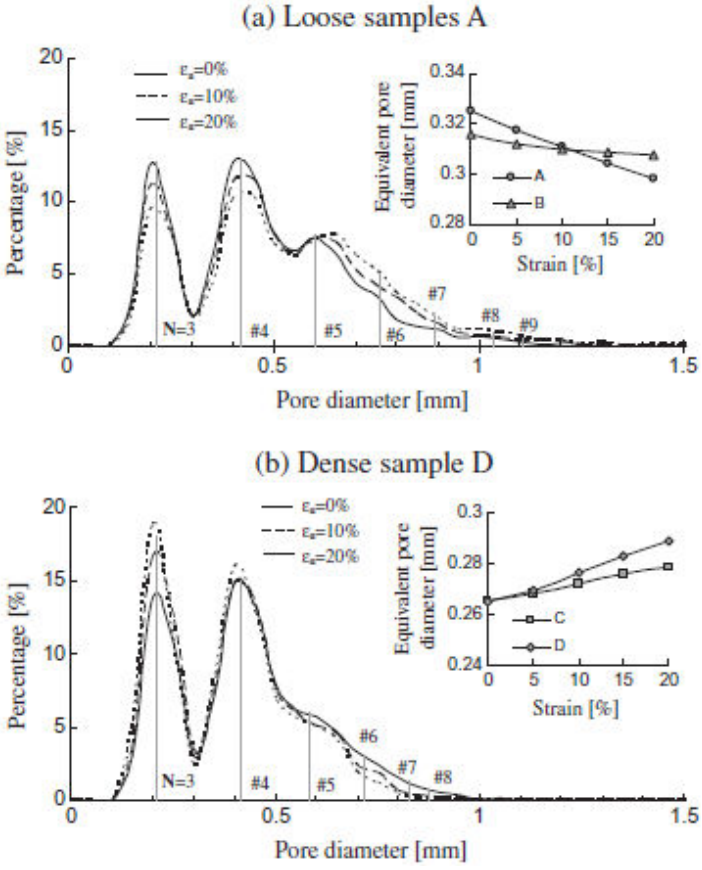

Figure 2-20 Pore size distribution (Kang, 2012)

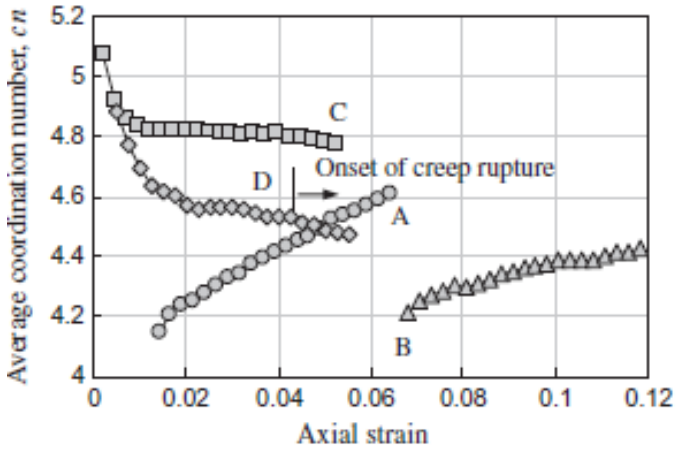

Figure 2-21 Evolution of average coordination number during creep (Kang, 2012)

Figure 2-22 illustrates above the scenario where the displacement of particles and evolution of pore spaces in samples A and D during creep were shown (Note: stage 0 = start of creep; stage 20 = end of creep). As creep proceeds, the large pores tend to split into small pores in the loose sample resulting in a contractive response while small pores are merged together to form large pores in the dense sample. The authors concluded that the pore split or union is a basic mechanism that determines unique pore characteristics for loose and dense samples, respectively, subjected to creep.

It was also noted that during creep, the pore orientation changed during the process of pore split and enlargement as revealed by the rose diagram in Figure 2-23. It can be seen that for sample A the uniformly oriented unit pore became vertically elongated (i.e. in the major principal stress direction) as creep proceeded. For sample B where creep starts at a higher stress ratio, the vertical orientation of pores is more pronounced before the creep starts and horizontal directivity became weaker than the sample A during creep. The dense samples C and D generally exhibited prominent development of vertical pores with creep. In all samples creep process finally led to more homogenised pore characteristic that exhibit similar orientation (preferred in the vertical direction) in the soil packing. The pores eventually have elongated perpendicular to the direction of loading collapse and those pores elongated along the axial loading direction

remained and then dominated during creep. Hence, a more stable particle arching elongated along the loading direction is gradually produced, which in turn decreases the overall creep rate and strengthens the soil properties. It was also observed that creep rupture does not result in major change in pore orientation while the inter-particle coordination number keeps decreasing.

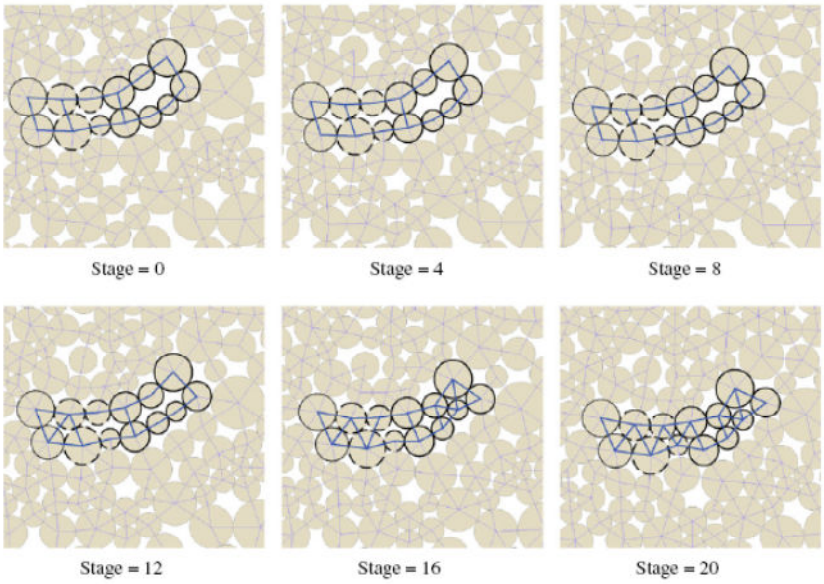

(a)

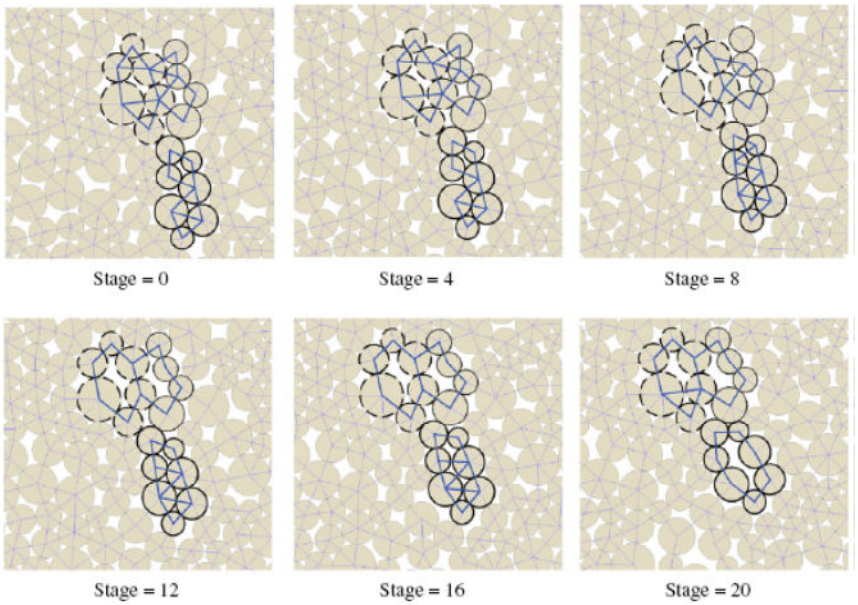

(b)

Figure 2-22 Evolution of pore space during creep (a) loose (b) dense

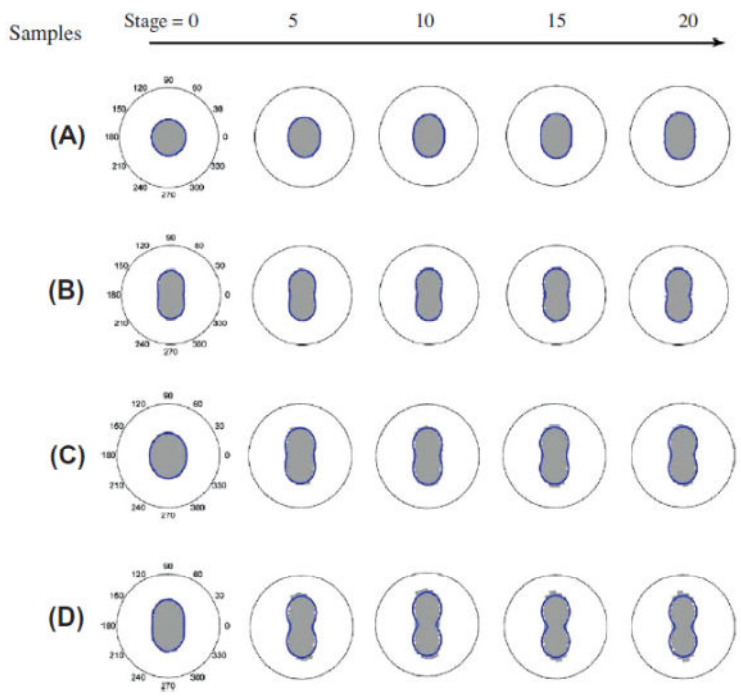

Figure 2-23 Change in pore orientation during creep (Kang et al, 2012)

2.4 Summary

Some key points from the literature review are:

- Sand aging has beneficial practical significance.
- Majority of *laboratory research* on soil aging and creep have examined clean sand, very little studies have been performed on silty sand.
- Few studies have been carried out on the effect of aging on triaxial monotonic undrained behavior
- Limited studies have been carried out on the effect of aging on triaxial one way cyclic undrained behavior.
- No direct observation has been attempted to link change in microstructure during aging to change in macro-mechanical behavior of silty sands.

3 Materials and Methods

3.1 Introduction

This chapter describes the material properties and outlines the procedures to investigate the effects that drained creep and aging have on macro-mechanical behavior particularly at small strains and for the microstructure of the material used in this study. These procedures include triaxial testing, both monotonic and cyclic, and one dimensional fabric testing. This chapter also describes some development to the existing triaxial apparatus.

3.2 Materials

3.2.1 Index properties

The materials used in this research program were reconstituted in the laboratory by mixing sand fraction and fine fraction (<0.075mm). It was decided to choose materials which are locally available to the Geomechanics Laboratory. It was decided to use the ejected sand fraction collected from Rydal Reserve Christchurch-New Zealand, one of the liquefied sites during Darfield's earthquake in 2010 (Canterbury, 2012). Natural Rydal Reserve material is a non-plastic silty sand with fines content of 15% with sand particle diameters ranging from 0.3mm to 0.075mm. The coefficient of uniformity C_u of the sand fraction only is 2.1 and the mean grain size D_{50} is 0.19mm (fine sand). Rydal Reserve's sand fraction is defined as poorly graded sand according to Unified Soil Classification System. The maximum and minimum void ratios, e_{max} and e_{min} are 1.026 and 0.645, respectively. It was thought that using a different colour of sand (grey) and fines (white) could help the quantification of microstructure of the silty sand during fabric testing. Thus the fines fraction from Rydal Reserve was replaced by fines fraction from silica flour 100, which was available in the Geomechanics Laboratory. This is non-plastic silt that passes no #200 sieve. Mineral composition of the silt is 99.8% of SiO_2 (see Appendix A). It was decided later to remove the particles sizes smaller than

0.032mm by wet sieving because of the difficulties in image analysis with very small grains. Thus final mean grain of size of silt is 0.042mm (coarse silt). The separate grain size distribution for sand fraction and silt are shown by Figure 3-1.

Figure 3-2 shows the grain size distribution of the sand-fines mixture used in this study. The combined material has a mean grain size D_{50} of 0.175, coefficient of uniformity C_u of 4.1 and coefficient of curvature C_c of 1.4. The mixture has specific gravity G_s of 2.64, and maximum and minimum void ratios e_{max} and e_{min} are 0.973 and 0.565, respectively.

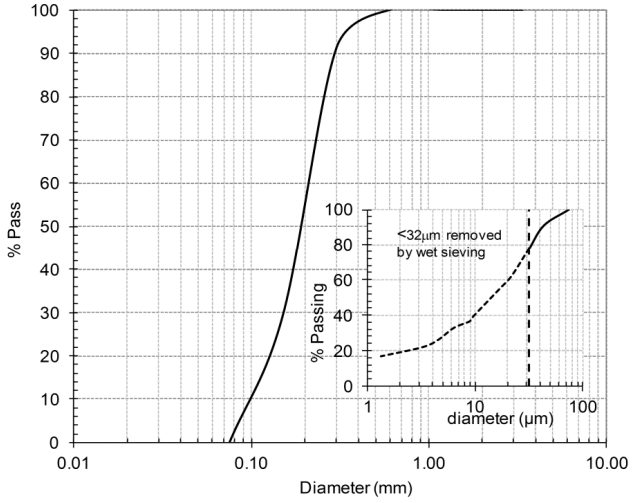

Figure 3-1 Grain size distribution of sand and silt fraction (inset)

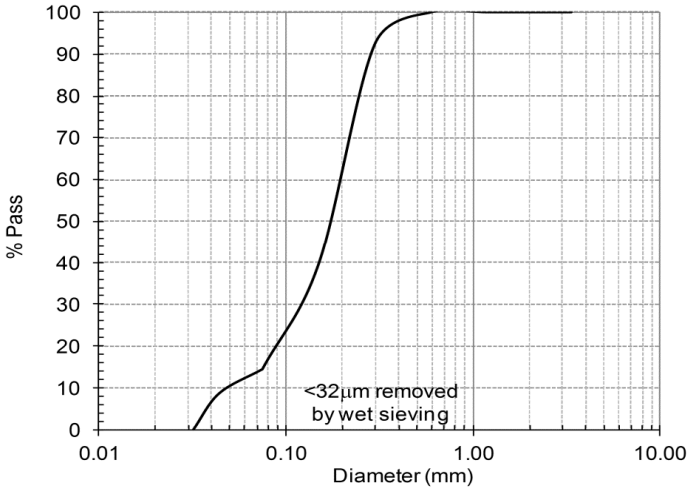

Figure 3-2 Grain size distribution of the sand-silt mixture used in this study

3.2.2 Particle shape and mineralogy

The scanning electron microscope (SEM) is an electron microscope that images the sample surface by scanning it with a high-energy beam of electrons in a raster scan pattern. The electrons interact with the atoms that make up the sample, producing signals that contain information about the sample's surface topography, composition and other properties such as electrical conductivity. Figure 3-3 shows a high resolution field emission, JEOL JSM 7000F scanning electron microscope at the Mechanical Engineering Department which was used for obtaining SEM images.

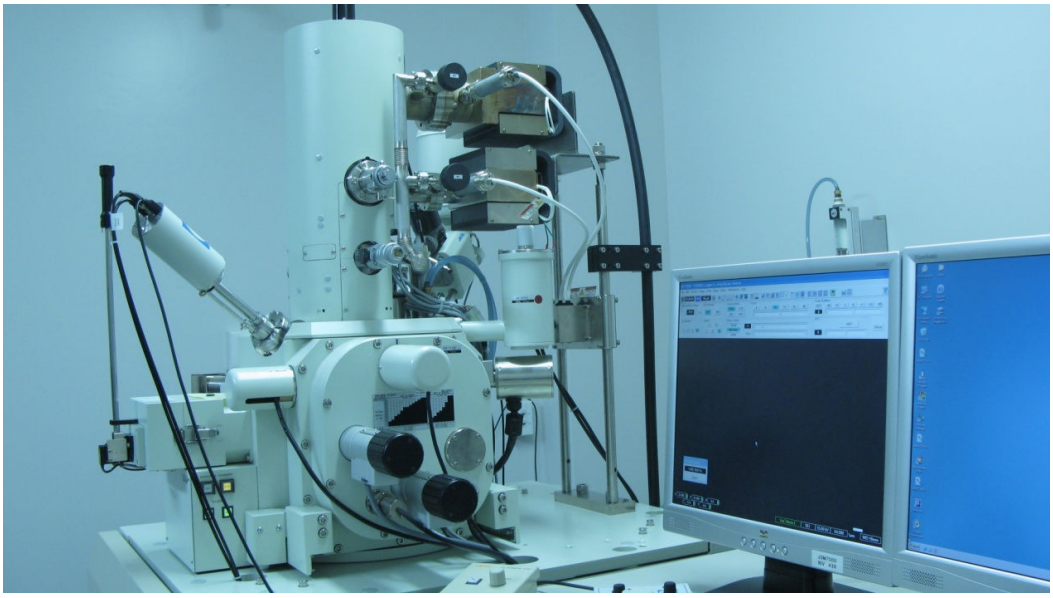

Figure 3-3 Scanning Electron Microscope

3.2.2.1 Particle shape

Micro-photographs of the material are shown in Figure 3-4 and Figure 3-5. It can be seen that visually the shape of the particles is *angular to sub-angular*. Based on the micro-photographs, which were converted into binary images, quantification of about 950 grains gives an average roundness (R) of 0.53 and sphericity (S) of 0.43. Roundness refers to the sharpness of the corners and edges of a grain. Roundness is defined as the ratio of the average radius of the curvature of the corners to the radius of the largest inscribed circle (Wadell, 1932). Sphericity

measures the degree to which a particle approaches a spherical shape. Sphericity is defined as the ratio between the diameter of a sphere with the same volume as the particle and the diameter of the circumscribed particles (Krumbein, 1941). All the shape descriptors above are automatically determined using *ImageJ* software. Based on the particle regularity , ρ, defined as (R+S)/2, (Cho *et al.*, 2006), the average ρ is 0.48 and this falls also into the *angular to sub-angular* category as classified below

ρ=0.75-0.9 rounded to sub rounded

ρ=0.65-0.75 sub rounded to sub angular

ρ=0.40-0.65 angular to sub angular

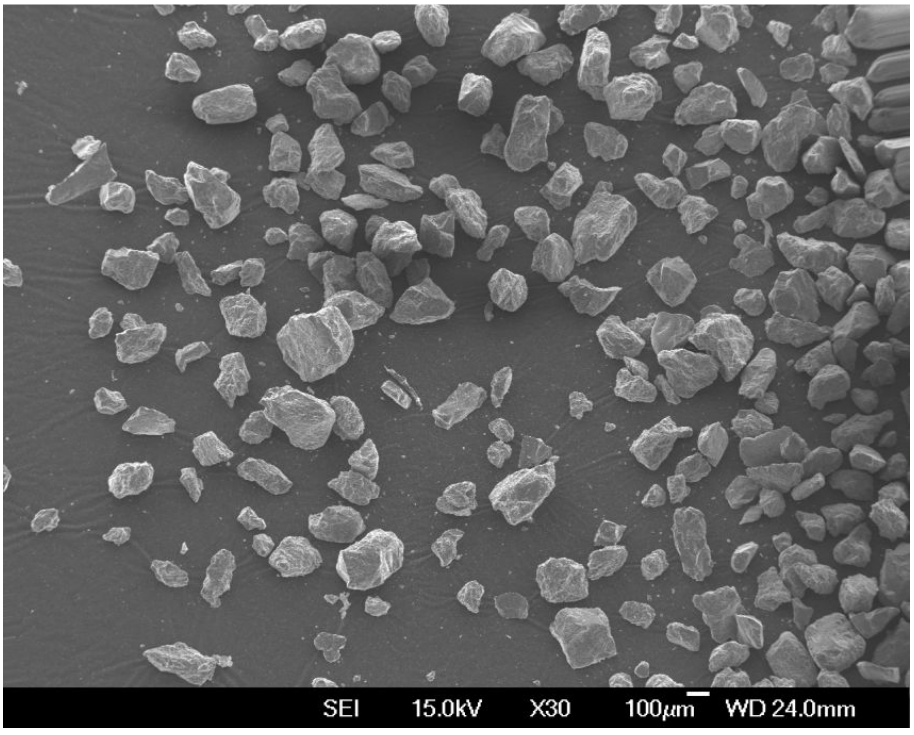

Figure 3-4 Microphotograph of sand used in this study

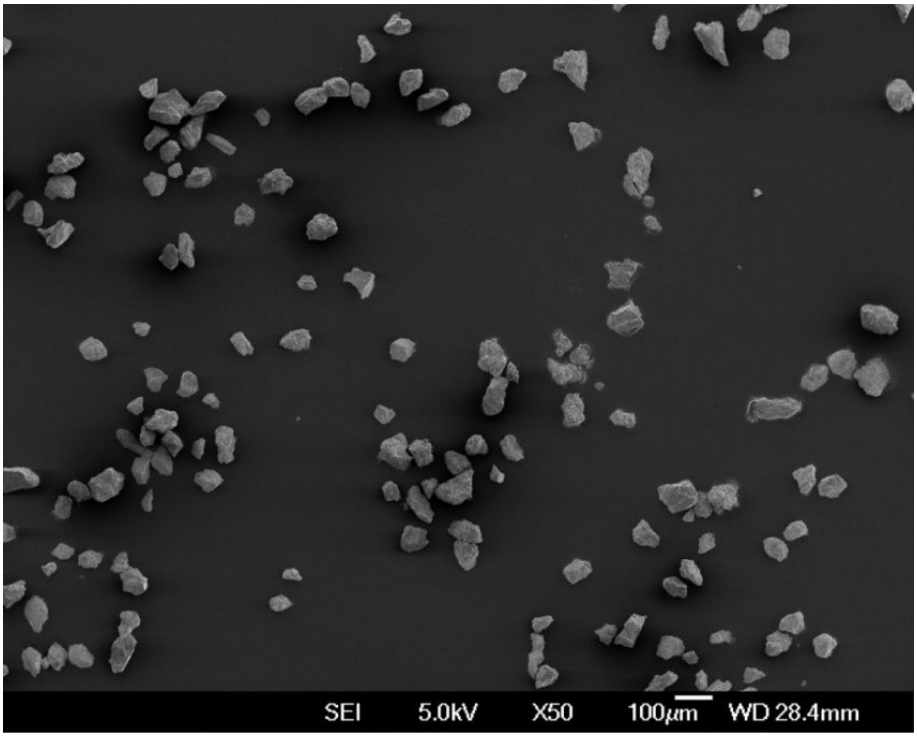

Figure 3-5 Microphotograph of silt used in this study

3.2.2.2 Mineralogy

SEM offers advantages that it can take photographs and analyze mineralogy of the material surface simultaneously. Two spectrums were taken and the percentage of the element by atomic weight is shown in Figure 3-7. It can be seen from Figure 3-6 that the material predominantly consisted of oxygen and silicon with average percentage of 49.6% and 37.9% respectively. Some aluminium and atrium was also found with average percentage of 6.5% and 1.9%. The mineralogical analysis shows some trace of organic matter (C, carbon based material) but the percentage is insignificant thus not shown in the figure. Therefore it can be expected that no chemical reactions occur during sample preparation and testing. This implies that aging mechanism in this study is mainly mechanical and not affected by chemical reaction.

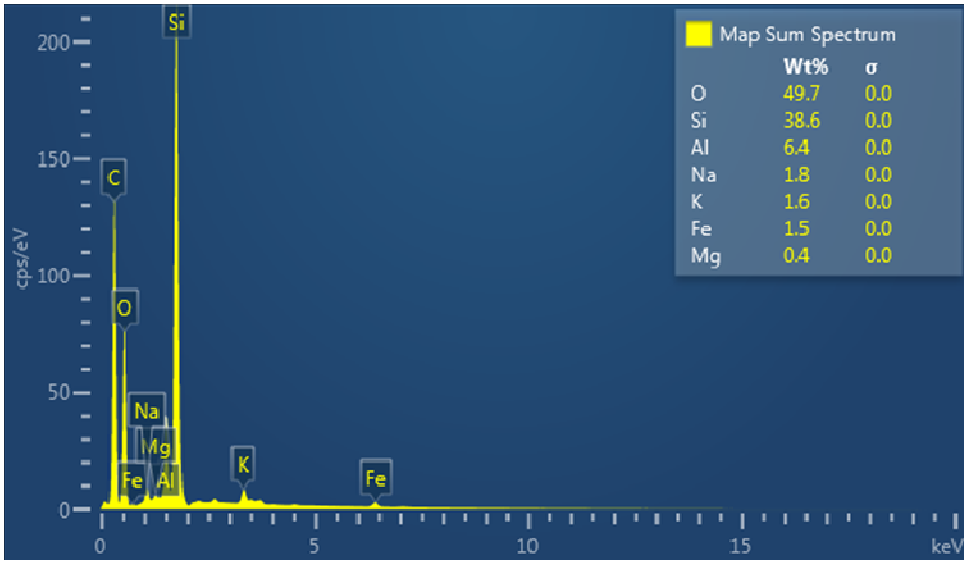

(a) spectrum-1

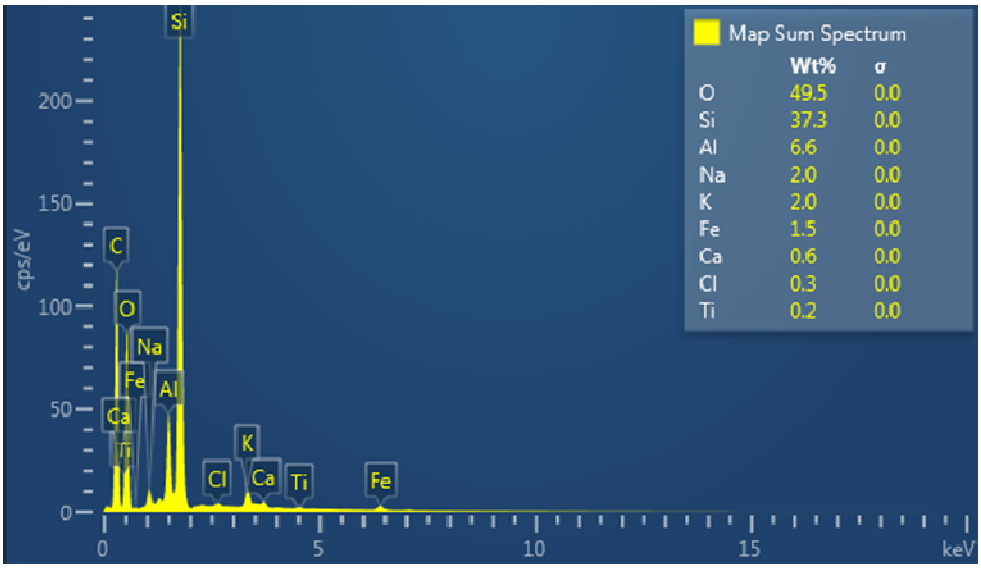

(b) Spectrum-2

Figure 3-6 Analytical spectrums of the material in this study

3.3 Experimental Method - Triaxial Tests

In this research, the general requirements of a triaxial testing system are:

- The stress and strain distributions inside the sample are sufficiently uniform so that the sample response represents "element" behavior
- Able to control cell pressure and axial load independently and precisely in particular to allow K_0 consolidation.
- Able to independently measure radial strain accurately during creep.
- Relatively stable stress measurement during creep especially for one week period.
- Able to measure axial strain accurately, free from bedding errors, and particularly over small strain range which is the main focus in this research.

To meet the research requirements of this project, a number of additional development to the existing apparatus and procedure were introduced, in particular the use of two local axial transducers and one radial local transducer (section 3.3.1.4 and 3.3.1.5) and a new separate data logging acquisition system of all local Linear Variable Differential Transformer (LVDT) transducers (i.e. 100 sample data per second).

3.3.1 Apparatus

The triaxial testing system employed for this study is schematically shown in Figure 3-7. A Perspex cylinder with top and bottom plate was used as the cell, so that a cylindrical sample (50mm in diameter and 100mm in height) and local (on specimen) transducers can be placed inside the cell. The cell was filled with de-aired water. Confining stress to the specimen was applied by water pressure. A Digital Pressure Volume Controller (DPVC) was used to apply/control cell pressure. The top and bottom platens of the specimen were connected to a second DPVC to control pore water pressure/volume inside the sample.

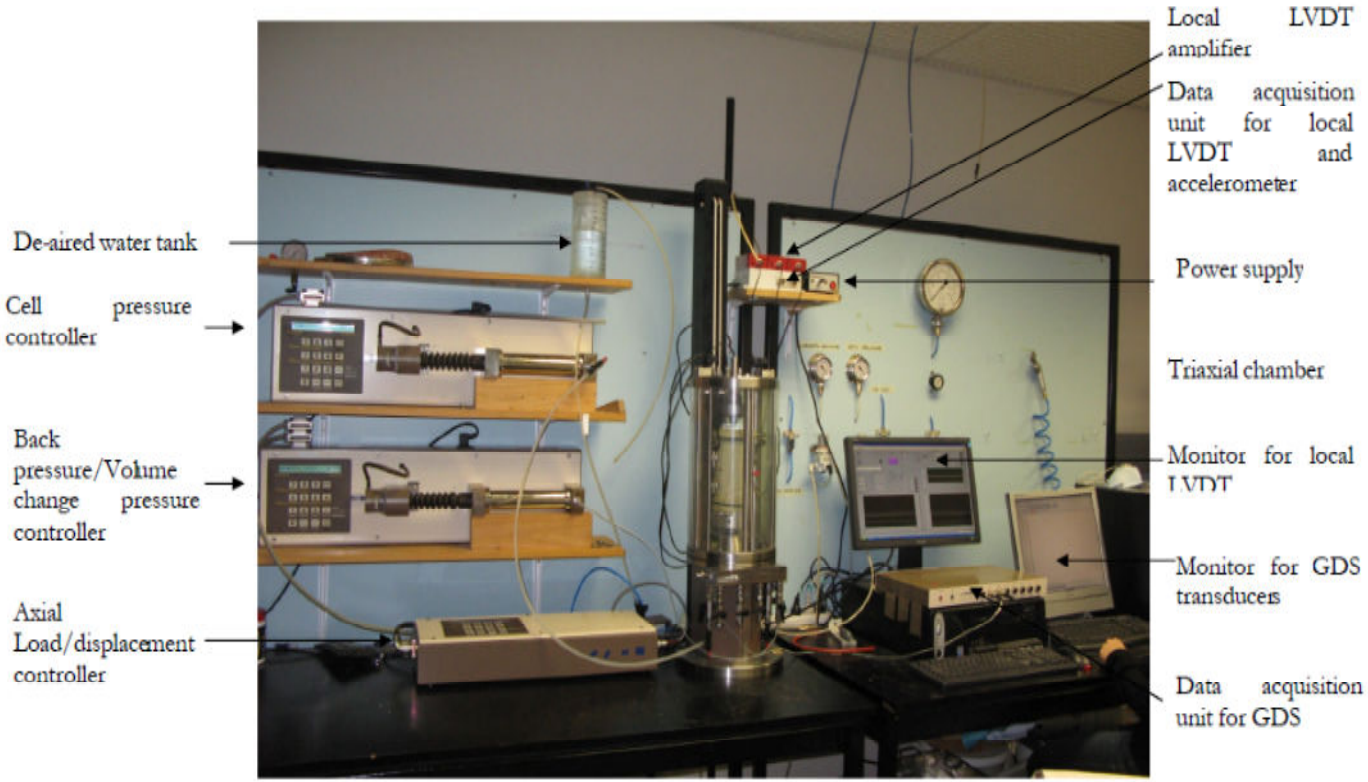

Figure 3-7 Overview of triaxial testing system

A force actuator controlled by a Geotechnical Digital System (GDS) digital controller was used to apply load to the bottom of the specimen. Therefore, the bottom platen was the moving platen and "free" movement was facilitated by a linear roller bearing. A submersible load cell located just above the top platen, i.e. between the top platen and the shaft, was used to record the axial force.

3.3.1.1 Axial force

The applied load on the sample was recorded by a submersible load cell (2kN capacity) positioned above the top platen of the specimen inside the Perspex cylinder so that the recorded data was unaffected by any inevitable frictional forces. The load cell is manufactured by GDS with an accuracy of ±0.1% of total capacity i.e. ±2N. Thus for a sample with diameter of 50mm the accuracy is within 1kPa.

3.3.1.2 Cell Pressure

The cell pressure was applied by water pressure using de-aired water by a GDS Digital Pressure Volume Controller (DPVC). A DPVC is a microprocessor controlled linear actuator for precise regulation and measurement of liquid pressure and liquid volume change. It can be directly connected to a computer for computer control via a General Purpose Interface Bus (GPIB).

The principle of DPVC in soil testing is illustrated in Figure 3-8 and detailed description is given in the GDS Handbook (2000). The DPVC consists of a pressure cylinder which is filled with de-aired water. De-aired water is pressurized by a piston moving inside the cylinder and the applied pressure is displayed via a Liquid Crystal Display (LCD). The piston is activated by a ball screw turned in a captive ball nut by a stepping motor and gearbox that move rectilinearly on a ball slide. The pressure inside the cylinder is detected by means of an integral pressure transducer. Control algorithms are built into the programmable memory to cause the motor to seek to a target pressure or step to a target volume change. The latter is achieved by counting the steps of the stepping motor.

The DPVC used for cell pressure had a maximum operational loading capacity of 2000kPa and a volume change capacity is 200 cc. The resolution of DPVC was 1kPa for pressure and 1 cu mm for volume change.

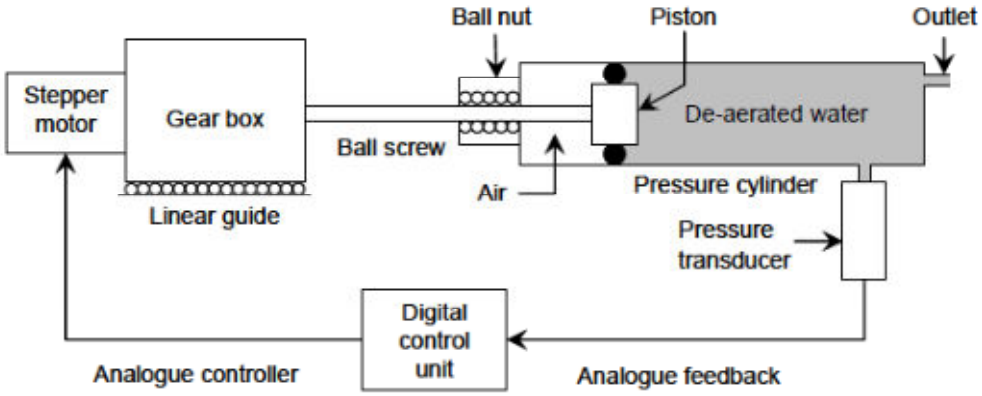

Figure 3-8 Schematic diagram of digital volume change controller (GDS Handbook, 2000)

3.3.1.3 Pore Water Pressure and Volume Change

The pore water pressure and the volume change of the soil specimen were monitored and controlled by another 200cc volume change capacity DPVC connected to both top and bottom drainage lines. The role of this DPVC depended on the testing conditions. Thus, in drained testing the DPVC was used to measure the volume change and controlled (kept constant) the pore water pressure. In undrained testing, it controlled (kept constant) the volume change and measured the pore water pressure. It can switch from one mode to another via computer control and therefore enables the shearing condition to switch smoothly from a drained condition to undrained condition during testing.

A pressure transducer was connected to the top platen of the specimen to have an alternative data source to cross check data from DPVC and to check pore water pressure uniformity (equilibrium) inside the sample.

3.3.1.4 Axial deformation

To properly understand the behavior of the soil during creep and its effect on undrained shear, a continuous and fast logging system is needed. External measurements are believed to be inadequate due to factors such as low resolution, seating errors, bedding errors (Baldi *et al*, 1988). Thus in addition to external measurements, on-specimen local LVDTs are required for accurate creep measurement and stiffness calculation particularly at small-strain values which are focus of this study.

Thus axial deformation of the sample was monitored by one external LVDT and two local/on-specimen LVDTs. The linear range of the local LVDT is ±5mm. LVDT are placed diametrically opposed and mounted on the specimen through the axial pads. Local axial strains are calculated as the average from both local LVDTs.

The axial pads (see Figure 3-9) that held the LVDT and reaction plate were redesigned and made so they were thicker in order to accommodate the use of enlarged platens. Based on some trials, the gauge length rod was also redesigned and remade so it has a niche thus making it easier to screw it to the axial pad

Initially the axial pads were pinned to the specimen but then this was discarded due to a leaking problem. Thus the axial pads were glued using instant contact adhesive i.e. *loctite* glue.

3.3.1.5 Radial deformation

Although for undrained shear, radial measurement is theoretically not significant (due to zero volumetric strain), direct measurement of radial change is important for measuring deformation during creep. Therefore radial deformation of the sample was monitored by local radial LVDT through an in-house made radial calliper, adapted from Bishop (1962). The radial LVDT has linear range ± 5mm thus the maximum radial strain is about 10% (for 50mm sample diameter). The calliper was mounted on the test specimen by means of two diametrically opposed

pads bonded to the membrane by *loctite* glue. The LVDT was positioned across the opening of the calliper where it measured the opening and closing of the jaws. The measurement position of the radial LVDT was the same distance from the centre of the positioning pads as they were from the hinge. Therefore the radial LVDT measurement was twice the equivalent change in specimen diameter.

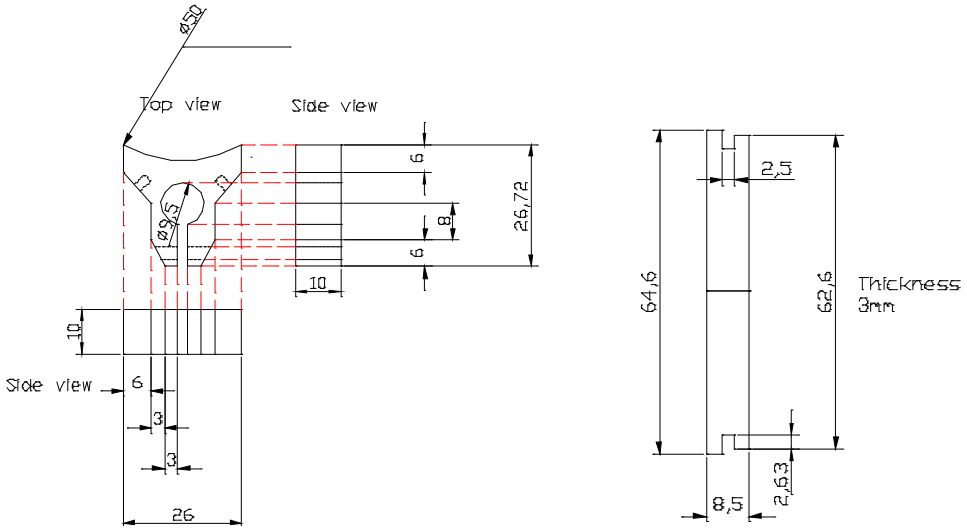

Figure 3-9 'In house' axial LVDT pads (a) and gauge length (b)

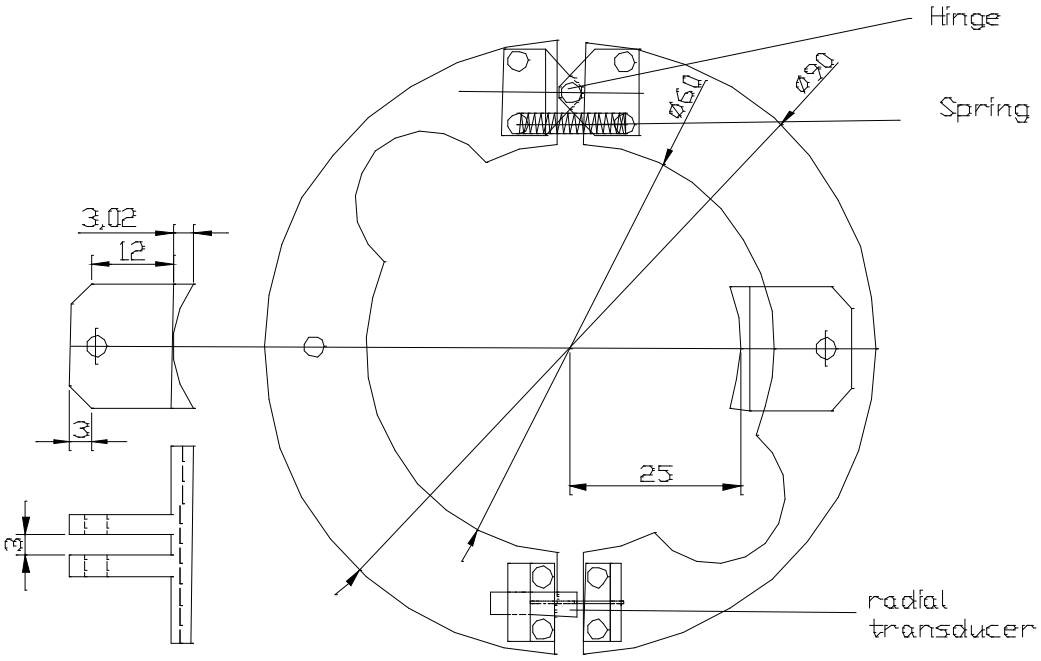

Figure 3-10 'In house' radial belt

3.3.2 Development of Local LVDT data logging system

Difficulties arose during the development of small strain measurement which attempted to utilize existing available local LVDTs. The difficulties were due to signal conditioning problem of the available submersible LVDTs (RDP type D5/200WRA/933) with the existing GDS data acquisition unit. The supply voltage of the 8 channels of GDS serial data acquisition unit is at ±5 Volt whereas the LVDTs supply voltage is at ±10 Volt. An effort was made by Mr John Koolos, laboratory technician, to utilize the LVDT with existing GDS data acquisition but it was unsuccessful. It was decided then to log the measurement of local LVDT by an 'in house' separate data acquisition unit.

Based on Shozen (2001) the magnitude of axial strain during aging was expected to be in the order of 0.1% thus the local LVDT needed to be able to read less than 0.01%. This strain is equal to a resolution of about 0.0065mm (the gauge length between the upper axial pad and lower axial pad being about 65 mm). The minimum required analogue to digital converter (ADC) bit resolution is calculated from Equation 3-1 below

$$ADC\ bit\ Resolution(n) = \frac{\log\left(\frac{V_D x E}{R x V_s}\right)}{\log(2)} + B \qquad \textbf{Eq. 3-1}$$

Where

V_d=full scale input voltage range (from amplifier if used) = 10V

V_d=full scale output voltage range =20V

R=resolution required in engineering units

E=engineering unit represented by Vs=10mm

n= bit resolution of the ADC

B=1 if bipolar range, 0 if unipolar; B=1 for this case

Thus

$$ADC\ bit\ Resolution(n) = \frac{\log\left(\frac{20x10}{0.0065x10}\right)}{\log(2)} + 1 \approx 13$$

It was decided to use ADC resolution of 14 bits. Back calculated from above equation the resolution is 0.00061mm which is equivalent to 0.00094% of strain. Because of other considerations, however, such as environmental noise (cell phones particularly introduce radio frequency noise) as well as noise within the signal conditioning system, this theoretical resolution is rarely attainable.

In addition to three local LVDT channels, accelerometers that measure acceleration in x, y, and z direction were installed to record any vibration in anticipation of aftershocks caused by the Canterbury earthquakes. A temperature sensor initially was planned to be installed into the data logging system but was not realized. Instead a USB temperature sensor connected to the PC was used to monitor the room temperature. Some complexity also was encountered during the software development for the data acquisition using LABVIEW^{TM} which eventually was solved. The whole development meant both hardware and software was finally ready to use at the end of February 2012. An overview of the local LVDT performance during creep and shear can be seen in Appendix B.

Another issue that arose was the research room temperature. It is generally well accepted that time dependent behavior of soils depends highly on temperature (Mitchell & Soga, 2005). Although this dependency is beyond the scope of the study it is deemed important to maintain the temperature during creep. The temperature control inside the Geomechanics research room did not work properly and continuously. This resulted in a high temperature variation (more than 5^0C) particularly between day and night, which affected, for example, the external volume change measurement, as illustrated in Figure 3-11. After some time, a temperature controlled room became available in the Environmental laboratory thus

the whole apparatus was moved into this laboratory. The temperature and humidity of the room were continuously controlled so the temperature variation is $\pm 0.5^0$C with the average temperature of 22^0C.

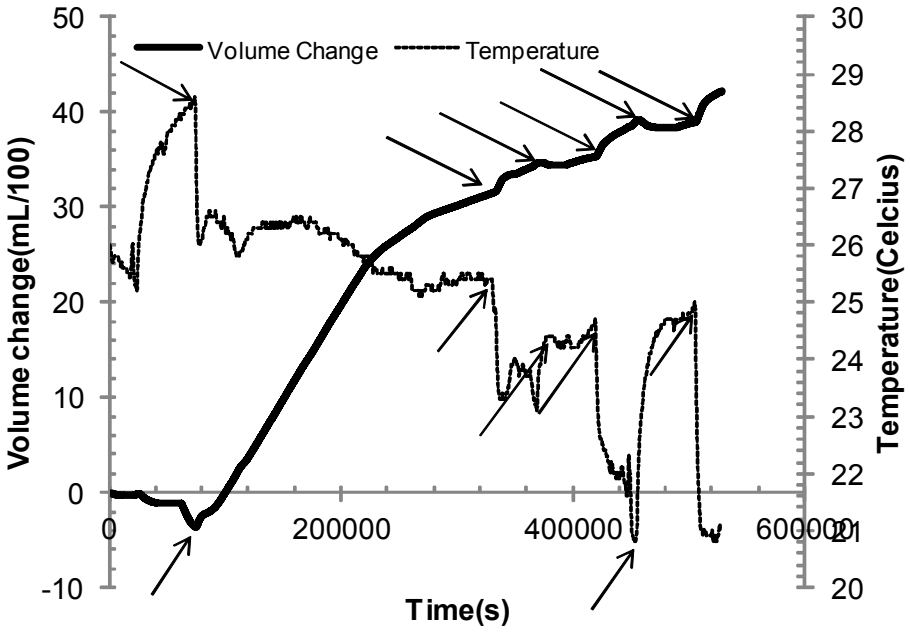

Figure 3-11 Temperature effect on volume change

3.3.3 Sample preparation

In order to avoid premature development of non-homogeneous deformation of the sample, some special techniques were employed such as enlarged platens, free ends, together with a moist tamping sample preparation method.

3.3.3.1 Enlarge platen with free ends

The frictional force at the contact between the end platen and the soil specimen is one of the reasons of premature development of non-homogeneous deformation during shearing. Therefore, Rowe and Barden (1964) and Lo (1985) proposed to use enlarged platens with free ends to reduce the frictional force and to delay the onset of non-homogeneous deformation significantly .

Initially, a pattern for the latex membrane (at the platens) was prepared by cutting a transparent sheet with a diameter slightly bigger than the sample diameter so that cutting the latex from this pattern would prepare a slightly larger end membrane than the sample diameter. This was done to ensure that soil particles would not come in contact directly with the platen at the periphery of the sample. One side of the membrane was lubricated with a thin film of high vacuum grease and placed on the enlarged platen. An enlarged platen was used to allow lateral expansion of soil during shearing. Air trapped between the membrane and platens, if any, was removed carefully.

3.3.3.2 Sample reconstitution

It was very difficult to mix sand with fines thoroughly at natural moisture content because fines form lumps even with a little moisture. The fines were first dried in an oven at 105^0c for 24 hours. The materials were then cooled down to room temperature in tightly sealed desiccators. Finally sand with fines was obtained by mixing the sand and fines in a dry state.

Several methods for preparing reconstituted samples in the laboratory have been reported in the literature. The choice of the sample preparation method depends on the objective of the study and achievability of testing requirements. The variation in achievable ranges of density based upon the sample preparation method greatly affects the deformational soil behavior. It is reported in the literature that different stress-strain responses can be found from different sample preparation methods, even at the same density (Ishihara, 1993; Vaid *et al.*, 1999). Therefore, it is most appropriate to compare soil behavior based on the same sample preparation method (Yamamuro & Covert, 2001). Considering the achievable range of densities required for this study (loose and dense), moist tamping, a method proposed by (Ladd, 1978), was mostly used in this study. For this method a predetermined amount of water (10%) was added to control the moisture content. Then the moist soil is put into the split mould, layer by layer (5 layers used in this study). For each layer the soil is then compacted to a specific height. Moist tamping produces a

consistent preparation method and avoids segregation problems (particularly for silty sand as used in this study). It is also found to give a good control over the global specimen density. While moist tamping does not replicate natural deposition, maintaining a consistent preparation method throughout testing ensured that all results were equally affected by the preparation method. Nevertheless, few samples were prepared later on by dry funnel pluviation (Bahadori *et al.*, 2008; Ishihara, 1993; Sitharam & Dash, 2008; Yamamuro & Wood, 2004). Dry funnel deposition involves deposition of dry material via a funnel into the bottom of a split mould. The material is placed in the funnel, which is raised along its axis of symmetry. The specimen's sedimentation was formed by placing the soil in a low energy state without any drop height. In order to achieve higher densities, the split mould can be tapped uniformly.

3.3.4 Sample set up

First, line marks were drawn on the rubber membrane to indicate the position for the local axial and radial pads. The specimen was reconstituted, confined inside the three split moulds along with the 'free end' enlarged base platen. The specimen was then locked at the base of the triaxial chamber. After that, the top cap including the plastic sleeve was slid carefully within the space between the top of the specimen and the extension cap which connects to the load cell. The specimen was moved so the top of the specimen just touched the top lubricated end membrane (e.g. load cell reading less than 0.002 kN). Drainage lines were then connected to the specimen. While targeting load cell to 0 kN, 15kPa of vacuum was applied to the top drainage line so the split mould could be removed. Local axial pads (i.e. top and bottom) including the gauge rods were then assembled for each side. These sets of local axial LVDTs were glued on the specimen by *instant loctite glue* at their positions. Care was taken such that the pair of local LVDTs was located diametrically so the radial belt could be installed with relative ease. Figure 3-12 shows the whole set up before the triaxial chamber was filled. After the chamber was filled the vacuum pressure on specimen was replaced by confining pressure, still targeting 0kN on the load cell. CO_2 was then percolated through the specimen

slowly enough (targeting 2-3 air bubbles/second) for about 1 hour in order to help the saturation process. Water was then percolated through the sample until no air bubbles were observed in the drainage line (about two hours in this study) and/or a minimal 1.5 times the volume of voids water was percolated. Some trials were performed to find the suitable different head between the de-aired water and glass container at the exit. It was decided that a head of about 0.3m was slow enough to prevent/minimize loss of fines during water percolation (collected water at the exit was relatively clear). The triaxial chamber was then filled with water. All the local LVDT readings and GDS controllers were then zeroed. To compensate the use of two separate data logging systems, both of them were started at the same time.

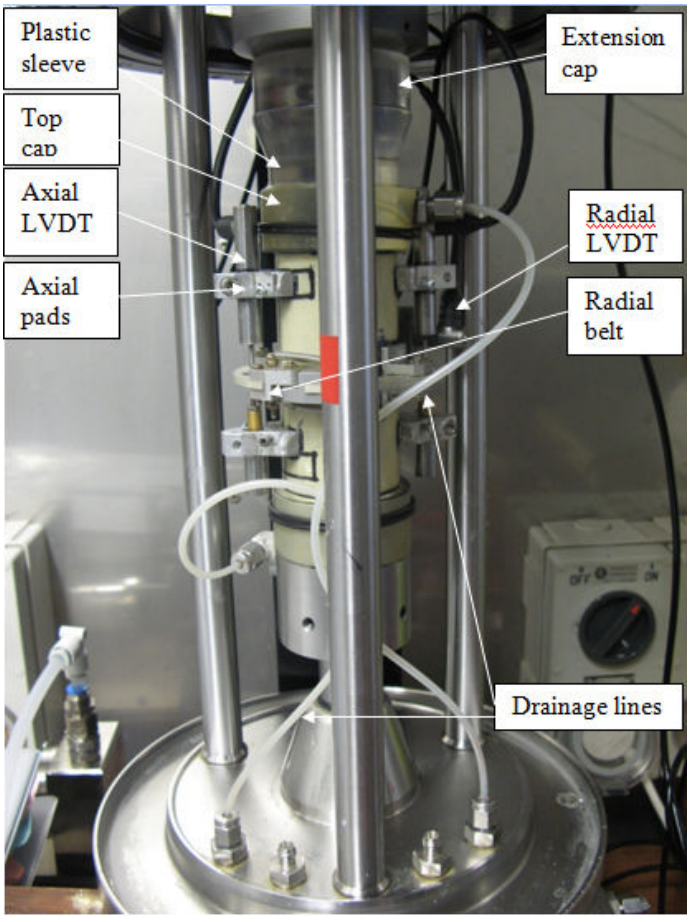

Figure 3-12 Specimen after set up inside the triaxial chamber

3.3.5 Saturation

The saturation was done by increasing the cell pressure and back pressure simultaneously while targeting 0kPa deviator stress. The B value was checked every 100kPa increment of back pressure. This is done using GDS Advance Loading Module. The final back pressure used in this study was 500kPa, as recommended by the GDS handbook (2000). The B value at this back pressure was found to be satisfactory i.e. ≥0.98. This relatively high back pressure was found later to be helpful during the K_0 consolidation.

3.3.6 Consolidation

The K_0 module program developed by GDS was used to perform K_0 consolidation. There are two methods to maintain zero lateral strain, either direct reading of the specimen diameter or using the volume change calculation. K_0 using direct reading is preferable; however the connection/splitter to tie the GDS data acquisition system and local data could not be made until the end of the study. Thus throughout this study K_0 consolidation were done based on volume change measurement. During K_0 consolidation, external axial displacement is adjusted slowly thus ensuring the diameter of the specimen remains constant, where the specimen diameter change is theoretically calculated from the back pressure volume change. The required inputs of this program module were the target confining and back pressures and the time to reach the target. The module increases them simultaneously at a certain loading rate. Trials were performed to choose a suitable loading rate which, in this study, was 15kPa/hour. This rate is considered reasonably slow enough to allow the sample to fully consolidate during loading, and no significant change in pore water pressure was observed during K_0 loading. In this study, consolidation is considered to be finish if no excess pore pressure was generated when the target consolidation stress is reached. Similar consideration was used by previous studies (e.g. Bowman, 2002; Lam, 2003)

The effective confining pressures used in this study were 30kPa, 60kPa and 120kPa, given that the focus was on creep at shallow depth. 30kPa was selected as the minimum confining pressure to avoid the influence of over consolidation due to 15kPa of vacuum pressure being applied during sample preparation. Using a high back pressure (i.e. 500kPa) proved to be useful in achieving accurate volume change measurement, thus maintaining practically zero radial strain of local and external measurement as exemplified in Figure 3-13. It can be seen that direct radial strain reading is well within the requirement e.g. Japanese Geotechnical Standard (JGS) requires that the lateral strain accuracy during K_0 consolidation is ±0.05% (JGS, 2000).

The deviator stress at the end of consolidation cannot be controlled using the K_0 module program and was found to be sensitive to the sample preparation. Thus careful attention was needed in to the sample preparation so that the mean effective stress at the end of consolidation between samples was reasonably close (± 2kPa). Figure 3-14 shows the relationship between K_0 values and mean effective stress for K_0 consolidated undrained tests in this study. It can be seen in Figure 3-14 that measured K_0 values decrease and converge to a certain ultimate value with the increase in effective mean pressure. The same trend was observed by Okochi and Tatsuoka (1984). This chart is used to check the repeatability of the sample preparation.

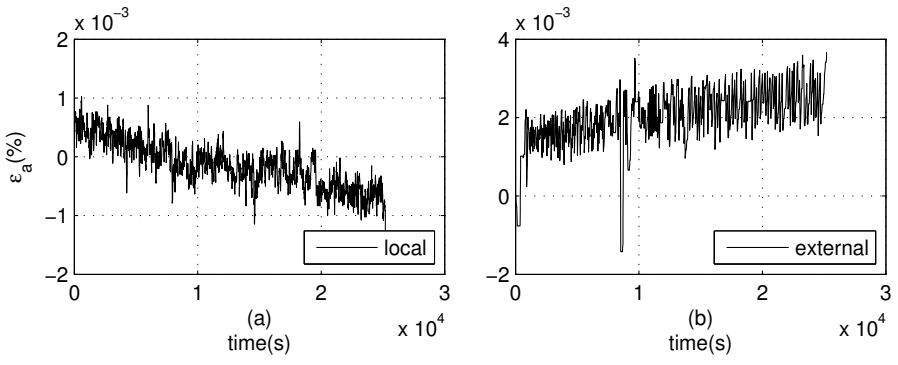

Figure 3-13 Radial strain control during K_0 consolidation(a) local (b) external

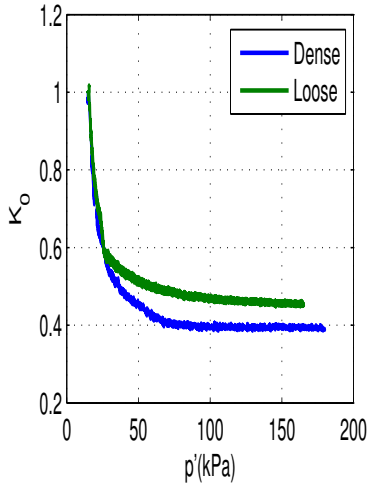

Figure 3-14 Relationship between K_0 and mean effective stress

3.3.7 Creep

Following the consolidation stage, a creep stage was performed by targeting constant cell pressure, back pressure and deviator stress for certain periods of creep – i.e. mainly one hour, one day and one week. It was important that these stresses during creep were reasonably stable i.e. within ±1kPa of the target value (see Appendix C).

3.3.8 Shear

Undrained monotonic loading was performed in a strain controlled manner using a strain rate of 0.01mm/s. This strain rate is commonly used for undrained tests on silty soil (JGS, 2000; Lade *et al.*, 2009). As the focus of this study is on small strain range, the majority of the tests were sheared up to about 1% strain; some tests were sheared beyond that for a repeatability check. For undrained cyclic loading, the specimens were sheared under stress control at a loading rate of 2 min per loading cycles. This loading rate was chosen considering the logging rate of the GDS data acquisition system (Rees, 2010).

3.4 Experimental Method- Fabric Tests

3.4.1 Specimen preservation

For quantification of soil microstructure using image analysis techniques, soil specimens reconstituted in the laboratory have to be preserved. Preservation of non-cohesive soil specimens can be accomplished by impregnating a curing agent into them. In this study, a low viscosity curing agent called EPO-THIN, a two part epoxy resin, manufactured by Buehler Inc. was impregnated into the specimen. Prior the impregnation of epoxy resin, a moist soil specimen had to be completely dried because the epoxy resins do not cure well in a moist environment.

An apparatus to preserve the soil fabric using resin developed by Massad (1998) which was adapted by Bowman (2002) was also used in this study. The resin impregnation chamber was constructed to include a pedestal and cap end-plates with a 50mm diameter by 70mm high split steel cylinder in between. The split cylinder was held together by three bulldog clips. Rubber O-rings at the bottom formed a seal between the cylinder and the lower pedestal. A central hole through the base pedestal, leading to a 1/4 inch BSP to 4mm push-fit connection, allowed the steady introduction of the resin up through the cylinder after assembly. Grooves were cut diametrically from the central hole, 5mm deep by 5mm wide, in a cruciform manner to facilitate the dispersion of resin sideways at the base during its application. The upper cap was free to move vertically as a piston within the cylinder as loads were applied via a ball bearing and weight hanger. Displacement at the surface of the sand was measured using a dial indicator placed on the hanger.

An interface chamber purchased from Geo-Test Instrument Corp. USA, with an in-built rubber membrane was used to separate the hydraulic control panel and the resin. Contact with resin after some tests could damage the manufacturer's Plexiglas made top cap thus it was replaced with in house made aluminium top cap. Resin was placed in the upper part of the interface chamber with water filling the lower section. Pressure was applied using a GDS Pressure Controller or, later, an

air-water interface to inject the resin into the base of the impregnation chamber via the rubber membrane. The air-water interface was connected to an automatic system for volume change. Modification of existing Visual Basic software for undergraduate triaxial testing was made to allow monitoring of the resin volume infiltrated. Precaution was taken to ensure air-bubbles were expelled from both sides of the interface chamber. This enabled an accurate assessment of the quantity of resin being used as the infiltration was carried out.

The sequence of operation used in the specimen preservation procedure consists of the following:

- Wipe the split steel cylinder/impregnation chamber, pedestal, and top cap with mould- release agent to facilitate removal of the sample after the test.
- Apply silicon sealant to the edges and base of the steel cylinder before assembly with the pedestal and lower O-ring. Apply also silicon grease at the edge of the stainless steel cylinder of the interface chamber to prevent leakage of resin during impregnation.
- Clamp the impregnation chamber using the three bulldog clips and seal the assembly
- Place fine metal gauze in the assembly base over the cruciform
- Pour soil into the impregnation chamber and reconstitute in four layers.
- Place gently the top cap on top of the levelled silty sand and apply loads for the required times before resin infiltration.

Monitor strain due to initial top cap loading and during aging up to one week using a dial gauge. Samples of the same density which show any discrepancy of strain during top cap loading, before the impregnation, are discarded and a new sample is made.

Initially the mix proportion (by weight) used was 100: 35: 12 for resin: hardener: acetone. The ratio was slightly modified from the ratio used by Masad (1998) and Bowman (2002), as particles were somewhat finer. As the same product was no longer produced, later on a new product of EPO-THIN (mixing ratio by weight is 5: 1.95) was mainly used for impregnation. Before mixing, the epoxy was heated for 10 minutes under 50^0C, thus eliminating the use of acetone. An attempt was also made to aid fabric visualisation by adding about 1% fluorescence epoxy dye. As silty sand is more compressible than clean sand at the same relative density (Lade *et al.*, 2009), a maximum pressure of 15kPa was used in this study for both dense and loose samples. The impregnation process typically took up to two hours. Samples were then left in the mould at least 48 hours before removal. The axial dial gauge measurement indicated that the typical average axial strain during epoxy intrusion and curing was 0.15%. This suggests that the disturbance to the microstructure is relatively small. This amount of strain is comparable to Yamamuro's *et al* findings (2008). After the mould had been removed (see Figure 3-16), the sample was left for two weeks to ensure that the resin was completely hard before cutting.

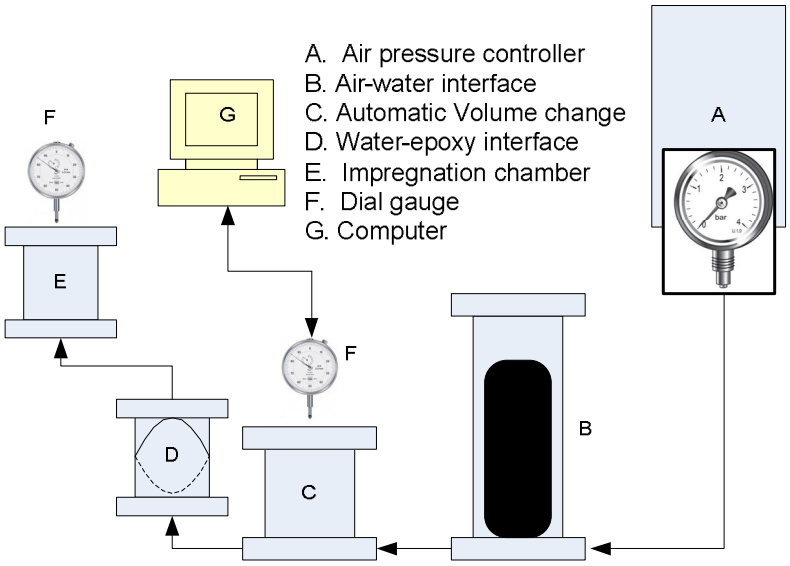

Figure 3-15 Impregnation set up

3.4.2 Coupon preparation

Once the epoxy impregnated specimen was fully cured, it was removed from the split steel cylinder. The specimens were then cut, ground, and polished in preparation for capturing the image. Best practices of coupon preparation were learned from Mr Rob Spiers (Geological Science Department technician) and Mr Kevin Stobbs (Mechanical Engineering Department technician).

Figure 3-16 Impregnated specimen

3.4.2.1 Cutting and sectioning

Initially all cutting and sectioning were done using an 18-inch (approx. 48mm) diamond blade, water cooled, slab saw shown in Figure 3-17 (a). Cuts with the slab saw caused concave, non-parallel surfaces because of blade flexure and operator error. When the sample was viewed under a microscope, the entire viewing surface would not be in focus. After some time, an ISOMET precision saw, Figure 3-17 (b), became available with a thinner wheel blade i.e. 0.6mm. However, the cutting depth of the available diameter of blade (3") was well below the diameter thickness of the specimen being sectioned. Later on a 5" wavering diamond blade was purchased, allowing sectioning with relatively flat and parallel surfaces. A new

jig was made for holding the specimen during the sectioning. The thinner wheel thickness of diamond wavering blade offers minimal kerfs loss and a cooler cut than that produced by other cutting methods. Specimen sectioning with a wavering saw results in minimal surface damage which reduces the number of subsequent grinding steps (Evans, 2005).

Thick sections, about 0.5mm and one thin section, about 30 microns were taken vertically from the middle part of the specimen.

(a) (b)

Figure 3-17 Diamond slab saw (left) and Isomet precision saw (right)

3.4.2.2 Manual grinding

The vast majority of research literature on epoxy-stabilized sand coupon surface preparation techniques for image analysis, e.g. Jang et al. (1999) and Evans (2005), describe the use of a lapping technique during initial grinding to obtain fast removal rates and superior surface flatness. This would have been a preferred method to use in this study but the necessary equipment was not available. Thus silicon carbide abrasive resin bonded to adhesive backed 8-inch paper disks was chosen for its uniform cutting, minimum surface distortion, and deformation.

Buehler Product's silicon carbide abrasive disks were used with DAP-2 8-inch grinder/polisher (see Figure 3-18) rotated at 150 rpm for 1 to 2 minutes. A steady stream of water was used to provide lubrication, prevent heat build-up, facilitate swarf removal, and evenly distribute the contact stresses. The coupon was rotated 90 degrees during each consecutive grinding step to help gauge removal rates of damage caused by previously used larger abrasive grit. The successive abrasive disks size used are nos. 180, 240, 320, 600. An additional abrasive disk no. 1200 then was used to grind manually by hand (following eight pattern), as transition to the polishing step. The sand/epoxy coupon and the polishing jig were thoroughly cleaned before switching to a finer size abrasive. The coupon was removed from the jig, washed and rinsed with water, and then dried with compressed air. The polishing jig was scrubbed with a brush and water, and then dried with compressed air.

An example of an image after grounding using no. 600 abrasive disks is shown in Figure 3-19. It can be seen that boundaries between the grains and epoxy are still not clear.

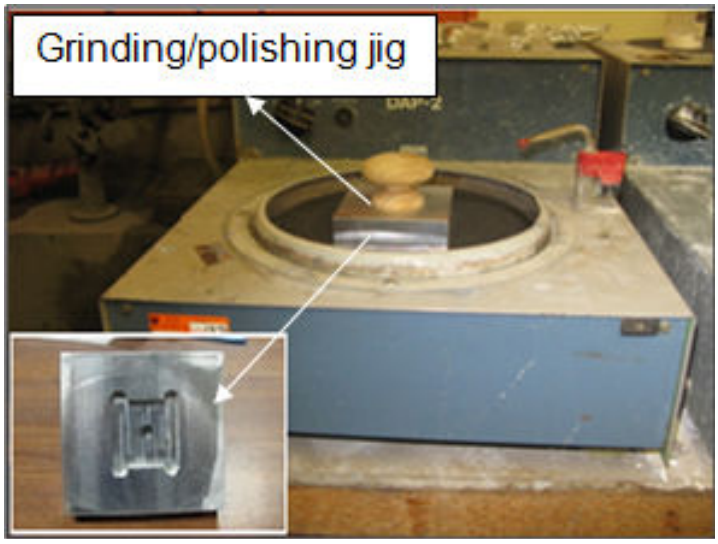

Figure 3-18 Grinder/Polisher machine and jig

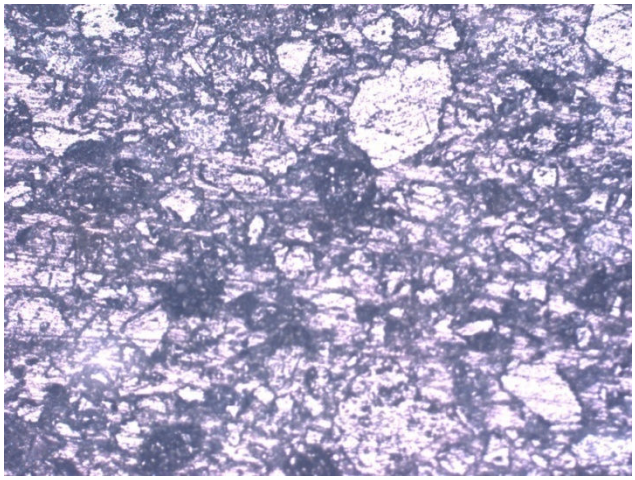

Figure 3-19 Example image after grounded using no. 600 abrasive disc

3.4.2.3 Manual polishing

In the final stage of preparation, a 0.3 mm alpha alumina powder was used to polish the sample following figure-of-eight patterns. This removed any scratches induced by the no. 1200 grit sandpaper without imparting any additional disturbance to the specimen.

3.4.3 Image capture

Two different types of microscopes were trialled for capturing images i.e. a light microscope and a scanning electron microscope (SEM). It was first thought that using a thin section was the best way for viewing the sample under a light microscope. However, the grains became too transparent and it was difficult to distinguish the grains and the pores of the sample as shown by Figure 3-20(a). A thick section was then trialled. Two light microscopes, one in the Geological Department and another one in the Mechanical Department, were used to capture images from the thick section. However the image result still did not help to differentiate between the grains especially fine grains and the pores as illustrated in Figure 3-20(b). Grain edges are also poorly defined especially for fine particles. In addition, the image reveals that some grains also are blackish in colour thus conversion into binary images would make some of the grains disappear. For a sample preserved with the addition of epoxy fluorescence dye, a fluorescence

microscope in the Biological Department was used. However the image result was also poor therefore discarded.

Later on SEM was attempted. Images can be obtained at magnification very much higher than those possible with the optical microscope. Two modes of SEM were attempted i.e. using a conventional scanning electron detector and a back scatter detector. The secondary electron mode produces images based on specimen surface topography. The back scatter mode on the other hand produces images based on atomic number. Areas with a higher atomic number will appear brighter than areas with a lower one. The later mode was introduced in geological science by Llyod (1987) and is still relatively not much used in geotechnical engineering.

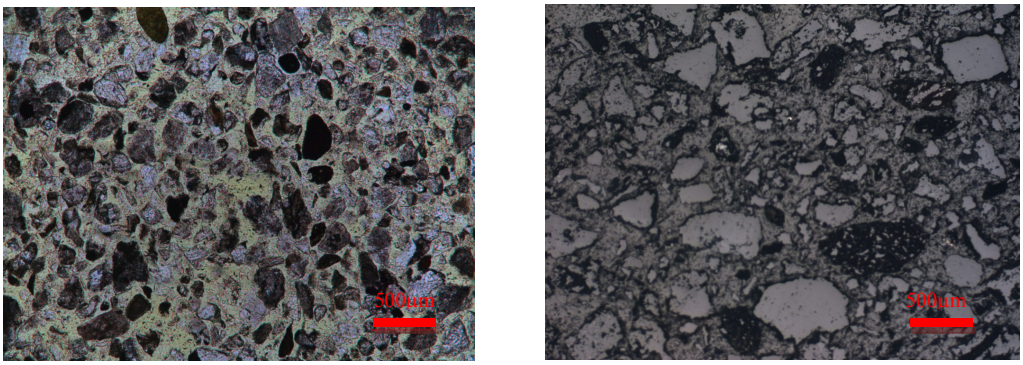

(a) (b)

Figure 3-20 Image sample under light microscope (a) thin section (b) thick section

Figure 3-21 shows image examples of the same area produced by both modes. It can be seen that secondary electron produces images that contain less detail compared to back scattered mode. Better and more accurate grain edge-definition is also achieved by back scattered mode. Accurate determination of grain edges allows the void distance relationship via mean free path (described in Section 6.2.2) to be examined. Thus it was decided to capture the images using SEM back scatter mode. It should be noted that the image from SEM represents only a small area of the whole section. One image in this study (45 x magnifications) for example covers the area of 13.3mm x 10.67mm.

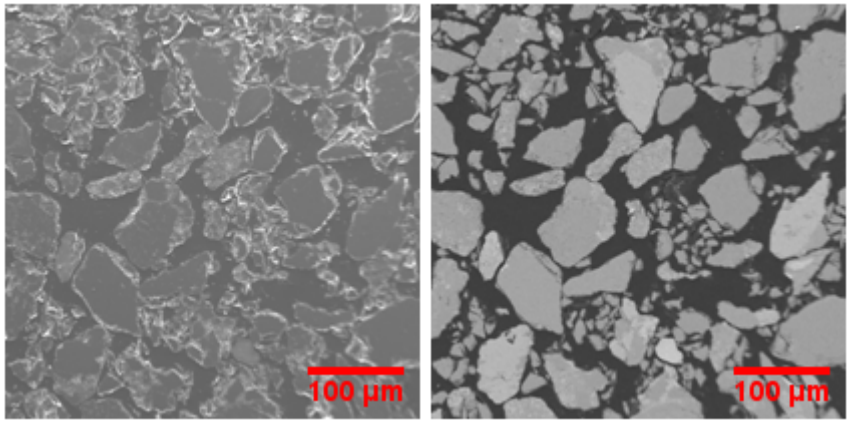

(a) (b)

Figure 3-21 SEM image from secondary electron (a) back scatter mode (b)

3.4.4 Image Processing

Image processing and specimen microstructure analysis were performed with *ImageJ* software. Colour (RGB) images from SEM were converted to 8-bit gray scale images. The gray scale images were processed to correct image defects and for image enhancement. Steps involved in this stage of the process included contrast expansion, correction for noise, segmentation/ thresholding and watershed. The goal of this stage was to minimize loss of data and, at the same time, enhance image quality so that consistent results could be obtained from the images after conversion

to a binary format. The algorithm for the automated process (a macro was written for consistency) is as below:

- Convert image to 8 bit grey scale
- Auto adjust brightness
- Auto adjust window
- Despeckle
- Segmentation / Thresholding
- Convert to binary image
- Fill holes if required
- Watershed

Auto adjustment of image brightness and window values ensures that the pixel values and image histograms are shifted to the optimum value level and image brightness and contrast are similar among different specimens. The despeckle function removes image noise from the image. The next step before conversion to a binary (black and white) image is called thresholding or segmentation. This process is designed to select the pixels within a range of brightness values that belong to the foreground and reject all of the other pixels in the background. The resulting image is displayed as a binary image, using black and white colours, to distinguish foreground and background regions. Watershed is then performed to separate the grains automatically. Finally some manual corrections were made where necessary due to imperfections of the watershed process. An example of image processing is shown in Figure 3-22.

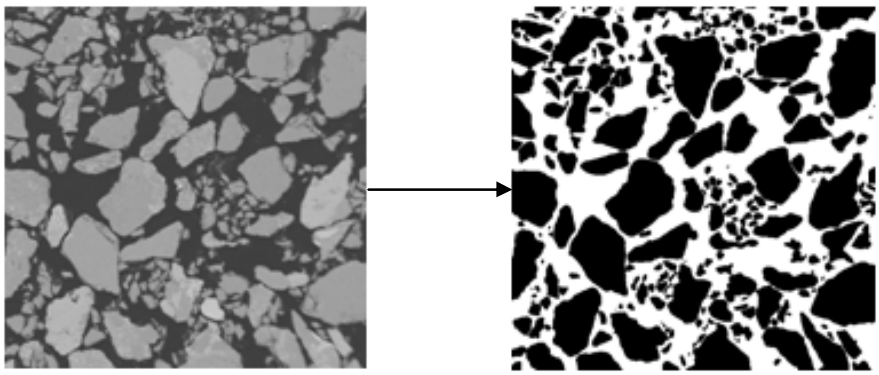

Figure 3-22 Example of image processing using *ImageJ*

3.4.5 Overview of preliminary image analysis

Void ratio (e) was commonly used as the parameter to overview the image analysis procedure, as used in Section 3.4.4. Void ratio is defined as

$$e = \frac{\text{Volume of void}}{\text{Volume of solid}} \qquad \textbf{Eq. 3-2}$$

As the captured image is in two dimensions, void ratio based on the image is defined as the ratio of the area of the void (white) to the area of the solid (black). Regardless of the issue that many factors can affect the measurement e.g. local density, it is expected that void ratio based on the image analysis should reasonably match the measured global void ratio based on weight and volume ((Evans, 2005; Jang & Frost, 1998). However, as the image captured by SEM represents only a small area of the whole section, it is necessary to utilize a statistical approach i.e. use some images than take the average. A representative elementary area for each image was determined by drawing a circular area which was enlarged until a relatively constant void ratio was obtained (Braham and Bear, 1985). For this study, it was found that a relatively constant void ratio was obtained at an area of about 130000 μm^2 which is equivalent to diameter of about 1292 microns (see Figure 3-23). This equivalent diameter value is about 9 times the mean diameter (±1400 particles) and comparable to the result from Masad (1998) who reported a value about 10 times the mean diameter of clean sand (±100 particles). However, it

should also be noted that even in one image, the number of objects is very large (>1000 particles) making image analysis tedious and challenging. By combining those factors, it was decided to take at least nine images from the left, right, bottom, middle and top of each section. The void ratio was then taken as the average of the void ratio from each image. As an example, for a dense sample of 70601H (see Chapter 6) the void ratio as prepared (measured by volume and weight) is 0.687 (including strain due to initial loading) whilst the void ratio based on the image analysis was 0.679. The variation in void ratio is 0.003. The results show that images analysis procedure used in this study is relatively acceptable.

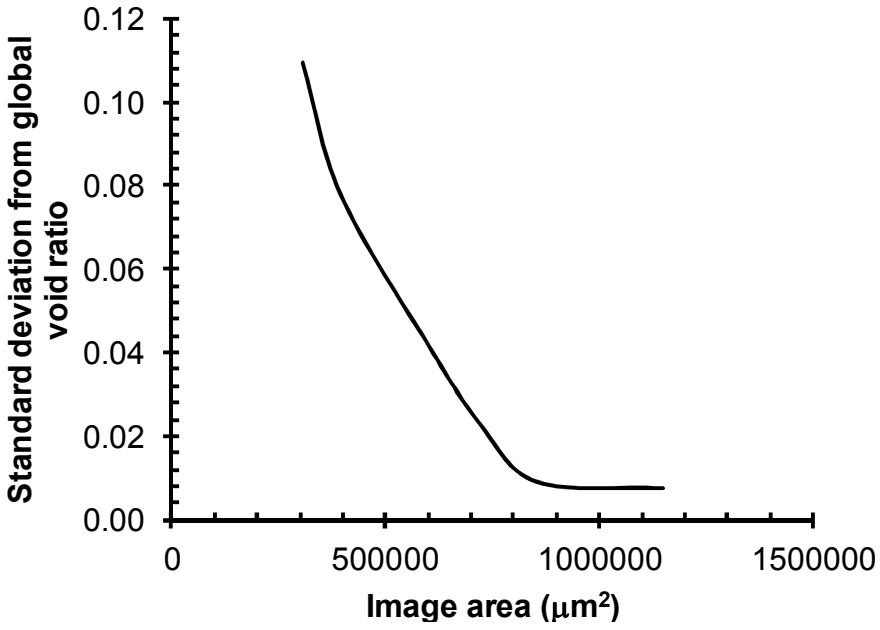

Figure 3-23 Determination of representative elementary area

3.5 Summary

This chapter presents materials and experimental methods developed and used in this study. The materials used are mainly non-plastic silty sand with fine content of 15%. The sand fraction obtained from ejected sand from Rydal reserve (D_{50} =0.19mm) and modified commercial silica flour 100 (D_{50}=0.042mm). The fine fraction was modified from original silica flour 100 by removing particles smaller

than 0.032mm in order to help image analysis. The samples were reconstituted mainly by moist tamping deposition with few tests prepared by dry funnel pluviation.

Regarding the experimental method there are two types of tests i.e. triaxial tests and fabric tests. For the triaxial test, a local measurements system has been developed to the existing GDS triaxial apparatus by utilizing three existing LVDTs transducers (2 LVDTs for axial strain and 1 LVDT for radial strain). In house radial belt for radial LVDT and axial local gauges and pads were made to accommodate enlarged base platen. A separate local LVDT data logging system with theoretical resolution of 0.0009% strain has been developed, capable of sampling 100 data per seconds. Local measurements show reasonable performance where local system generally gives stiffer response than external system. For fabric test, the use of new EPO-THIN has been introduced for the preservation of relatively compressible silty, eliminating the use of acetone. A modified impregnation setup has been developed involving the use of air-water interface from conventional triaxial apparatus to inject the epoxy resin into the sample at maximum 15kPa pressure. The average strain during epoxy intrusion and curing is approximately 0.15%, indicating relatively small disturbance to the microstructure. Thus the preservation method can be used thereafter. For the coupon preparation, the use 1200 abrasive discs for manual grinding were introduced. Furthermore, SEM with back scattered electron detector was used to capture the image from the coupon. The captured images revealed clear contrast between grains and the epoxy filled resin, in addition better grain edge definition, making the image analysis easier without much of the mathematical morphological process.

In summary, overall triaxial and fabric test methodology provided the required quality of the purpose of this research study.

4 Observation of Creep

4.1 Introduction

This chapter describes strain development during creep stages, before commencement of shearing. The majority of the creep observations follow K_0 consolidation because it is generally accepted that in the level ground, free field the stresses condition exhibit K_0 condition (e.g. Fourie & Tshabalala, 2005; Sawada, 2007). In addition, most of the studies of creep have been performed following isotropic consolidation, while limited studies have been done following K_0 consolidation. The last reason is to approximately mimic the fabric tests (Chapter 6) which were performed under zero lateral strain (K_0 condition).

A total of 29 creep tests were performed at three different effective confining pressures and two soil densities, three aging times and two sample preparation methods as summarized in Table 4-1. Low pressures were used in this study because the effects of creep under such low effective confining pressures on silty sand have not been much investigated. This may be relevant, for example, to study time effects on freshly deposited or disturbed soils such as in the case of hydraulic fills, submarine slopes, mine tailings, and post-liquefaction state of soils behavior following earthquakes.

Both local and external strains are presented, as none of the measurement systems are considered 'perfect'. The local system is relatively reliable for measuring average axial strain because it is 'free' of sample end effects. However the radial local system measures the strain only at a discrete point on the sample i.e. mid-height of the sample and may be affected by necking, bulging and other localized deformation. On the other hand measurement of external axial strains could suffer from sample bedding in addition to apparatus compliance. The external radial strain measures 'average' radial strain change across the whole sample height. Together both systems may complement each other to give clearer pictures of sample deformation in terms of both local and overall strains.

Table 4-1 Summary of performed creep tests

No	Method	Dr (%)	σ'_3(kPa)	σ'_1(kPa)	σ'_3/σ'_1	Test ID	Aging Time
1	MT	67.4	120	306	0.39	CKoU-1	1 hour
2	MT	67.4	120	307	0.39	CKoU-2	1 day
3	MT	67.6	120	306	0.39	CKoU-3	1 week
4	MT	67.1	60	149	0.40	CKoU-4	1 hour
5	MT	67.2	60	149	0.40	CKoU-5	1 day
6	MT	67.4	60	149	0.40	CKoU-6	1 week
7	MT	67.5	30	67	0.45	CKoU-7	1 hour
8	MT	67.3	30	67	0.45	CKoU-8	1 day
9	MT	67.3	30	67	0.45	CKoU-9	1 week
10	MT	67.6	30	30	0.99	CIU-10	1 hour
11	MT	67.8	30	30	1.00	CIU-11	1 day
12	MT	67.4	30	30	0.99	CIU-12	1 week
13	MT	39.8	120	261	0.46	CKoU-13	1 hour
14	MT	40.0	120	261	0.46	CKoU-14	1 day
15	MT	39.4	120	260	0.46	CKoU-15	1 week
16	MT	39.7	60	125	0.48	CKoU-16	1 hour
17	MT	39.8	60	126	0.48	CKoU-17	1 day
18	MT	39.6	60	125	0.48	CKoU-18	1 week
19	MT	39.4	30	57	0.53	CKoU-19	1 hour
20	MT	39.8	30	57	0.52	CKoU-20	1 day
21	MT	39.9	30	58	0.52	CKoU-21	1 week
22	DD	69.6	60	113	0.53	CKoU-22	1 min
23	DD	69.2	60	112	0.53	CKoU-23	1 day
24	DD	69.5	60	60	1.00	CIU-24	1 min
25	DD	69.5	60	60	1.00	CIU-25	1 day
26	MT	68.4	60	60	1.00	CIU-26	1 min
27	MT	70.0	60	60	1.00	CIU-27	1 day
28	MT	38.4	30	30	1.00	TWIU-34	1 hour
29	MT	38.9	30	30	1.00	TWIU-35	1 week

Note:
MT=moist tamping; DD=dry pluviation; Dr=relative density

4.2 Definitions

Local strains are presented in terms of calculated volumetric and shear strain data along with the measured axial and radial strain. Local volumetric strain is defined as

$$\varepsilon_v = \varepsilon_a + 2\varepsilon_r \quad \textbf{Eq. 4-1}$$

Shear strain is defined as

$$\varepsilon_s = 2/3(\varepsilon_a - \varepsilon_r) \quad \textbf{Eq. 4-2}$$

where ε_a is axial strain (compression positive) and ε_r radial strain (compression positive) of the sample. For external systems, axial (ΔH) and volumetric changes (ΔV) are measured. Volume change is determined from volume of water coming into and out of the sample. External radial strain is then calculated from change in diameter (ΔD) as given by equation below

$$\varepsilon_{re} = \frac{D_{new} - D_{initial}}{D_{initial}} x100\% \quad \textbf{Eq. 4-3}$$

$$D_{new} = \sqrt{\frac{4A_{new}}{\pi}} \quad \textbf{Eq. 4-4}$$

$$A_{new} = \frac{(V_{initial} + \Delta V)}{(H_{initial} - \Delta H)} \quad \textbf{Eq. 4-5}$$

Where $D_{initial}$,$V_{initial}$ and $H_{initial}$ are initial diameter, volume and height respectively., while external shear strain is calculated with the same equation of Eq. 4-2.

In this thesis, the state of stress is described using "Cambridge q-p' "stress invariants.

Deviator stress is defined as

$$q = (\sigma'_1 - \sigma'_3) \qquad \textbf{Eq. 4-6}$$

Mean effective stress is defined as

$$p' = \frac{1}{3}(\sigma'_1 + 2\sigma'_3) \qquad \textbf{Eq. 4-7}$$

where σ'_1 and σ'_3 are major and minor principal stresses.

4.3 Creep Following K_0 Consolidation

When the final consolidation pressure was reached, constant deviator stress, back pressure and cell pressure were targeted via *GDSLab* software. The sample was then left for a certain period of time of 1 hour, 1 one day or 1 week, and strain development was monitored during this period.

4.3.1 K_0 consolidation

Figure 4-1and Figure 4-2 show typical strain and stress paths respectively during K_0 consolidation, i.e. before the creep stage for dense samples (CKoU-2; CKoU-5; CKoU-8) and loose samples (CKoU-14; CKoU-17; CKoU-20). The letter in the legend represents density while the numbers represent effective confining pressure. Figure 4-1 demonstrates, as expected for K_0 consolidation, the slope of the strain path is equal to unity for all confining pressures. Figure 4-2 shows that the stress paths for three confining pressures appear to be almost on top of each other. However further observation reveals that the stress paths are slightly different. Higher confining pressure results in slightly less steep gradient. This may be explained with Figure 3.11 where the K_0 value ($=\sigma'_3/\sigma'_1$) is decreasing as mean effective stress increases and practically reaches a constant value when the mean

effective stress is higher than 100kPa. Each end point for a different confining pressure therefore has a different stress ratio, R (=1/K_0), and effective mean stress (p') as presented in Table 4-2. Thus when comparing creep at different confining pressures for each density, we are actually comparing creep due to combined effects of stress ratio and mean effective stress. In addition, the table shows that the axial strain during K_0 consolidation is greater for higher confining pressure, for both dense and loose samples. The table also reveals that higher confining pressures during K_0 consolidation tends to decrease the volumetric compressibility, m_v.

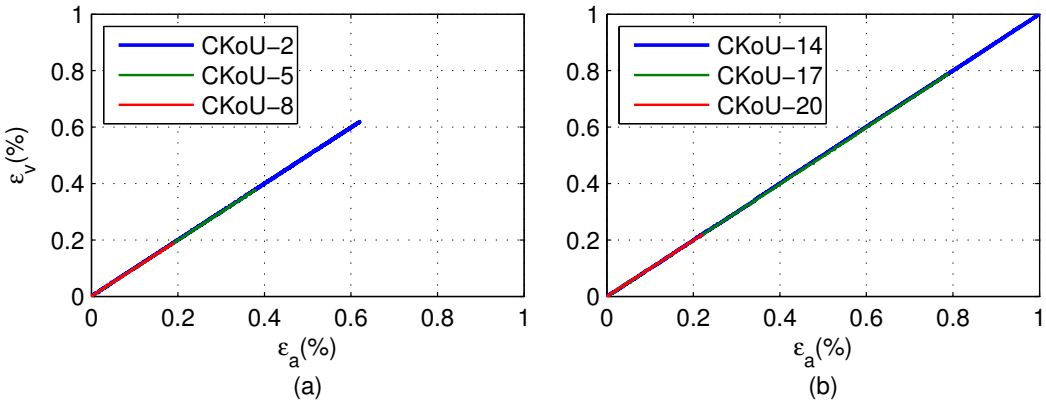

Figure 4-1 Typical strain path before creep i.e. 1 day of aging samples at 120, 60 and 30 kPa confining pressure (a) dense samples: CKoU-2; CKoU-5; CKoU-8 (b) loose samples: CKoU-14; CKoU-17; CKoU-20

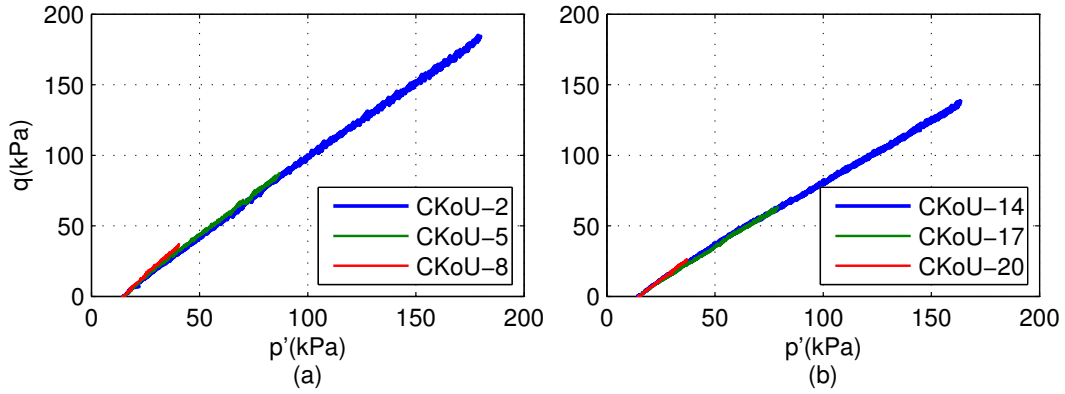

Figure 4-2 Typical stress path before creep i.e. .e. 1 day of aging samples (a) dense samples: CKoU-2; CKoU-5; CKoU-8 (b) loose samples: CKoU-14; CKoU-17; CKoU-2 at 120, 60 and 30 kPa confining pressure, respectively

Table 4-2 Typical stress conditions at the end of K_0 consolidation i.e. when creep starts

σ'_3 (kPa)	Dense					Loose				
	p' (kPa)	q (kPa)	R	ε_a (%)	m_v (1/kPa)	p' (kPa)	q (kPa)	R	ε_a (%)	m_v (1/kPa)
30	40	36	2.21	0.19	7.47E-05	26	26	1.87	0.22	2.1E-04
60	88	88	2.47	0.38	5.23E-05	63	63	2.05	0.79	1.6E-04
120	180	186	2.55	0.62	3.75E-05	141	137	2.14	1.00	7.9E-05

Note: m_v= volumetric compressibility

$m_v = d\varepsilon/d\sigma = \varepsilon_a/(p'-p'_o)$; p'_o=15kPa

4.3.2 Dense moist tamped samples

Figure 4-3 shows the development of creep strains for dense samples at 60kPa confining pressure for 1 hour, 1 day and 1 week of creep time, respectively i.e. CKoU-4, CKoU-5 and CKoU-6. The figure presents typical trends for creep of a dense moist tamped sample. Similar trends were observed for dense samples at higher and lower confining pressure used in this study (see appendix D).

Figure 4-3(a) and (b) demonstrates the development of axial strain for CKoU-4, CKoU-5 and CKoU-6 samples with logarithmic time in seconds from both local and external measurement, respectively. Generally, for the material used in this study and for the same creep time, strains measured externally are typically 40% to 80% higher than strains measured locally. External axial strain represents an 'average' of behavior across the whole height of cylindrical sample. On the other hand local axial data is taken at the average of approximately the mid-point of the sample across 65mm gauge length. As briefly discussed in Chapter 3, the difference between external and local measurement is due to issues such as bedding effects and apparatus compliance. However, as creep due to apparatus compliance should be relatively constant (Bowman, 2002), then larger external strain is likely due to bedding effects at the ends of the sample.

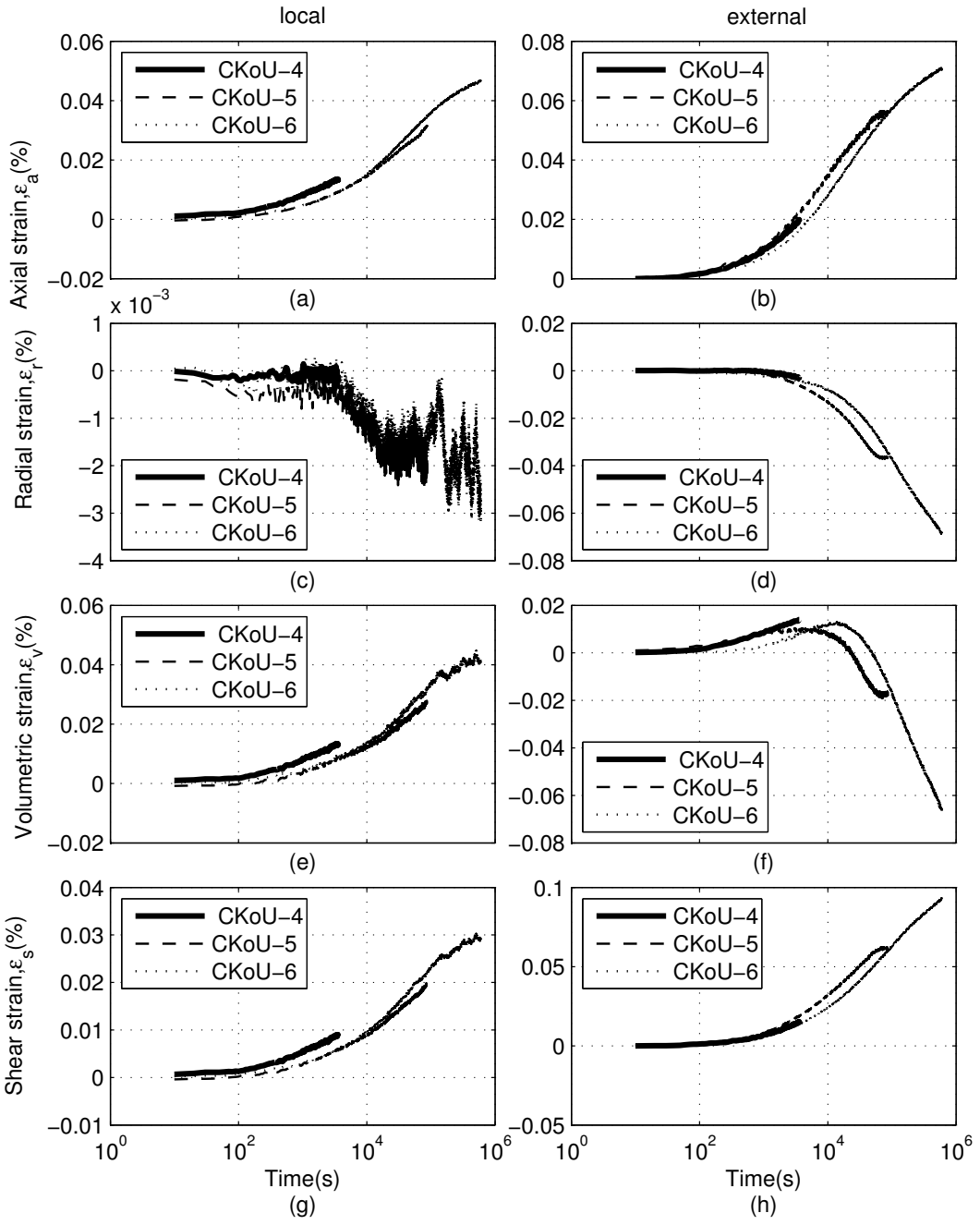

Figure 4-3 Typical strains development during creep of dense samples at 60 kPa confining pressure (CKoU-4, CKoU-5 and CKoU-6) for 1 hour, 1 day and 1 week of creep time, respectively

Both of the measurement systems show axial creep strain is in compression. This is because when creep starts (end of K_0 consolidation), axial stress is greater than radial stress. Positive axial strains increase with time at a decreasing strain rate.

The development of radial strains with time is illustrated in Figure 4-3(c) and (d). The first thing to be noted that local radial strains are more jagged compared to local axial or external radial strain. This may be explained due to the fact that local radial LVDT measures strain at discrete point along the mid-height of the sample whereas local axial and external radial measure 'average' strain across the gauge length and full height of the sample respectively. Thus the local radial LVDT is likely to be more sensitive to localized factors such as bulging due to uneven loading and local void ratio variation. Moist tamped samples are generally accepted to be less uniform than pluviated samples even for reconstituted clean sand (Frost & Park, 2003; Vaid *et al.*, 1999). As the material used in this study contains 15% of fines, the effect of non-uniformity is expected to be more pronounced. Similar to axial strain, both local and external measurements show that negative radial strain tends to increase with time. Negative value of radial strain shows that the sample expands over time in the radial direction.

Figure 4-3(e) and (f) presents development of volumetric strain with time. It is interesting to observe that the local system shows that the soils, up to one week of aging, generally appear to be still in the initial compression stage. Conversely, the external volumetric strain demonstrates that the soils start to dilate at about 10^4 seconds (2.8 hours). This may be explained by what is being measured by both systems. Local volumetric strain was calculated from a discrete radial strain measurement made at the mid-height of the sample, and axial strain made over a 65mm gauge length (see Eq. 4-1). Local volumetric strain assumes constant strains over certain volume but is based on the assumption that strains actually vary locally. While external strain is measured from the volume change across the whole cylindrical sample. External radial strains being calculated from volume change assuming uniform 'average' strains (discussed further in 4.5.1). The external system revealed that volumetric strain of one week sample is more dilative compared to

one day sample due to higher shear stress developed in one week aged sample as compared to that after one day. A similar tendency between local and external volumetric strains for creep is also observed for higher and lower confining pressures.

Regarding shear strains, all samples up to one week of aging exhibited positive shear strains, as presented in Figure 4-3(g) and Figure 4-3(h). Again this is due to axial stress at the beginning of aging being greater than radial stresses. Both local and external systems show a similar trend with regard to the shear stresses.

4.3.3 Loose moist tamped samples

The development of strains during creep of loose samples (CKoU-16, CKoU-17 and CKoU-18) is illustrated by Figure 4-4 (a) to (h). Likewise with dense samples, the figures are typical of creep strains for 60kPa confining pressure but also represent general behavior for higher and lower confining pressure used in this study (see appendix E). Figure 4-4 (a) and (b) shows that axial strain increases in compression with time at a decreasing strain rate for both local and external measurement. This is a similar trend to that of axial strain of dense samples.

Negative radial strains for loose samples, locally (Figure 4-4 (c)) and externally (Figure 4-4 (d)), generally follow the same trend as dense ones where a longer period of creep tends to increase the strain. Surprisingly, there is not so much difference between local radial strain of dense and loose samples. This is likely related to the fact that those numbers (in particularly for one hour aging) are close to the actual resolution of the LVDT.

In terms of volumetric strain development, loose samples, up to one week of aging are still contracting and show no tendency to dilate, as shown by Figure 4-4 (f) and Figure 4-4 (g).

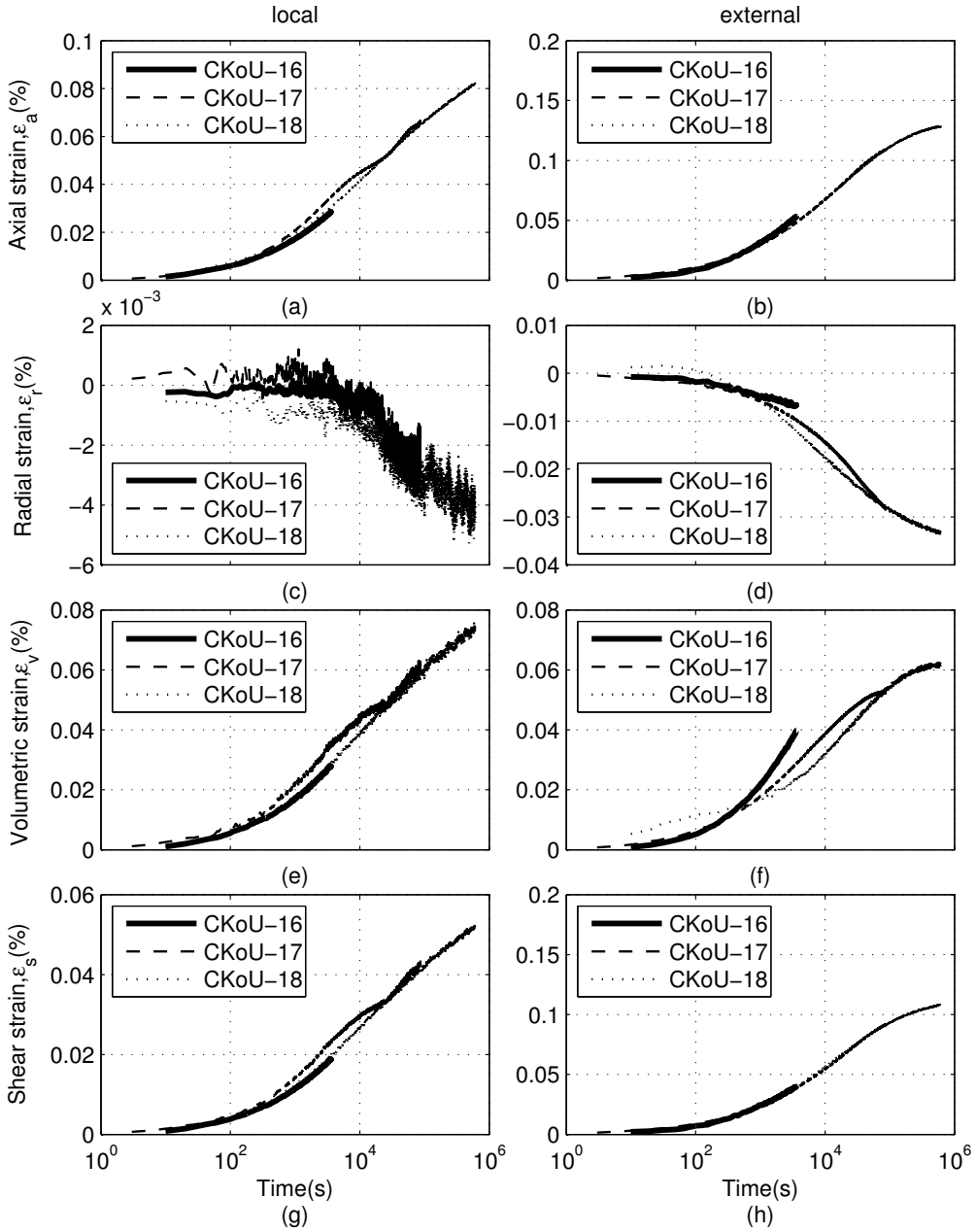

Figure 4-4 Typical strains development during creep of loose sample at 60 kPa confining pressure (CKoU-16, CKoU-17 and CKoU-18) for 1 hour, 1 day and 1 week of creep time, respectively

4.3.4 Combined effects of confining pressure and stress ratio

Table 4-2 explicitly shows that it is difficult to investigate the effect of confining pressure only on creep following K_0 consolidation. Although the stress

paths for different confining pressures appear to be on top of each other, the stress ratio (R) is slightly different, particularly for 30kPa confining pressure.

Figure 4-5 and Figure 4-6 demonstrate the combined effect of confining pressure and stress ratio on dense samples for one day (CKoU-2, CKoU-5 and CKoU-8) and one week of aging (CKoU-3, CKoU-6 and CKoU-9), respectively (effect of confining pressure only on creep is discussed in 4.4.2). Despite of lower compressibility (see Table 4-20), local axial strain is greater for higher confining pressure samples. Consistent trends are shown by external axial strain. (Gu *et al.*, 2014), based on DEM, found that axial strain at small strain range increases with increasing in stress ratio. The trends are illustrated by Figure 4-6(a) and (b). This indicates a significant effect of stress ratio and mean effective stress for the same sample at the same density. In short, the combined effect of increased confining pressure and stress ratio increases the magnitude of creep induced strain following K_0 consolidation. It implies that following a disturbance, deeper soil in the field condition tends to creep more than shallower soil.

An interesting trend is shown by radial strains of dense samples, as shown in Figure 4-6(c) and (d). It appears that lower confining pressures result in greater dilative radial strains for both local and (eventually) external measurement. This may relate to the nature of dense soils that lower confining pressure causes the soils to become more dilative (Alim *et al.*, 2006; Fukushima & Tatsuoka, 1984). This is supported by external volumetric strain in Figure 4-6(f) which shows that the sample at 30kPa is the most dilative followed by the sample at 60kPa and 120kPa, respectively. Although local volumetric strains in Figure 4-6(e) do not show dilation, the figure shows that 30kPa sample is the least contractive followed by 60kPa and 120kPa Regarding shear strain, generally as expected, higher confining pressure results in higher shear strain during creep as shown in Figure 4-6(g) and (h).

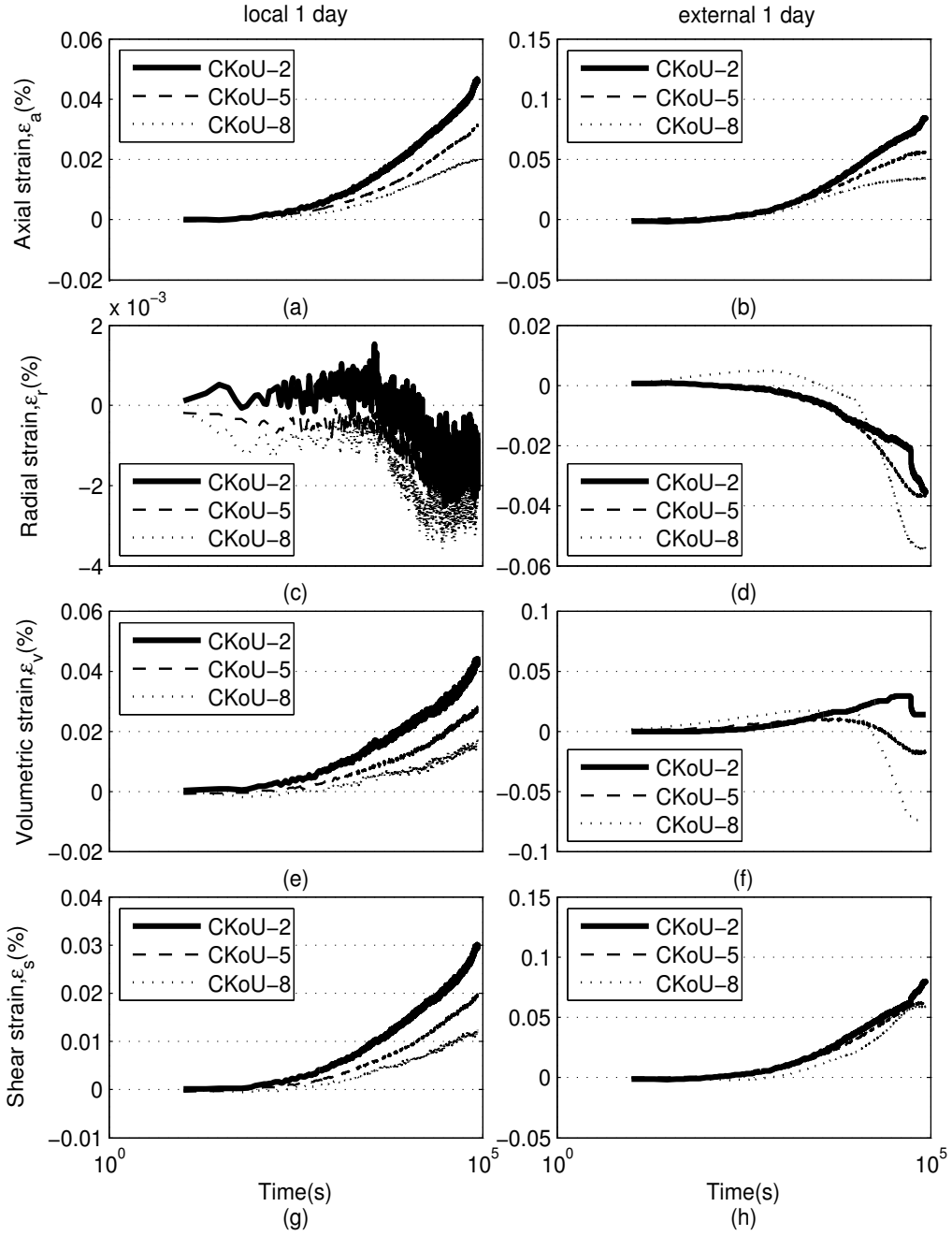

Figure 4-5 Creep of K_0 consolidated dense samples i.e. 1 day creep (CKoU-2, CKoU-5 and CKoU-8) at 120, 60 and 30 kPa confining pressure, respectively

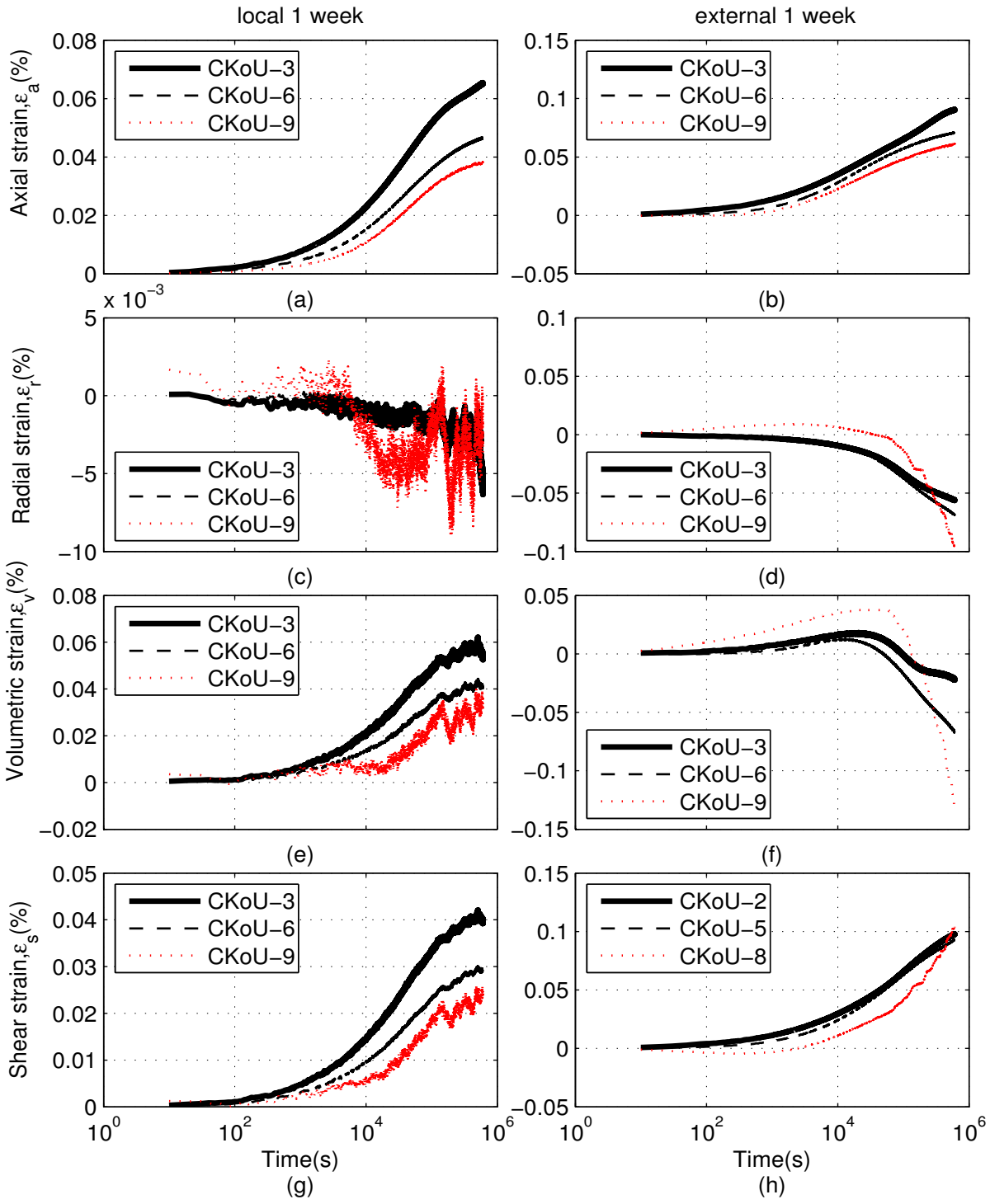

Figure 4-6 Creep of K_0 consolidated dense samples i.e. 1 week creep (CKoU-3, CKoU-6 and CKoU-9) at 120, 60 and 30 kPa confining pressure, respectively

For loose samples, combined effects of confining pressure and stress ratio on creep for one day and one week are presented in Figure 4-7 and Figure 4-8. The general trends between local and external strain, particularly volumetric strain, are more consistent with each other compared to the dense samples. Local and external axial strains are greater for high confining pressures than for lower confining pressures. This is due to the fact that higher confining pressure means higher stress ratio and mean effective stress. Gu *et al.* (2013), based on DEM of dense samples, reported that higher stress ratio during anisotropic loading result in higher volumetric strain. Both local and external measurements reveal that radial strains are higher for higher confining pressure. Generally this tendency also is observed for volumetric strains, which are contractive, and shear strains. Shear strains, locally and externally, are in the positive direction.

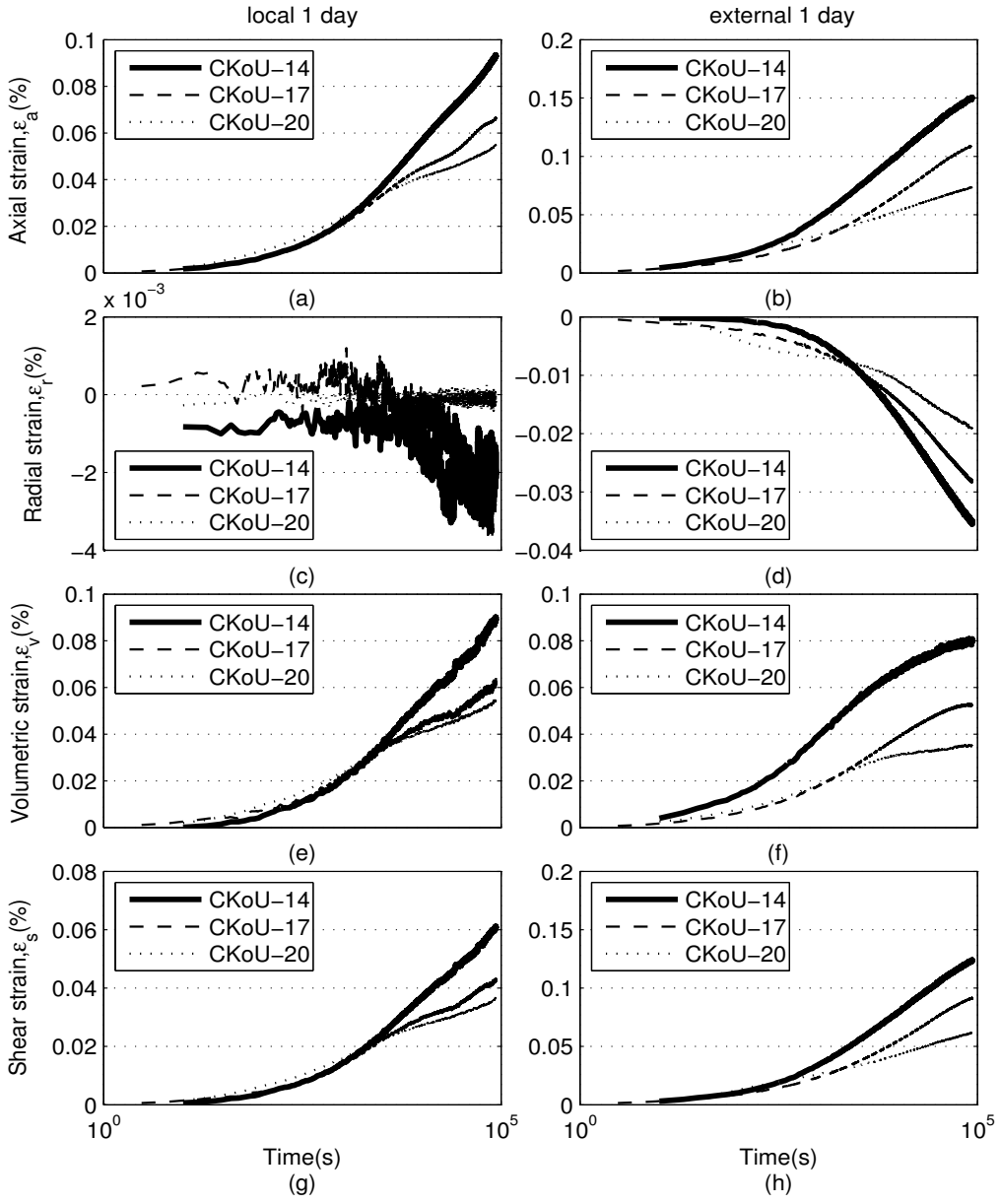

Figure 4-7 Creep of K_0 consolidated loose samples i.e. 1 day creep (CKoU-14, CKoU-17 and CKoU-20) at 120, 60 and 30 kPa confining pressure, respectively

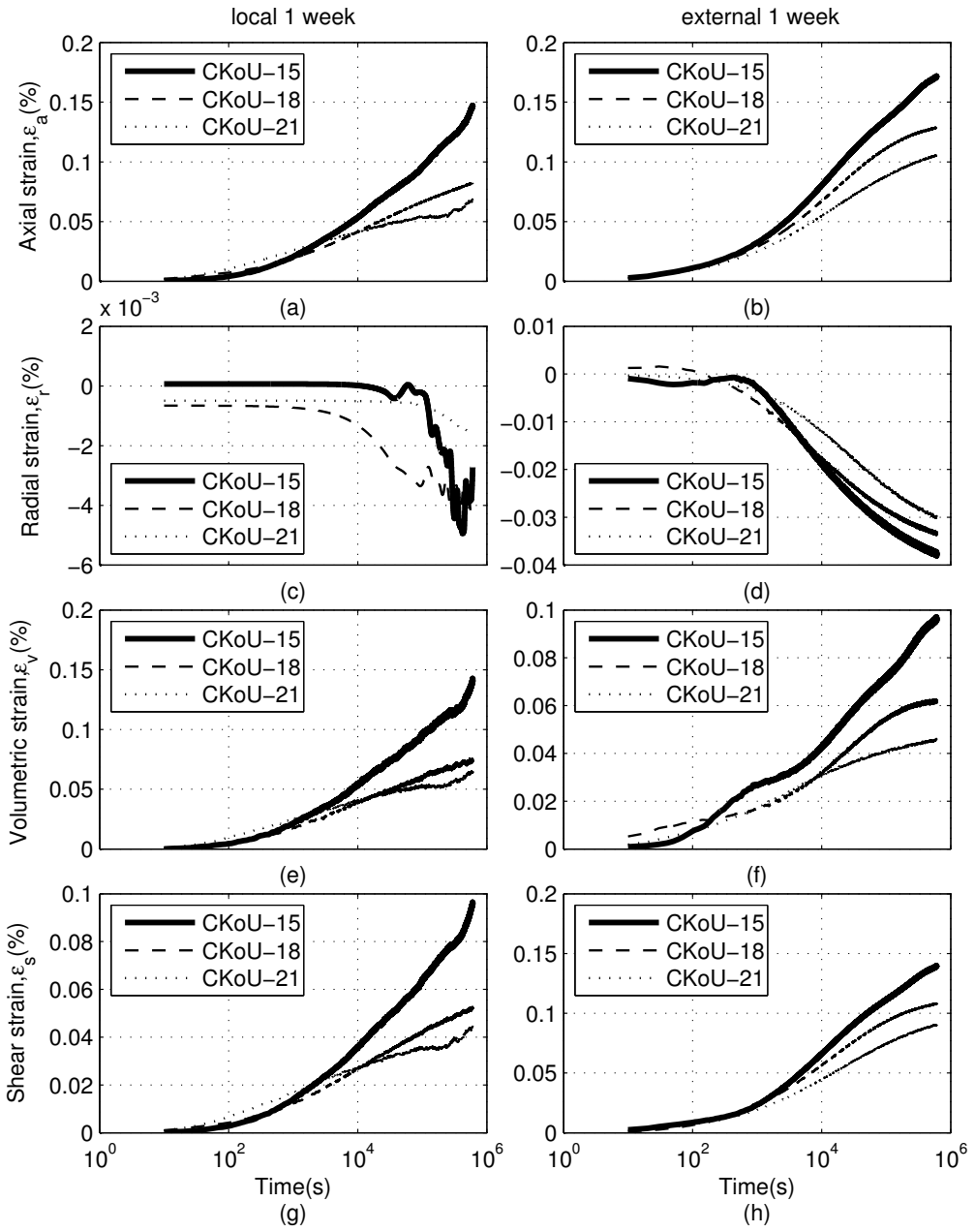

Figure 4-8 Creep of K_0 consolidated loose samples i.e. 1 week creep (CKoU-15, CKoU-18 and CKoU-21) at 120, 60 and 30 kPa of confining pressure, respectively

4.4 Creep Following Isotropic Consolidation

4.4.1 General

Comparing creep of isotropic and K_0 consolidated samples can be viewed from two different perspectives – i.e. whether K_0 consolidation or isotropic consolidation is used as a reference. If we deem K_0 consolidation as the reference then there are two possibilities. Firstly, the isotropic consolidated sample is aimed at the same mean effective stress of the K_0 consolidated sample, which basically means comparing creep at different stress ratios (e.g. Mejia,1988; and Howie *et al* , 2002). Secondly, the isotropic sample is consolidated to the same effective confining pressure as the K_0 sample first, and then is sheared to the same end points of the consolidation stress path of the K_0 consolidated sample (Ibraim *et al.*, 2009). On the other hand, if we use the isotropically consolidated sample as the reference, for the GDS apparatus used in this study, it means comparing creep of samples which are aimed at the same effective confining pressure of consolidation. Thus we compare creep due to the combined effects of different mean effective stress and stress ratio. This case was chosen for this study considering the fact that isotropic consolidation is still the common practice in the industry.

4.4.2 Loose moist tamped samples

Examples of creep following isotropic consolidation on loose samples at 30 kPa confining pressure (TWIU-34 and TWIU-35) for 1 hour and 1 week of creep time, respectively, are presented Figure 4-9.

Both local (Figure 4-9 (a)) and external (Figure 4-9 (b)) systems show that axial strains are increasing with time. Likewise, the volumetric strains are also increasing (meaning compressing) with time. One hour sample shows that shear strain, locally (Figure 4-9(e)) and externally (Figure 4-9 (f)) is approximately zero, which was expected. However the one week sample shows that positive shear strains are developing. It suggests some microstructural changes are occurring over

time causing shear, despite the fact that shear strain is zero when creep starts. Overall the local and external measurements are very similar throughout.

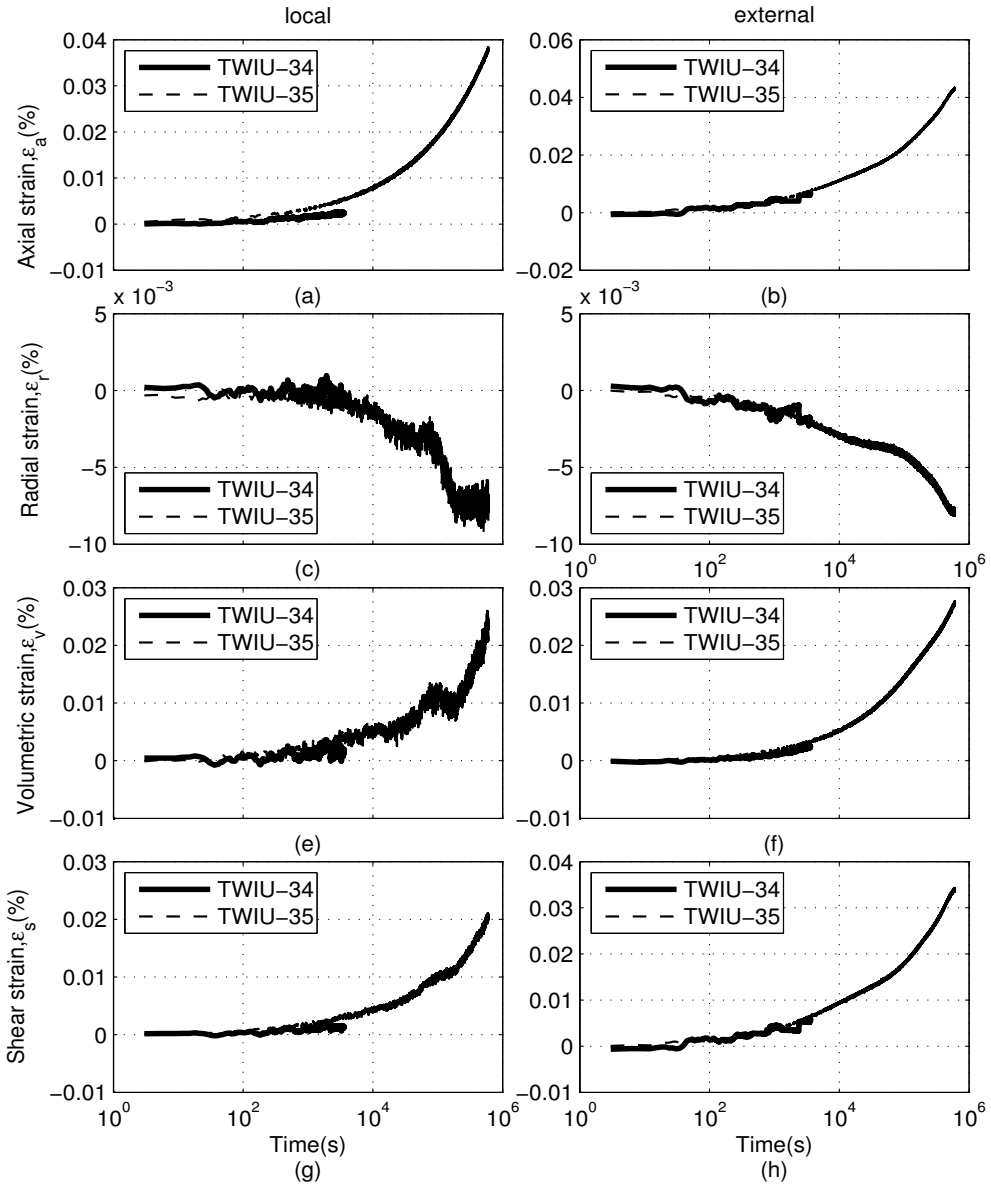

Figure 4-9 Strains of isotropically consolidated loose samples at 30kPa confining pressure (TWIU-34 and TWIU-35) for 1 hour and 1 week creep, respectively

4.4.3 Dense moist tamped samples

4.4.3.1 Effect of moist tamping on samples at low confining pressure

One set of tests on dense samples at 30 kPa confining pressure (CIU-10, CIU-11 and CIU-12) for 1 hour, 1 day and 1 week creep time, were performed for creep following isotropic consolidation. Figure 4-10 shows all strains developed from both local and external measurements.

It can be seen from Figure 4-10(a) that local axial strain tends to increase with time up to about $3x10^5$ seconds (≈ 3.5 days) and then starts to decrease but the sample is still in compression. One possible explanation is that particle rearrangements due to creep vary from time to time thus fluctuation is not uncommon. On the other hand, Figure 4-10(b) shows an unexpected result, where external axial strain for one week aging becomes negative indicating swelling. One possible explanation is that to the amount of energy used during tamping was higher than the mean effective stress at the end of consolidation. Frost and Park (Frost & Park, 2003), in their critical assessment of the moist tamping method, reported that the amount of energy required to prepare dense moist tamped samples is significantly higher than that required to prepare loose samples, as illustrated in Figure 4-11. The figure implies that there is a minimum initial confining stress if we want the moist tamped sample to be normally consolidated, regardless of whether the soil is clean sand or silty sand. It is likely that that low confining pressure used here (30kPa) is less than the applied stress experienced by the soil during the compaction i.e. the soil tends to be over-consolidated. Therefore unloading occurs during creep. Whereas for K_0 consolidated samples at the same confining pressure and density (CKoU-8 and CKoU-9), axial strains are in compression. This is likely that the mean effective stress at the end consolidation is higher than the applied stress during tamping. It is interesting to observe and compared the creep of a dense dry pluviated sample following isotropic consolidation of dense sand, with no pre-stress applied (see section 4.4.4).

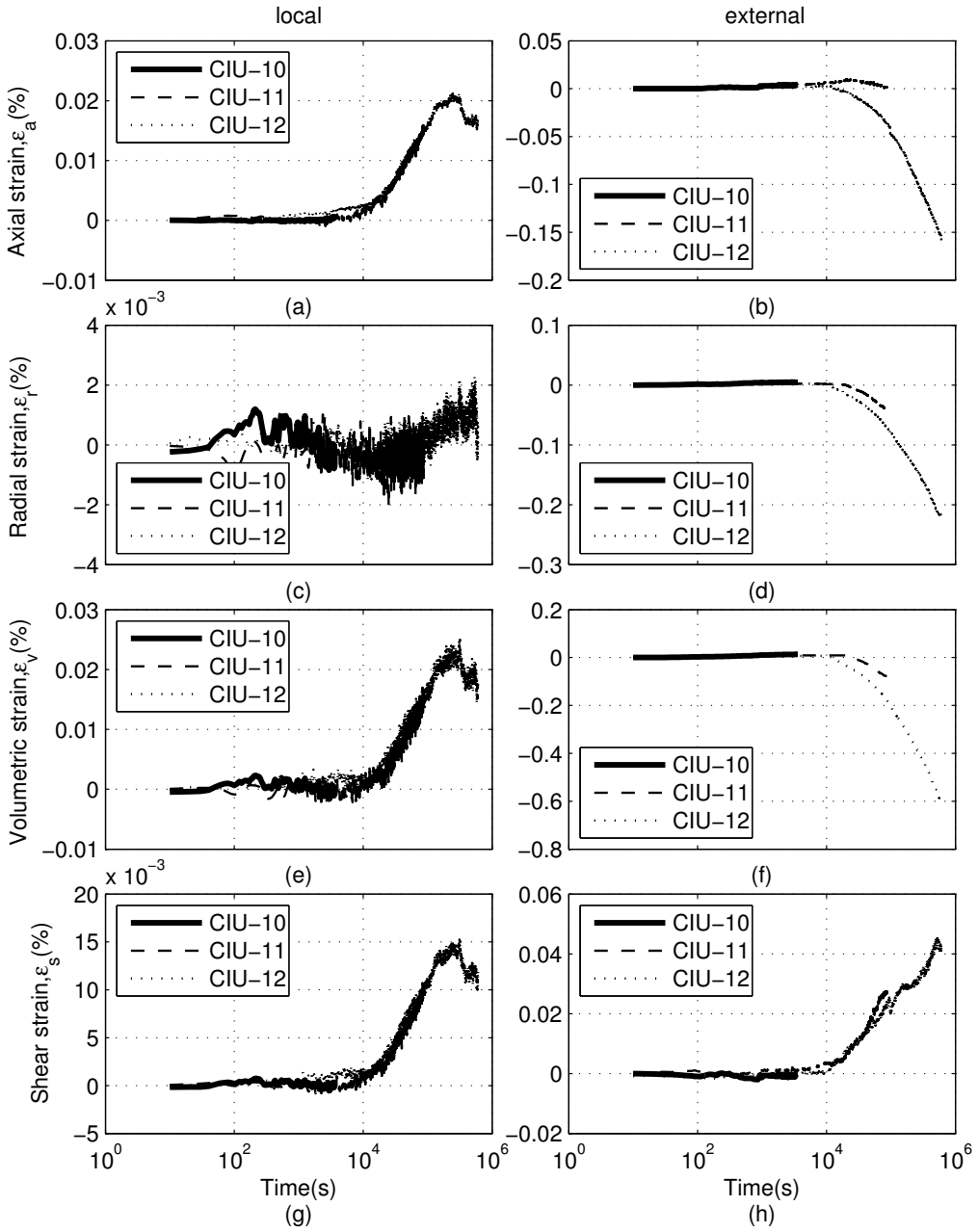

Figure 4-10 Strains of isotropically consolidated dense samples at 30kPa confining pressure (CIU-10, CIU-11&CIU-12) for 1 hour, 1 day and 1 week of creep

Up to one day creep, local radial strain, shown by Figure 4-10(c), is practically zero. Then the radial strain tends to increase in compression. This may explain why the local axial strain starts to decrease from 3.5 days. However Figure 4-10(d) shows the opposite trend to local strains where the external radial strains are expanding with time. Again, this may be due to variation in local void ratio at the mid-height of the sample (where local strain been measured), which differ from the average across the whole cylindrical sample. External volumetric strain demonstrates that the sample swells more with time whereas local volumetric strain is still in compression but starts to change direction toward swelling after 3.5 days. The different trend in volumetric strain locally and externally is likely due to variation in localized factors such as void ratio. Moist tamped samples (clean sands) are known to be less uniform in terms of void ratios compared to other methods of deposition (Frost & Park, 2003; Vaid *et al.*, 1999). Figure 4-10(g) shows that local shear strains follow the same trend as local axial strain because local radial strain is very small compared to local axial strain. On the other hand external shear strain increases with time at a decreasing rate.

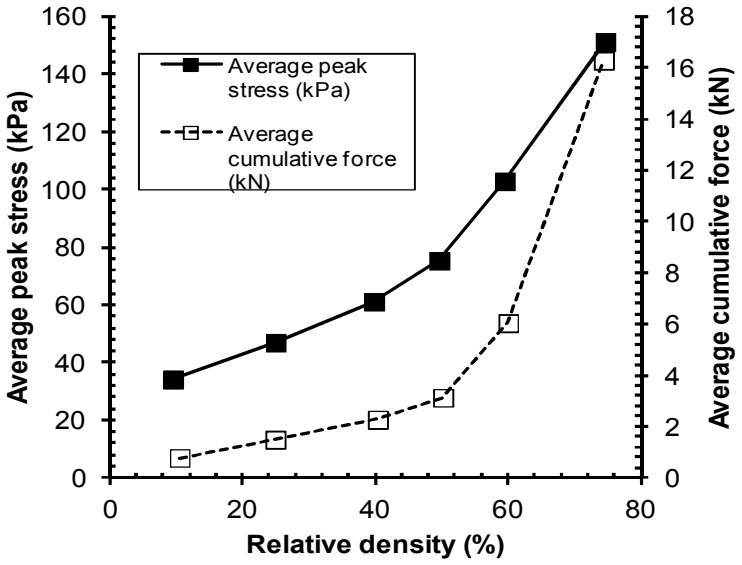

Figure 4-11 Average peak stress and cumulative force during tamping for various relative densities (Frost & Park, 2003)

4.4.3.2 Effect of confining pressure

Unlike creep following K_0 consolidation, investigating the effect of confining pressure on creep following isotropic consolidation (CIU-11&CIU-27) is relatively simple because the stress ratio at the beginning of the creep is equal to unity. This is illustrated in Figure 4-12, based on test CIU-11 for 30kPa confining pressure and CIU-27 for 60kPa confining pressure.

The first main feature is that overall (externally) the sample at 30kPa confining pressure appears to swell more than the sample at 60kPa, as shown by volumetric strain in Figure 4-12(b). Additionally the 60kPa sample appears to experience "delayed" swelling due to higher confining pressure. This external behavior supports the observation of the combined effects of confining pressure and stress ratio on creep following K_0 consolidation as discussed in section 4.3.4. However, again the overall global behavior was not manifested locally at the mid-height of the sample, as in Figure 4-12(e). Local volumetric strain for samples at both confining pressures are still in compression with the 30kPa sample being less compressive (or contractive) than the 60kPa sample. The next feature is regarding shear strain. Externally, the 30kPa sample exhibits increasing positive shear strain with time, whereas 60kPa sample develops negative shear strain. Locally, shear strains have the same trend as volumetric strain where the 30kPa sample develops less shear strain than the 60kPa sample.

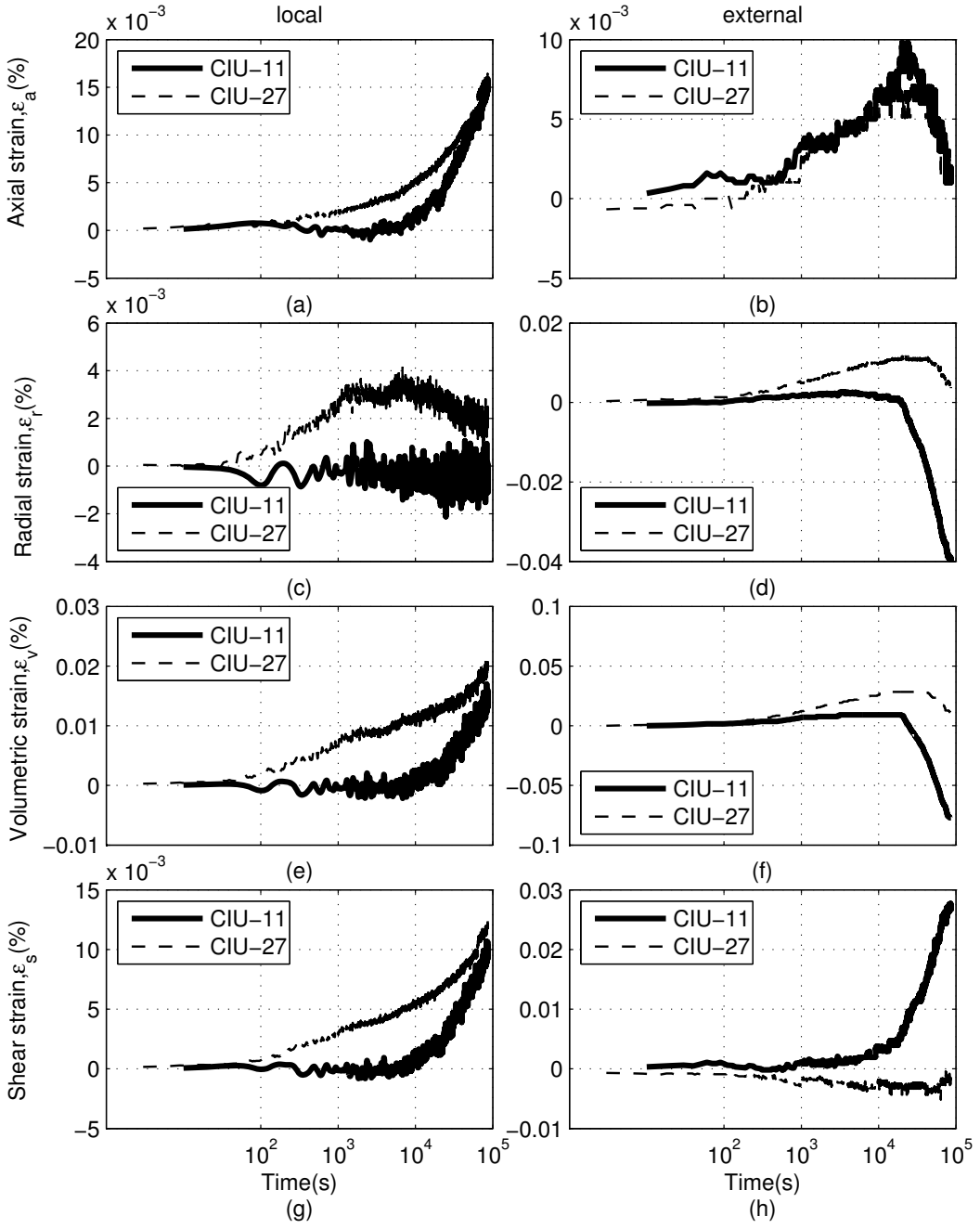

Figure 4-12 Strains of isotropically consolidated dense samples of 1 day creep (CIU-11 &CIU-27) at 30 kPa and 60 kPa of confining pressure, respectively

4.4.4 Dry pluviated samples

A few tests were done on samples with different methods of preparation i.e. dry funnel pluviation (see 3.3.2). Only dense cases were tested because medium dense to dense samples could be prepared using dry pluviation. Additionally it is interesting to see whether the 'different' trend between local and external strains as found in dense moist tamped samples would also be observed for dry pluviated samples, which are more uniform (Frost & Park, 2003; Vaid *et al.*, 1999).

Figure 4-13 shows creep of dense dry pluviated samples at 60 kPa confining pressure which was K_0 consolidated (CKoU-22 and CKoU-23) for one minute and 1 day aging, respectively. The figure shows that axial strain is compressive, similar to the behavior of moist tamped samples. Figure 4-13 (a) and Figure 4-13 (b) show that local and external axial strains are relatively similar in term of the magnitude (external axial strain is only slightly greater than local one) Figure 4-13 (c) and Figure 4-13 (d) show that in term of radial strain, K_0 consolidated sample is in expansion, locally and externally. Regarding volumetric strain, Figure 4-13 (e) and Figure 4-13 (f) show that up to $2x10^4$ s≈5.6 hours (when volumetric strains are still in contraction), local and external volumetric strains are relatively similar in magnitude. Despite of that we still see different trends between local and external volumetric strain as in dense moist tamped samples i.e. locally the soil is still in contraction whereas externally the soil shows dilative behavior. Figure 4-13 (c) and Figure 4-13 (d) show that up to $2x10^4$ s≈5.6 hours (when external volumetric strain start to dilate), local and external volumetric strains are relatively similar in magnitude. One possible explanation is because the material used in this study is silty sand whereas the material used by (Frost & Park, 2003; Vaid *et al.*, 1999) to assess the uniformity of sample preparation is clean sand. The presence of fine grains adds to the anisotropy of the sample hence creates more variation in local factors such as void ratio compared to clean samples prepared by the same method. For shear strain, a similar trend was observed locally and externally.

Figure 4-14 shows creep of dense dry pluviated samples at 60 kPa confining pressure which was isotropically consolidated (CKoU-24 and CKoU-25) for one minute and 1 day aging, respectively. The figure demonstrates that local and external axial strains are generally positive indicating compression. This is likely because dry pluviated method does not involve pre-stressing during its deposition as in the moist tamped sample. Therefore the soil tends to be normally consolidated with minimum swelling tendency. This supports observation before that swelling tendency for dense moist tamped samples i.e. CKoU-11 and CKoU-12 (see Figure 4-10) is because the samples experience higher applied stress during tamping than mean effective stress at the end of consolidation. Both local and external radial strains indicate that the sample, up to one day aging, is in compression. Similarly, volumetric strains from local and external system suggest the sample is in compression. Likewise, local and external shear strains are in positive direction. And as expected, the magnitude of shear strain is much less in the isotropic sample than the dry pluviated sample.

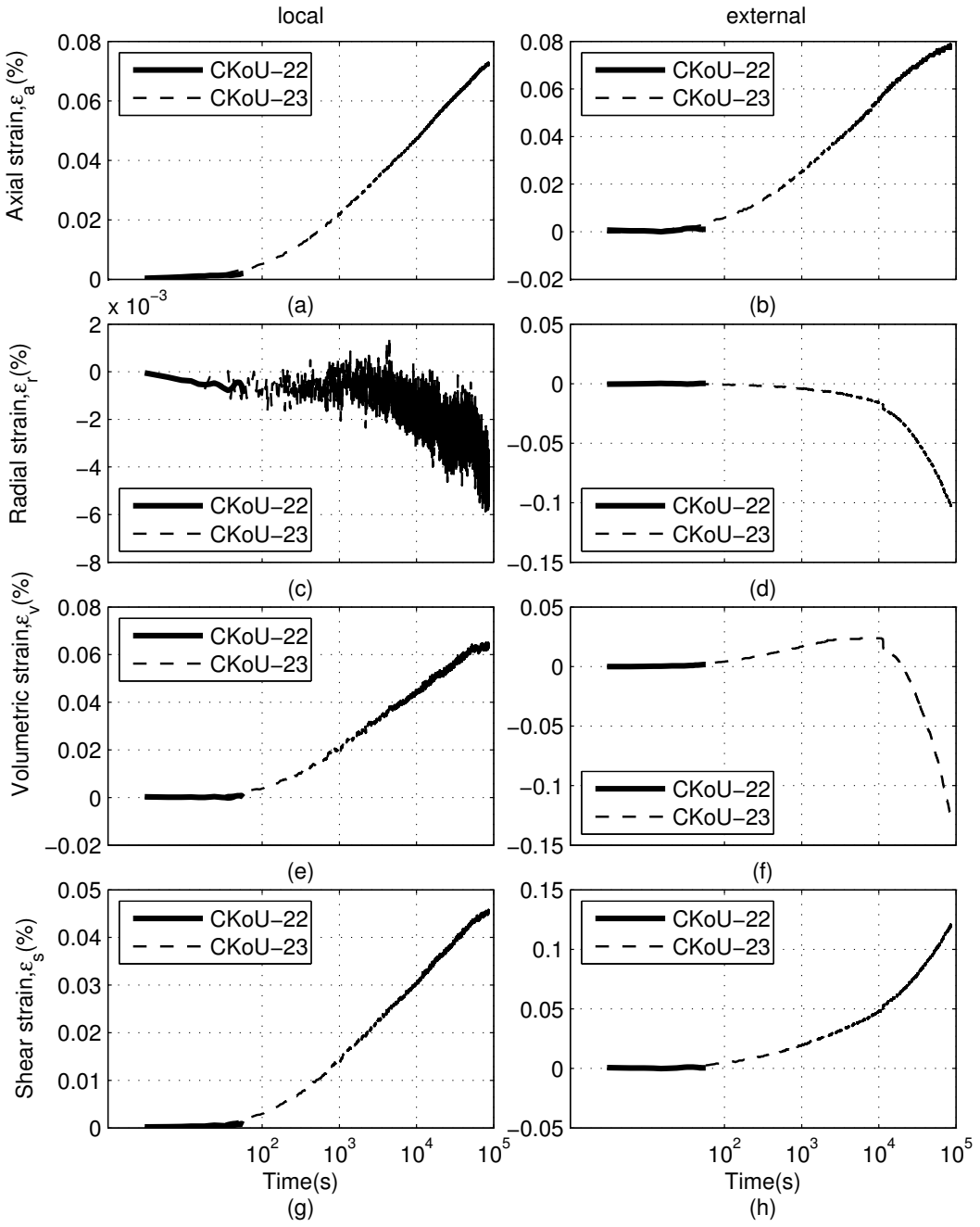

Figure 4-13 Strains of K_0 consolidated dry pluviated dense samples at 60kPa confining pressure (CIU-22&CIU-23) for 1 min and 1 day creep time

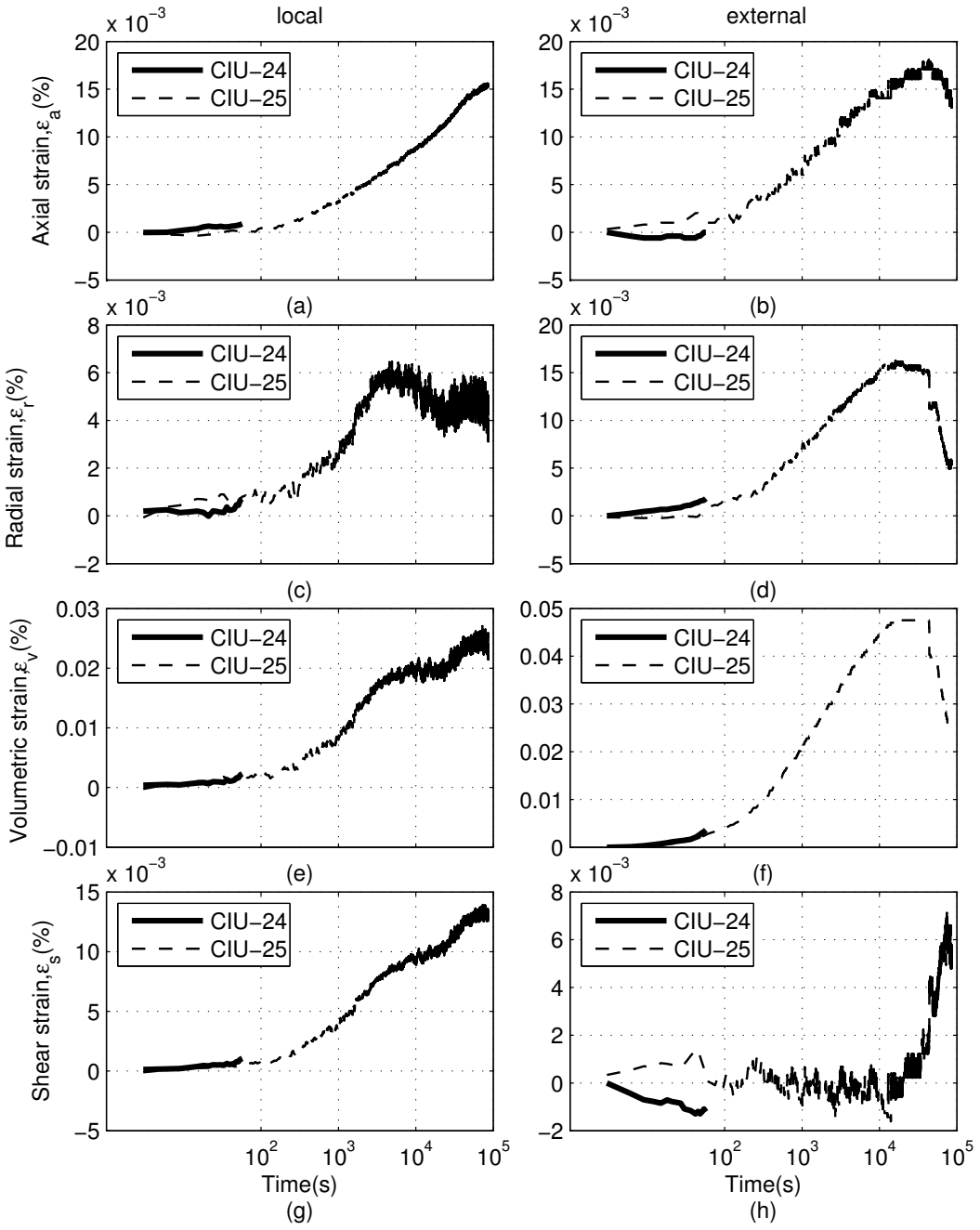

Figure 4-14 Strains of isotropically consolidated dry pluviated dense samples at 60kPa confining pressure (CIU-24&CIU-25) for 1 min and 1 day creep time

4.5 Discussion

4.5.1 Local and external measurement

The figures in the previous section (section 4.3 and 4.4) show that there appear to some differences (either magnitude of strain or trend) in local and external measurements. Some possible explanations are explained below:

(a) Due to difference in what is being measured

Local volumetric strain was calculated from a discrete radial strain measurement made at the mid-height of the sample, and axial strain made over a 65mm gauge length (see Eq. 4-1). Thus local volumetric strain is sensitive to local variation factors such as local void ratios and bulging due to uneven loading. External volumetric strain is measured from the volume change across the whole cylindrical sample and external axial strain. External radial strains are calculated from volumetric strain and axial strain assuming uniform 'average' strains.

(b) Due to non-uniform creep strains at the end of the sample

Bowman (2002) used fixed ends for all of her tests on creep of uniform sand at high stress ratio. Bowman (2002) thought that barrelling at the mid-height of the sample had something to do with the difference between local (where radial expansive strain was greater locally) and external strains that were developed. This study used frictionless ends where two layers of membranes (with high vacuum grease in between) were put at both ends of the sample. It seems by having this; the end of the sample may have expanded more than the middle as sketched in Figure 4-15. Even for K_0 consolidated samples higher axial strain was observed for the external measurements than for the local ones. This suggests that compliance at the ends is still important and cannot be ignored.

Considering the potential strain errors and the measured strains (see Appendix B), local axial strain is well within the sensitivity of the transducer whereas the

measured local radial strain is beyond the sensitivity of the transducer. Despite of this, the tendency is quite consistent across the tests that radial strain tends to expand over time. In term of external measurement, local axial strain is also beyond the sensitivity of the transducer whilst some of the volumetric strains are within the sensitivity of the volume change. It should be noted however that external measurement both axial and volumetric are affected by bedding error. Nevertheless, a consistent tendency of dilation was observed for longer aging duration.

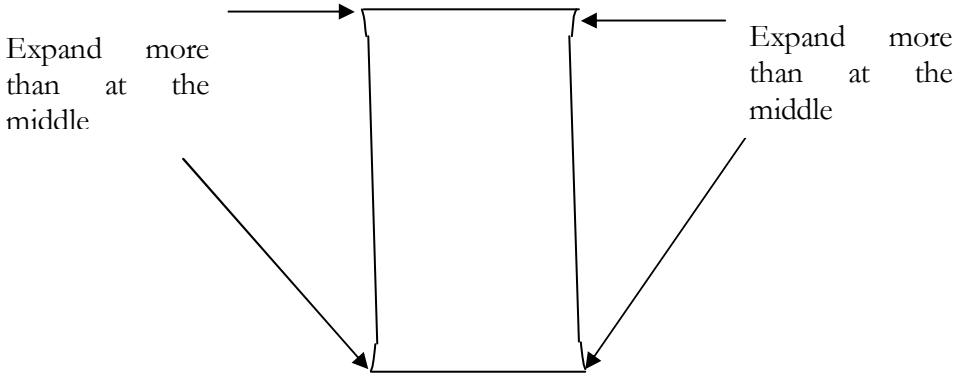

Figure 4-15 Suggested non-uniform creep strains between both end of the sample and that in the middle due to the use of lubricated ends

4.5.2 Creep behavior of K_0 consolidated samples

4.5.2.1 Dense moist tamped samples

Dense moist tamped samples show that axial strains from local (Figure 4-3(a)) and external (Figure 4-3(b)) measurements increase in compression with time at a decreasing strain rate. This decreasing strain rate suggests that the deformation can be categorized as primary creep (Wang *et al.*, 2014). This was expected because creep was performed before the maximum deviator stress was reached. The relationship between times, on logarithmic scale, and axial strains is not linear for both local and external measurement as reported by previous studies who investigated creep of very dense dry pluviated clean sand with prepared relative density close to 100% (e.g. Lade & Liu, 1998). It should be noted however that Lade and Liu (1998) appear to record the data at discrete points, not

continuously as used in this study. A similar trend as in this study was reported by Bowman (2002), who performed approximately one day creep of dense clean sand (Dr=±70%). The tendency of increasing axial strain at a decreasing rate is similar to the increase in shear wave velocity (V_S) during aging as demonstrated from SCPT (Howie & Amini, 2004), resonant column test (Wichtmann *et al*, 2004) and bender element (Gao *et al.*, 2011), as explained in Chapter 2. This indicates that shear wave and axial creep strains are somehow related. Shear wave propagates through contacts between the grains, and as axial creep strain develops, some changes in contact between the grains occur which may be manifested in the change of shear wave velocity during aging.

Both local (Figure 4-3 (c)) and external (Figure 4-3 9d)) systems show that negative radial strain tends to increase with time which suggests some expansion in the radial direction with time. A similar observation was reported by Bowman (2002) for dense air pluviated clean sand. This suggests if the radial direction is restrained, there will be an increase in radial stress during aging as hypothesized by Bowman and Soga (2002). Jirathanathaworn *et al.* (2009) observed an increase in radial stress, via photo-elastic method, during sustained loading of glass rods. Field observations from dilatometer tests have indicated that during aging the horizontal stress index increases (Saftner, 2011a). These observations add to the Bowman's (2002) hypothesis that radial stress increases during aging of dense soils, and the increase may occur not only at high stress (deep soil) but also low stress (shallow depth soils).

There appears to be different trend of volumetric strain development locally (Figure 4-3(e)) and externally (Figure 4-3 (f)) with time. Local system shows that the soils, up to one week of aging, generally appear to be still in the initial compression stage, no dilation yet. Whereas external volumetric strain demonstrates that the soils start to dilate at about 10^4 seconds (2.8 hours). This may be explained by what is being measured by both systems. Local volumetric strain was calculated from a discrete radial strain measurement made at the mid-height of the sample, and axial strain made over a 65mm gauge length (see Eq. 4-1). Local volumetric strain

assumes constant strains over certain volume but is based on the assumption that strains actually vary locally. Thus local volumetric strain is sensitive to local variation factors such as local void ratios and bulging due to uneven loading. While external strain is measured from the volume change across the whole cylindrical sample. This issues is further discussed in 4.5.1

Shear strains from local (Figure 4-3 (g)) and external (Figure 4-3(b)) measurements show that they are increasing with time. Similar tendency was also observed by Bowman (2002) for dense air pluviated clean sand.

4.5.2.2 Loose moist tamped samples

A similar trend of axial creep for loose K_0 consolidated samples as for dense ones is observed from Figure 4-4 (a) and Figure 4-4(b), local and external measurements, respectively, where axial strain increases in compression with time at a decreasing strain rate. This is in accordance to Shozen (2001) and Lam (2003) who performed aging tests on loose Fraser River sand.

Neglecting one hour measurement, external radial strain measurement on the other hand gives some interesting insights. Despite higher axial strains, loose samples tend to have lower radial measurement. Theoretically as the deviator stress during creep was targeted to be constant (in addition to the constant back pressure and cell pressure) it reasonable to expect some immediate changes in the radial strain due to axial creep strain. One possible explanation is that dense soils have a higher particle coordination number than loose soils (Alim *et al.*, 2006; Wang *et al.*, 2008). Due to this, it is reasonable to expect that even a small change in the axial strain of dense samples causes immediate change in radial strain. On the other hand, higher axial strain in loose samples may be due to local structure collapse (Bowman, 2002), which does not result in radial expansion. With greater volumetric contractive strains, as suggested by Murayama *et al.* (1984), local structure collapse is more likely to occur in loose sand at higher stress ratio due to kinematically unrestrained conditions.

4.5.2.3 Mechanics approach to volume change during creep

Based on the general trend of creep for both dense and loose samples, a conventional mechanics approach is used to understand the behavior. The behavior can be divided into two components i.e. pure shear and pure volumetric strain (Bowman, 2002). This approach is illustrated in Figure 4-16 and Figure 4-17, for dense and loose samples respectively (initial sample dimensions are represented by a red dashed line).

Results for loose samples, local and external volumetric strains have similar behavior i.e. contracting. On the other hand, for dense samples, what happen earlier for external volumetric strain (i.e. dilation after contraction), is still happening locally but it is taking more time to be manifested. Similar observation also was found by Bowman for dense clean sand (2002). Hence external volumetric strain is used here for this approach. Following K_0 consolidation, both dense and loose samples are in compression with the axial stress being greater than the radial stress. Therefore for pure shear both samples induce a positive shear strain (axial compression with time and radial expansion with time).

For dense soil, added to this is the pure volumetric response which is changing from contractive to dilative with time with a degree of shearing with time (Bowman, 2002). The contractive mechanism mainly involves particle rearrangement into a tighter packing. This particle rearrangement may be facilitated by abrasion and grinding of particle surface asperities; breaking or crushing of particle surface protrusions and sharp particle corners and edges; and fracturing of particles (Mesri & Vardhanabhuti, 2009). As this study was performed under low stresses, the particle rearrangement of dense samples is likely due to the first and second factors only. Dilative mechanisms involve evolution of pore space, particle sliding and rolling. These occur as the force chain networks are being redistributed toward a more stable fabric. After some time, pore evolution then becomes the dominant process. With time, small pores merge and larger pores are then formed (causing expansion in the lateral direction) as the shear strain increases. As the

larger pores are formed, the average coordination number (inter-particle contact per particle) decreases (Kang *et al.*, 2012). In terms of pore orientation, with time more pores are elongated toward the direction of the principal stress (see Chapter 6 for further discussion). A pore space elongated along the major principal stress direction is more stable than that along the minor principal stress (Iwashita & Oda, 2000).

For loose samples, as creep proceeds, larger pores enclosed by larger numbers of grains start to collapse (due to contractive response), forming smaller, pores with a higher average coordination number. This collapse can explain why radial expansion in loose samples is less than in dense samples. Likewise, the pore orientation also evolves toward major principal direction thus forming more stable arching.

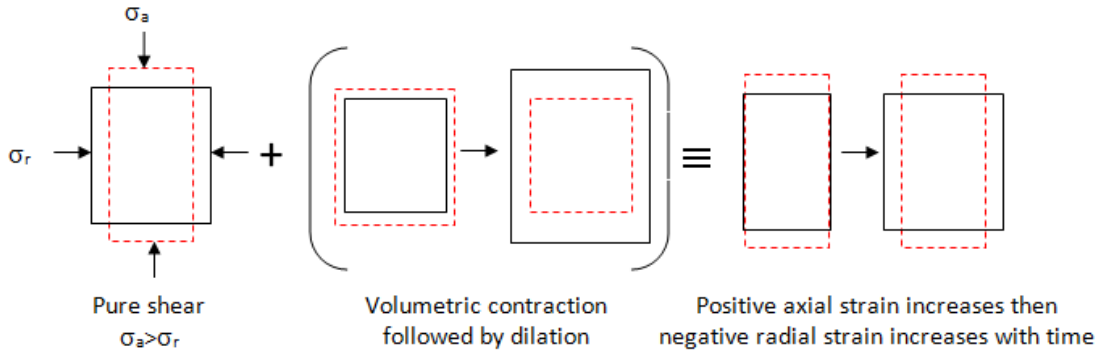

Figure 4-16 Development of strain with time for dense sample (after Bowman, 2002)

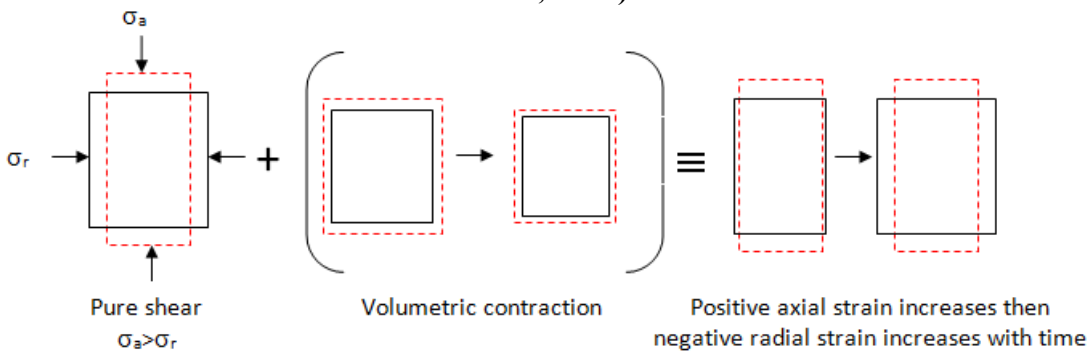

Figure 4-17 Development of strain with time for loose sample (after Bowman, 2002)

4.5.2.4 Creep comparisons: dense versus loose

Generally for the same confining pressure and period of creep, axial strains for loose samples tend to be greater than those of dense samples as exemplified by Table 4-3. This occurs despite loose samples generally having a lower stress ratio for K_0 condition. Hence, the mean effective stress is lower than for dense samples (see Table 4-2). Previous studies show that higher stress ratio causes higher creep strain (Howie *et al.*, 2002; Lam, 2003; Mejia *et al.*, 1988). Likewise higher mean effective stress results in more creep strain (Lam, 2003). This suggests that density has a more significant effect on creep, because the compressibility of loose samples at 60kPa confining pressure is approximately three times the compressibility of dense samples at the same confining pressure (see Table 4-2). This relatively higher compressibility is likely to cause local structure collapse, as suggested by Bowman and Soga (2002) which in turn causes higher axial creep. This local structure collapse is likely to occur for sand that contains a relatively low amount of fines (Yang & Wei, 2012). It should be noted that this trend may be different for other type of soils than used in this study. Wang *et al* (2008) found that loose *Ottawa* sand exhibited less axial creep compared to dense sand, whereas axial creep strains in loose *Toyoura* sand are higher than in the dense case. Wang *et al* (2008) believed that the effect of density on aging varies with the type of sand. There is no explanation by Wang et al (2008) about what does type of sand mean but the Author of this thesis believes this is likely due to different particle shapes of Ottawa (round shape) and Toyoura sand (angular shape). Soga *et al*. (2001) reported that particles shape influences creep behavior where angular particles are more liable to creep. Interestingly, the difference between axial strains for loose and dense samples tends to decrease as the period of creep increases. For example, one week of aging for loose samples results in approximately 1.7 times the local axial strain of dense sample. However, for one day and one hour creep period, loose samples exhibit axial strain 2.1 and 2.2 times that of dense samples. The same trend was observed from external measurements.

In general as shown by the local measurements, looser samples tend to develop greater volumetric contractive strains. Table 4-3 also demonstrates that loose samples tend to experience greater shear strain with time than dense samples. This tendency is also in accordance with observations from numerical modelling (Wang *et al.*, 2008), who reported that the mean contact shear force after aging of loose samples tends to higher than for dense samples. This is likely to be due to lesser overall restraint of particle movement.

Table 4-3 Creep comparison of dense and loose K_0 consolidated samples

Strain		Dense			Loose		
		1 hour	1 day	1 week	1 hour	1 day	1 week
ε_a(%)	Local	0.013	0.032	0.047	0.028	0.067	0.079
	External	0.019	0.056	0.07	0.054	0.109	0.129
ε_r(%)	Local	-0.0002	-0.002	-0.003	-0.0002	-0.002	-0.004
	External	-0.003	-0.036	-0.069	-0.007	-0.028	-0.033
ε_v%)	Local	0.013	0.028	0.041	0.028	0.063	0.071
	External	0.013	-0.016	-0.068	0.040	0.053	0.063
ε_s(%)	Local	0.009	0.023	0.033	0.019	0.046	0.055
	External	0.015	0.061	0.093	0.041	0.091	0.108

4.5.3 Creep comparisons: K_0 consolidated versus isotropically consolidated samples

4.5.3.1 Loose moist tamped samples

Two sets of tests were available to compare creep following K_0 and isotropic consolidation on loose samples i.e. CKoU-19 vs. TWIU-34 (Figure 4-18) and CKoU-21 vs. TWIU-35 (Figure 4-19).

Loose isotropic samples exhibit less axial strain than K_0 samples both locally and externally, due to lower stress ratio compared to K_0. Likewise for the volumetric strains which are in compression both locally and externally. A similar tendency is also observed for positive shear strain development both locally and externally. In short, isotropic consolidated samples creep less (axial, volumetric and shear) than K_0 consolidated samples.

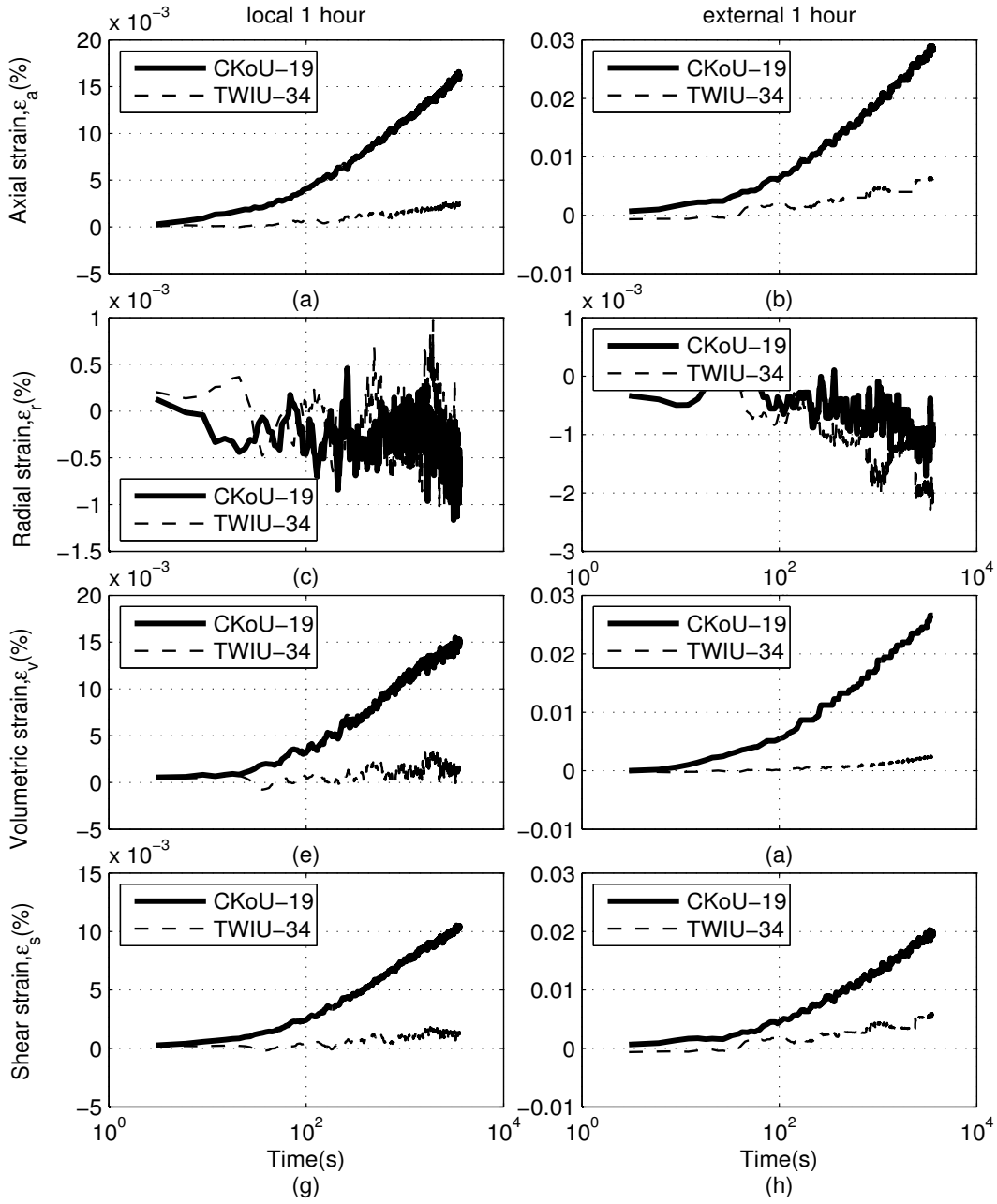

Figure 4-18 Comparison of 1 hour creep of loose moist tamped samples at 30 kPa confining pressure following K_0 and isotropic consolidation (CKoU-19&TWIU-34)

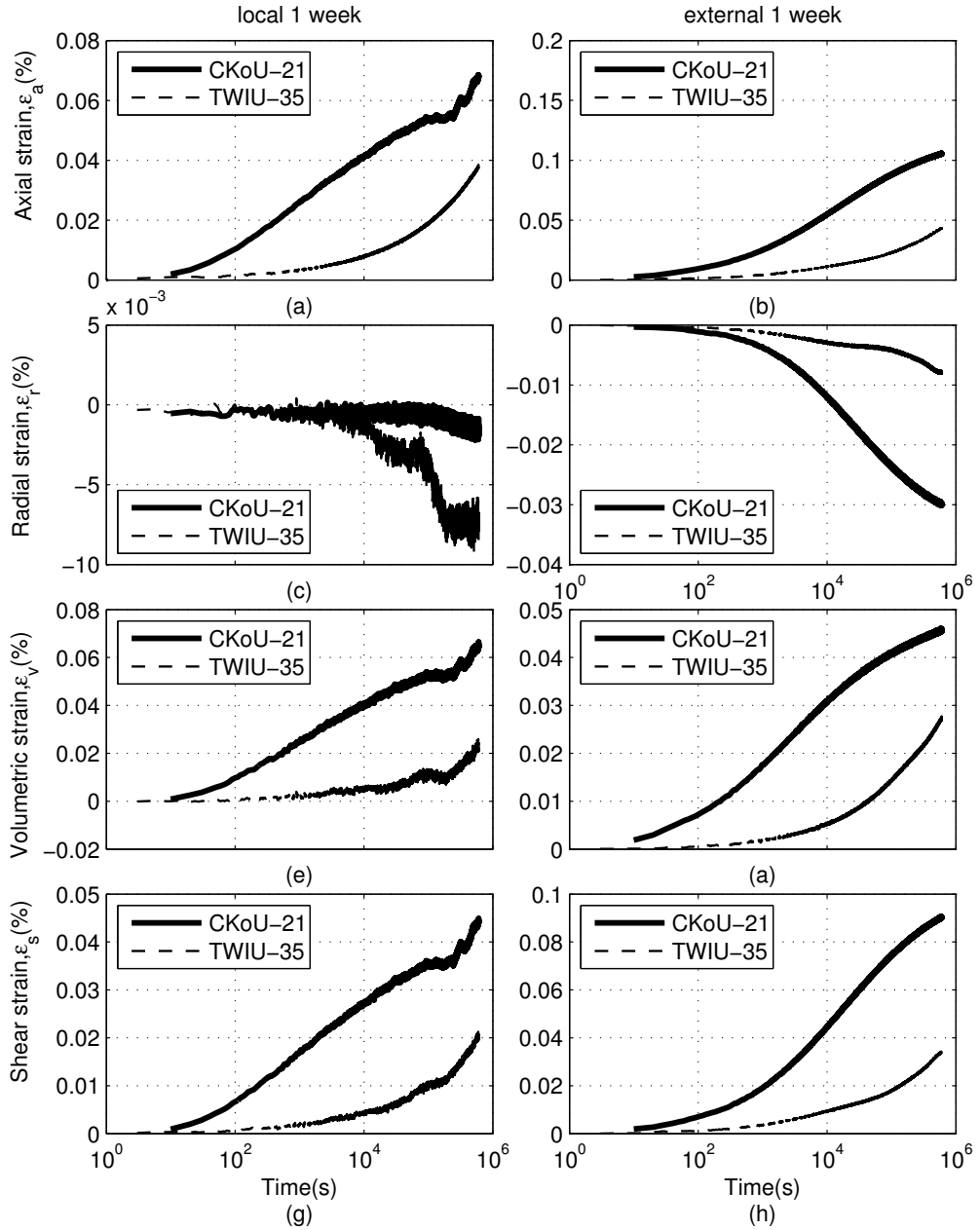

Figure 4-19 Comparison of 1 week creep of loose moist tamped samples at 30 kPa confining pressure following K_0 and isotropic consolidation (CKoU-21&TWIU-35)

4.5.3.2 Dense moist tamped samples

Creep comparisons following K_0 and isotropic consolidation of dense samples at 30kPa confining pressure are illustrated in Figure 4-20 (CKoU-8&CIU-11) for 1 day creep and in Figure 4-21 for 1 week creep. Creep comparisons for samples at 60 kPa confining pressure for 1 day of creep are shown in Figure 4-22 (CKoU-5&CIU-27).

It can be seen from Figure 4-20 (a) and (b) and Figure 4-21 (a) and (b) that K_0 consolidated samples exhibit more axial strain than isotropic consolidated samples due to a higher stress ratio and mean effective stress at the start of creep. The figure also reveals that there is a tendency of delay in the development of axial strain of the isotropic sample. This is likely due to the axial and radial stresses being equal, thus it takes some time for shear strain to develop. In terms of radial strain, up to one day aging time, the K_0 consolidated sample also exhibits more negative strain (expansion) than the isotropic consolidated sample. However for one week aging time, the isotropic sample expands more than the K_0 sample. Volumetrically, up to one day aging time, the K_0 consolidated sample, according to local measurement, tends to develop greater strain in contraction although external measurement shows both being dilative. Figure 4-21 (e), (f) shows a continuation tendency at the end of one day aging time i.e. according to external measurement, the isotropic sample dilates more than the K_0 sample. This is likely due to higher degree of swelling of the one week sample compared to the one day sample. Regarding the shear strain, it is clear that the isotropic sample develops less strain than the K_0 sample.

Similar to 30kPa samples, for samples at 60 kPa local and external axial strains of K_0 consolidated samples are more compressive than isotropic samples. In terms of radial strains, the K_0 consolidated samples expand faster and greater than the isotropic samples. Regarding shear strain, K_0 consolidated samples generate more positive shear strain.

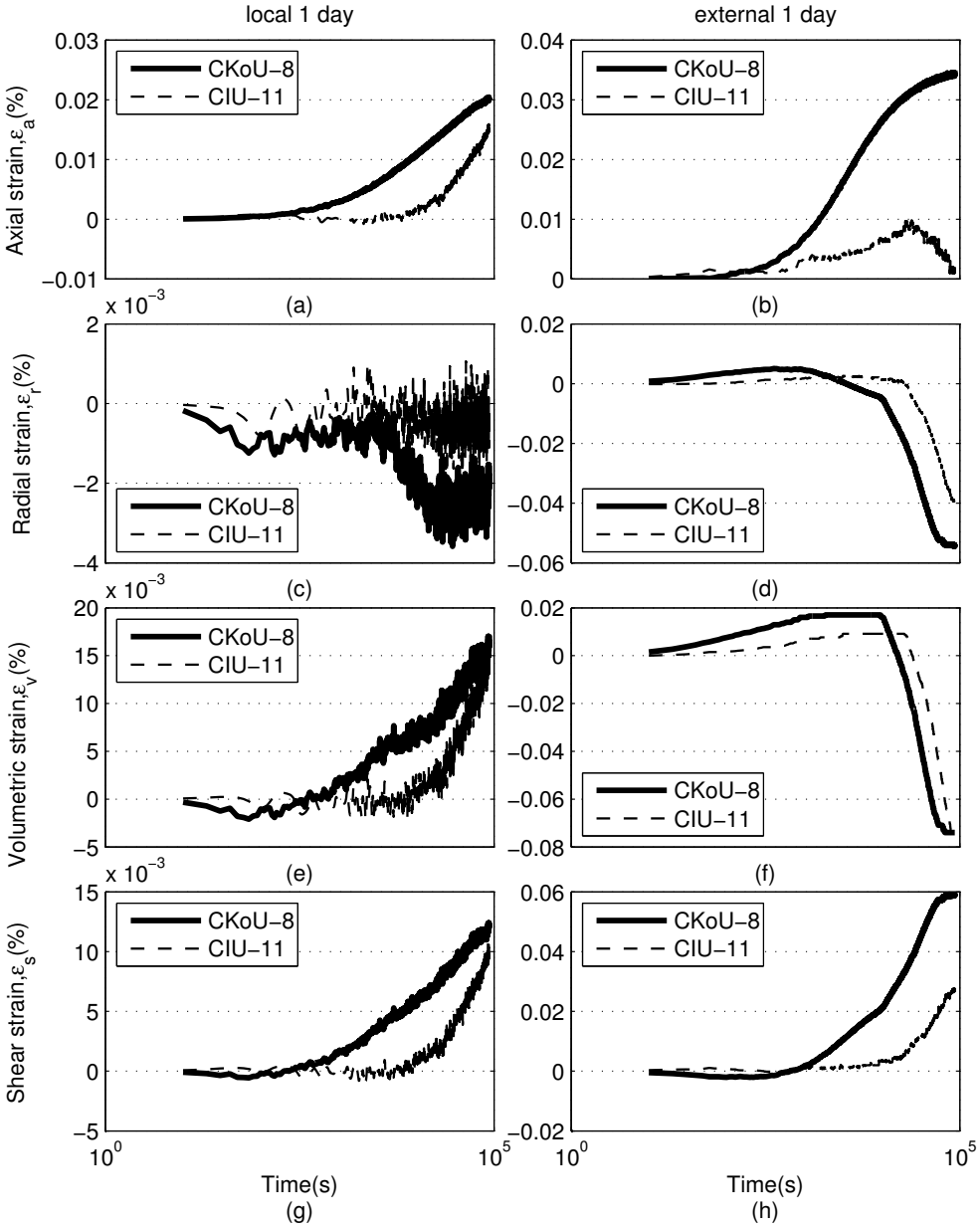

Figure 4-20 Comparison of 1 day creep of dense moist tamped samples at 30kPa confining pressure following K_0 and isotropic consolidation (CKoU-8 &CIU-11)

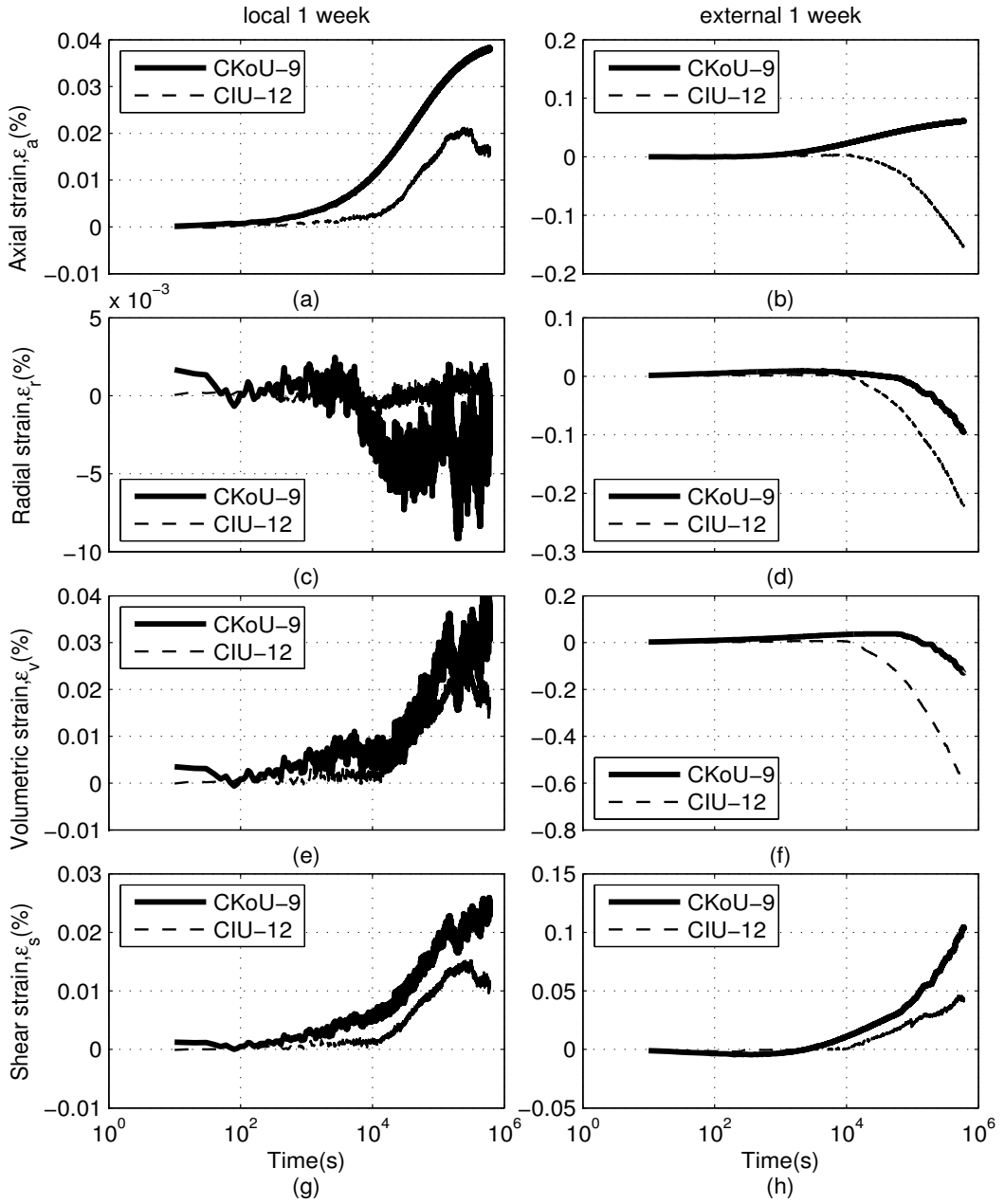

Figure 4-21 Comparison of 1 week creep of dense moist tamped samples at 30kPa confining pressure following K_0 and isotropic consolidation (CKoU-9 & CIU-12)

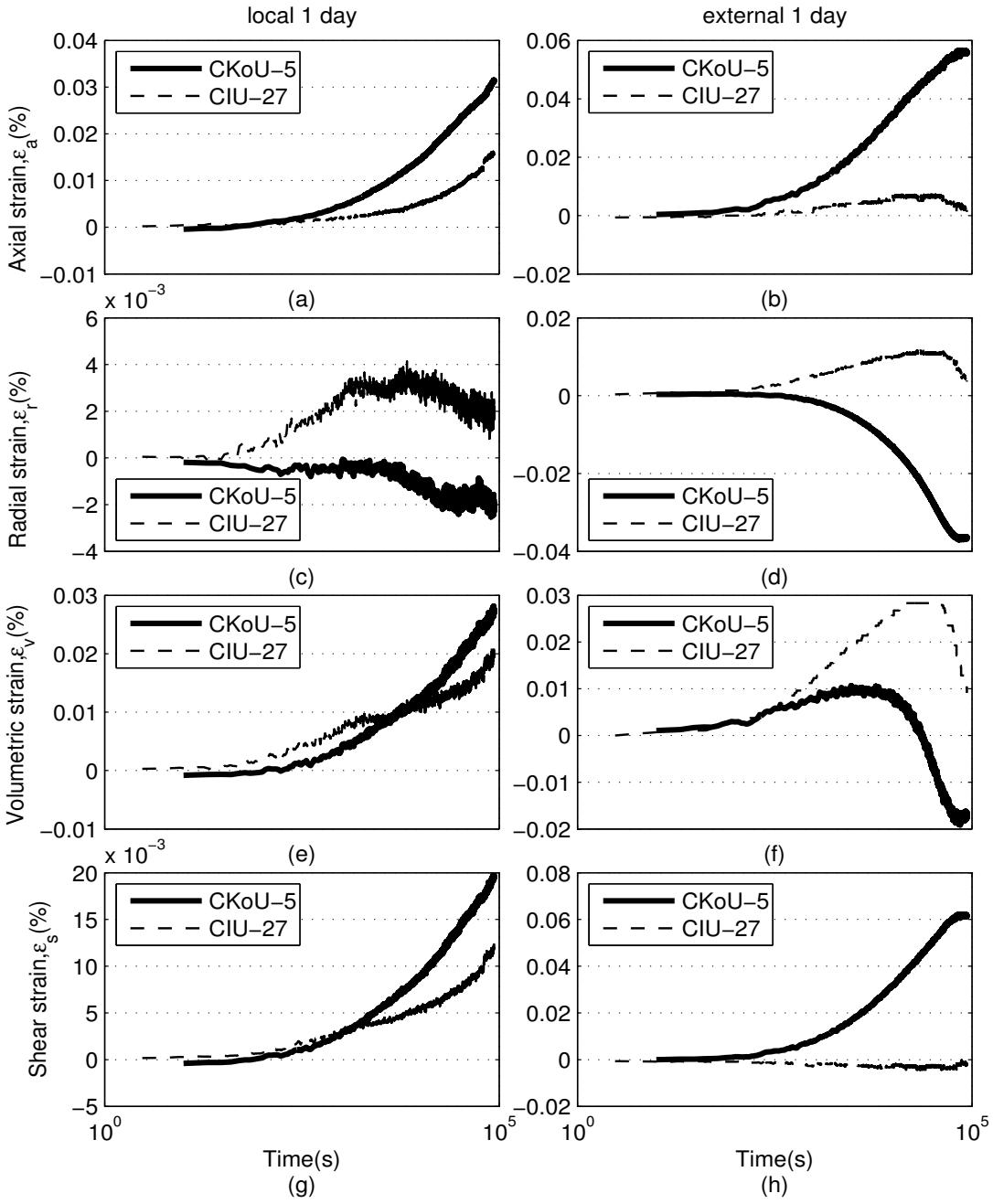

Figure 4-22 Comparison of 1 day creep of dense moist tamped samples at 60kPa confining pressure following K_0 and isotropic consolidation (CKoU-5&CIU-27)

4.5.3.3 Dense dry pluviated samples

Figure 4-23 shows strains of dense dry pluviated samples at 60 kPa confining pressure which were consolidated isotropically (CIU-25) and K_0 consolidated (CKoU-23) for one day creep. Generally similar trends, as in the case of dense moist tamped samples (section 4.5.3.2), were observed when comparing strains of K_0 and isotropically consolidated of dry pluviated samples. The dense dry pluviated K_0 consolidated sample develops more axial strain than the isotropic consolidated sample. The radial strain of K_0 dry pluviated sample exhibits expansion whereas that of the isotropically consolidated sample exhibits compression. Locally, volumetric strain of K_0 consolidated sample is more dilative than that of the isotropically consolidated sample. Finally, the K_0 consolidated sample develops more shear strain, locally and externally, than the isotropically consolidated sample.

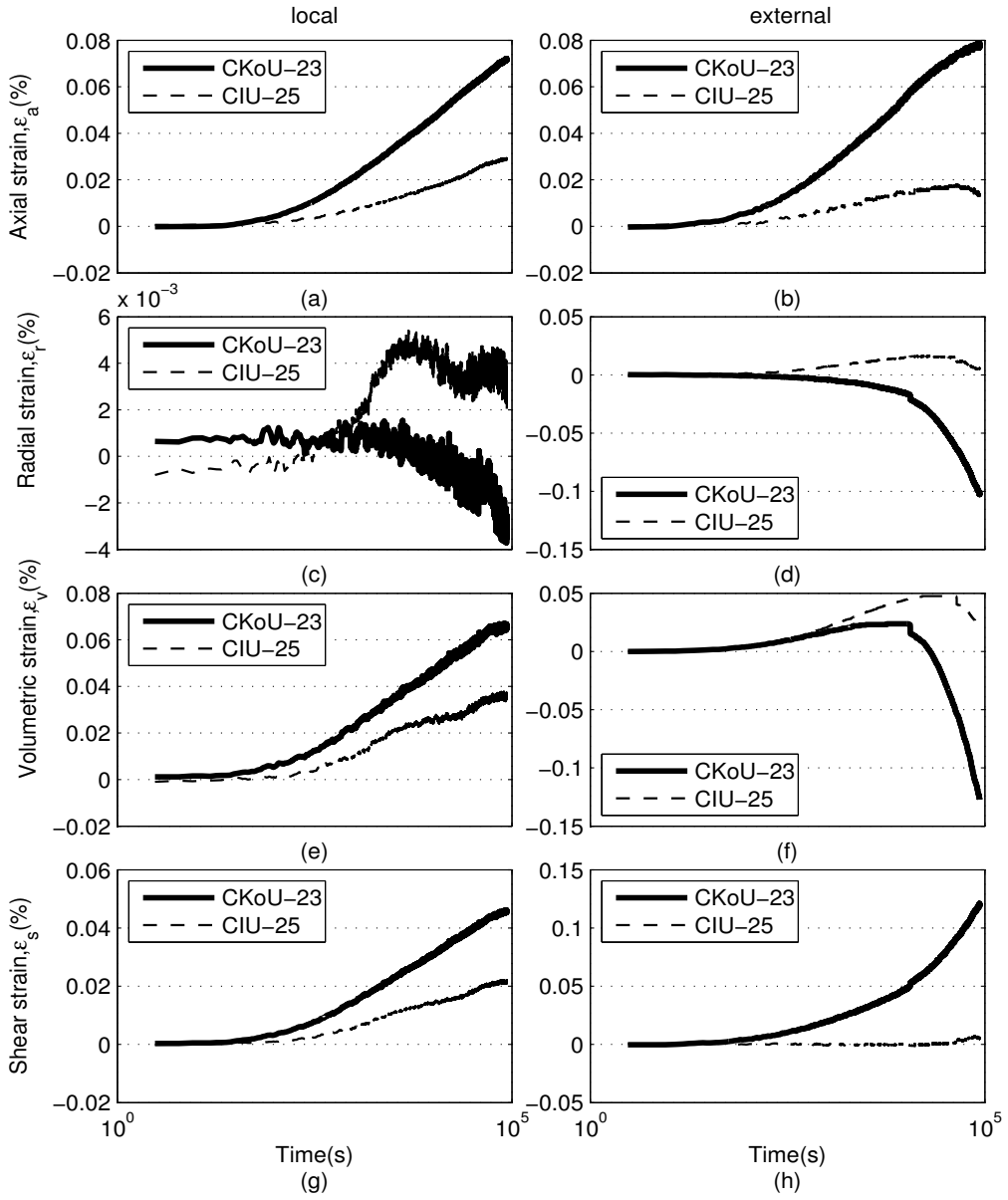

Figure 4-23 Comparison of 1 day creep of dense dry pluviated samples at 60kPa confining pressure following K_0 and isotropic consolidation (CKoU-23&CIU-25)

4.5.4 Creep comparisons: moist tamped versus dry pluviated samples

A comparison of creep of dry pluviated (CIU-25) and moist tamped (CIU-27) samples at approximately the same density following isotropic consolidation is shown in Figure 4-24.

The dry pluviated sample is more compressive than the moist tamped sample both locally and externally as presented in Figure 4-24 (a) and (b). This is likely because low energy deposition such as dry pluviation produces more unstable grain contacts i.e. compared to high energy deposition such as moist tamping (Yamamuro & Wood, 2004). Dry funnel pluviation produces fabric which has a preference for horizontal grain orientation whereas moist tamped produces a fabric in which grain orientation is fairly random with a slight bias towards the vertical (Jang & Frost, 1998; Yusa & Bowman, 2013). Therefore, dry pluviated samples produce fabric with contact normals less concentrated in the vertical direction compared to moist tamped samples (Yimsiri & Soga, 2010). Thus moist tamped samples have higher stiffness and more dilative behavior compared to dry pluviated samples (e.g. Ibrahim & Kagawa, 1991a; Lee, 2001). Furthermore, an interesting trend was observed from external axial strain. Both dry pluviated and moist tamped samples initially showed increase of axial strain with time and then this started to decrease at approximately the same time. The tendency of decreasing axial strain is not seen from local measurements, which showed increase till the end of creep time.

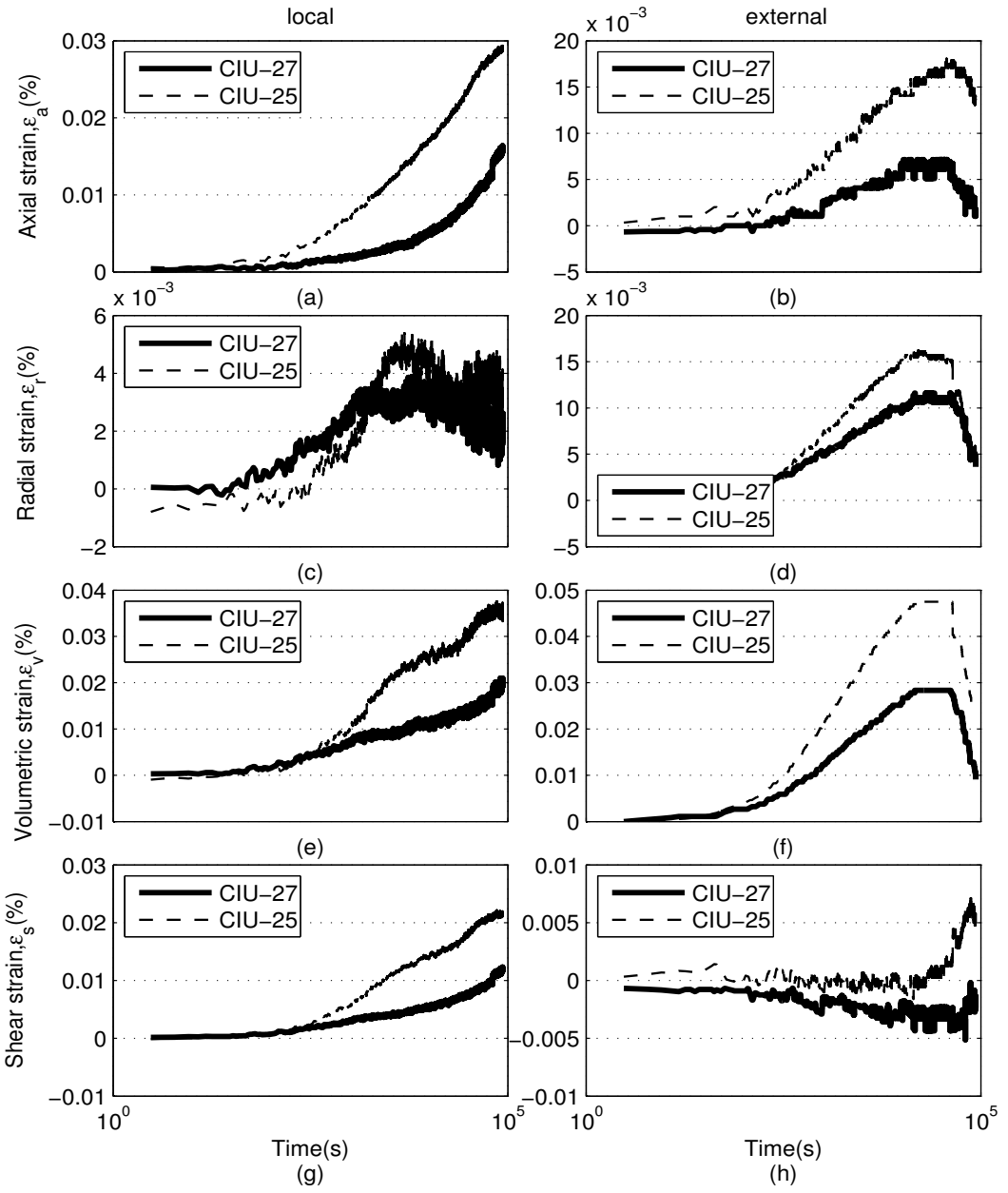

Figure 4-24 Creep comparison of 1 day creep at 60kPa confining pressure following isotropic consolidation for dense moist (CIU-27) and dry pluviated sample (CIU-25)

Figure 4-24(c) and (d) demonstrates that the dry pluviated sample exhibits greater radial strain compared to the moist tamped one. This in turn makes the volumetric strain of the dry pluviated sample also higher than the moist tamped one. Both dry pluviated and moist tamped samples show signs of changing creep strain direction at approximately 40000s. The moist tamped sample changes direction toward dilation at a lower volumetric strain than the dry pluviated sample. Local volumetric strains at the mid-heights of the samples, on the other hand, show no sign of changing direction; they are still increasing with time. Furthermore, local shear strains for both moist tamped and dry pluviated sample increase in a positive direction with time. An interesting trend was observed externally. The dry pluviated sample appears to have a delay in the development of positive shear strain. The shear strain commences to kick in at about 20000 seconds as the magnitude of radial strain is almost equal to axial strain before that time. The moist tamped sample, on the other hand, overall shows very small negative shear strain.

4.5.5 Overview of factors affecting creep used in this study

Bowman (2002) categorized factors affecting creep be into two i.e. inherent factors (e.g. density, particle shape, initial fabric or depositional method) and induced factors (e.g. stress path, loading rate, creep period). Density and initial fabric are the inherent factors used in this study. Induced factors used in this study are creep period and consolidation stress paths before creep (K_0 and isotropic consolidation). Particularly for K_0 consolidation, the induced factor is actually due to the combination of stress ratio (R) and mean effective stress or effective confining pressure. For isotropic consolidation, it is due mean effective stress. As both inherent and induced factors affect creep simultaneously, it is quite difficult to say which one is the most significant factor. Higher mean effective stress, for example, generally results in greater creep (Figure 4-12). Creep is more pronounced at higher stress ratio (e.g. Shozen, 2001 and Lam, 2003). However, Table 4.3 (in addition to Table 4.2) demonstrates that loose samples (low stress ratio and mean effectives stress) compared to those of dense sample (higher stress ratio and mean

effective stress), exhibit higher creep. This suggests that density has more significant effects on creep. For tests at the same density and stress ratio (Figure 4-24), moist tamped samples develop greater axial and volumetric strain than dry pluviated samples. This suggests the importance of initial fabric on creep. However as no tests were conducted on loose dry pluviated samples, no comparison can be made regarding the effect of initial fabric relative to other factors. Regardless, the author believes density in combination with initial fabrics have significant effects on creep.

4.6 Summary

The following summary can be drawn regarding creep following K_0 and isotropic consolidation.

1. Following K_0 consolidation, axial creep is in compression. Positive axial and negative radial creep tends to increase with time at a decreasing rate.

2. As the time increases, volumetric creep over all the whole cylindrical body tends to follow the fundamental behavior of soils in which dense soils initially contract and then dilate, while loose soil contract. This is accordance with the observations by Wang et al. (2014) from DEM results, who thought that what happens during creep at decreasing strain rate is simi[l]ar to strain hardening during the pre-peak process of triaxial shearing. For dense soils in this study, for aging less than about 10^4 seconds volumetric strain is still in contraction after which dilation starts. For loose soils in this study, volumetric creep becomes greater as the aging time increases.

3. Shear strains for both K_0 consolidated and isotropic samples increase with time and are in the positive direction.

4. Creep following K_0 consolidation tends to be greater than creep of isotropically consolidated samples. This is due to the higher stress ratio of K_0 sample at the beginning of creep. This applies to both dense and loose samples.

5. For creep following K_0 consolidation, higher confining pressure causes greater axial, volumetric and shear creep for both dense and loose samples. Higher confining pressure during consolidation results in a higher stress ratio. Thus higher confining pressure means greater mean effective stress and stress ratio at the beginning of creep which in turn means greater creep.

6. For creep following isotropic consolidation, higher confining pressure results in greater creep due to in the higher mean effective stress. This supports observation of creep following the K_0 consolidation, as pointed above.

7. Externally, radial strain of K_0 consolidated dense sample is lower for higher confining pressures but the directions tend to be the same. Conversely, loose samples tend to have greater external radial strain for higher confining pressure used in this study.

8. Similar to dense moist tamped samples, K_0 consolidated dry pluviated samples develop greater creep than isotropic samples. Up to one day of aging, the radial strains of isotropic samples are still in compression whereas K_0 consolidated samples are expanding. Regarding the volumetric strain, at the mid-height of the sample the K_0 consolidated sample is more contractive; however over the whole cylindrical sample, the K_0 consolidated sample it is more dilative than the equivalent isotropic sample.

9. For one day of aging following isotropic consolidation, dry pluviated samples exhibit greater axial creep than moist tamped samples, locally and externally. Volumetric strains of dry pluviated samples are also higher than those of the moist tamped samples. A similar trend was observed for shear strains.

10. Creep is result of inherent and induced factors that works simultaneously. In this study the inherent factors are density and initial fabric while the induced factors are period of creep and combination of stress ratios and mean effective stress.

11. Density, in particular, appears to have more significant effects on creep magnitude and creep strain direction compared to stress ratio and mean effective stress.

12. Initial fabric has a significant role in creep development.

5 Aging Effects on Undrained Small-Strain Stiffness

5.1 Introduction

This chapter presents the results and some aspects of triaxial testing for this research program. The triaxial tests are mainly undrained due to the limited previous studies of the creep induced aging effects on the mechanical behavior of non-plastic silty sand. The first part of this chapter reviews the importance of small-strain stiffness and undrained behavior of silty sand. The following sections then explain and discuss results from monotonic and cyclic undrained tests. Triaxial tests generate a large quantity of data thus this chapter summarizes them by showing typical results of each class of testing.

5.2 Review

5.2.1 Importance of small-strain stiffness

In recent years, there has been growing acceptance that under working loads, soil below foundations experiences shear strain of less than 0.5% with average shear strains typically below about 0.1% (Burland, 1989). Jardine (1992) categorized strain into three groups i.e. very small-strain (<0.001%), small-strain (between 0.001% and 0.1%) and large strain (>0.1%). Small-strain stiffness firstly has been recognized to be important from soil dynamic analyses. Seed and Idriss (1970) concluded that shear modulus and damping depend on the amount of shear strain. However, nowadays it has been acknowledged that small-strain stiffness also plays an important role in static behavior. This acknowledgment was dictated by the fact that the typical strain of geotechnical structures is between 0.01% and 0.5%, as illustrated in Figure 5-1 (Mair, 1993). For retaining walls and foundations the strain ranges are within 0.01% and 0.1%. The figure reveals that conventional soil testing generally measures strain which is larger than the strain level relevant to practical problems. The figure also implies the necessity of the use of local strain gauges to

measure strain which is relevant to practical problems. Therefore in this chapter, the effects of creep induced aging are presented based on local strain measurement.

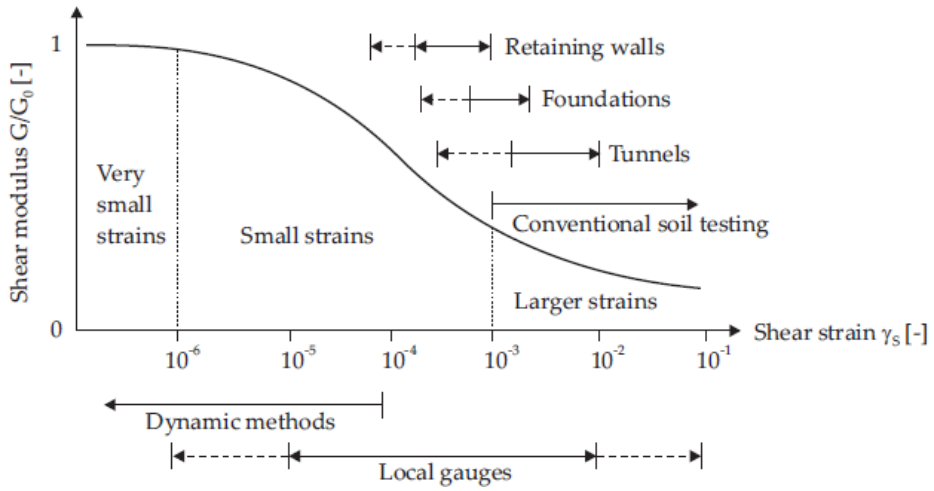

Figure 5-1 Typical shear strains in geotechnical engineering (Atkinson & Sallfors, 1991)

Previous laboratory studies on sand aging (e.g. Howie *et al.*, 2002; Wang & Tsui, 2009; Yan *et al.*, 2010) revealed that time has significant effect on stiffness. Most of the studies of sand aging have focused on very small-strain stiffness due to the characteristics of dynamic loading tests such as resonant column tests (e.g. Wang & Tsui, 2009; Witchman, 2005) or those using bender elements (e.g. Yan *et al.*, 2010). In addition, previous laboratory studies, particularly for triaxial tests, were mainly performed under drained condition (see Table 2.2) and were mainly performed on clean sand. This study focuses on the effect of creep induced aging on undrained small-strain stiffness of silty sand, which is relatively less investigated and is common in nature. Yamamuro and Lade (2011) revealed that many cases of static failure of granular soils occurred in silty sands.

5.2.2 Undrained behavior of silty sand

5.2.2.1 Dense silty sand

Yamamuro and Wood (2004) performed a series of undrained triaxial tests on dense silty sand (DR≈84%) with fines content of 20%, reconstituted by three

different methods i.e. slurry deposition (SD), dry funnel deposition (DFD) and air pluviation (AP). The results revealed that there was no significant difference in the behavior i.e. they all demonstrated stable behavior as illustrated in Figure 5-2.

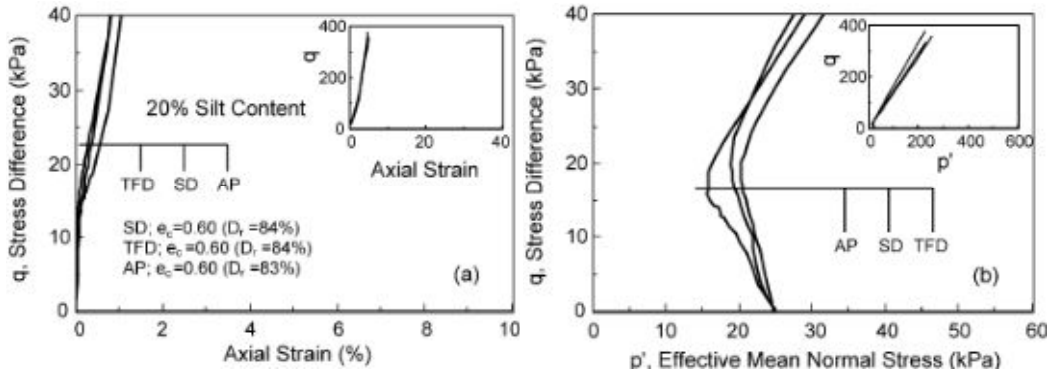

Figure 5-2 Undrained behavior of dense silty sand (Yamamuro & Wood, 2004)

5.2.2.2 Loose silty sand

Lade and Yamamuro (Lade & Yamamuro, 1997) identified that there are four characteristic types of undrained monotonic loose behavior of silty sand namely static liquefaction, temporary liquefaction, temporary instability and instability (see Figure 5-3). Characteristics of each type are as follows:

- Static liquefaction is characterized by the development of high pore-water pressure which results in zero effective confining pressure and zero deviator stress at low axial strains (Yamamuro & Lade, 1997).

- Temporary liquefaction occurs at higher stresses than the static liquefaction region and is characterized by an initial peak in the deviator stress, followed by a decline (Yamamuro & Lade, 1997).

- Temporary instability occurs at much greater stress than the temporary liquefaction region, and it occurs in a region similar to the temporary liquefaction region with two differences: (1) the amount that the deviator stress increases above the initial peak to effective stress failure is not as large as that exhibited by temporary liquefaction; (2) the soil exhibits increasing

contractiveness with increasing confining pressure (Yamamuro & Lade, 1997).

- The instability region is located at higher pressures than those of the temporary instability region and is characterized by the deviator stress achieving an initial peak, whereupon it declines and never increases above the initial peak before reaching effective stress failure (Yamamuro & Lade, 1997).

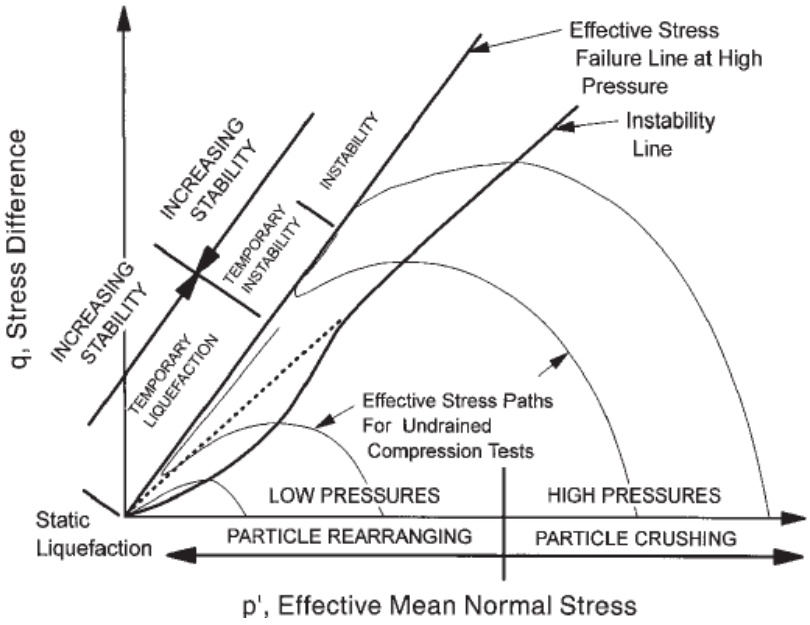

Figure 5-3 Undrained behavior of loose silty sand (Lade & Yamamuro, 1997)

5.3 Undrained Monotonic Compression Test

The purpose of these tests was to investigate the effect of creep on silty sand stiffness, particularly at small-strain (<0.1%). In this section, results are presented for monotonic undrained compression for both K_0 and isotropically consolidated tests.

A total of 27 monotonic undrained tests were performed at three different effective confining pressures and two densities, three aging times and using two sample preparation methods. The type of tests was chosen due to the reasons as explained in Section 4.1. Table 5-1 lists the conditions of each monotonic undrained test.

5.3.1.1 Shear stage stress path

This study focuses on the small-strain range thus most of these shear stages were stopped at about 1% of strain. Figure 5-4 shows examples of shear stress path for dense samples (CKoU-3, CKoU-6, and CKoU-9) and loose samples (CKoU-CKoU-18, and CKoU-21) for 1 week aging time. It can be seen from Figure 5-4 that generally while the mean effective stress at which the tests start is different, the stress paths eventually join on top of each other at larger deviator stress. The same figures reveal that strain hardening and strain softening is consistent for all dense and loose samples, respectively. Using K_0 consolidation (controlling lateral strain rather than axial effective stress) at different confining pressures (so different mean effective stress) means that stress ratios are also different. Therefore differences in shear stage response are due to combined effects of confining stress and stress ratio. The stress ratio at the end of consolidation, before shear stages, can be seen from Table 4.2 in Chapter 4. For loose samples, in particular, maximum deviator stress, q_{peak}, increases as effective mean pressure and the initial deviator stress (stress ratio) at the end K_0 consolidation, q_{static}, increase. This was expected, since higher confining pressure results in higher deviator stress.

Table 5-1 Samples Tested in Monotonic Undrained Test

No	Method	Dr (%)	σ'_3(kPa)	σ'_1(kPa)	σ'_3/σ'_1	Test ID	Aging Time
1	MT	67.4	120	306	0.39	CKoU-1	1 hour
2	MT	67.4	120	307	0.39	CKoU-2	1 day
3	MT	67.6	120	306	0.39	CKoU-3	1 week
4	MT	67.1	60	149	0.40	CKoU-4	1 hour
5	MT	67.2	60	149	0.40	CKoU-5	1 day
6	MT	67.4	60	149	0.40	CKoU-6	1 week
7	MT	67.5	30	67	0.45	CKoU-7	1 hour
8	MT	67.3	30	67	0.45	CKoU-8	1 day
9	MT	67.3	30	67	0.45	CKoU-9	1 week
10	MT	67.6	30	30	0.99	CIU-10	1 hour
11	MT	67.8	30	30	1.00	CIU-11	1 day
12	MT	67.4	30	30	0.99	CIU-12	1 week
13	MT	39.8	120	261	0.46	CKoU-13	1 hour
14	MT	40.0	120	261	0.46	CKoU-14	1 day
15	MT	39.4	120	260	0.46	CKoU-15	1 week
16	MT	39.7	60	125	0.48	CKoU-16	1 hour
17	MT	39.8	60	126	0.48	CKoU-17	1 day
18	MT	39.6	60	125	0.48	CKoU-18	1 week
19	MT	39.4	30	57	0.53	CKoU-19	1 hour
20	MT	39.8	30	57	0.52	CKoU-20	1 day
21	MT	39.9	30	58	0.52	CKoU-21	1 week
22	DD	69.6	60	113	0.53	CKoU-22	1 min
23	DD	69.2	60	112	0.53	CKoU-23	1 day
24	DD	69.5	60	60	1.00	CIU-24	1 min
25	DD	69.5	60	60	1.00	CIU-25	1 day
26	MT	68.4	60	60	1.00	CIU-26	1 min
27	MT	70.0	60	60	1.00	CIU-27	1 day

5.3.2 K_0 consolidated samples

Undrained secant stiffness at certain strain (i.e. 0.02% and 0.06%) and initial modulus (G_0), which are the focus of this chapter, are obtained from the deviator stress-shear strain curve. It should be noted that for the undrained condition, shear strain (ε_s) is equal to axial strain (ε_a) because volumetric strain is zero (see Eq. 4-1 and Eq. 4-2).

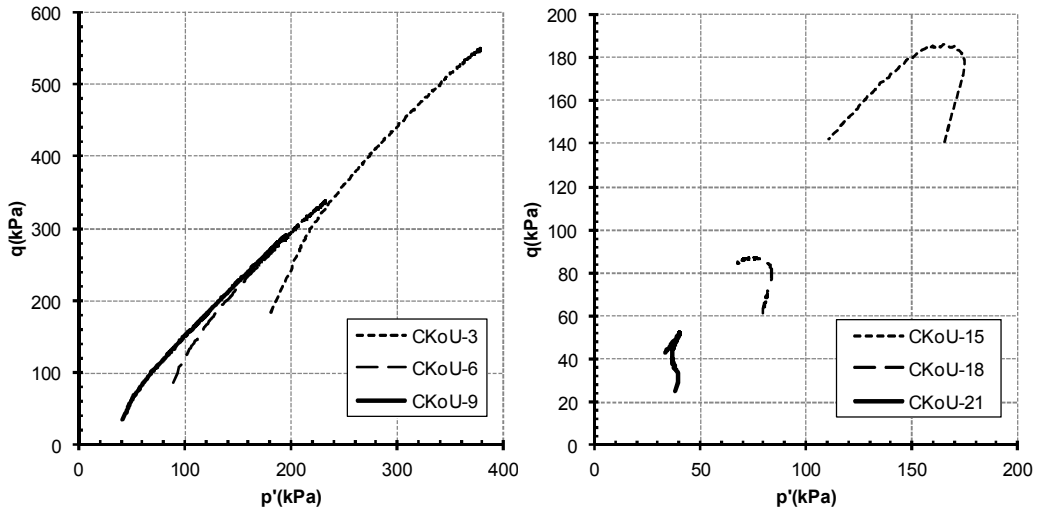

(a) (b)

Figure 5-4 Stress paths obtained from K_0 consolidated samples after 1 week aging (a) dense i.e. CKoU-3, CKoU-6&CKoU-9 (b) loose i.e. CKoU-15, CKoU-18&CKoU-21 at 120, 60 and 30 kPa confining pressure, respectively

5.3.2.1 Effects on stress-strain relationship

In order to study the effect of drained creep induced aging, a group of tests were performed. Three consolidation pressures were chosen and each sample was aged for one hour, one day and one week. Figure 5-5 shows a typical set of results for dense samples i.e. CKoU-1, CKoU-2 and CKoU-3 for 1 hour, 1 day and 1 week of aging times, respectively. Following the consolidation stage, the samples were aged at relatively constant creep stress ratio, $R=\sigma_1'/\sigma_3' \approx 2.6$. The black thick line represents a sample that aged for one hour, the black dash line for sample that was

aged for one day and the black dot line represents sample that was aged for one week.

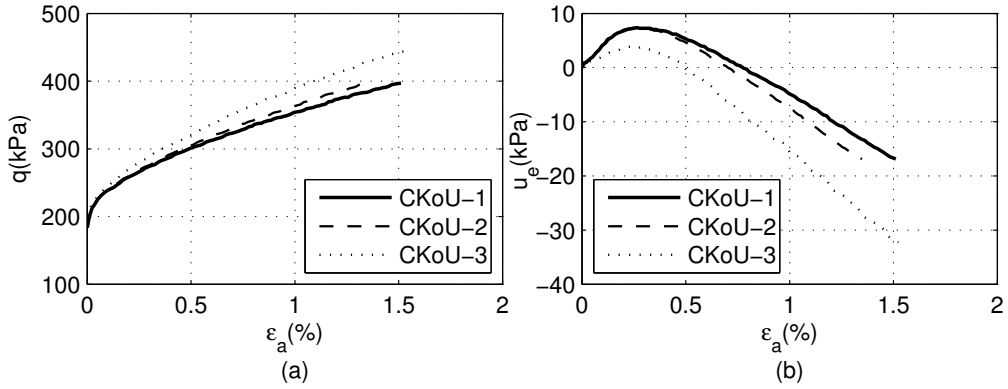

Figure 5-5 Example of aging effects on stress-strain response of K_0 dense samples at 120 kPa confining pressure (CKoU-1 – 1 hour, CKoU-2 –1 day and CKoU-3 – 1 week of aging time, respectively)

Figure 5-5 stress-strain curves show that the deviatoric stress tends to increase continuously and exhibit stain hardening behavior during the shearing process, due to their dilative feature and therefore negative pore pressure. This is typical dense soil behavior under undrained condition (Gu *et al.*, 2014; Yamamuro & Wood, 2004). Figure 5-5(a) also shows that there is an increase in deviator stress for samples with a longer period of aging. Generally there was a slight change between one hour and one day aging, but there was a slightly higher change between one hour and one week. This was also true for samples at lower consolidation pressures and aged over the same time, as listed in the Table 5-1. Figure 5-5(b) presents a typical excess pore pressure versus axial strain relationship for dense samples. The first thing to see is that no sample experienced a large increase in pore pressure, as expected for dense samples. All the samples exhibited a peak positive pore pressure at about the same strain i.e. 0.3% and then a decrease before the pore pressure changed from positive to negative. It can be seen from the figure that soil that was aged longer tended to generate lower positive excess pore pressure. The figure also shows that a longer period of aging makes the sample become more dilative. In

addition, aging tends to change the contractive behavior into dilative behavior at a lower strain.

The effects of aging on shearing for loose samples are exemplified by Figure 5-6. The stress-strain relationships in Figure 5-6(a) show that all samples experience strain softening. In general, samples that were aged longer show higher peak deviator stress up to about 0.7%, but after that, more aged samples soften faster (reduce deviator stress more quickly with strain). Unlike dense samples which show less change, there appears to be significant change between one day and one hour aged samples. In terms of pore pressure response as shown in Figure 5-6(b), the effect of aging time is not very distinct when compared to the dense soil behavior. The one week sample generally shows less mean pore pressure generation up to about 0.5% strain, compared to the rest of the samples. At strain larger than 0.5% the one week sample exhibits larger excess pore pressure.

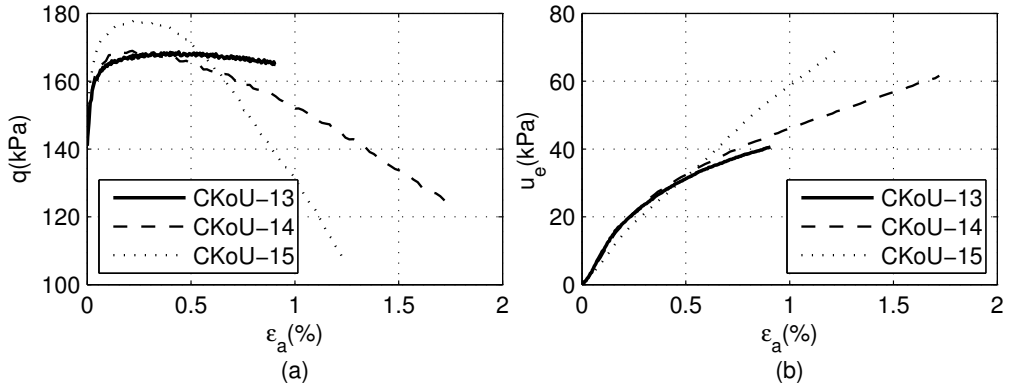

Figure 5-6 Example of the influence of aging on stress-strain response of loose samples at 120 kPa confining pressure (CKoU-13-1 hour, CKoU-14-1 day and CKoU-15-1 week aging, respectively)

5.3.2.2 Effects on small-strain stiffness

As the focus of this study is on undrained stiffness at small-strain (<0.1%), the following figures in the rest of this chapter will be in terms of stiffness. Undrained secant stiffness or secant shear modulus at certain shear strain (G) is obtained from the gradient between the initial point at zero strain and the point (strain) in question. Initial shear modulus (G_0) was determined from the initial part

of the q versus ε_s curve (tangent stiffness). For consistency of G_0 determination, regression was performed on data points with shear strain less than 0.01%. The range of the regression was taken considering the resolution of the LVDTs and minimum data logging time of the GDS apparatus.

Figure 5-7 illustrates stress-strain curves for all dense K_0 consolidated samples at strain of about 0.1% for three aging times (1 hour, 1 day and 1 week respectively) and three confining pressures i.e. 120 kPa, R=2.6 (CKoU-1, CKoU-2&CKoU-3); 60 kPa, R=2.47 (CKoU-4 CKoU-5 and CKoU-6); and 30 kPa, R=2.21 (CKoU-7 CKoU-8 and CKoU-9). The figure shows that more aged samples, for all confining pressures, have stress-strain curves above younger samples, indicating stiffer response. To allow clearer comparison of stiffness, as the samples at different confining pressure were sheared at different initial stress ratios, incremental deviator stress Δq, i.e. the difference between the current deviator stress and that at the beginning of shearing, is also presented in Figure 5-8 (Lam, 2003). Figure 5-8 shows a similar trend as in Figure 5-7. In addition Figure 5-8 shows that samples at higher confining pressures are stiffer than those at lower pressures.

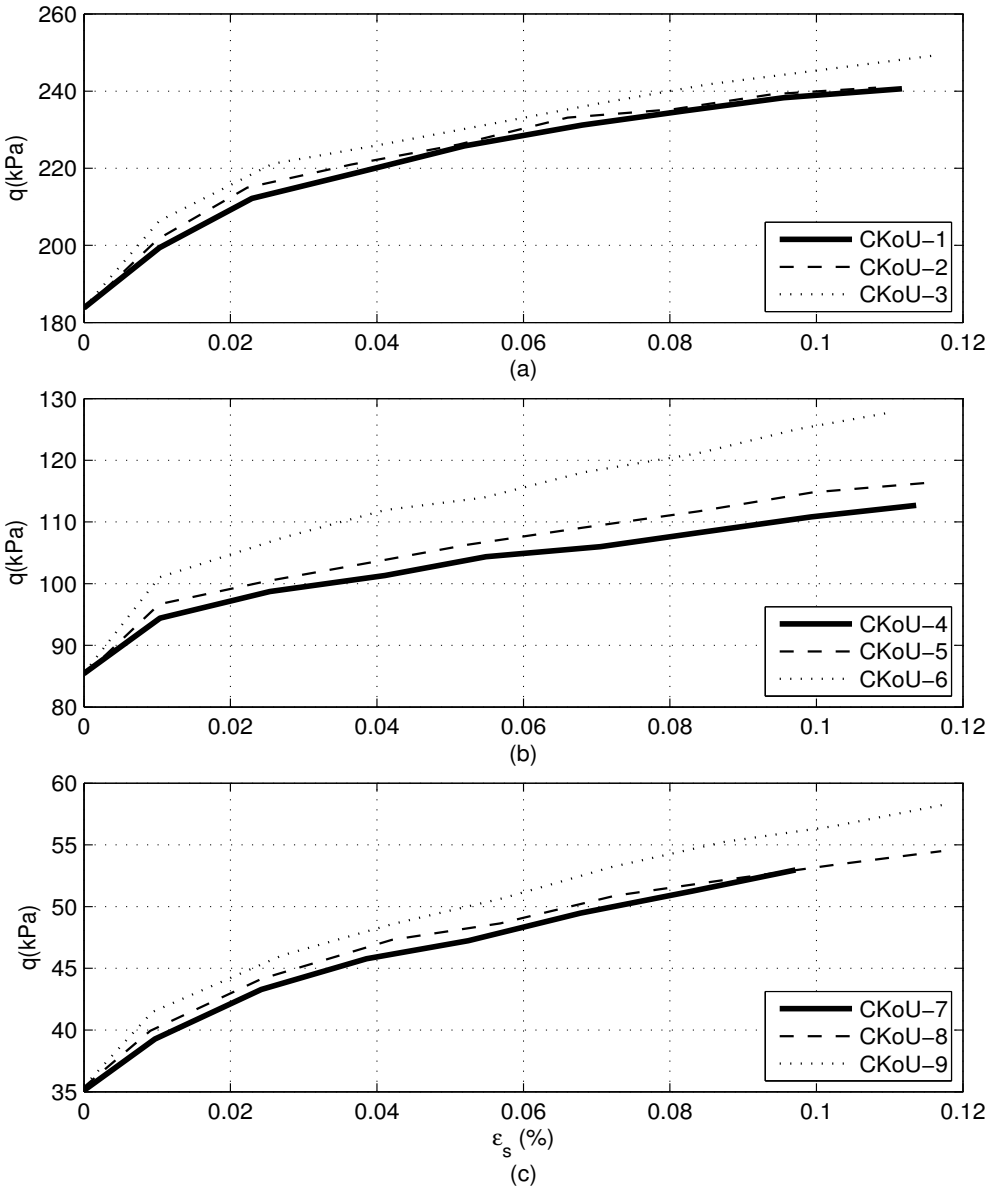

Figure 5-7 Small-strain q versus ε_s of dense K_0 consolidated samples for 1 hour, 1 day and 1 week of aging times respectively at (a) 120kPa (CKoU-1, CKoU-2&CKoU-3); (b) 60 kPa (CKoU-4, CKoU-5&CKoU-6) and (c) 30kPa (CKoU-3, CKoU-6&CKoU-9) of confining pressure

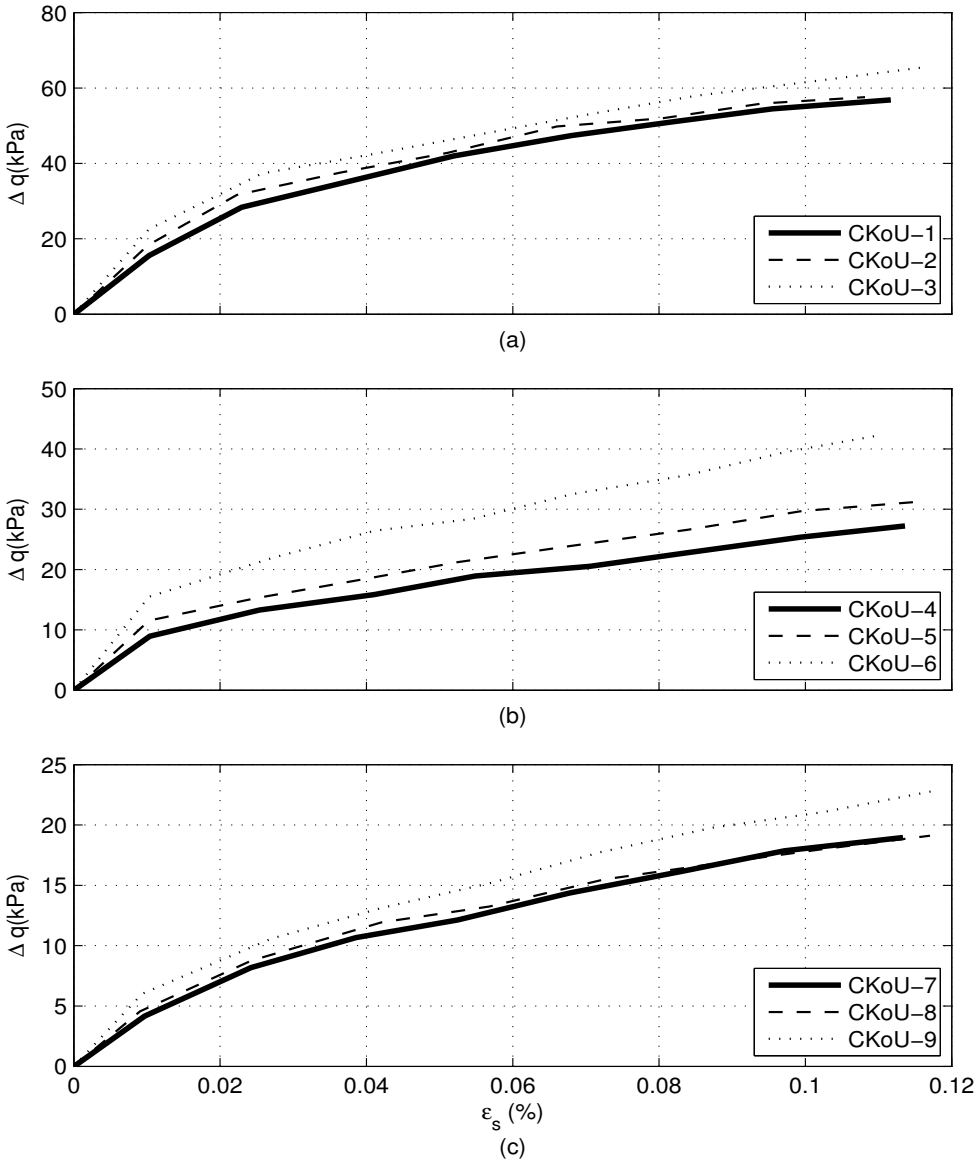

Figure 5-8 Small-strain Δq versus ε_s of dense K_0 consolidated samples for 1 hour, 1 day and 1 week of aging times, respectively at (a) 120 kPa (CKoU-1, CKoU-2&CKoU-3), (b) 60 kPa (CKoU-4, CKoU-5&CKoU-6) and (c) 30 kPa (CKoU-3, CKoU-6&CKoU-9) of confining pressure

Effect of aging on stiffness can be seen more clearly in terms of shear modulus (G) as shown in Figure 5-9. The figure shows that shear modulus of more aged samples lie above younger samples. It can be seen also that the manifestation of the aging effect on undrained stiffness tends to diminish with increasing shear strain. This indicates that aging is mostly manifested at small strain as reported by other researchers who performed studies on clean sand (see Section 2.2.2.3).

Neglecting time effects, Figure 5-10 show that samples at higher confining pressure with the same aging time have higher shear modulus, which shows a reasonable trend of confining pressure effects on shear modulus. For example, shear modulus at 0.02% strain for dense samples for 1 hour aging time i.e. CKoU-1(120 kPa), CKoU-4 (60 kPa) and CKoU-7 (30 kPa) are 132.4, 64.4 and 36.4 MPa, respectively. Negussey (1984) reported that higher confining stress led to stiffer stress-strain response and strength. In addition, Gu *et al.* (2013), based on DEM, shows that small-strain modulus increases with increase of confining pressure. In contrast, higher stress ratio reduces small-strain stiffness (Lam, 2003; Richart & Yu 1984; Tatsuoka & Hoque, 2004). This suggests that the effect of confining pressure outweighs the opposite effect of stress ratio. This was reasonable considering, for example, that ratio of confining pressure between CKoU-1 and CKoU-7 is 4 whilst the ratio of stress ratios between them is only 1.15.

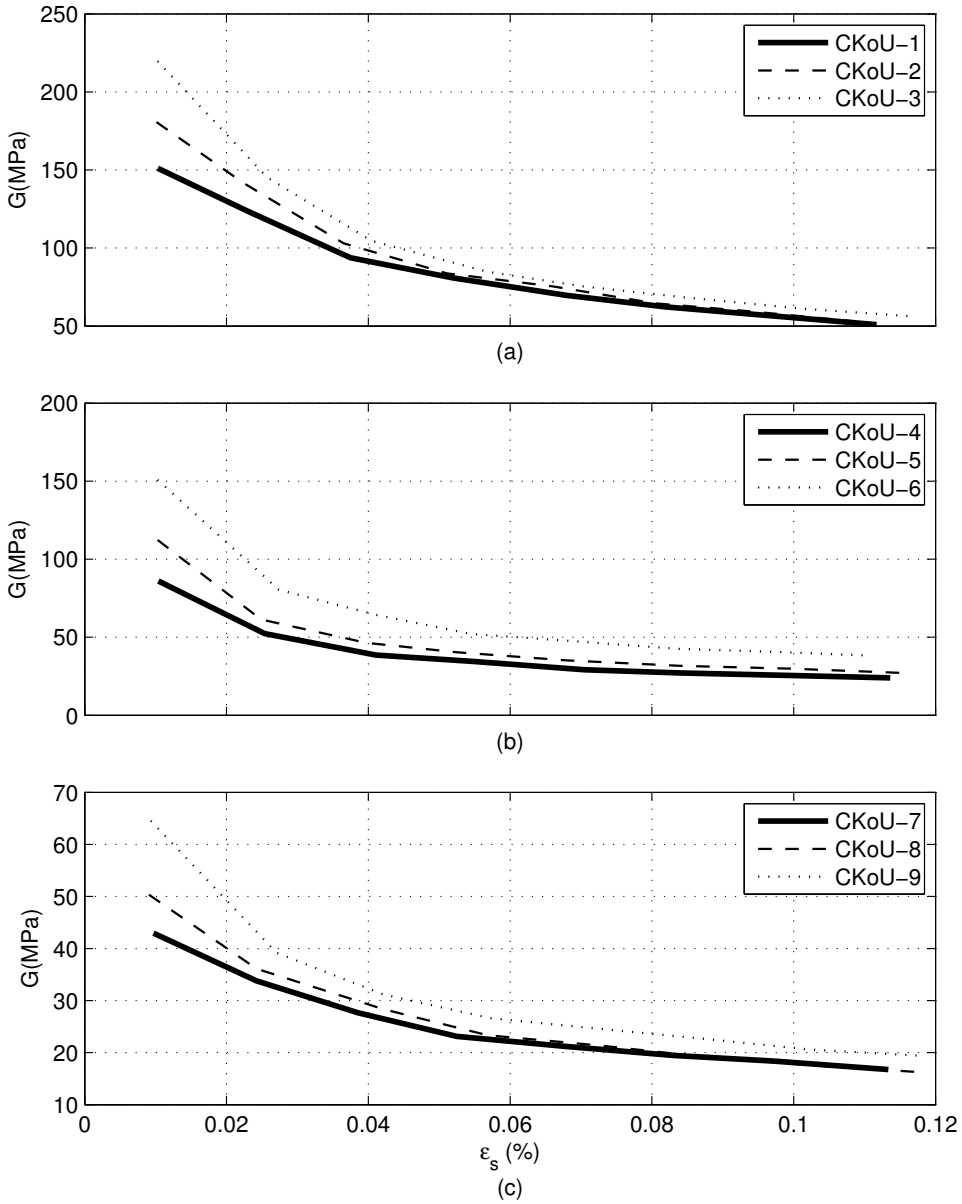

Figure 5-9 Shear modulus of dense K_0 consolidated samples for 1 hour, 1 day and 1 week of aging times, respectively at (a) 120 kPa (CKoU-1, CKoU-2&CKoU-3), (b) 60 kPa (CKoU-4, CKoU-5&CKoU-6) and (c) 30 kPa (CKoU-3, CKoU-6&CKoU-9) of confining pressure

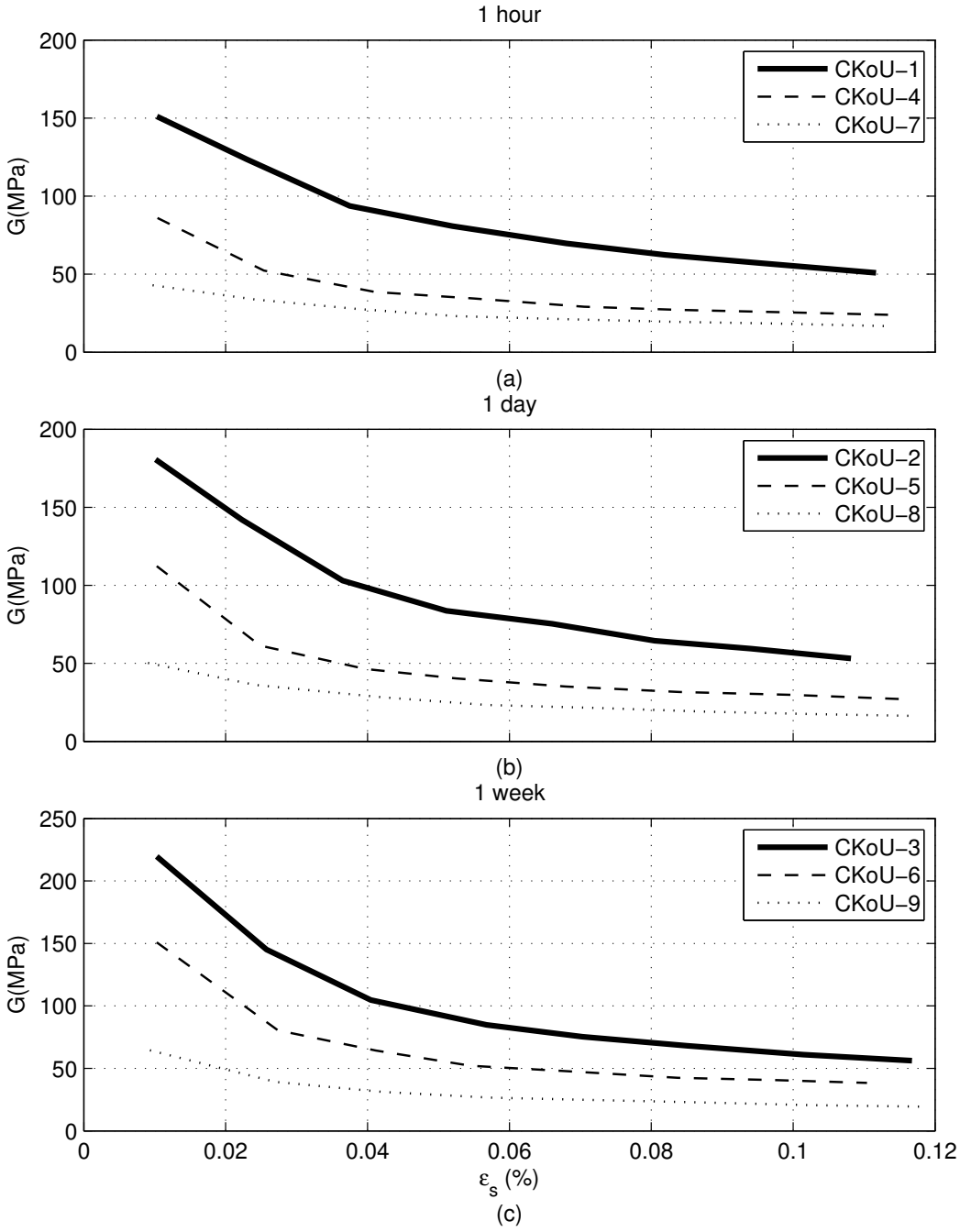

Figure 5-10 Shear modulus dense K_0 consolidated samples for (a) 1 hour (CKoU-1, CKoU-4& CKoU-7), (b) 1 day (CKoU-2, CKoU-5& CKoU-8) and (c) 1 week (CKoU-3, CKoU-6& CKoU-9) of aging time

Stress-strain curves, q versus ε_s at small-strain range for all loose K_0 consolidated samples for 1 hour, 1 day and 1 week respectively at three confining pressures, i.e. 120 kPa (CKoU-13, CKoU-16&CKoU-19); 60 kPa (CKoU-14 CKoU-17 and CKoU-20) and 30 kPa (CKoU-15 CKoU-18 and CKoU-21) of confining pressures, are shown in Figure 5-11. The corresponding Δq versus ε_s plot is shown in Figure 5-12. Both figures generally show similar aging effect as in the case of dense samples i.e. stiffer response with age.

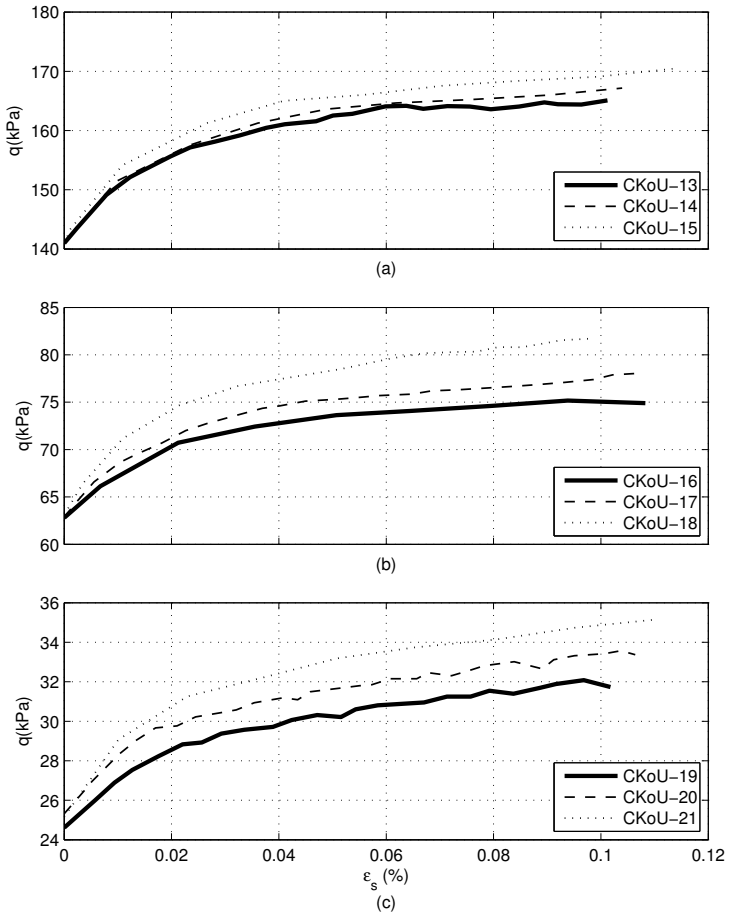

Figure 5-11 Small-strain q versus ε_s of loose K_0 consolidated samples for 1 hour, 1 day and 1 week of aging times, respectively at (a) 120 kPa (CKoU-13, CKoU-14&CKoU-15), (b) 60 kPa (CKoU-16, CKoU-17&CKoU-18) and (c) 30 kPa (CKoU-19, CKoU-20&CKoU-21) of confining pressure

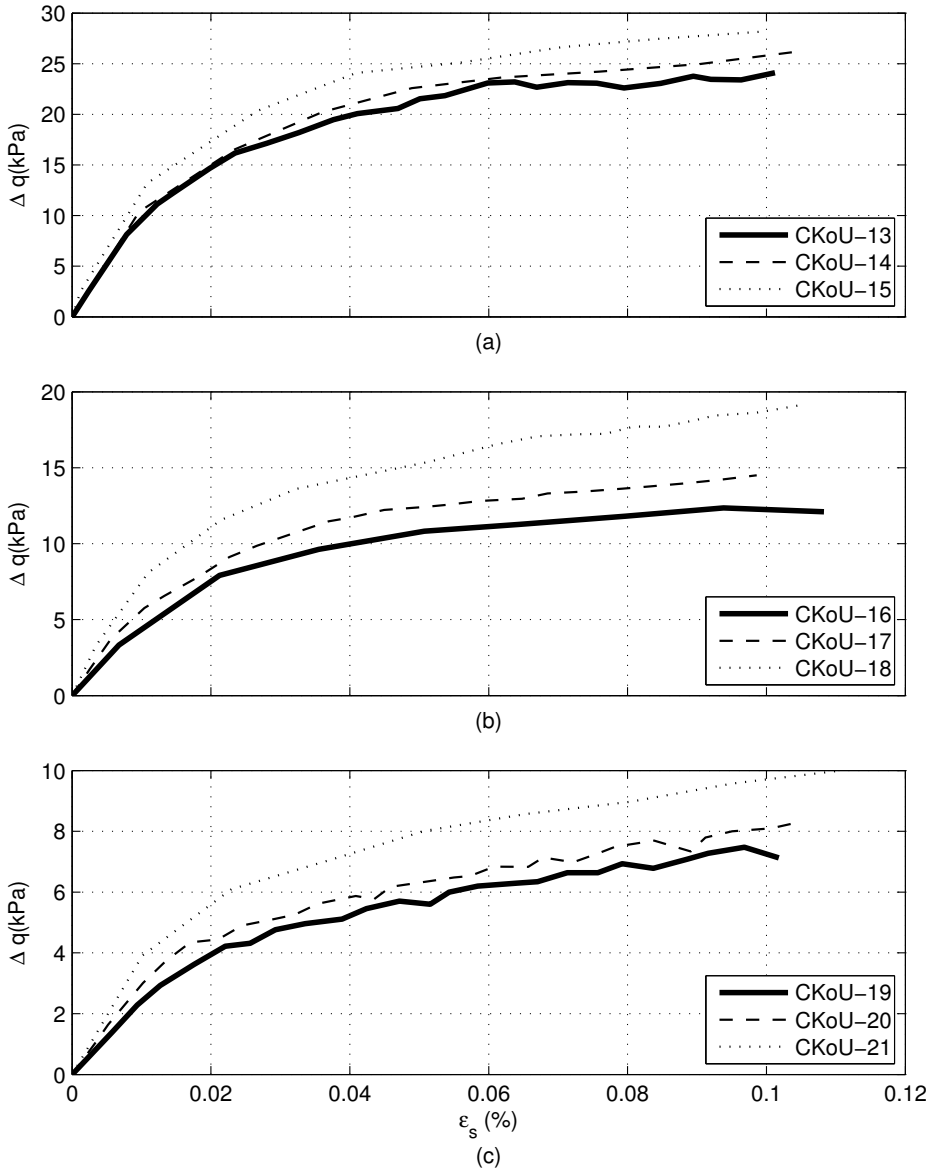

Figure 5-12 Small-strain Δq versus ε_s of loose K_0 consolidated samples for 1 hour, 1 day and 1 week of aging times, respectively (a) 120 kPa (CKoU-13, CKoU-14&CKoU-15), (b) 60 kPa (CKoU-16, CKoU-17&CKoU-18) and (c) 30 kPa (CKoU-19, CKoU-20&CKoU-21) of confining pressure

In terms of shear modulus, aging effects on loose samples are illustrated in Figure 5-13. As in the case of dense samples, obvious effects of aging on loose samples can be seen clearly at small strains.

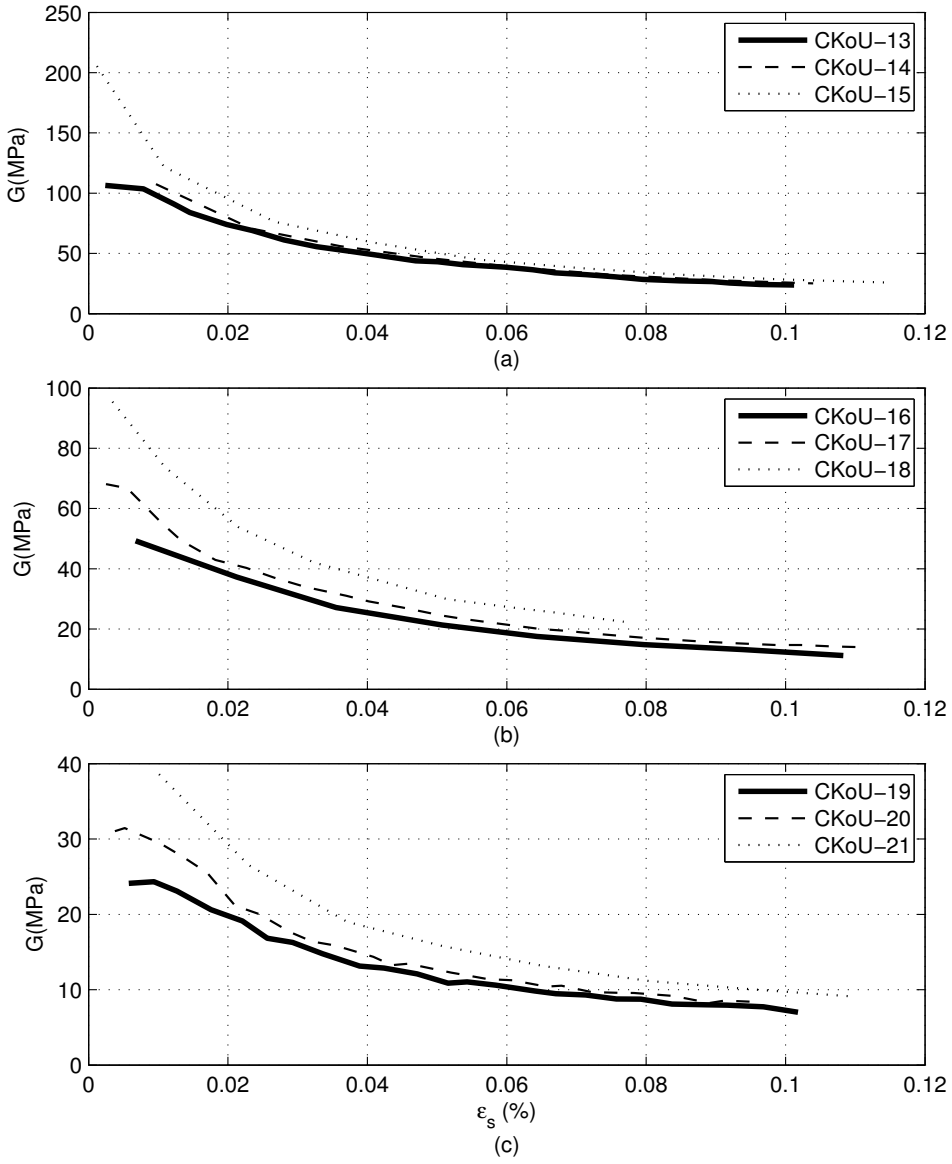

Figure 5-13 Shear modulus of loose K_0 consolidated samples for 1 hour, 1 day and 1 week of aging times, respectively at (a) 120 kPa (CKoU-13, CKoU-14&CKoU-15), (b) 60 kPa (CKoU-16, CKoU-17&CKoU-18) and (c) 30 kPa (CKoU-19, CKoU-20&CKoU-21) of confining pressure

5.3.3 Isotropically consolidated samples

Aging effects following isotropic consolidation on loose granular soils have been relatively much investigated (e.g. Howie et al, 2002; Shozen, 2001 and Lam 2003). This sub-section presents aging effects following isotropic consolidation on dense silty sand which is less studied, and which can be important when considering the time-dependent behavior of mechanically densified soil.

Figure 5-14 illustrates effects of aging on stress-strain response and undrained stiffness of dense soil (CIU-10 and CIU-12) following isotropic consolidation along with the corresponding K_0 consolidated samples (CKoU-7 and CKoU-9). It can be seen from Figure 5-14(a) that for the same aging time, stress-strain relations of isotropic consolidated samples tend to be above those of K_0 consolidated samples. This suggests that isotropic consolidated samples have stiffer response compared to K_0 consolidated samples, as supported by greater undrained stiffness shown by Figure 5-14(b). This is due to the lower stress ratio of isotropic samples.

Figure 5-15 shows aging effects for isotropic consolidated samples (60 kPa confining pressure) of 1 minute and 1 day of aging times, respectively for dense moist tamped samples (CIU-26 and CIU-27) and dry pluviated samples (CIU-24 and CIU 25). A different (shorter) initial aging time from other tests was chosen as 1 minute as an attempt to see early effects of aging (see 5.3.4.3). As can be seen from Figure 5-15(b) moist tamped samples produce stiffer stress-strain responses compared to dry pluviated samples. Stiffer response and higher shear modulus at small-strain range due to aging are obvious from Figure 5-15, for both moist tamped and dry pluviated sample. This suggests regardless of the method of preparation, time has significant effects on small- strain mechanical properties.

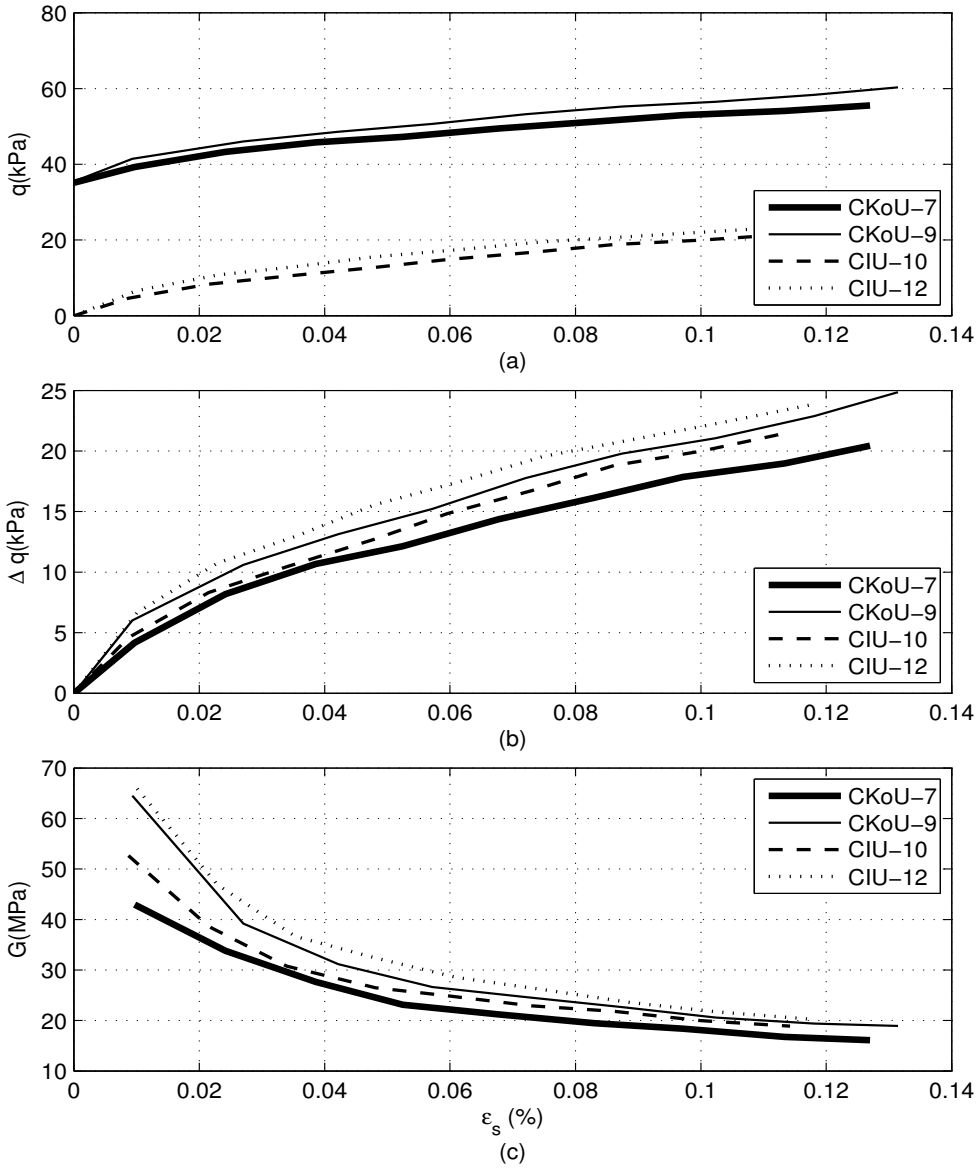

Figure 5-14 Aging effects of 30 kPa confining pressure for 1 hour and 1 week of aging time, respectively on dense isotropically consolidated i.e. CIU-10&CIU-12 (p'=30kPa) and dense K_0 consolidated samples i.e. CKoU-7&CK$_0$U-9 (p'=40.4 kPa)

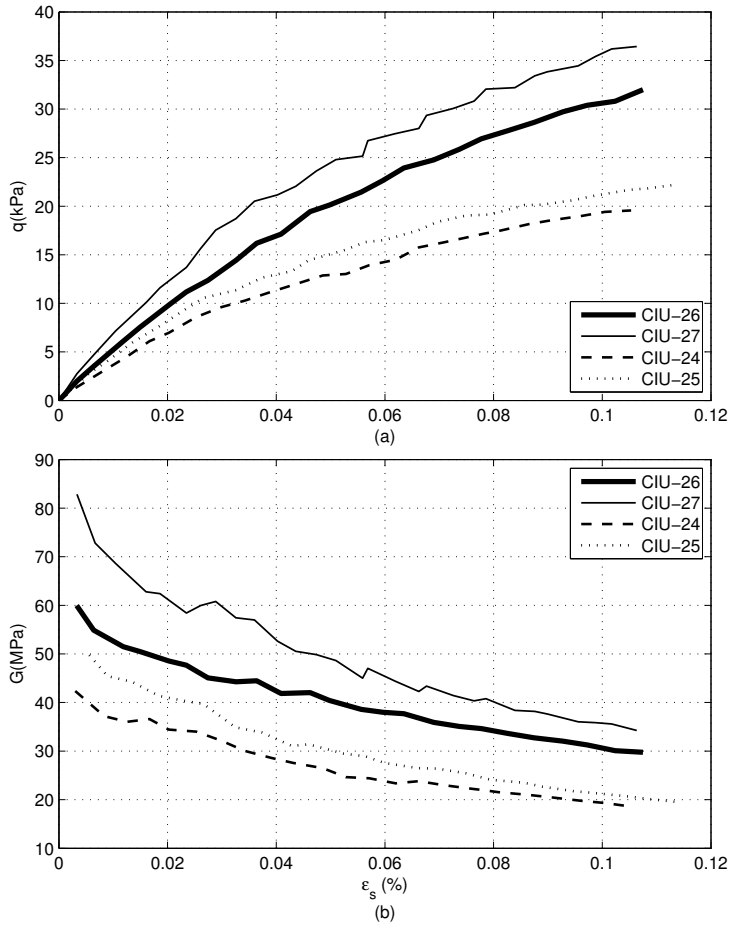

Figure 5-15 Shear modulus of isotropic consolidated dense samples (60 kPa confining pressure) for 1 minute and 1 day of aging time, respectively for moist tamped (CIU-26&CIU-27) vs. dry pluviated (CIU-24&CIU-25) preparation

5.3.4 Discussion

5.3.4.1 Aging effects on stress-strain relationship

It has been shown that generally more aged K_0 consolidated samples result in stiffer stress-strain relationship, at least up to about 1% of strain in this study (Figure 5-5 for dense samples and Figure 5-6 for loose samples). Dense samples show that more aged samples generate lower pore-pressure, which suggests more dilative behavior of older samples. A similar observation of pore pressure response has been reported by Lade et al (1997) who performed creep, following a

proportional loading, up to 1690 min on clean sand under very high effective confining stress (5050kPa) and stress ratio of 2.72. The stress-strain curve for loose samples (Figure 5-6) shows that older samples tend to behave in a more brittle manner than younger samples. This might be attributed to the fact that during creep induced aging, axial and radial strain (thus volumetric and shear strain) are developing (see Chapter 4). This strain development during aging may cause more homogenized force chains, thereafter enhancing the interlocking and associated dilatancy (Wang *et al.*, 2008).

A similar trend was observed for dense isotropically consolidated samples (Figure 5-14 and Figure 5-15), where aging results in a stiffer response. The trend applies to lower (30kPa) and higher (60kPa) confining pressure and both moist tamped and dry pluviated samples. Figure 5-7 and Figure 5-11 suggest that samples at higher confining pressure have stiffer stress-strain response. This is keeping in with Negussey's observation (1984) who reported that higher confining stress led to stiffer stress-strain response. Figure 5-7 and Figure 5-15 (a) demonstrate that, under 60 kPa of confining pressure and the same aging time, stress-strain curves of dense moist tamped samples lie above those of dry pluviated samples, meaning a stiffer stress-strain response. This is in accordance with previous studies (e.g. Ibrahim & Kagawa, 1991a; Lee, 2001). Furthermore, isotropically consolidated samples have stiffer stress-strain response compared to K_0 consolidated samples. This is in accordance with previous laboratory findings (e.g. Lam, 2003; Richart & Yu 1984; Tatsuoka & Hoque, 2004) where higher stress ratio was found to reduce small-strain stiffness. Gu *et al.* (2014), based on numerical modelling, also found a similar trend of the effect of stress ratio on small-strain stiffness.

5.3.4.2 Aging effects on small-strain undrained stiffness

Effects of aging on small-strain stiffness of K_0 consolidated samples can be seen clearly in terms of shear modulus (G) as shown in Figure 5-9 and Figure 5-13. The figures show that the net effect of confining pressure and stress ratio on aging of K_0 consolidated samples is a higher shear modulus with age.

Figure 5-9 and Figure 5-13 also show that manifestation of aging effect on undrained stiffness tends to diminish with increasing shear strain. This indicates that aging is mostly manifested at small-strain as reported by other researchers (e.g. Howie *et al.*, 2002; Suarez *et al.*, 2009b). It can be seen that generally aging time tends to increase the initial shear modulus, G_0 and undrained secant stiffness, $G_{0.02\%}$ and $G_{0.06\%}$ significantly. DEM simulations by Wang et al (2008) suggest that contact creep changes during aging makes the force chains more homogeneous. Aging reduces the stress concentration of the strong force chain networks thus minimizing the risk of force buckling. Additionally, due to contact creep, the weak force chain gains higher normal forces (i.e. higher shear resistance) hence lower shear stress. This makes the particles more difficult to slide past each other. These changes in force chain properties eventually result in a more stable force chain network and thereafter higher initial stiffness. However how this homogenization occurs in silty sand is still elusive. A further hypothesis of aging mechanism of dense silty sand, based on creep observation (see Chapter 4) and microstructure change during aging, is discussed in Chapter 6.

5.3.4.3 Quantification of rate of increase in stiffness due to aging

Gain in stiffness due to time effects is commonly quantified by two parameters i.e. the coefficient of shear modulus increase with time, I_G, and the coefficient of shear modulus increase relative to shear modulus at 1000 minutes , N_G (Anderson & Stokoe, 1978). I_G and N_G are given by:

$$I_G = \frac{\Delta G}{\log\left(\frac{t_2}{t_1}\right)} \qquad \textbf{Eq. 5-1}$$

$$N_G = \frac{I_G}{G_{(1000\ \min)}} 100\% \qquad \textbf{Eq. 5-2}$$

where ΔG is shear modulus increase for one logarithmic cycle of time, t_1= reference time and t_2=aging time. It was thought that ideally aging effects should be quantified to the condition immediately after aging starts, as the longer time passing by the creep rate reduce more. As the minimum aging time for K_0 consolidated samples in this study is 1 hour, thus N_G is defined relative to 1 hour aging time instead of 1000 min.

In order to quantify and compare the rate of stiffness increase due to aging, results from K_0 consolidated samples (Figure 5-9 and Figure 5-13) and isotropically consolidated samples (Figure 5-14(b) and Figure 5-15(b)) are presented in Table 5-2 and Table 5-3, respectively. Initial shear modulus (G_0) and shear modulus at 0.02% ($G_{0.02\%}$) and 0.06% ($G_{0.06\%}$) are chosen for comparison as the aging effects tend to be greater, and thus more obvious, at smaller strains.

Table 5-2 Aging effects on undrained shear modulus (G_0, $G_{0.02\%}$ and $G_{0.06\%}$) of K_0 consolidated samples

Test ID	σ'_3 (MPa)	Aging time (min)	G_0 (MPa)	$G_{0.02\%}$ (MPa)	$G_{0.06\%}$ (MPa)	$I_{G(0)}$ (MPa)	$I_{G(0.02\%)}$ (MPa)	$I_{G(0.06\%)}$ (MPa)	$N_{G(0)}$ (%)	$N_{G(0.02\%)}$ (%)	$N_{G(0.06\%)}$ (%)
Dense											
CKoU-1	120	60	151	132	75						
CKoU-2	120	1440	181	149	79	21.4	12.1	2.4	14.1	9.1	3.2
CKoU-3	120	10080	220	173	83	30.8	18.1	3.3	20.4	13.7	4.4
CKoU-4	60	60	86	64	33						
CKoU-5	60	1440	112	78	38	19.0	10.1	3.7	22.1	15.7	11.4
CKoU-6	60	10080	151	111	50	29.2	20.8	7.9	33.9	32.3	24.2
CKoU-7	30	60	43	36	22						
CKoU-8	30	1440	50	40	23	5.4	2.6	0.5	12.5	7.2	2.4
CKoU-9	30	10080	65	49	26	9.7	5.7	1.8	22.6	15.7	8.2
CKoU-1	120	60	151	132	75						
Loose											
CKoU-13	120	60	95	74	38.5						
CKoU-14	120	1440	107	81	39	9.1	5.4	0.6	9.6	7.3	1.6
CKoU-15	120	10080	123	91	43	12.6	7.5	2.0	13.3	10.2	5.1
CKoU-16	60	60	45	38	19						
CKoU-17	60	1440	58	45	21	9.1	4.5	1.9	20.2	11.8	10.4
CKoU-18	60	10080	75	58	27	13.6	8.8	3.9	30.2	23.1	20.8
CKoU-19	30	60	24	20	10						
CKoU-20	30	1440	30	22	11	4.5	1.8	0.6	19.1	9.0	6.2

Table 5-3 Aging effects on undrained shear modulus (G_0, $G_{0.02\%}$ and $G_{0.06\%}$) of isotropically consolidated samples

Test ID	σ'_3(kPa)	Aging time (min)	G_0 (MPa)	$G_{0.02\%}$ (MPa)	$G_{0.06\%}$ (MPa)	$I_{G(0)}$ (MPa)	$I_{G(0.02\%)}$ (MPa)	$I_{G(0.06\%)}$ (MPa)	$N_{G(0)}$ (%)	$N_{G(0.02\%)}$ (%)	$N_{G(0.06\%)}$ (%)
CIU-10	30	60	53	40	25						
CIU-12	30	10080	71	52	29	8.2	5.4	1.8	15.7	13.4	7.2
CIU-24	60	1	37	35	24						
CIU-25	60	1440	45	41	28	2.7	2.0	1.2	7.5	5.9	5.0
CIU-26	60	1	53	49	38						

(a) Dense K_0 consolidated samples

Table 5-2 reveals that for the same aging time, dense K_0 consolidated samples at higher confining pressure have greater initial shear modulus. It should be remembered that that for K_0 consolidated samples, higher confining pressure also means slightly higher stress ratio (see Table 4-2). Therefore the results shown by Table 5-2 are due to effects of different stress ratios and confining pressures. The same table reveals that the values of I_G and N_G at 0.02% strain are always larger than those at 0.06% strain. Again this shows that the aging effect is more pronounced at smaller strain and suggests that the rate of increase in stiffness increases as the shear strain decreases (Howie *et al.*, 2002; Wang & Tsui, 2009). It also appears from Table 5-2 that N_G values tend to increase up to a confining pressure of 60kPa, as indicated by a higher aging rate for samples at 60kPa compared to 30kPa. However N_G values for dense samples at 120kPa tend to be lower than for samples at 60kPa. This suggests the effect of confining pressure outweighs the effect of stress ratio on the aging rate.

(b) Loose K_0 consolidated samples

Table 5-2 again shows that the aging manifestation for loose K_0 consolidated samples is more pronounced at smaller strains, as indicated by higher values of $I_{G(0.02\%)}$ compared to $I_{G(0.06\%)}$. It can be seen also that the increase in shear modulus is higher for 60kPa samples (R=2.05) compared to 30kPa samples (R=1.87). This indicates the effect of stress ratio on stiffness increase is more dominant than the confining pressure i.e. confining pressure is doubled whilst stress ratio increases about 9%. However at 120kPa confining pressure the stiffness increase tends to be lower than that at 60kPa. This suggests that the effect of confining pressure is greater than the effect of stress ratio. As stress ratios are different for loose and dense samples, no conclusion could be drawn regarding the effect of density alone on stiffness increase of K_0 consolidated samples. However, Table 5-2 indicates that at 30kPa confining pressure, loose samples, despite having lower stress ratio, tend to produce more stiffness increase with age than dense samples. This may relate to

the fact that loose samples initially have a less homogenized force chain network compared to dense samples (Wang & Tsui, 2009), as indicated by the relatively greater amount of creep of loose samples than that of dense samples (see Table 4.3). Low confining pressure i.e. 30kPa may help prevent local structure collapse, as suggested by Bowman (2002). Another possible explanation is that loose samples have lower "rotational frustration" compared to dense samples (Lupogo, 2009). Rotational frustration is a measure of how easy particles rotate under loading. A further discussion, based on change in degree of particle orientation during aging, is discussed in chapter 6. In contrast, at 60 kPa and 120kPa confining pressures, N_G values of dense samples tend to be higher than those of loose samples. This suggests a greater aging rate of dense samples compared to loose samples. This is likely due to local structure collapse of loose samples, which is more likely to occur at higher confining pressure. Wang *et al.* (2009) reported that at 50 kPa confining pressure, the aging rate of loose clean sand was greater than that of dense sand, whilst at 100 kPa, dense sand samples developed larger aging rate than loose samples. Thus changes in aging rate behavior for this study occur at lower confining pressure (60 kPa instead of 100kPa) than the findings of Wang *et al*. (2009). This is likely due to the presence of fines. *Salgado et al.* (Salgado *et al.*, 2000) reported that the addition of fines to clean sand resulted in lower small-strain stiffness. Therefore it is likely that the presence of fines lowers the stress level at which the relative aging rates change between dense and loose sample. Despite this, the results in this study are generally consistent with the findings of Wang *et al*. (2009).

(c) Comparing K_0 and isotropically consolidated samples

Table 5-3 presents results of the aging effect on undrained stiffness for isotropically consolidated samples. Based on the table, we can compare the increase in undrained stiffness between dense K_0 consolidated samples (CKoU-7 and CKoU-9) and dense isotropically consolidated samples (CIU-10 and CIU-12) for 1 hour and 1 week of aging time, respectively. It can be seen than in general I_G and N_G values of isotropically consolidated samples are lower than those of K_0 consolidated samples. As an example, for initial stiffness, I_G and N_G values for the isotropically

consolidated tests are 8.24MPa and 15.65%, respectively, whilst for K_0 consolidated tests they are 9.7MPa and 22.58%, respectively. This suggests that the K_0 samples gain more stiffness than isotropic samples with time. This is likely due to higher stress ratio of K_0 sample. Additionally it may be due to the stress history of the dense isotropic samples, particularly CIU-12. That is, it is likely that during tamping the sample experiences higher stress than the mean effective consolidation stress, as suggested by Frost and Park (2003). This makes the sample behave as 'over-consolidated', as indicated by swelling of axial strain (see Figure 4.14). The 'over-consolidated' samples tend to have more stable packing with a more homogenized force chain network than those of normally consolidated samples. Similar observations, based on resonant column tests, of the effect of over-consolidation on aging rate was reported by Wang et al. (2009).

(d) Comparing moist tamped and dry pluviated samples

Table 5-3 shows that moist tamped samples have larger undrained shear modulus than those of dry pluviated samples. This is in accordance with previous studies (e.g. Ibrahim & Kagawa, 1991a; Lee, 2001). In terms of stiffness gain, Table 5-3 shows that I_G and N_G values of moist tamped samples tend to be greater than those of dry pluviated samples. As an example, for the selected moist tamped soil tests, I_G and N_G values for the initial shear modulus are 5.3MPa and 9.91%, respectively, compared to 2.73MPa and 7.46%, respectively, for dry pluviated soil tests. This suggests that if time effects are considered in design, a proper reconstitution method reflecting natural deposition for laboratory testing should be used. Otherwise it may overestimate the effect of time on small-strain stiffness.

Regardless of the magnitude of increase in stiffness, it can be said aging has significant effects on undrained small-strain stiffness. Thus care must be taken in laboratory practices because holding time may result in significant differences in stiffness over the small-strain range even if the samples are identical in density and procedure. Murashev (1997) reported that shear modulus of undisturbed samples

(older samples) were higher than reconstituted ones (younger samples) even the densities were identical.

(e) Qualitative aging comparison of silty sand and clean sand

A comparison of small-strain stiffness gain between silty sand in this study and clean sand from literature review study was attempted. It is realized that the comparison is not ideal because the conditions are not exactly the same (see table Table 5-4). Despite this, it is thought that the comparison may open up more insight about the effects of fines on aging.

Table 5-4 Qualitative comparison of stiffness increase between silty sand and clean sand

Ref.	USCS	Shape	Creep	Dr (%)	p' (kPa)	t_2 (min)	t_1 (min)	$G_{(t=t1)}$ (Mpa)	$G_{(t=t2)}$ (Mpa)	I_G (Mpa)	N_G (%)
CIU-26&CIU-27	SM	SA-A	isotropic	70	87	1440	1	53.4	70.2	5.3	9.9
Wang et al (2008)	SP	A	isotropic	77	100	2880	1	103.4	109.0	1.6	1.6

SA= sub angular; A= angular; In Wang *et al.* G was taken at 0.0005% strain; In this study G in the table refer to G_0 ; SM=silty sand; SP=poor gradeed clean sand

The table shows that the tests in this study and those from Wang et.al (2008), despite some differences e.g. mean effective stresses and aging time, are relatively similar considering they both were conducted on dense samples, under isotropic consolidation. The table shows that I_G and N_G values of silty sand (SM) i.e. 5.3 and 9.91 respectively are greater than clean sand (SP) i.e. 1.6 and 1.56 respectively. It appears that silty sand tends to gain more increase in stiffness with time compared to clean sand. This may be due to greater creep of silty sand. Wang *et al.* (2009) suggests that sand with higher fines content gains more increase in stiffness. It should be noted that fines used in the study of Wang *et al.* (2009) was kaolin (i.e. non-plastic clay), which may suggest that chemical aging mechanisms also play a role due to a certain extent. A further study of the effect and type of of non-plastic fines content on aging of silty sand is needed.

5.4 Undrained Cyclic Compression Test

5.4.1 General

Early work by Hardin and Black (1968) concerning the response of soil to dynamic loading showed a very small hysteresis loop under cyclic loading in a strain range not exceeding 0.01%. In the previous section it was shown that aging affected small-strain stiffness which in turn may affect also cyclic resistance.

There are two loading conditions in cyclic triaxial test i.e. two-way loading (include stress reversal or alternating sign of q) or one-way loading (only compression or extension cyclic loading), as illustrated in Figure 5-16. Different stress paths during cyclic triaxial tests will give different soil response. One-way loading in compression is more stable than two-way loading, whether they are isotropic or anisotropic (De Gennaro *et al.*, 2004; Ghionna & Porcino, 2006).

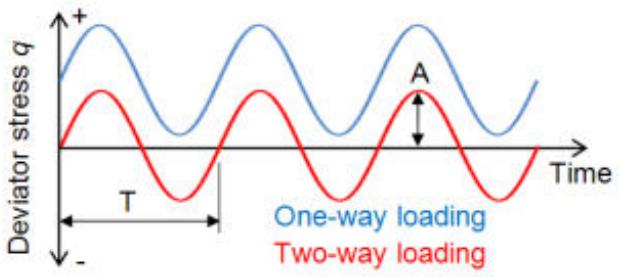

Figure 5-16 One way and two way cyclic loading. Note A=loading amplitude, T=loading period (Rees, n.d.)

Aging effects under two-way cyclic loading have been relatively more investigated by previous researchers compared to one-way cyclic loading (see Section 2.2.2.5). Recently, Saftner (2011b) performed two-way cyclic loading tests of loose moist tamped clean sand (CSR=0.225 and CSR=0.175) and found that increasing holding time, i.e. aging following isotropic consolidation, increased the number of cycles to initiate liquefaction across different values of CSR as shown Figure 5-17. Due to the limited investigation of aging effects on cyclic resistance

under one-way cyclic loading, this study focuses on this matter. One-way cyclic loading is relevant to the development of deformations in natural slopes, embankment slopes, dams and quay wall backfills during earthquake loading (Arangelovski & Towhata, 2007).

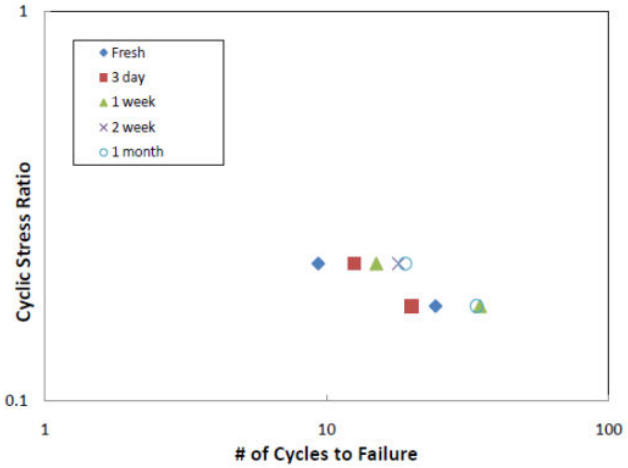

Figure 5-17 Aging effects on two-way cyclic resistance (Saftner, 2011)

In this study, one-way cyclic loading of triaxial tests were performed to evaluate the number of cycles to trigger strain-softening (N) at a given cyclic stress ratio (CSR), where CSR is defined as the ratio of shear stress (equal to half of deviator stress) to initial effective confining pressure. The number of cycles (N) in this study was taken as the number of cycles to trigger strain softening and consequent liquefaction, from a plot of p' versus q, as illustrated in Figure 5-18. Table 5-5 presents a list of cyclic tests in this study.

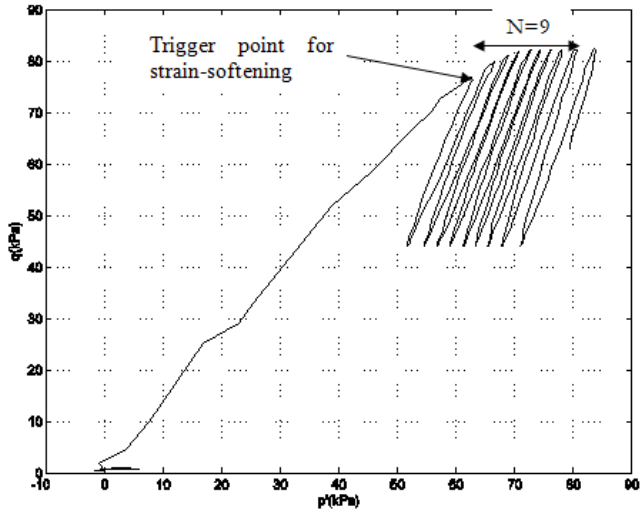

Figure 5-18 Definition of number of cycles to trigger strain-softening (N) used in this study

Table 5-5 Samples Tested in Cyclic Test

No	Method	Dr (%)	σ'_3(kPa)	K_0	Test ID	Aging Time (min)	CSR
28	MT	40.56	60	0.4793	OWKoU-28	1 min	0.12
29	MT	38.76	60	0.4803	OWKoU-29	1 day	0.12
30	MT	40.28	60	0.4761	OWKoU-30	1 week	0.12
31	MT	39.85	60	0.4793	OWKoU-31	1 min	0.18
32	MT	39.71	60	0.4803	OWKoU-32	1 day	0.18
33	MT	40.11	60	0.4761	OWKoU-33	1 week	0.18

5.4.2 Results

Figure 5-19 shows the stress-strain relationship for one-way cyclic loading of samples with a mean effective stress of 60kPa and CSR=0.12 (OWKoU-28, OWKoU-29 and OWKoU-30) for 1 min, 1 day and 1 week of aging time. The corresponding stress path is shown in Figure 5-20.

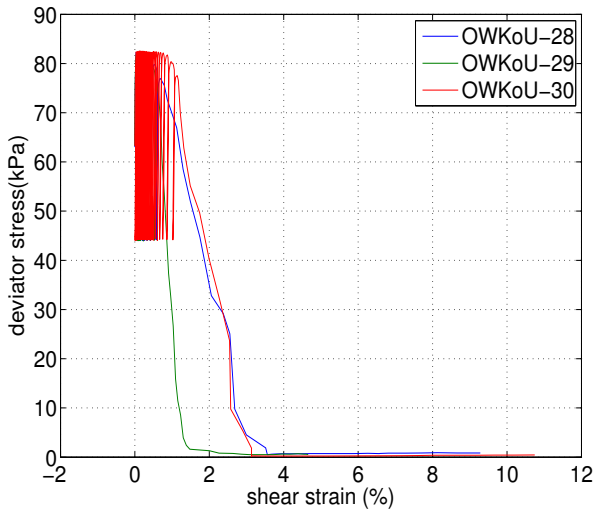

Figure 5-19 Stress-strain relationship of K_0 consolidated samples under one-way cyclic loading at σ'_3=60kPa; CSR=0.12 for 1 min (OWKoU-28), 1 day (OWKoU-29) and 1 week (OWKoU-30) of aging time

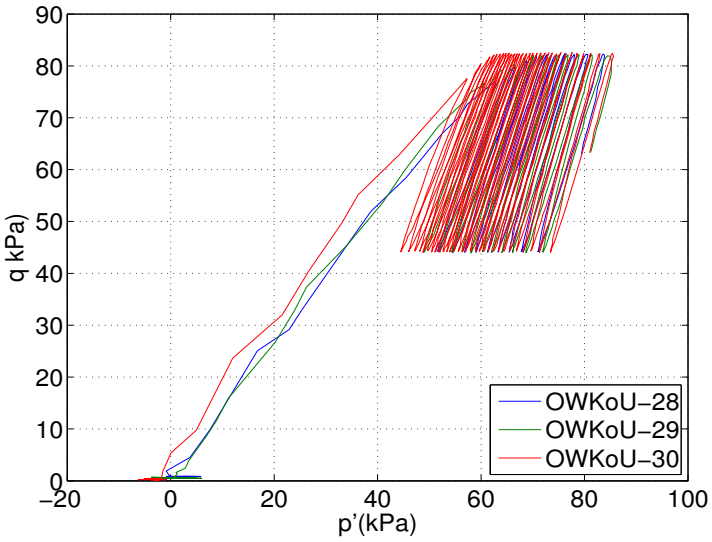

Figure 5-20 Stress path of K_0 consolidated samples under one-way cyclic loading at σ'_3=60kPa; CSR=0.12 for 1 min (OWKoU-28), 1 day (OWKoU-29) and 1 week (OWKoU-30) of aging time

Figure 5-21 shows the stress-strain relationship for one-way cyclic loading samples with mean effective stress of 60kPa and CSR=0.12 (OWKoU-28, OWKoU-29 and OWKoU-30) for 1 min, 1 day and 1 week of aging time. The corresponding stress path is shown in Figure 5-22.

Figures 21-24 show that all samples experience strain softening and reach zero deviatoric stress at different levels of strain. Aging effects on the number of cycles to trigger strain softening is discussed in the following section.

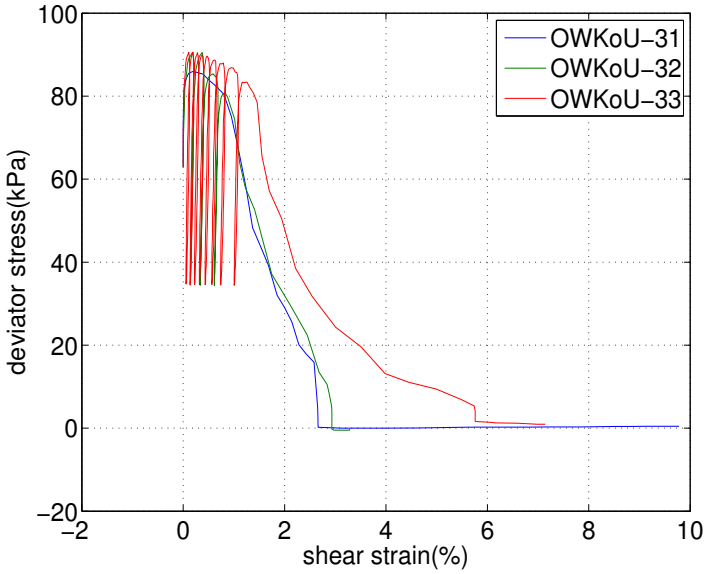

Figure 5-21 Stress-strain of loose K_0 consolidated samples at σ'_3=60kPa under one-way cyclic loading; CSR=0.18 for 1 min (OWKoU-31), 1 day (OWKoU-32) and 1 week (OWKoU-33)

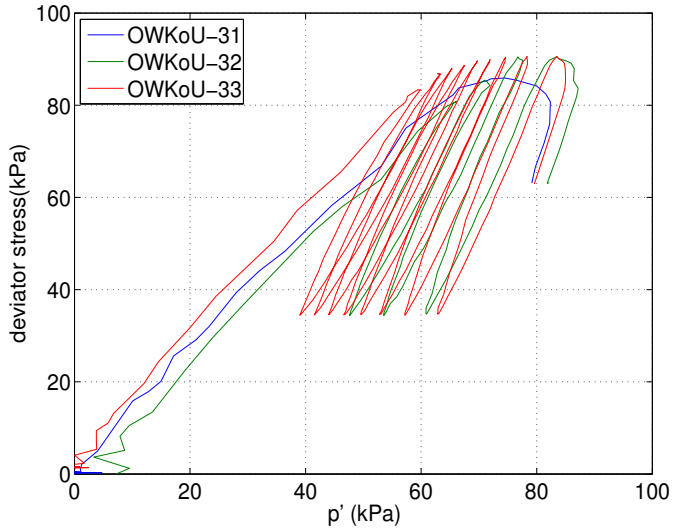

Figure 5-22 Stress path of loose K_0 consolidated samples under one-way cyclic loading at σ'_3=60kPa; CSR=0.18 for 1 min (OWKoU-31), 1 day (OWKoU-32) and 1 week (OWKoU-33) of aging time

5.4.3 Discussion

Figure 5-23 shows aging effects on the number of cycle to initiate liquefaction for both loose K_0 consolidated samples in Figure 5-21 (CSR=0.12) and Figure 5-22 (CSR=0.18). The figure clearly shows that the number of cycles to trigger strain softening and consequent liquefaction increases with aging time. It appears from the figure that the aging effect is more pronounced at lower CSR. For CSR=0.12 samples, the number of cycles increases from N=9 for 1 minute of aging to N= 12 and N=31 for 1 day and 1 week of aging sample, respectively. For CSR=0.18 samples, the number of cycles increases from N=1 for 1 minute of aging to N=4 and N= 9 for 1 week 1 day and 1 week of aging sample, respectively. Smaller CSR value means smaller strains thus more cycles are needed to destroy aging effects. Wang *et al.* (2009) reported that the effects of aging can gradually diminish when shear strains are higher. In addition, Bowman (2002) reported that very small load cycles tended to accelerate the dilatancy tendency of dense clean sand, thus enhancing aging.

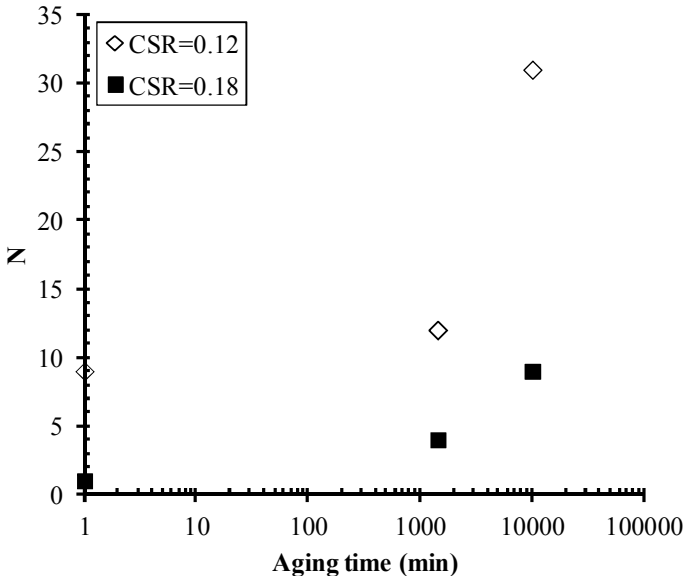

Figure 5-23 Aging effects on number of cycles to trigger strain-softening and consequent liquefaction under one way cyclic test

5.5 Summary

In accordance with the results of the previous sections, the following trends can be concluded:

1. Initial shear modulus (G_0) and undrained small-strain secant shear modulus increases with aging duration. This applies to dense and loose, moist tamped and dry pluviated sample, either K_0 or isotropically consolidated.

2. The rate of stiffness gain is higher at smaller strain than larger strain, with the tendency of diminishing at larger strain.

3. Loose K_0 consolidated samples, at 30kPa confining pressure used in this study, tend to gain more in small-strain stiffness compared to dense samples. However, at 60kPa and 120kPa, dense samples gain more in small-strain stiffness than loose samples.

4. Dense isotropically consolidated samples in this study tend to have a lower stiffness increase (over small-strain range) with aging time than the corresponding K_0 consolidated samples.

5. Dense moist tamped samples exhibit higher rate of stiffness increase (at small-strain range) compared to dense dry pluviated sample.

6. It appears that non-plastic silty sand produces more increase in small-strain stiffness with time than clean sand. This may be due to greater creep of silty sand. More research is needed to investigate the effect of non-plastic fines content and type on aging.

7. The number of cycles required triggering cyclic softening and liquefaction for one way cyclic loading condition increases with the aging duration. In addition the aging effect is more pronounced at lower CSRs

6 Microstructure Study of Aging of Silty Sand

6.1 Introduction

Microstructural study of soil in geotechnical engineering, either indirectly from numerical modelling or directly from image analysis, has gained some appreciation in recent years. The study of microstructure has enabled us, for example, to explain why various deposition methods result in different stress-strain relationship (Vaid *et al.*, 1999; Wanatowski & Chu, 2008; Wood *et al.*, 2008); it also has shed light on deformation and the localization mechanism of sheared granular materials (Alshibli & Sture, 1999).

This chapter focuses on shedding light on the aging mechanism of silty sand. It is realized that due to the presence of fines, change in the microstructure (if manifested) would be more subtle than that has been investigated by Bowman (2002) for dense clean sand, which involved approximately 2700 particles per fabric test. Thus a statistical approach was used by involving a larger number of grains i.e. approximately 10000 particles per fabric test in this study.

In addition, most of the direct microstructure studies of granular material have been performed on clean sand. Direct microstructural study of granular soil is relatively limited due to the difficulty in preserving it with minimal disturbance. Even rarer is the study of the microstructure of 'undisturbed' granular soil due to the cost of obtaining it in-situ. This chapter describes some insights via tests on the microstructure of 'undisturbed' sand and silty sand obtained by the gel-push sampling technique, in addition to reconstituted tests.

A total of 14 fabric tests (see Table 4-1) were performed (SEM images can be found in Appendix F). Each sample was reconstituted in the impregnation cylinder (see Figure 3.15 in Chapter 3 for the impregnation setup) to the desired density. The reconstituted sample was approximately 5 cm in diameter and 4 cm in height. A top cap was put on top of the levelled sample carefully. Then the sample was loaded

accordingly in the vertical direction. The vertical effective stress applied for each fabric test was matched to the K_0 consolidation stage of the triaxial tests that were also carried out (see table 4.1). Vertical strain due to initial top cap loading, hanger and weight were monitored. Samples of the same density which showed any discrepancy of axial strain during top cap loading and weight application were discarded and a new sample was made. The loaded samples then were aged for a certain aging time before being impregnated by epoxy resin (see section 3.4.1 in Chapter 3 for further detail).

Table 6-1 shows the fabric tests used in this study. Two undisturbed samples were used to gain some knowledge about the undisturbed microstructure of silty sand, whilst 12 samples were reconstituted with different densities, aging time and sample preparation methods in order to obtain a better understanding of the aging mechanism of sand with fines.

Table 6-1 Creep tests

No	Test ID	Method	Dr(%)	σ'_v(kPa)	Aging time
1	40301H	MT	40	57	1 hour
2	40301W	MT	40	57	1 week
3	40304M	MT	40	57	4 months
4	40308M	MT	40	57	8 months
5	40601H	MT	40	125	1 hour
6	40601W	MT	40	125	1 week
7	40601H_DD	DD	40	125	1 hour
8	40601W_DD	DD	40	125	1 week
9	70301H	MT	70	67	1 hour
10	70301W	MT	70	67	1 week
11	70601H_DD	DD	70	113	1 hour
12	70601W_DD	DD	70	113	1 week
13	gp-A	UD	na	80	-
14	gp-B	UD	na	50	-

MT= Moist tamped

DD= Dry pluviated

UD= Undisturbed from gel push sampling

6.2 Review

6.2.1 Overview of theoretical microstructure of silty sand

A theoretical microstructure of soil containing large and fines particles was originally proposed by (Terzhagi, 1956). The structure of silty sand named 'metastable' was proposed by him to explain submarine flow slides. Similar structure type, as illustrated by Figure 6-1(a) was also suggested by (Hanzawa, 1980) to explain quick behavior of Arabian silty sands.

A particle microstructure, where smaller particles sit between the larger particles (Figure 6-1) may develop and result in high volumetric compressibility. For spherical particles, smaller particles can sit between larger particles if the diameter of the larger particles is at least 6.5 times that of the fines ones (McGeary, 1961).When sheared sand particles become closer and in better contact, this results in increasing dilatancy tendency as illustrated by Figure 6-1(b) (Yamamuro & Lade, 1997). As the mean diameter of sand used in this study is approximately 4.7 times the mean diameter of silt (see Chapter 3) then silt particles cannot easily occupy the voids between the sand particles. Of course this does not consider other factors such as particle shape and the variation in particle size around the mean.

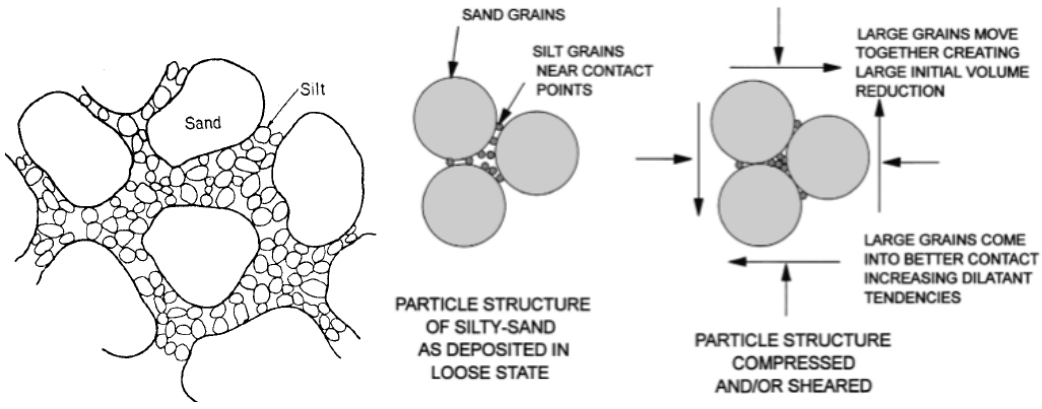

(a) (b)

Figure 6-1 Theoretical microstructure of silty sand (a) metastable structure (Hanzawa, 1980); (b) sheared silty sand (Yamamuro & Lade, 1997)

Additionally, fines content (beyond the scope of this study) also plays an important role in the behavior of silty sand. A transition fines content exists which separates sand-dominated or silt-dominated behavior. The transition fines content can be indicated by a plot of extreme void ratio and fines content (Yang, 2004). For the material in this study the transition zone is approximately 20-40% fines by weight, as shown in Figure 6-2. As the fines content in this study is 15%, below the transition fines content, then the overall behavior is expected to be sand dominated. In terms of force chains, not all fines particles are part of the network, as illustrated in Figure 6-3 (Voivret *et al.*, 2009). Force chains are path of force propagation in granular materials due to interplay between the contact geometry and force distribution (http://web.physics.ucsb.edu/~complex/research/granular.html). In the figure, force chains are represented by black lines; thicker lines are the stronger force network. Moreover, Yamamuro *et al.* (2008) postulated that there are five types of grain contact in silty sand structure: Large-Large (L-L) which refers to stable sand to sand contact; Large-Small-Large (L-S-L) represents relatively unstable sand-fines-sand and Large-Small-Void (L-S-V) referring to sand-fines-void and fines with no contact with sand. The last type of grain contact is considered have no role in the force chain network (passive contact), only increasing the density.

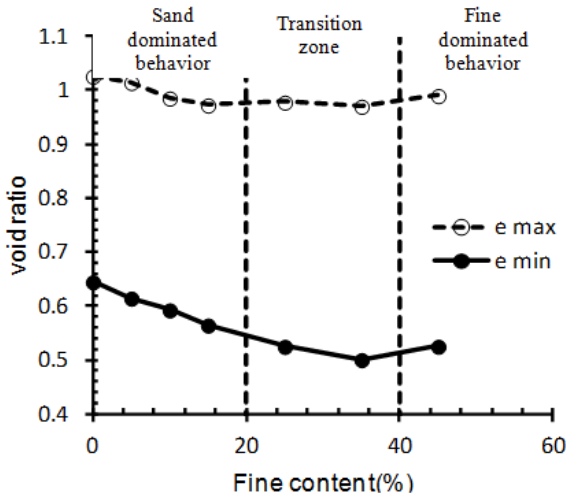

Figure 6-2 Variation of void ratio and fines content for material used in this study

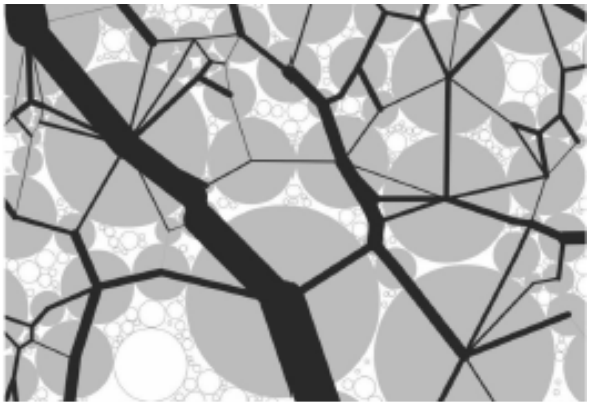

Figure 6-3 Typical Force chain network in polydisperse (well graded) granular material (Voivret *et al.*, 2009)

6.2.2 Fabric measurements

There are various fabric measurements used by different researchers such as contact anisotropy (e.g. Oda, 1972), particle orientation (e.g. Ibrahim & Kagawa, 1991a) and void ratio (e.g. Alshibli & El-Saidany, 2001). Contact anisotropy deals with the contact points between the particles. This measure is easier to be obtained from numerical modelling rather direct microstructure observation as used in this study. Given the difficulties in measuring contact points in real granular soils, particularly sand with fines, true contact points in a two dimensional plane as used in this study would be even more difficult to obtain and can be misleading. Therefore this measure is not used in this study. This study is concentrated on retrieving some basic trends of microstructure changes during aging of silty sand thus it was felt that particle orientation and void ratio are adequate as the measures.

6.2.2.1 Particle orientation

The orientation of a non-spherical particle can be represented by the inclination of the long axis of the particle to a reference axis (Mitchell & Soga, 2005). The true long three dimensional axis of a particle is difficult to determine. Thus in this study particle orientation is defined by the angle of the apparent long axis of the projected particle in two dimensions (vertical plane in this study). Particle orientations are generally expressed by a histogram (Oda, 1972) or rose

diagram (Ibrahim & Kagawa, 1991b). As this method of presentation is largely a visual one, it is felt that a rose diagram will give a more intuitive feel for the orientation distribution. Therefore in this study, rose diagram is used. An approximately circular rose diagram indicates a random particle orientation, whereas a non-circular rose diagram means more particles are aligned in a specific direction. Measurement of the angles in this study was obtained using the *angle* option within *Image-Pro Analyzer 7.0* software. *Angle* defines the angle between the vertical axis and vertical orientation of the major axis of ellipse equivalent to the particle, such that vertical is represented by 0^0 whilst horizontal is represented by 90^0.

Particle orientation distribution can be analyzed by circular statistics (Fisher, 1993). The Fisher distribution function $P_{dA}(\alpha)$ gives the normalized probability of finding a unit vector direction within an angular area dA, at angle of α from true mean direction (at which α=0). The Fisher distribution is defined as:

$$P_{dA}(\alpha) = \frac{\kappa}{2\pi \sinh(\kappa)} \exp[\kappa . \cos(\alpha)] \sin(\alpha) \qquad \text{Eq. 6-1}$$

The influence of different scales of structure on the behavior of soil is unknown. A soil with a relatively large number of fines particles (silt), as used in this study, may have different scales of interest. The results of rose diagrams in which all fines are included, for example, will be controlled by the fines particles although the large particles may form the major force columns and govern the soil's mechanical behavior. To avoid bias related to particle size, a weighted value for the orientation of each particle is displayed here. A comparison between weighted and non-weighted values can be seen in Appendix G.

The properties of particle orientation distribution can be obtained by the resultant vector length (R), mean resultant length (r), and mean angle (α_m):

$$R = \sqrt{\left\{\sum_{i=1}^{N}[l_i.sin\,(2\alpha]\right\}^2 + \left\{\sum_{i=1}^{N}[l_i.cos\,(2\alpha]\right\}^2} \quad \text{Eq. 6-2}$$

$$r = \frac{R}{\sum_{i=1}^{N} l_i} \quad \text{Eq. 6-3}$$

$$\alpha_m = \frac{1}{2}tan^{-1}\left(\left\{\sum_{i=1}^{N}[l_i\,sin\,(2\alpha_i]\right\} / \left\{\sum_{i=1}^{N}[l_i\,cos\,(2\alpha_i]\right\}\right) \quad \text{Eq. 6-4}$$

where l_i is the length of long axes of the particle, N is the number of measurements, α is the angle between the unit vector and the true direction and r is a simple measure of the concentration. The value of r ranges from zero to one. Higher r value indicates more orientated data.

Another parameter that also often be used to measure degree of cluster is von-Mises concentration parameter, κ, which can be estimated from the equation below (Butler, 1992)

$$\kappa = \frac{N-1}{N-R} \quad \text{Eq. 6-5}$$

In this study r and κ are referred to degree of orientation. An increase in r or κ indicate a more orientated data and a reduction in anisotrophy of the orientation.

In this study, rose diagrams and Fischer statistical analysis were drawn and calculated by the aid of Geo-Orient ver. 9.5.0 developed by Dr. Rod Holcombe (http://www.holcombe.net.au/).

6.2.2.2 Void ratio

There are essentially two different ways to measure distribution of voids. The first method, which was introduced by Oda (1976), is to locate the centroid of particles and link them to produce polygons, representing individual void elements. The second method is to measure the mean free path between particles by use of scanning line which passes through both particles and voids (Kuo, 1998). Bowman (2002) argued that interlocking of particles may cause soils to age. Interlocking particles are more related to particle edges rather than particle centroids, so that a mean free path method was used in this study to measure the distribution of spatial distance between particles. The displacement and orientation of the lines are varied. A representative void is then produced by summing over those found on a number of scanned lines in each direction. The directions of the scanning lines used here were vertical and horizontal as illustrated in Figure 6-4, commensurate with principal vertical and axisymmetric radial stresses.

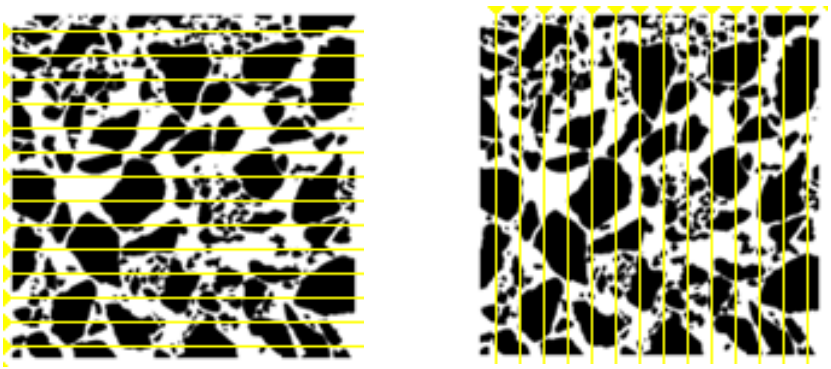

Figure 6-4 Mean free path

In this study spatial or void distance is determined with the aid of the *calliper* tool within **Measure** menu in the *Image-Pro Analyzer 7.0*. The calliper tool measures distance according to particle edge and different colour between the particle (black) and void (white). Combined with the calliper tool, two macros were written in Visual Basic for Applications (VBA) to automate the making of the detection line and measuring the void distance over the sample length. The first macro was to automate the measurement in the horizontal direction whilst the

second one in the vertical direction. For edge detection, the smoothing option was set to the minimal value so that relatively close particles were treated as separate. The shift distance of the calliper was set to be small enough (i.e. 10 pixels) so it could pass through the fines particles (minimum size is 15 pixels). The output for each calliper line of an image was transferred into a text file. Another macro was written in Microsoft Excel to combine all the files automatically into one. Bowman (2002) suggested the use of variance and kurtosis as statistical measures to asses particle interlock. For an interlocked structure to have the same average density as an unlocked one there must be areas where particles are more clustered and more loosely packed, compared to the unlocked structure. In another words particle interlock should relatively increase with variance. Variance (s^2) is defined as

$$s^2 = \frac{\sum(x - x_m)^2}{n} \qquad \text{Eq. 6-6}$$

where x is the log of void distance along the sample length, x_m is mean void distance and n is the number of void distances. It should be noted, however, that the material used in Bowman's study was clean sand whereas the material in this study contains about 15% of fines; therefore the ratio of the variance to mean was also used in this study in an attempt to measure interlock. It is a normalized measure of whether a set of data is clustered or dispersed, and also is called the index of dispersion. It answers the question of how big is the variance of the distribution relative to mean of the distribution. It was thought that higher ratio of variance to mean indicates a more interlocked structure.

Kurtosis is a measure of peakedness of the curve compared to a truly normal curve. In this study it is a measure of relative number of closely packed particles and large void gaps. It is formulated as below:

$$\beta = \left[\frac{n(n+1)}{(n-1)(n-2)(n-3)}\sum\left(\frac{x - x_m}{s}\right)^4 - \frac{3(n-1)^2}{(n-2)(n-3)}\right] \qquad \text{Eq. 6-7}$$

Bowman (2002) argued that the more interlocked structure has more negative kurtosis value, corresponding to a flatter distribution.

6.3 Microstructure changes of dense samples

6.3.1 Orientation distribution

6.3.1.1 General

Two sets of fabric tests on dense samples were performed i.e. one set on dry pluviated sand (70601H-DD and 70601W-DD) and one set on moist tamped sand (70301H and 70301W). Approximately 10000 particles were analyzed per test for particle orientation. Results for those tests are visualized by rose diagram and presented in term of Fischer statistics for the particle orientation. Separate analysis for 'sand size' particles and 'fines particles' are also performed in order to see anisotropy between large and small grains. It is realized that it will be difficult to determine which particles are fines (less than 75 micron in diameter in a sieve analysis) due to the two dimensional projection. Effort was trialled to differentiate fines from sand based on the material composition utilizing tools on SEM. The silica flour manufacturers, i.e. Sibelco reported that the silica flour that was used as fines in this study is almost pure quartz with silica dioxide i.e. 99.8% (see Appendix A). It was assumed that the materials impurities are greater for natural sand. Based on the assumptions, it was thought that fines size particles in two dimensional projections are most probably sand. However, SEM material element composition suggests that some of the sand size particles have high degree of purity also (see Figure 6-5). Thus it is still difficult to differentiate fine size particles whether they are fines or sand. In addition the number of fines size particles involved in each fabric test is relatively large i.e. approximately 7000 (see Table 6-2). Therefore it was deemed that required time to check material composition for each fines particle is not practical. Regardless it can be determined that particles having a feret minimum equal to or larger than 75 micron can be classified as sand size. Feret minimum is the smallest the distance between two parallel tangents of the particle at an arbitrary angle, and is often used as the diameter equivalent to a sieve analysis (Sympatech GmBH, 2013). In this study, the rest of the particles are assumed to be fines particles. This assumption results in a higher fines content than the fines

content determined from the particle size distribution. For example it was found that the fines fraction to total area of the images for dense moist tamped and dry pluviated sample is approximately 12-13% (see Table 6-2), which is equivalent to a fines content of approximately 26% (when it is actually 15%). However, the separation is aimed to retrieve some basic trends of apparent orientation of larger particles (sand) and fines particles; therefore the approach used is deemed adequate for this purpose.

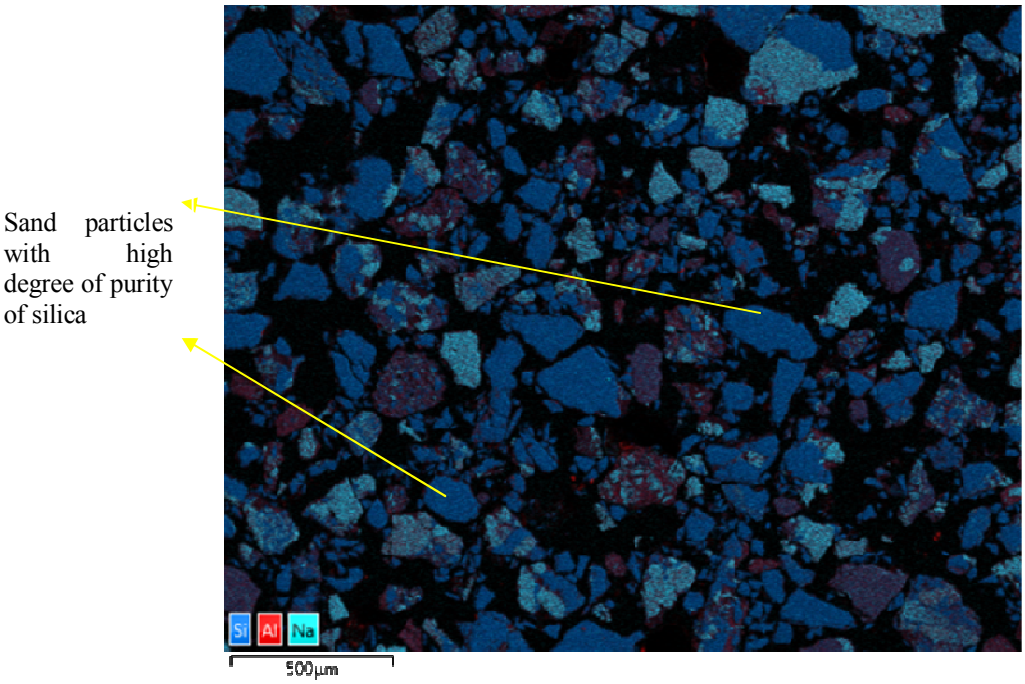

Figure 6-5 Surface map of element

6.3.1.2 Moist tamped versus dry pluviated sample

A general visual observation from these sets of rose diagrams (see Figure 6-6 and Figure 6-7) is that the moist tamped method produces fabric which is more isotropic than the dry pluviated method. This is supported by r and κ values (see Table 6-2) of the moist tamped samples which are less than those of dry pluviated samples, indicating higher isotropy. This is in accordance with previous studies of clean sand fabric such as Park (1999) and Jang and Frost (1998). This study shows that a similar trend is observed for silty sand. Table 6-2 shows sand particles are

more orientated than 'fines' both in moist tamped and dry pluviated samples. In addition the table also shows that 'fines' in the moist tamped samples are much less orientated than in the dry pluviated sample, with r and κ values close to zero.

Table 6-2 Fischer statistical analysis for orientation of dense dry pluviated samples (70601H-DD&70601W-DD) and moist tamped samples (70301H&70301W)

Sample		%fraction*	e	N	α_m	r	κ
70601H-DD	All	59	0.684	10633	84±0.9	0.178	0.360
	Sand	46	1.174	1808	81.2±0.9	0.299	0.630
	'fines'	13	5.453	8825	87.9±1.6	0.121	0.240
70601W-DD	All	59	0.687	9221	89.1±0.8	0.205	0.420
	Sand	47	1.132	1705	87.5±0.9	0.299	0.630
	'fines'	12	8.018	7516	91.5±1.4	0.148	0.300
70301H	All	60	0.679	9430	174.5±3.1	0.054	0.110
	Sand	48	1.306	1689	5.1±3.3	0.080	0.160
	'fines'	12	7.097	7741	162.3±4.8	0.045	0.090
70301W	All	59	0.683	10907	1.9±2.9	0.057	0.110
	Sand	47	1.324	1719	0.6±1.8	0.150	0.300
	'fines'	12	7.038	9188	34.2±5.4	0.005	0.010

e=void ratio; N=number of particle

*to total area

6.3.1.3 Dense dry pluviated sample

Figure 6-6 gives the orientation for 70601H-DD and 70601W-DD tests, of one hour and one week aging time. Mean directions are indicated by a small black arrow. It can be seen that dry pluviation produces fabric that tends to have the long axis of particles horizontally orientated. A general trend also can be observed that sand and 'fines' tend to have similar orientation. The results from the rose diagram are supported by the Fischer statistics in Table 6-2, which give overall mean orientation of 84°or 264° (due to the bi-directional nature of the orientated data the mean angle of x° could be represented also by x+180°) and 89° or 269.1°, for one hour and one week aging time, respectively. To avoid confusion, the mean angles for the rest of this chapter are presented only in x°).

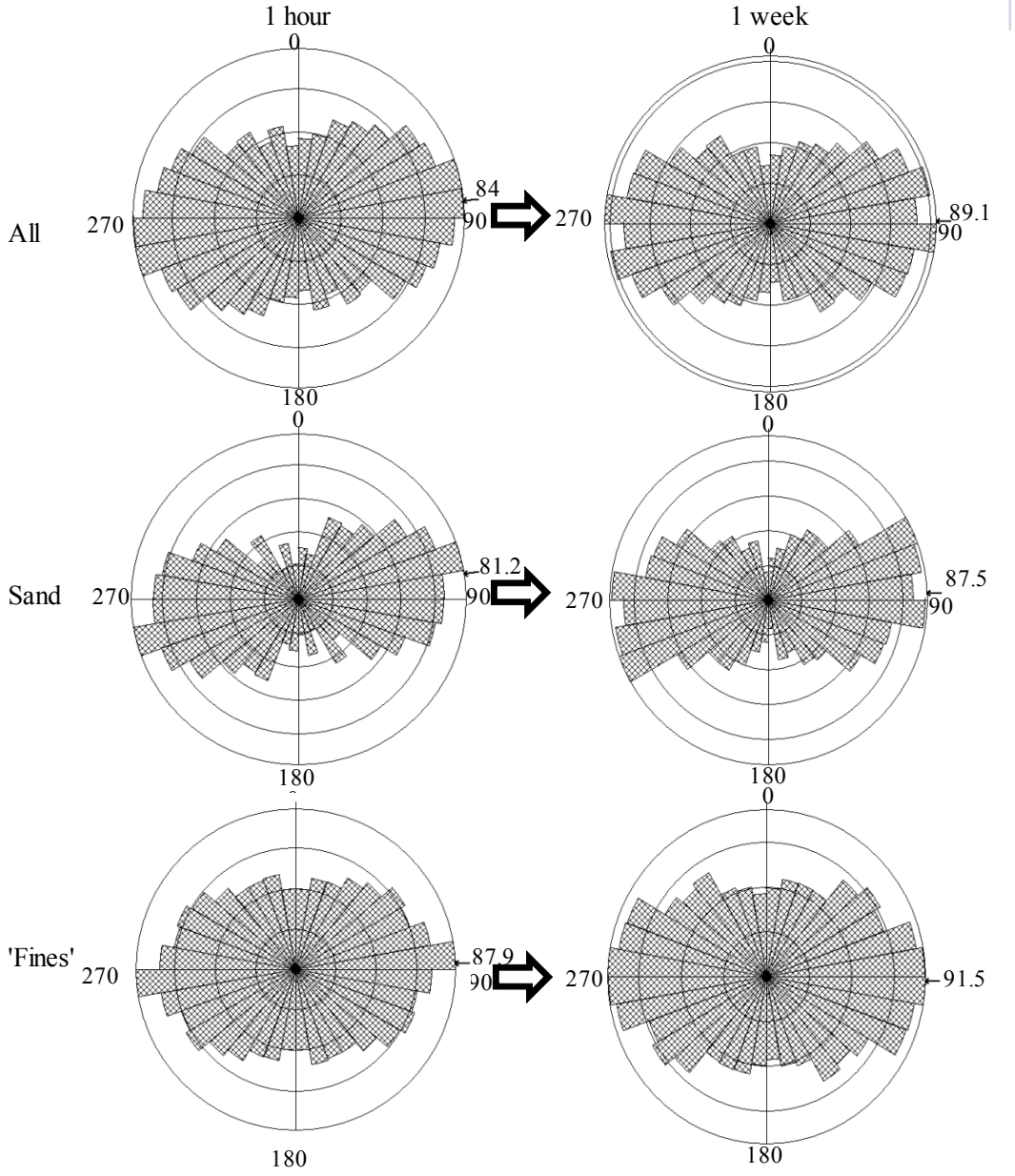

Figure 6-6 Change in grains orientation for dense dry pluviated sample at σ'_v =113kPa i.e. 70601H_DD (left) and 70601W-DD (right)

Figure 6-6 shows that the mean orientation changes from 84° to 89°. As particles initially are slightly inclined from the horizontal and major principal stress direction is vertical, it can be seen that with time particles tend to push away toward horizontal axis. A similar tendency of particle rotation was found from separate rose diagrams of sand and 'fines'. It can be seen also that as the soil ages the degree of

orientations tend to increase. For all particles, κ value increases from 0.36 (one hour) to 0.42 (one week). A similar trend was found with r i.e. increase from 0.18 at one hour to 0.2 at one week. Interestingly, for sand only, κ and r are relatively the same over time. This indicates much of the change in the degree of orientation occurs in the 'fines' as shown by κ which increases from 0.24 to 0.3 or r which increases from 0.121 to 0.148. Although some sand particles may be included in the 'fines' size category, it can be said that change in the degree of orientation is contributed mainly from 'fines'. This also indicates that although theoretically the force column consists mainly of sand size particles (based on Figure 6-2), in dense silty sand, fines may have a significant role in the force column network and they may contribute relatively significantly during aging. This also suggests more fines fill the voids between the sand grains for dense samples and they have more contact (either between them or with sand) than those in loose samples, as discussed also in section 6.4 . Thevanayagam and Mohan (2000) postulated that in loose silty sand (fine content less than the transition fine content), the fines tend to just float in the voids between the sand and have less role in the force chain network.

6.3.1.4 Dense moist tamped sample

Figure 6-7 presents the orientation for 70301H and 70301W tests, of one hour and one week aging time. The mean direction of all particles for the 1 hour sample is 174.5° whilst for one week it is 1.9.° Change in the mean particle orientation also occurs for separate sand and 'fines' analysis (see Table 6-2). It is interesting to note that the degree of orientation appears to be the same despite a slight increase of r value. On the one hand, it can be seen clearly from the table that as the sample ages, there is a significant increase in the value of r and κ of sand size particles, i.e. from 0.08 to 0.15 and from 0.16 to 0.3, respectively. On the other hand, there is a decrease in the degree of orientation of 'fines' size particles e.g. κ change from 0.09 to 0.01.

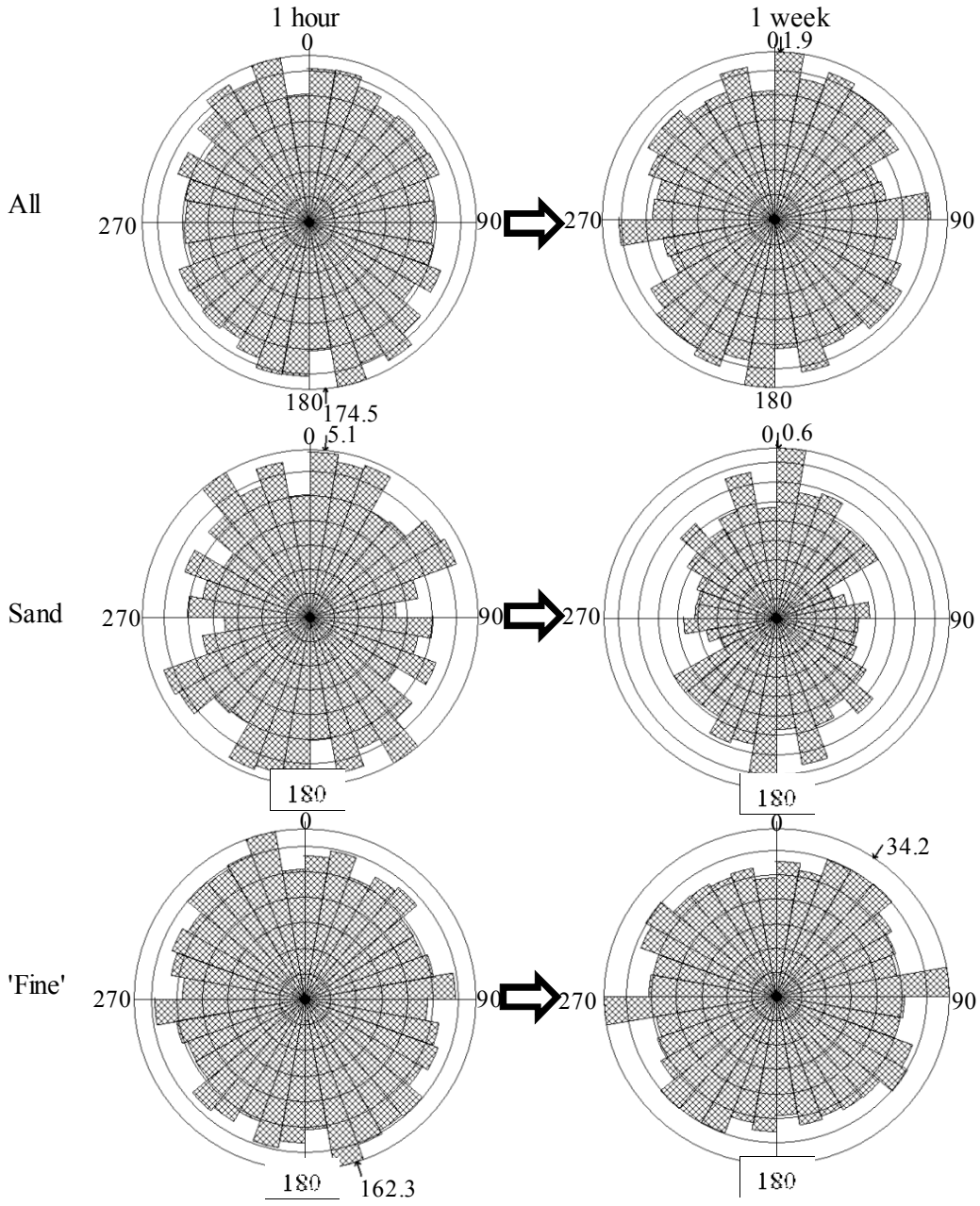

Figure 6-7 Change in grains orientation for dense moist tamped sample at σ'_v =67kPa i.e. 70301H_MT (left) and 70301W-MT (right)

6.3.2 Spatial distance distribution

6.3.2.1 General

Figure 6-8 shows a typical distribution of particle spacing on a histogram, based on 70301H, which gives a highly positive-skewed distribution. This indicates that there are large number areas with closer void distance than areas with greater void distance. In order to be meaningful, this type of distribution should be transformed to approach normality (Chatfield, 1983). A fitting distribution analysis gives a log normal distribution as the best fit. Thus all data and statistical analysis were performed on log form.

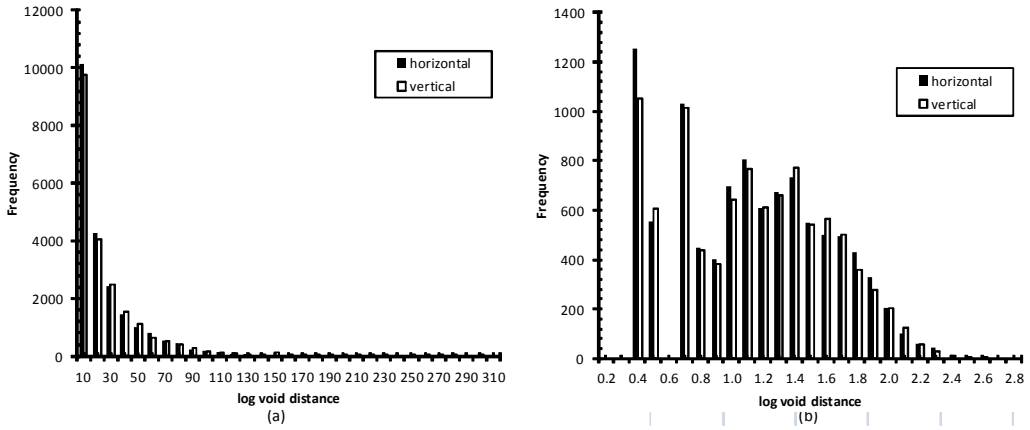

Figure 6-8 Typical void distance distribution based on 70301H in arithmetic (a) and log (b) scale

Spatial void distance analysis was performed mainly on all particles. However as the fine content in this study indicates a sand-dominated behavior (see Figure 6-2), additional spatial analysis was also performed on sand size particles throughout all the samples in this study. It is realized that spatial analysis on sand particles could be influenced by artifices in the data (an apparent lessening of the number of sand particles). Based on weight-volume relationship of prepared samples in the fabric test, we can calculate than the fractions of sand in dense and loose condition are 51% and 48% respectively (see Appendix H). Based on image analysis, the sand fraction for dense and loose samples ranges from 46-48 % (Table 6-3) and 41-46 % (see Table 6-5) respectively. Those ranges indicate that the sand

fraction for the dense samples from image analysis is equivalent to 77-85% of the prepared sample. For the loose samples, the range is equivalent to 79-85% of the prepared sample. This suggests separate sand analysis for spatial distance distribution can reasonably be attempted, considering that the overall behavior is sand-dominated as indicated by Figure 6-2.

Table 6-3 Void distance analysis for dense dry pluviated (70601H_DD&70601W_DD) and moist tamped (70301H&70301W) samples at σ'_v =113kPa

Sample		% Frac.	e	N	mean		variance		kurtosis		Varian / Mean	
					V	H	V	H	V	H	V	H
70601H_DD	All	59	0.684	10633	1.056	1.097	0.176	0.181	-0.681	-0.623	0.167	0.165
	Sand	46	1.174	1808	1.523	1.569	0.254	0.258	-0.267	-0.168	0.167	0.164
70601W_DD	All	59	0.687	9221	1.087	1.125	0.197	0.205	-0.759	-0.684	0.182	0.182
	Sand	47	1.132	1705	1.473	1.512	0.260	0.274	-0.325	-0.378	0.177	0.181
70301H	All	60	0.679	9430	1.081	1.069	0.239	0.245	-0.859	-0.875	0.221	0.229
	Sand	48	1.306	1689	1.517	1.506	0.308	0.304	-0.409	-0.448	0.203	0.202
70301W	All	59	0.683	10907	1.088	1.085	0.233	0.236	-0.920	-0.910	0.215	0.217
	Sand	47	1.324	1719	1.397	1.503	0.331	0.300	-0.768	-0.405	0.237	0.200

6.3.2.2 Moist tamped versus dry pluviated sample

Table 6-3 shows that, for all particles, the absolute difference between mean log void distance in the vertical and horizontal direction is greater in dry pluviated samples than in moist tamped samples (i.e. 0.042 compared to 0.011). This suggests that initial fabric of dry pluviated sample is relatively anisotropic whilst moist tamped samples tend to be near isotropic. Dry pluviated samples generally have lower void distance in the vertical direction compared to the horizontal one. A similar observation was found by (Masad, 1998). This is due to closely spaced gaps in the vertical direction of horizontally orientated fabric. The table also shows that initially the moist tamped sample (70301H) generally has higher variances (i.e. 0.239 vertically and 0.245 horizontally) are than those of the dry pluviated sample (70601H_DD) (i.e. 0.176 vertically and 0.181 horizontally). Similar to variance, variance to mean ratio or index of dispersion values of the moist tamped sample are larger than those of the dry pluviated sample. This indicates that initially that the particles of the moist tamped sample are more clumped. In term of kurtosis, the

dense moist tamped sample generally have lower kurtosis values (i.e. -0.859 vertically and -0.875 horizontally) than those of the dry pluviated sample (i.e. -0.681 vertically and -0.623 horizontally). Lower kurtosis suggests a flatter curve distribution (Bowman, 2002). This suggests that the moist tamped sample is more structured than dry pluviated sample. Overall it can be said that moist tamped sample is more isotropic than dry pluviated sample. Additionally moist tamped sample start already clustered and structured, thus there is less room for particle movement towards structuring than for the dry pluviated sample.

6.3.2.3 Dense dry pluviated sample

Figure 6-9 shows a plot of mean void distance in the horizontal and vertical directions when data in each direction from test 70601H_DD and 70601W_DD are combined (18 data points in each direction). In general there is medium and significant[1] linear relationship between mean log void distance and void ratio as shown by coefficient correlation r (square root of R^2). For horizontal and vertical direction r=+0.55 and r=+0.56 respectively.

Figure 6-10 presents plots of mean void distance versus void ratio for all particles for tests 70601H_DD and 70601W_DD. It can be seen from the figure that overall there are slight changes over time in the mean void distance both horizontally and vertically. Table 6-3 shows that mean log void distance in vertical direction increases from 1.056 for the one hour sample to 1.087 for the one week sample. Horizontally it increases from 1.097 to 1.125. The increases suggest growth in voids both in the horizontal and vertical direction. In term of coefficient of correlation (r) between mean log void distance and void ratio, it was found that for the horizontal direction, r=+0.32 (not significant) and r=+0.69 (significant) for one hour and one week samples, respectively. Vertically r=+0.37 (significant) and r=+0.5 (significant). Further examination however shows that there is a strong significant linear relationship for sand particles (both in the horizontal and vertical

[1] It should be noted that for a random data sets of 9, 18 and 27 points, the critical r values corresponding to 95% confidence interval are 0.602, 0.468 and 0.367. Values higher than critical r are considered significant. (Chatfield, 1983)

directions and for one hour and one week samples) as shown by Figure 6-11 with r ranging from +0.89 to +0.95. This is likely due to the more anisotropic nature of dry pluviated samples as revealed by Table 6-3. Accepting a linear relationship, it can be seen that mean log void distance or spacing tends to increase with time both in the vertical and horizontal direction. The increases are 3.5 and 2.5% for vertical and horizontal direction, respectively. Again these increases in mean log spacing indicate void expansion or growth.

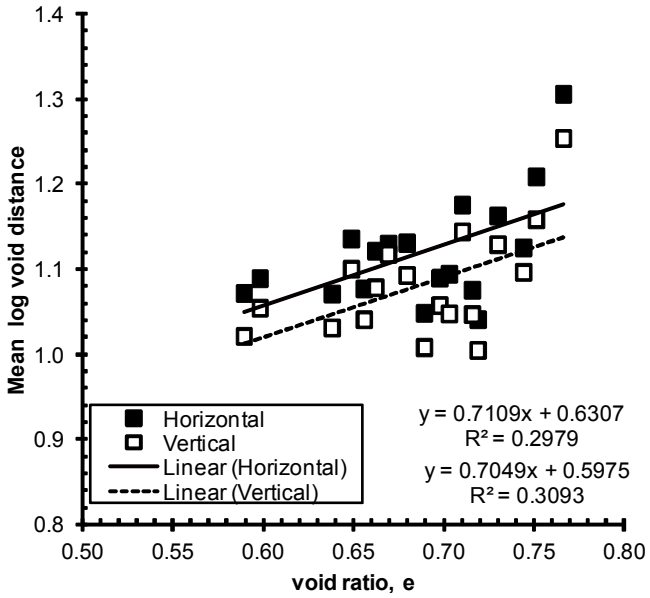

Figure 6-9 Mean log void distance for dense dry pluviated samples (all) at σ'_v =113kPa co i.e. combined data of 70601H_DD&70601W_DD: (a) horizontal (b) vertical

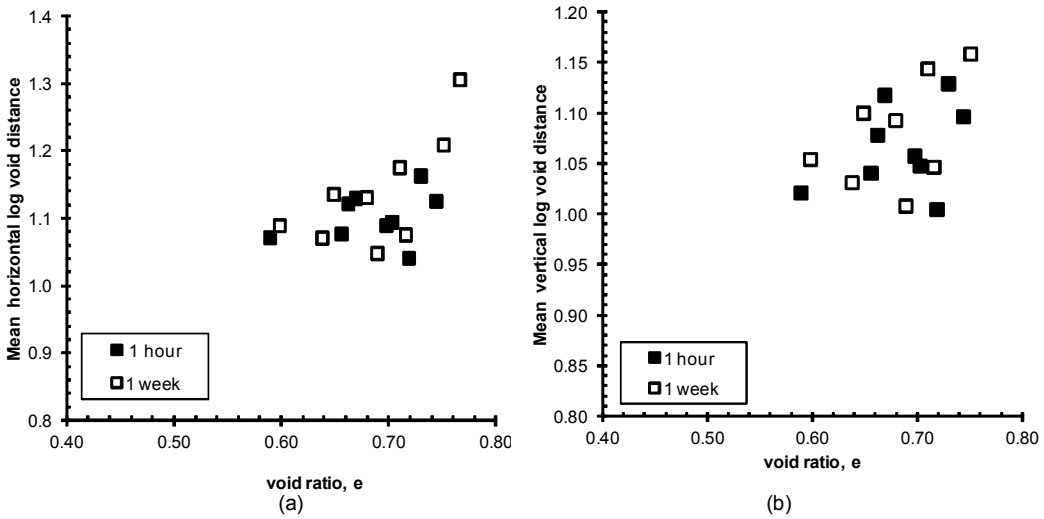

Figure 6-10 Mean log void distance for dense dry pluviated samples (all) at σ'_v =113kPa co i.e. 70601H_DD&70601W_DD: (a) horizontal (b) vertical

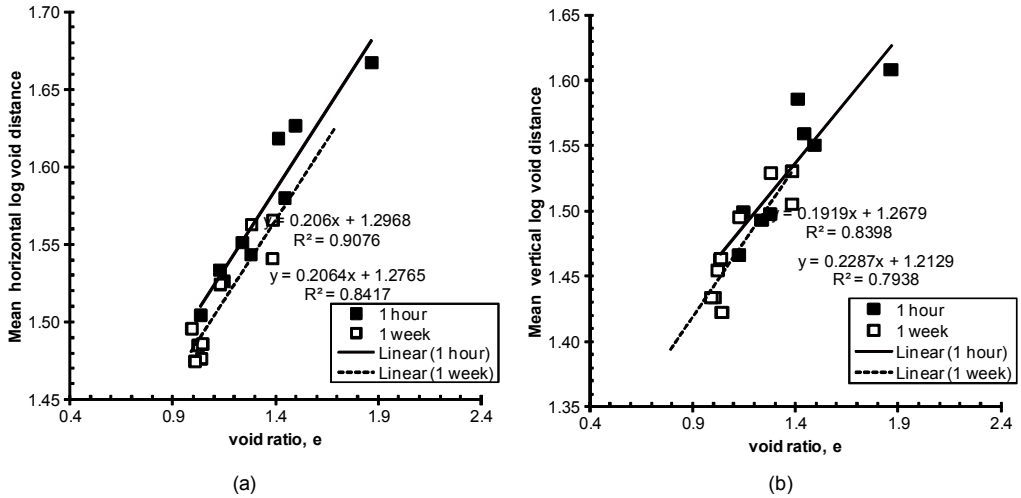

Figure 6-11 Mean log void distance for dense dry pluviated sample (sand) at σ'_v =113kPa co i.e. 70601H_DD&70601W_DD: (a) horizontal (b) vertical

Figure 6-12 shows plots of variance versus void ratio. It can be seen from the figure that generally variances both in horizontal and vertical direction change with time. The figure reveals that variances of the one week sample tend to be above those of the one hour sample. Table 6-3 supports the observation from Figure 6-12 that variances are increasing with time, horizontally and vertically, for all particles and sand particles. A similar observation was reported by (Bowman & Soga, 2003) on dense air pluviated fine sand, which produced a similarly horizontally orientated fabric. For all particles, variance increases from 0.176 to 0.197 vertically, while

horizontally it increases from 0.181 to 0.205. For sand particles only, vertically, variance increases slightly from 0.254 to 0.260. Whilst horizontally, variance increases from 0.258 to 0.274. This indicates that with time under load, particles clustered together, thus increasing variance of void distance, most notably for all particles. It should be noted that the one hour sample shows no relationship between variance and void ratio with r=-0.07 horizontally and r=-0.08 vertically. The one week sample shows a significant linear relationship with r=+0.62 both in the horizontal and vertical direction.

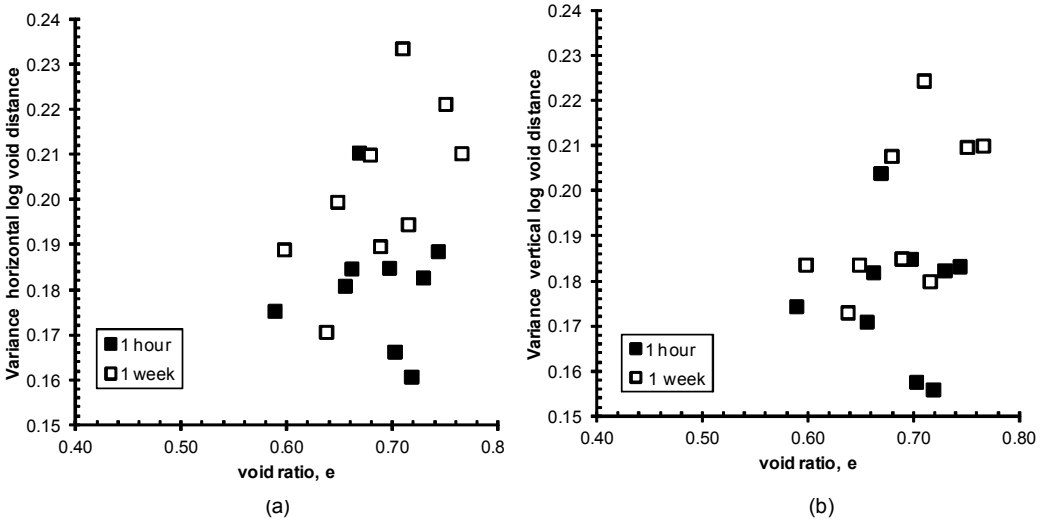

Figure 6-12 Variance log void distance for dense dry pluviated sample (all) at $\sigma'_{v=}$ 113kPa co i.e. 70601H_DD&70601W_DD: (a) horizontal (b) vertical

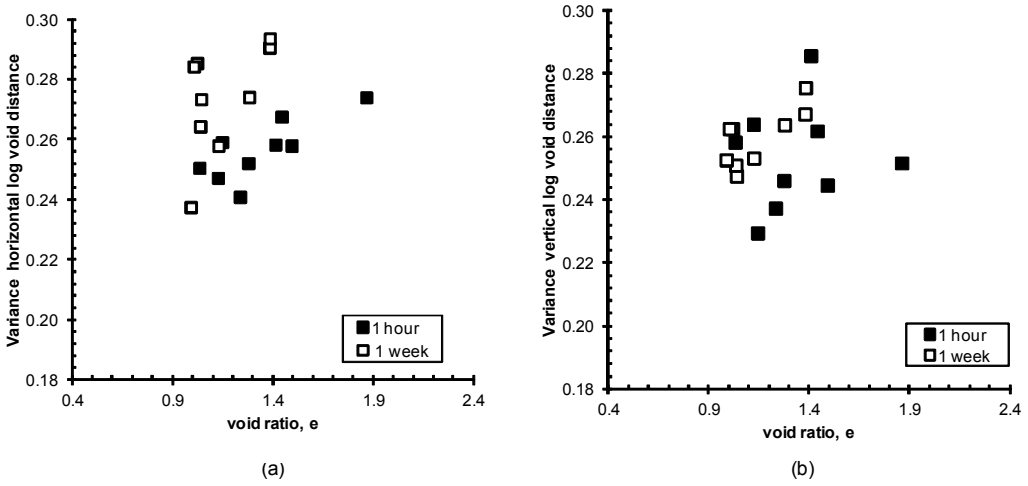

Figure 6-13 Variance log void distance for dense dry pluviated sample (sand) at $\sigma'_{v=}$ 113kPa co i.e. 70601H_DD&70601W_DD: (a) horizontal (b) vertical

Figure 6-14 illustrates the relationship between kurtosis and void ratio. The figure generally shows that kurtosis values change with time. Kurtosis values of the one week sample tend to be above (lower value) those of the one hour sample. Based on kurtosis, a similar trend was observed for moist tamped and dry pluviated samples that aged samples generally have lower kurtosis values, as observed also by (Bowman, 2002). Kurtosis values decreased from -0.681 to -0.742 vertically and from -0.623 to -0.683 horizontally (see Table 6-3). It should be noted that there is no significant linear correlation between kurtosis and void ratio as represent by low r values i.e. r=-0.07; r=-0.47 (horizontal) and r=-0.2 and r=-0.25 (vertical).

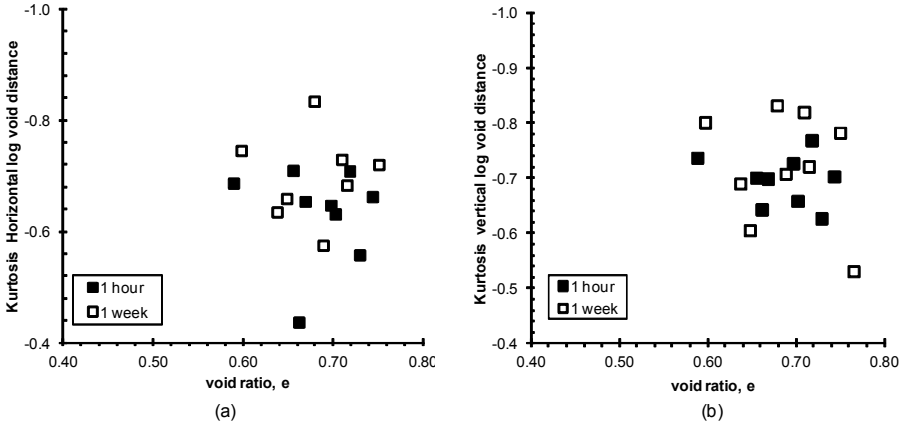

Figure 6-14 Kurtosis log void distance for dense dry pluviated sample (all) at σ'_v =113kPa co i.e. 70601H_DD&70601W_DD: (a) horizontal (b) vertical

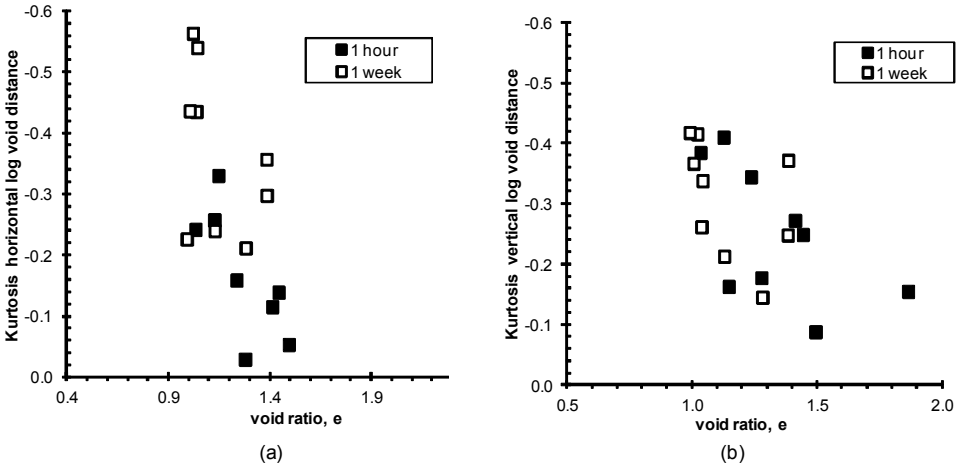

Figure 6-15 Kurtosis log void distance for dense dry pluviated sample (sand) at σ'_v =113kPa i.e. 70601H_DD&70601W_DD: (a) horizontal (b) vertical

Figure 6-16 and Figure 6-17 show plot of index of dispersion against void ratio for all and sand particles respectively. The one week sample has a larger of index of dispersion both in the vertical i.e. from 0.167 to 0.182 and horizontal direction i.e. from 0.165 to 0.182 (see Table 6-3). A similar tendency to increase also applies to sand particles alone. It should be noted that there is no significant linear relationship between the index of dispersion and void ratio, with maximum r=-0.38. Similarly no correlation was found for sand particles alone with maximum r=-0.37

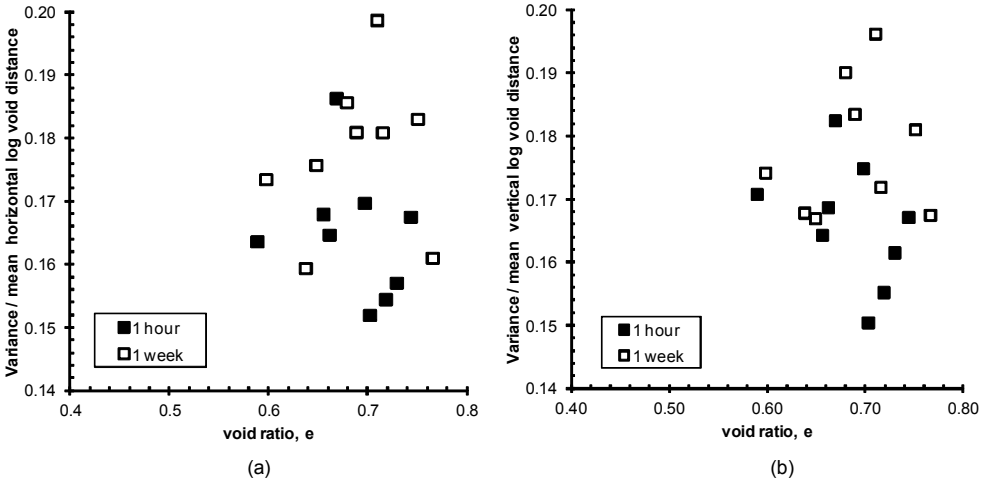

Figure 6-16 Variance/mean void distance (all) for dense dry pluviated sample at σ'_v =113kPa co i.e. 70601H&70601W: (a) horizontal (b) vertical

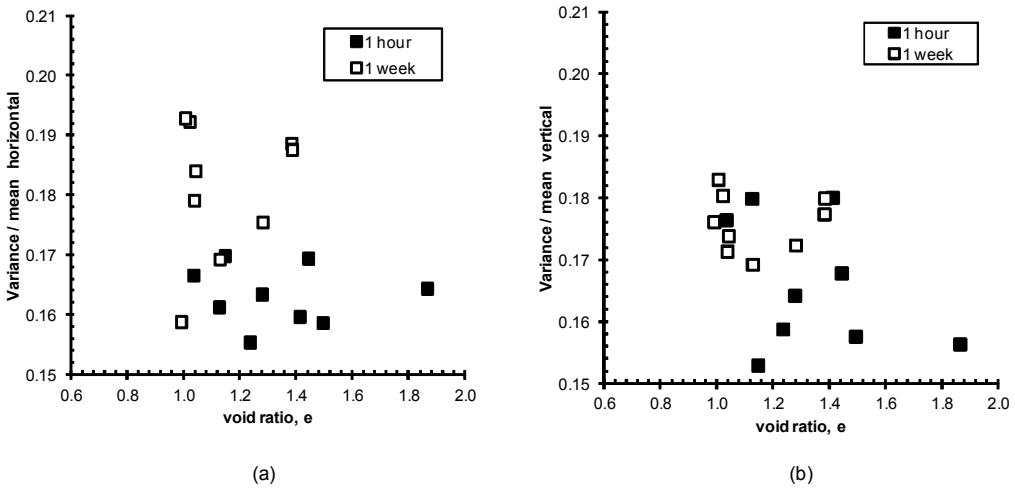

Figure 6-17 Variance/mean void distance (sand) for dense dry pluviated sample at σ'_v =113kPa co i.e. 70601H&70601W: (a) horizontal (b) vertical

6.3.2.4 Dense moist tamped sample

Figure 6-18 and Figure 6-19 show a plot of mean void distance for dense moist tamped silty sand for 1 hour and one week aging time (all and sand particles respectively). The figure shows there is a slight change in the mean log void distance both in horizontal and vertical direction. Based on Table 6-3, for all particles, generally mean log void distance or spacing tends to increase with time both in the vertical and horizontal direction. For moist tamped samples the mean log void distance increased by 0.7% and 1.4% in the vertical and horizontal direction, respectively. For sand size particles, however, the opposite was found where mean log void distance tended to decrease, particularly in vertical direction.

For all particles, there is a significant linear relationship between mean void distance and void ratio. In the horizontal direction, r values for one 1 hour and one week are 0.63 and 0.92, respectively, whilst in vertical direction they are 0.89 and 0.88, respectively. Those r values are greater than those of the moist tamped samples. For sand particles, initially there is no significant linear relationship in horizontal direction but at one week the relationship became strong with r= 0.9. In vertical direction there is no significant linear relationship.

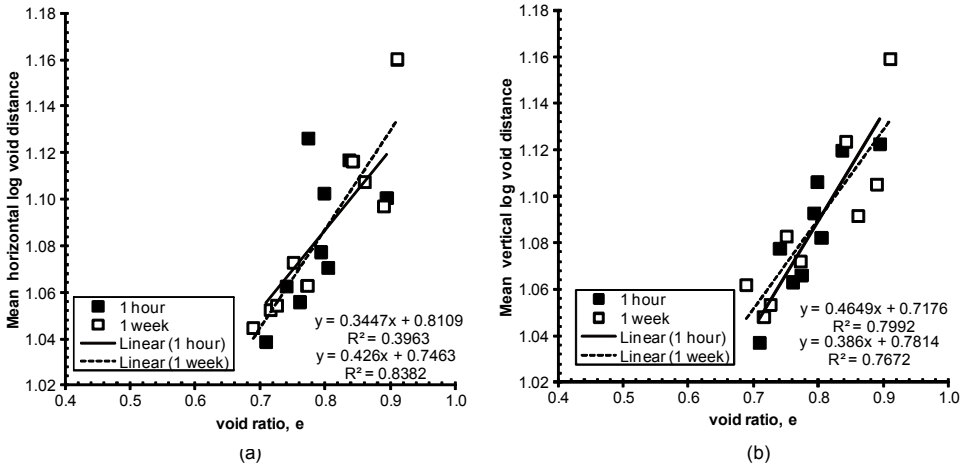

Figure 6-18 Mean log void distance (all) for dense moist tamped sample at σ'_v= 67kPa i.e. 70301H and 70301W): (a) horizontal (b) vertical

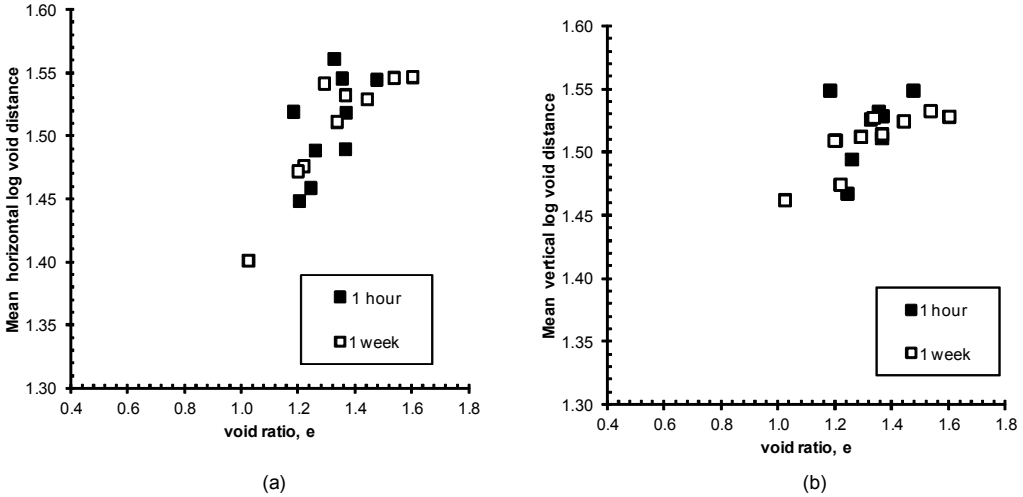

Figure 6-19 Mean log void distance (sand) for dense moist tamped sample at σ'_v= 67kPa i.e. 70301H and 70301W): (a) horizontal (b) vertical

Figure 6-20 (all particles) and Figure 6-21 (sand particles) present a plot of variance (all particles) of log void distance for dense moist tamped silty sand for 1 hour and one week aging time. There is a slight decrease in variance with time (see Table 6-3). Vertically variance decreases from 0.239 to 0.233 whilst horizontally variance decreases slightly from 0.245 to 0.236. This suggests the particles are less clustered. Interestingly, however, variance in sand tends to increase in the vertical direction (from 0.308 to 0.331) whilst horizontally it appears to be only a slight decrease (from 0.304 to 0.300). This suggests more strong void structure between the sand (L-L grain contact), due to merged voids, forming in the vertical direction whereas weak horizontal void structure collapses. Generally, for all particles, the linear relationship between the variance void distance and void ratio is not significant (r critical=0.602) with r =+0.68 (1 hour horizontal) and r=+0.53 (1 week horizontal) and r=+0.38 (1 hour vertical) and r=+0.46 (1 week vertical). Variances of moist tamped sample tend to be lower in the vertical direction than in the horizontal direction. For sand particle, initially no significant linear relationship was found but at one week the relationship became significant.

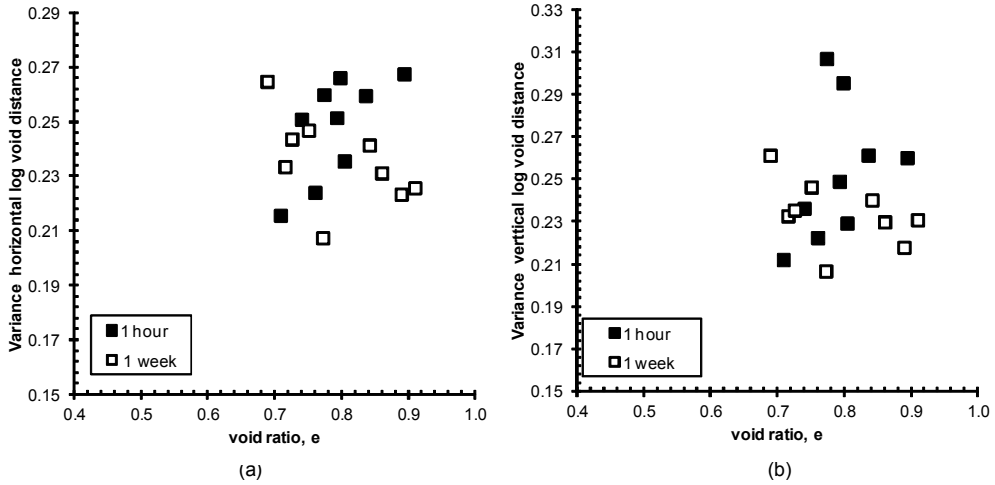

Figure 6-20 Variance log void distance (all) for dense moist tamped sample at σ'_v =67kPa i.e. 70301H_ and 70301W: (a) horizontal (b) vertical

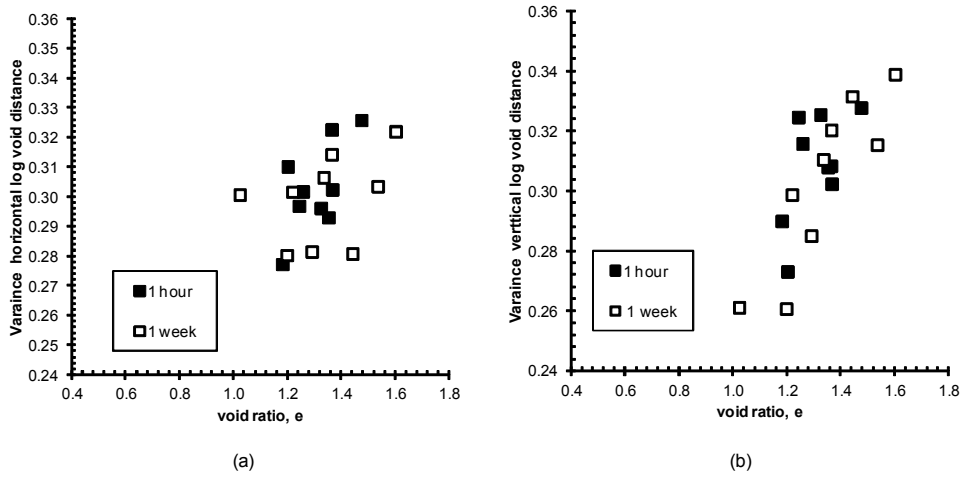

Figure 6-21 Variance log void distance (sand) for dense moist tamped sample at σ'_v =67kPa i.e. 70301H_ and 70301W: (a) horizontal (b) vertical

Plot of kurtosis versus void ratio are illustrated in Figure 6-22 (all particles) and Figure 6-23 (sand particles). For all particles, the kurtosis value decreases with time from -0.859 to -0.920 vertically and from -0.875 to -0.910. A lower kurtosis value for aged samples was also reported by Bowman (2003) for dense clean sand. For sand particles, values of kurtosis become lower vertically (from -0.409 to -0.768) and slightly increase horizontally (from -0.448 to -0.405). This is in accordance with change in variance which predominantly occurs vertically. For all particles, correlation values r in the horizontal direction are +0.57 and +0.92 for 1

hour and 1 week aging time, respectively, whilst in the vertical direction r=+0.21 and r=+0.79. This shows that for one hour, the linear relationship between kurtosis and void ratio is not significant (r critical=0.602) whereas for one week it is significant. For sand particles there is no significant linear relationship in both directions.

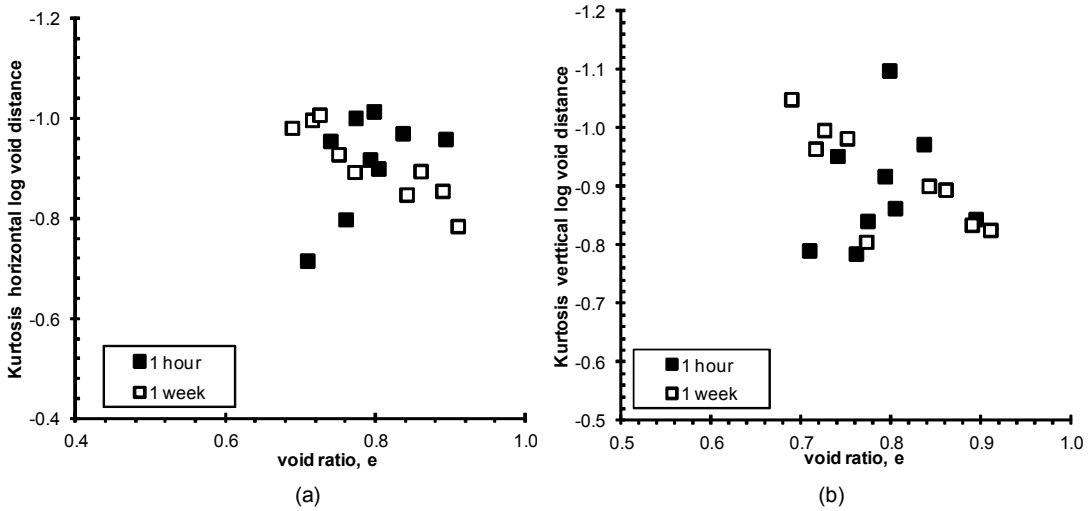

Figure 6-22 Kurtosis log void distance (all) for dense moist tamped sample at σ'_v =67kPa i.e. 70301H_ and 70301W: (a) horizontal (b) vertical

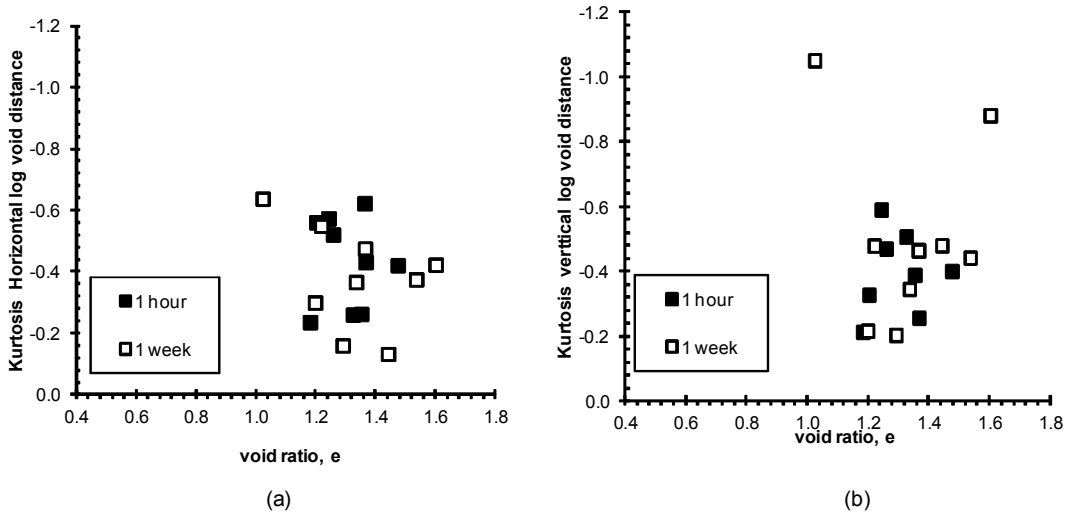

Figure 6-23 Kurtosis log void distance (sand) for dense moist tamped sample at σ'_v =67kPa i.e. 70301H_ and 70301W: (a) horizontal (b) vertical

The relationship between variance to mean ratio and void ratio are shown by Figure 6-24 (all particles) and Figure 6-25 (sand only). For all particles, Table 6-3 shows that variance to mean ratio decreases with time i.e. vertically (from 0.221 to 0.215) and decreases horizontally (from 0.229 to 0.217. For sand only, variance to mean ratio tends to increase vertically from 0.203 to 0.237 and slightly decrease horizontally (0.202 to 0.200). Vertically the tendency is similar to moist tamped samples, but horizontally, moist tamped samples show a reduction in the index of dispersion. Generally the linear trend against void ratio is relatively medium but significant. In the horizontal direction r=+0.62 and r=-0.77 for one hour and one week aging time, respectively, whilst vertically r=+0.22 and r=-0.75. There is no significant linear relationship for sand particles only.

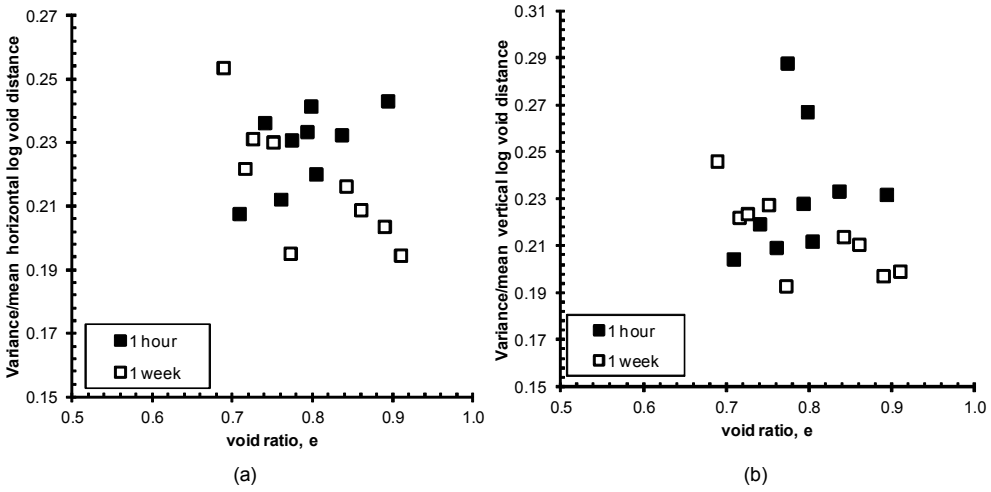

Figure 6-24 Variance/mean log void distance (all) for dense moist tamped sample at σ'_v =67kPa i.e. 70301H_ and 70301W (a) horizontal (b) vertical

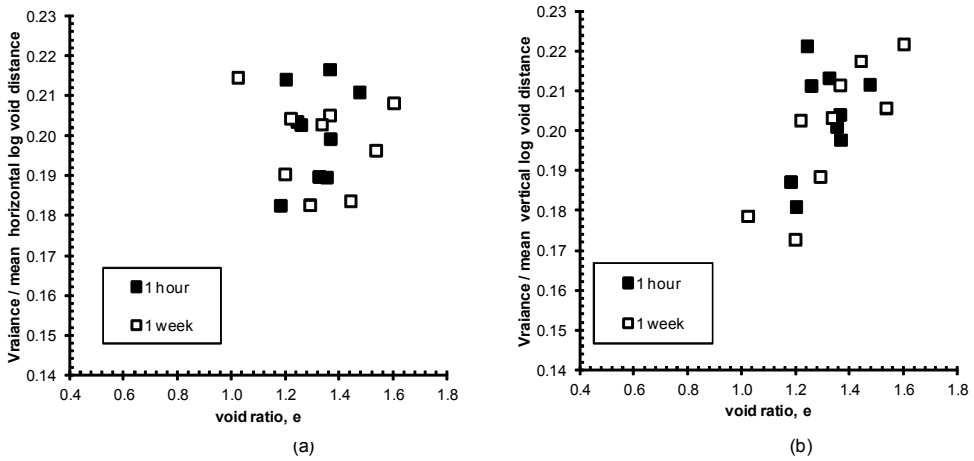

Figure 6-25 Variance/mean log void distance (sand) for dense moist tamped sample at σ'_v =67kPa i.e. 70301H_ and 70301W (a) horizontal (b) vertical

6.4 Microstructure changes of loose samples

6.4.1 Orientation distribution

6.4.1.1 Moist tamped versus dry pluviated sample

Similar to dense samples, the rose diagrams in Figure 6-27 and Figure 6-28 show that loose moist tamped samples (40601H and 40601W) are more isotropic than loose dry pluviated samples (40601H_DD and 40601W_DD). Likewise r and κ values of loose moist tamped samples are less than those of loose dry pluviated samples, indicating higher isotropy of moist tamped samples (see Table 6-4). The same trends as for dense samples are found where sand particles are more orientated than 'fines'. Additionally 'fines' of moist tamped samples are less orientated than those of dry pluviated sample as suggested by lower values of r and κ values.

6.4.1.2 Loose moist tamped sample

Four sets of fabric tests up to 8 months were carried out to investigate microstructure changes in loose moist tamped samples i.e. 40301H, 40301W, 40304M and 40308M. Longer tests were attempted considering that many previous studies (e.g. Baxter & Mitchell, 2004; Bowman, 2002) suggested that the aging effect (thus microstructure change) is less profound in loose sand compared to

dense sand. However many longer term aging case studies in the field were found following ground improvement works on relatively loose soil. Moist tamped samples were used for long term tests because it is the main preparation method used in this study and in the literature on silty sand. In addition, one set of tests on loose moist tamped samples at higher loading stress (40601H and 40601W) and one set on loose dry pluviated samples were also performed (40601H and 40601W). Fischer statistical analysis results for all loose samples are presented in Table 6-4 Rose diagrams are shown by Figure 6-26 to Figure 6-28.

Table 6-4 Fischer statistical analysis for orientation of loose samples

Sample		%fraction*	e	N	α_m	r	κ
40301H	All	53	0.883	9830	173.8±5.7	0.03	0.06
	Sand	42	1.402	1629	3.9±5.2	0.05	0.1
	'fines'	11	6.944	8201	156.5±8.2	0.03	0.05
40301W	All	54	0.854	10046	141.8±4.6	0.05	0.10
	Sand	41	1.421	1577	151.1±4.2	0.09	0.18
	'fines'	13	6.773	8469	141.6±8.5	0.03	0.07
40304M	All	55	0.827	10606	90.3±1.3	0.13	0.27
	Sand	41	1.461	1619	88.4±1.3	0.20	0.42
	'fines'	14	6.161	8987	92.9±2.4	0.09	0.18
40308M	All	54	0.848	9725	97.5±1.8	0.12	0.25
	Sand	42	1.387	1656	99.7±1.8	0.20	0.41
	'fines'	12	7.292	8069	94.9±4.4	0.07	0.13
40601H	All	53	0.877	9485	177.9±2.3	0.07	0.14
	Sand	40	1.481	1598	0.1±1.8	0.15	0.30
	'fines'	13	6.213	7887	169.5±8.9	0.02	0.05
40601W	All	54	0.856	10297	176±3.4	0.05	0.10
	Sand	43	1.341	1582	173.8±2.8	0.10	0.20
	'fines'	11	7.310	8715	4+-10.9	0.02	0.04
40601H-DD	All	53	0.873	10678	86.5±1.1	0.20	0.42
	Sand	44	1.248	1892	86.5±0.8	0.31	0.65
	'fines'	9	5.658	8786	87.1±1.3	0.14	0.29
40601W-DD	All	54	0.852	10553	89.6±0.8	0.20	0.40
	Sand	46	1.188	1792	90.5±0.8	0.32	0.68
	'fines'	8	6.288	8761	88.2±1.7	0.12	0.25

e=void ratio; N=number of particle

*to total area

Figure 6-26 illustrates the change in particle orientation for long term tests under 30kPa confining pressure. As can be seen from the figure, particles tend to rotate with time. Surprisingly for 4 months and 8 months samples further significant changes occur where particle orientation tends to shift from toward-vertical initially to towards-horizontal. Initially, from one hour to one week, mean orientations of all particles are toward the vertical i.e. from 173.8° for the one hour sample to 142.4° for the one week sample. Then, 4 and 8 months samples have mean orientations of 90.3° and 97.5°, respectively. A similar trend of particle rotation is also observed in sand and 'fines'. This suggests that under loading, structuration in terms of particle orientation changes is a continuous process. Table 6-4 demonstrates that with time particles align together in terms of orientation, as indicated by a higher value of r or κ with time. For example, r and κ value of all particles of 1 week and 4 months samples increase about 1.7 and 4.5 times the value at one hour. The table also shows that sand particles have greater tendency to align at a particular orientation compared to fines-sized particles. For sand, the 4 months sample has r and κ approximately 4 times that of r and κ of one hour sample, whilst for fines sized, it is 3.6 times.

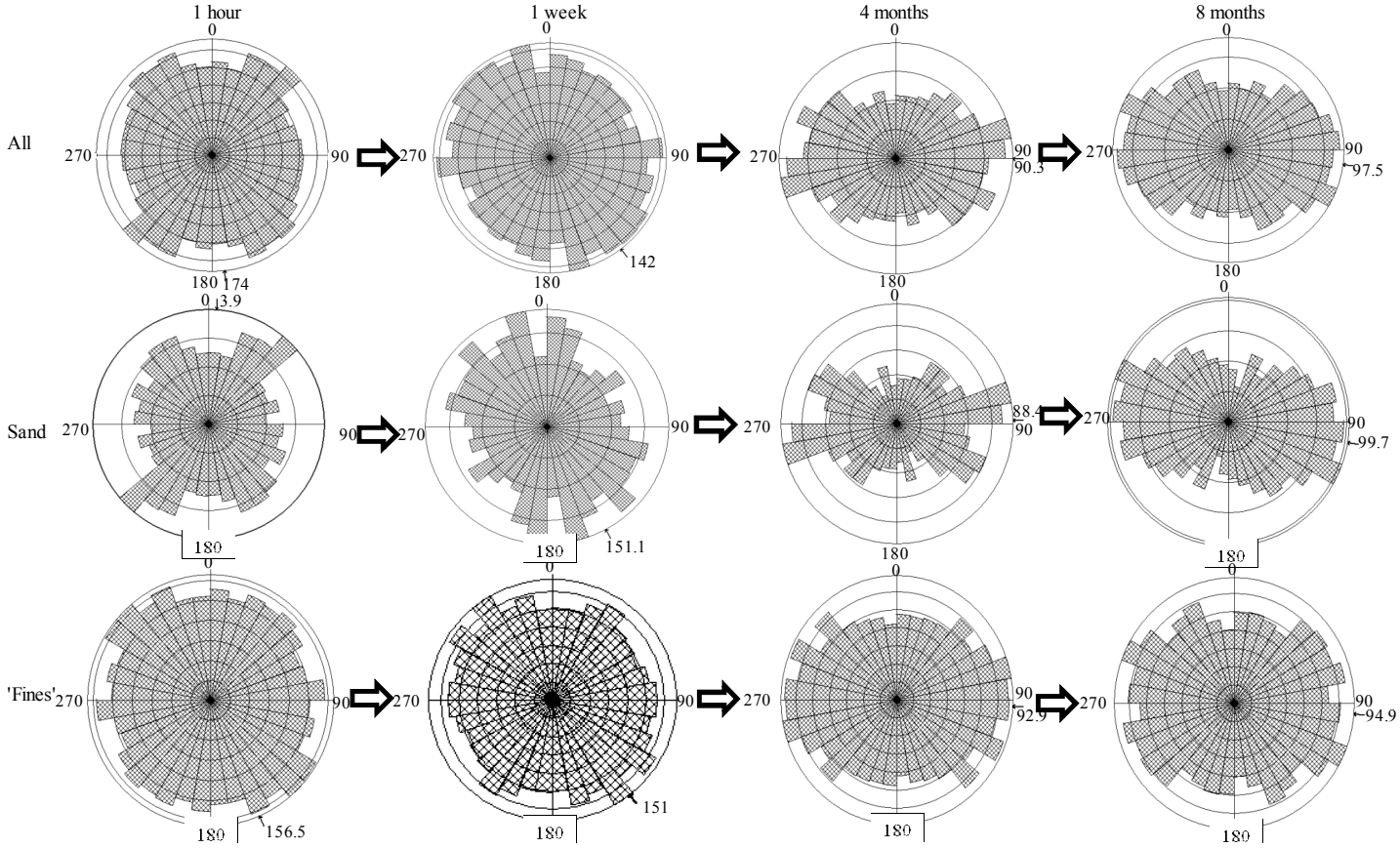

Figure 6-26 Change in grains orientation for loose moist tamped samples (40301H, 40301W, 40304m and 40308m) at σ'_v=57kPa

Figure 6-27 demonstrates change in particle orientation of loose moist tamped samples aged at higher vertical effective stress i.e. 40601H and 40601W. The first thing to be noted is that generally the sample at higher vertical effective stress has a greater degree of orientation, particularly in sand. The initial degree of orientation, r, at 60kPa confining pressure is 0.15 compared to 0.05 for the 30kPa sample. Particle rotation with time was also observed at higher vertical effective stress, however in contrast to tests at lower vertical effective stress, the degree of orientation tends to be lower with time. It can be seen that change in degree of orientation is greater in sand (from κ= 0.3 to κ=0.2) compared to "fines" which was relatively constant with a slight decrease from κ=0.05 to κ=0.04. Samples at lower vertical stress also demonstrated a similar tendency that greater change in degree of orientation occurs within sand-sized particles (from κ= 0.09 to κ=0.05) whereas the orientation of "fines" tends to be relatively constant. This indicates that for loose samples many fines are floating in the voids i.e. L-S-V grain contact. This is in accordance with observation from DEM of polydisperse granular material (Imole *et al.*, 2013; Kumar *et al.*, 2014).

6.4.1.3 Loose dry pluviated sample

Figure 6-28 shows change in particle orientation for loose sample under effective vertical stress of 125kPa for dry pluviated samples i.e. 40601H_DD and 40601W_DD. Mean orientation changes from 86.5° for the one hour sample to 89.6° for the one week sample. It appears that the absolute change of mean orientation for the moist tamped samples (i.e. 177.9°-176°=1.9°) is slightly less than that of dry pluviated samples (i.e. 86.5°-89.6°=2.5°).

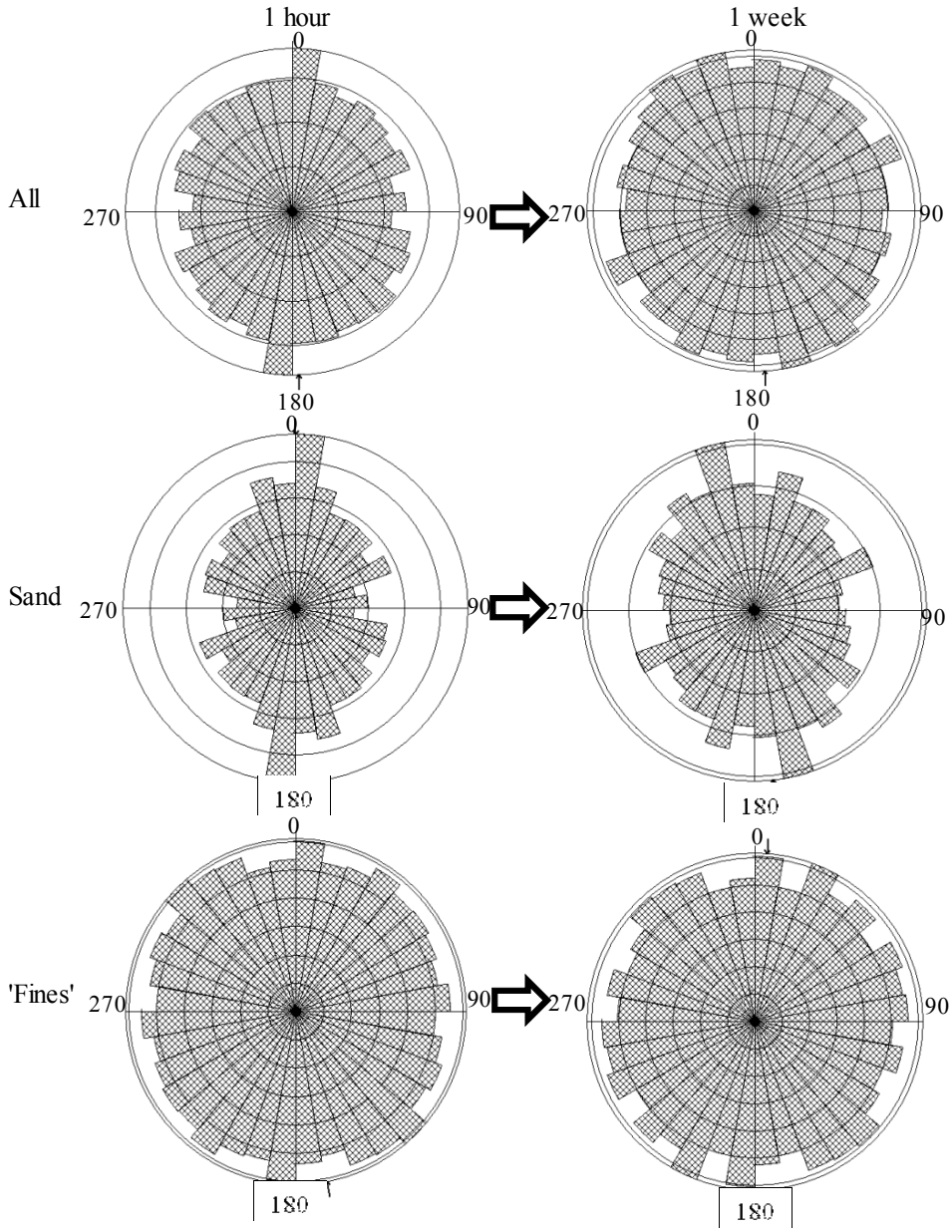

Figure 6-27 Change in orientation of loose moist tamped samples at σ'_v=125kPa i.e.40601H (left) and 40601W (right)

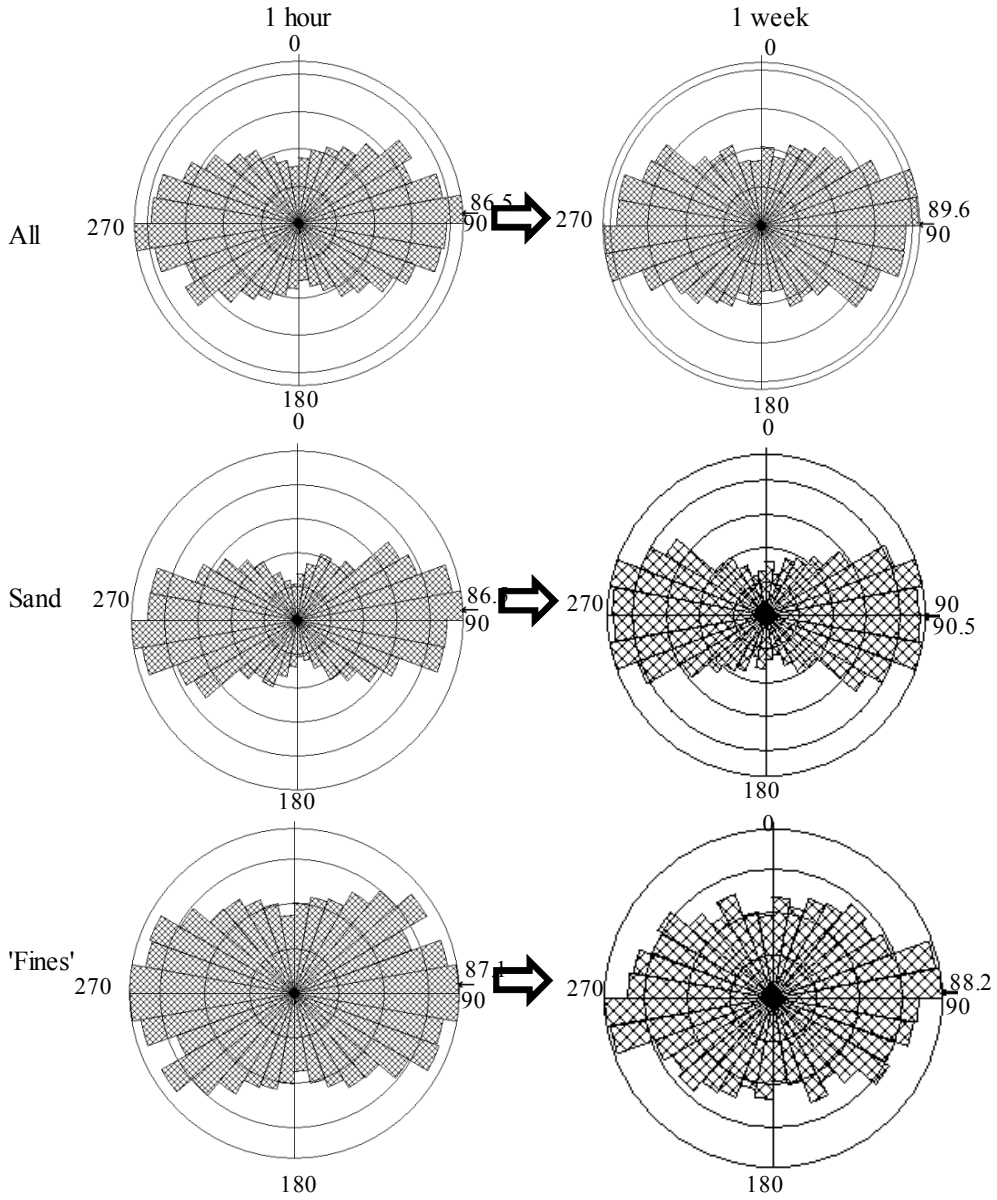

Figure 6-28 Change in orientation of loose dry pluviated samples at σ'_v=125kPa i.e. 40601H-DD (left) and 40601W-DD (right)

6.4.2 Spatial distance distribution

6.4.2.1 General

Table 6-5 shows void distance statistical analyses for all loose fabric tests. Generally loose samples have greater mean log spacing compared to dense samples,

which is expected due to their higher void ratio. For example sample 40301H has mean log spacing of 1.127 and 1.108 in the vertical and horizontal direction, respectively, compared to sample 70301H (see Table 6-3) which has mean log spacing of 1.081 and 1.069. The loose dry pluviated sample at 1 hour (40601H_DD) aging time shows lower vertical mean log void distances than those in the horizontal direction for all particles (V=1.064;H=1.079). This was expected for a fabric with horizontally preferred orientation. On the other hand, initial loose moist tamped samples (40601H) demonstrate that vertical mean log void distance is nearly the same as the horizontal mean log void distance (i.e. V=1.064; H=1.079)

6.4.2.2 Moist tamped versus dry pluviated

Two sets of fabric tests were performed to investigate microstructure changes of different fabric i.e. 40601H&40601W and 40601H_DD&40601W-DD. It can be seen from Table 6-5 that generally the difference between mean log void distances in the vertical and horizontal directions are less in moist tamped soil than that in dry pluviated soil. The difference for moist tamped samples is 0.002 and 0.007 for 1 hour and 1 week, respectively, whilst for dry pluviated sample they are 0.015 and 0.037. This suggests that in terms of void distance, moist tamped soil is more isotropic than dry pluviated, soil as seen for dense sample (see section 6.3.2.2)

Table 6-5 Void distance analysis for loose samples

Sample		% Frac.	e	N	Mean		Variance		Kurtosis		Var. / Mean	
					V	H	V	H	V	H	V	H
40301H	All	53	0.883	9830	1.127	1.108	0.250	0.246	-0.966	-0.893	0.222	0.222
	Sand	42	1.402	1629	1.518	1.538	0.312	0.297	-0.445	-0.382	0.205	0.193
40301W	All	54	0.854	10046	1.112	1.096	0.242	0.251	-0.820	-0.838	0.218	0.229
	Sand	41	1.421	1577	1.549	1.548	0.314	0.330	-0.376	-0.509	0.203	0.213
40304M	All	55	0.827	10606	1.074	1.091	0.229	0.247	-0.797	-0.982	0.213	0.226
	Sand	41	1.461	1619	1.527	1.586	0.289	0.299	-0.361	-0.315	0.189	0.189
40308M	All	54	0.848	9725	1.082	1.117	0.258	0.255	-0.967	-0.941	0.238	0.228
	Sand	42	1.387	1656	1.520	1.560	0.285	0.285	-0.328	-0.254	0.187	0.183
40601H	All	53	0.877	9485	1.136	1.138	0.259	0.257	-0.959	-0.897	0.228	0.226
	Sand	40	1.481	1598	1.572	1.586	0.307	0.288	-0.286	-0.161	0.195	0.182
40601W	All	54	0.856	11297	1.054	1.047	0.232	0.232	-0.924	-0.919	0.220	0.222
	Sand	43	1.341	1582	1.511	1.507	0.312	0.301	-0.464	-0.417	0.206	0.200
40601H_DD	All	53	0.873	11678	1.064	1.079	0.190	0.187	-0.745	-0.770	0.179	0.173
	Sand	44	1.248	1892	1.492	1.499	0.261	0.264	-0.321	-0.202	0.175	0.176
40601W_DD	All	54	0.852	10553	1.051	1.088	0.196	0.189	-0.787	-0.699	0.186	0.174
	Sand	46	1.188	1792	1.477	1.523	0.267	0.281	-0.331	-0.276	0.181	0.184

6.4.2.3 Loose moist tamped sample

a) 4030 samples

Figure 6-29 shows plot of mean log void distance with combined data from test 40301H, 40301W, 40304M and 40308M in each direction. In general there is a significant[2] linear correlation between mean log void distance and void ratio with r=+0.6 in the horizontal direction and r=+0.57 in the vertical direction. Figure 6-30 illustrates a plot of mean log-distance (all particles) for loose moist tamped samples for each aging time. The figure suggests that there are changes in mean log void distance as the samples age. The sample, up to 4 months, shows that mean log void distance tends to be lower both vertically and horizontally (see Table 6-5). Vertical mean log-distance values for one hour, one week and four months are 1.127, 1.112 and 1.074, respectively, whilst horizontally, they are 1.109, 1.096 and 1.091, respectively. This indicates that up to four months loose moist tamped samples are still contracting or compressing, although at four months the orientation has changed from toward-vertical to toward-horizontal. For 8 months sample, mean log-distance increases slightly; from 1.074 to 1.082 in the vertical direction and 1.091 to 1.117 in the horizontal direction. This increase, at 8 months of aging, indicates void growth. For sand particles, Figure 6-31 indicates some changes in the mean log void distance with time, despite no significance linier relationship between void ratio and log void distance. However, there is no consistent trend of change in mean log void distance overt time as shown by Table 6-5. It appears that after 8 months mean log void distance tends to be back as in the one hour sample. While in the horizontal direction, 8 months sample suggests a slight increase in mean log void distance compare to one hour sample.

[2] Critical r value for 36 data points is 0.320 (Chatfield, 1983)

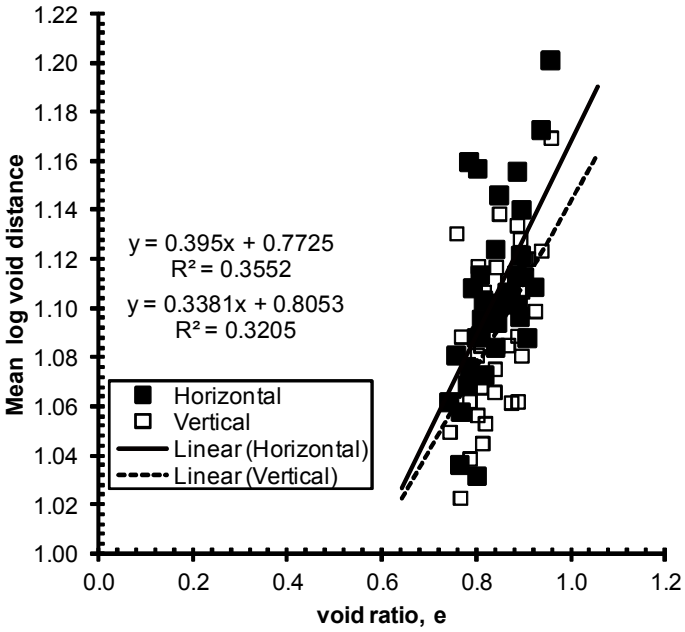

Figure 6-29 Mean log void distance (all) for loose moist tamped samples (40301H, 40301W, 40304M and 40308M) at σ'_v=57kPa

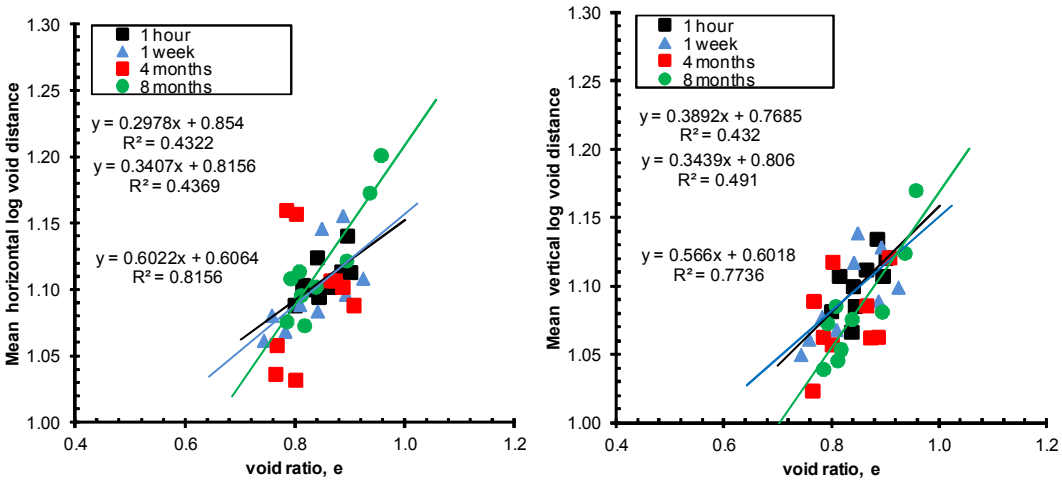

(a) (b)

Figure 6-30 Mean log void distance (all) for loose moist tamped samples at σ'_v=57kPa for each aging time (40301H, 40301W, 40304M and 40308M)

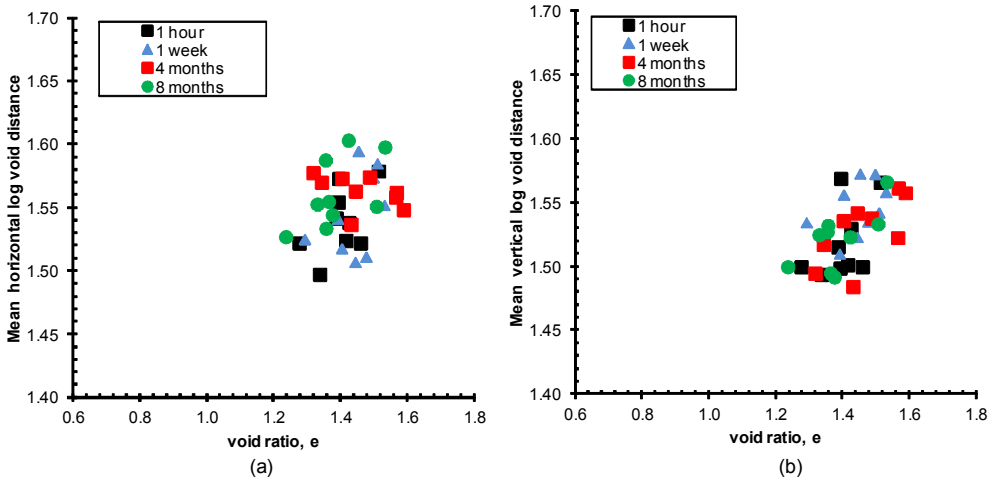

Figure 6-31 Mean log void distance (sand) for loose moist tamped samples at σ'_v=57kPa for each aging time (40301H, 40301W, 40304M and 40308M)

Figure 6-32 shows plot of variance of log void distance (all particles) for loose moist tamped samples. The figure in general indicates that some changes occur as the sample ages. Based on Table 6-5, with the exception of the horizontal variance for one week which tends to increase, for up to four months generally the variance decreases with time vertically and horizontally. The log mean variance in the vertical direction decreases from 0.25 at one hour to 0.229 at 4 months, whilst horizontally it barely changes (0.246 to 0.247). This is likely because moist tamped soil starts already structured and clustered as explained in section 6.3.2.2. This tendency of variance decreasing in the loose samples is also found for 40601H and 40601W. In general there is no significant linear relationship between variance and void ratio. For example, in the horizontal direction, r=+0.55 and r=+0.27 for 1 hour and 4 months respectively, indicating no significant relationship (critical r for 9 points is 0.602). In the vertical direction, r=+0.25 and =r+0.22 accordingly, indicating also no significant linear relationship. Figure 6-33 presents the relationship of void ratio and variance for sand particles. The figure suggests some change in the microstructural occur with time. In term of the relationship between void ratio and variance, no significant correlation was found. It appears from Table 6-5 that one week sample has almost the same variance (vertically), but 4 months

and 8 months sample indicate lower variance. Horizontally, 8 months sample also indicate lower variance compare to the initial one hour sample.

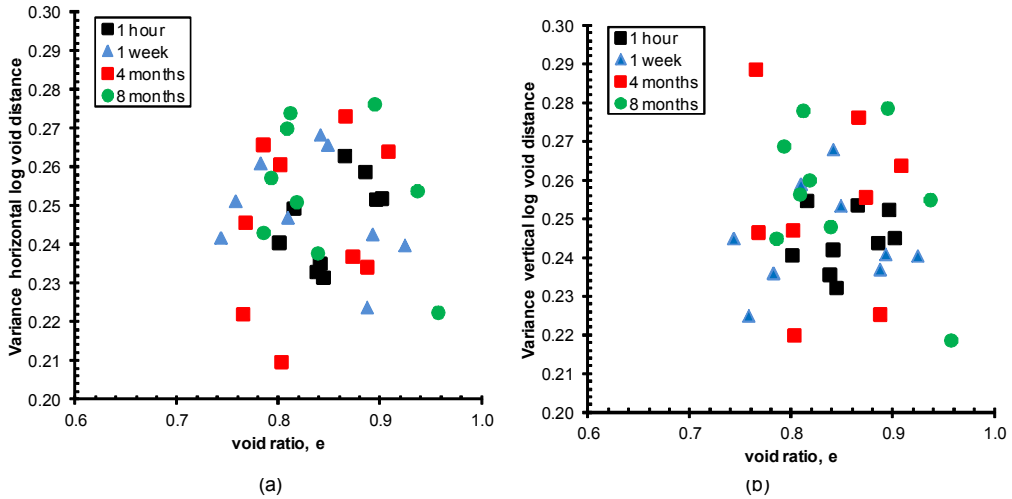

Figure 6-32 Variance log void distance (all) for loose moist tamped samples at σ'_v=57kPa i.e. 40301H, 40301W, 40304M and 40308M

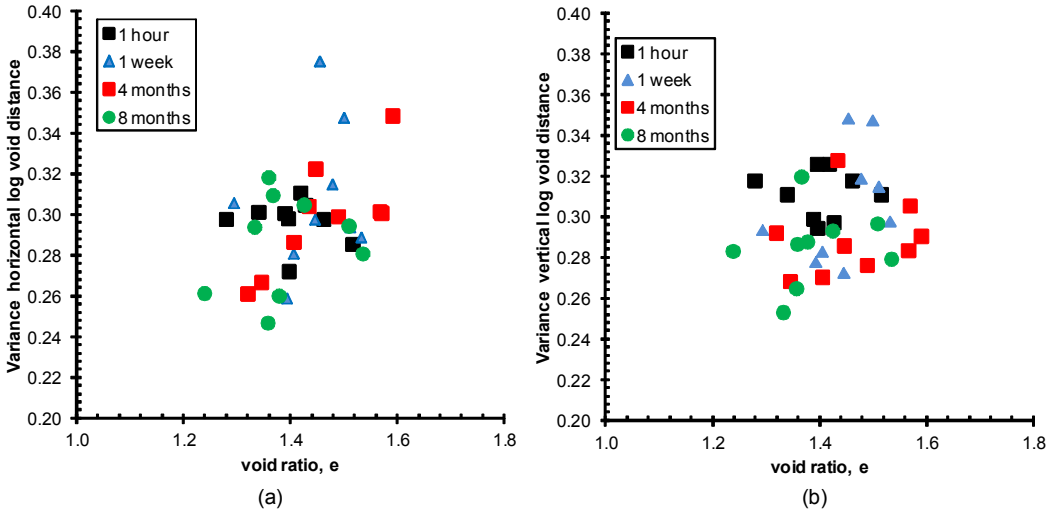

Figure 6-33 Variance log void distance (sand) for loose moist tamped samples at σ'_v=57kPa i.e. 40301H, 40301W, 40304M and 40308M

Plots of kurtosis of log void distance against void ratio (all particles), for loose samples are illustrated in Figure 6-34. Vertically, values of kurtosis up to 4 months tend to be larger with time e.g. from -0.966 at 1 hour and -0.797 at 4 months (see Table 6-5). A similar tendency is shown also by sand particles with a kurtosis value equal to -0.445 at 1 hour and -0.361 at 4 months. Horizontally, Table 6-5 shows no clear trend of kurtosis with time. However, it appears from the table as the particle orientation becomes horizontally orientated the kurtosis value tends to be lower with time i.e. β=-0.893 at 1 hour; β=-0.982 at 4 months and β=-0.941 at 8 months. For sand particles, Figure 6-35 also implies some microstructural changes did occur with time, despite no significant linier relationship between void ratio and the kurtosis. Table 6-5 shows that in vertical direction, kurtosis tends to increase with time (i.e. -0.445 at one hour and -0.328 at 8 months). Similarly in horizontal direction, the kurtosis tends to be higher over time (i.e. 0.382 at one hour and -0.254 at 8 months).

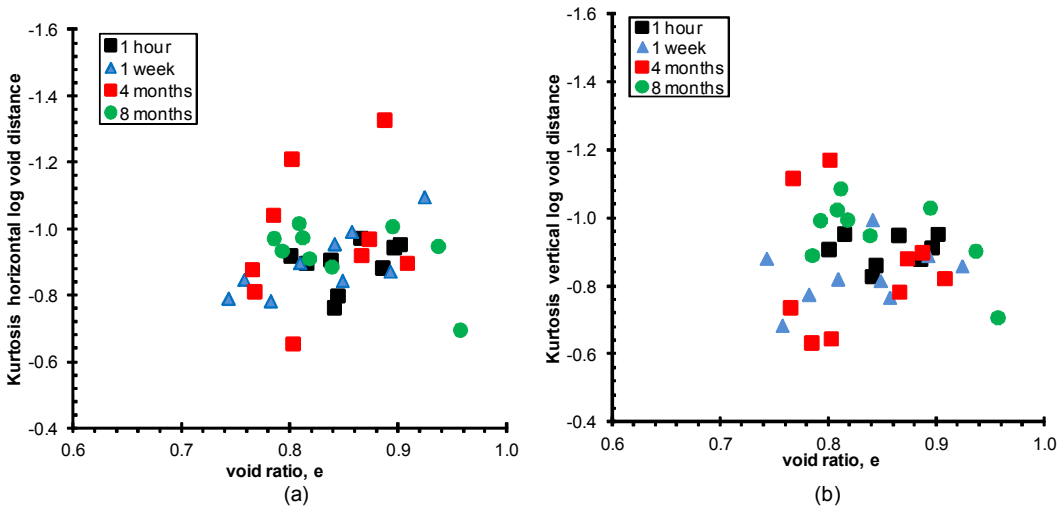

Figure 6-34 Kurtosis log void distance (all) for loose moist tamped samples at σ'_v=57kPa i.e. 40301H, 40301W, 40304M and 40308M

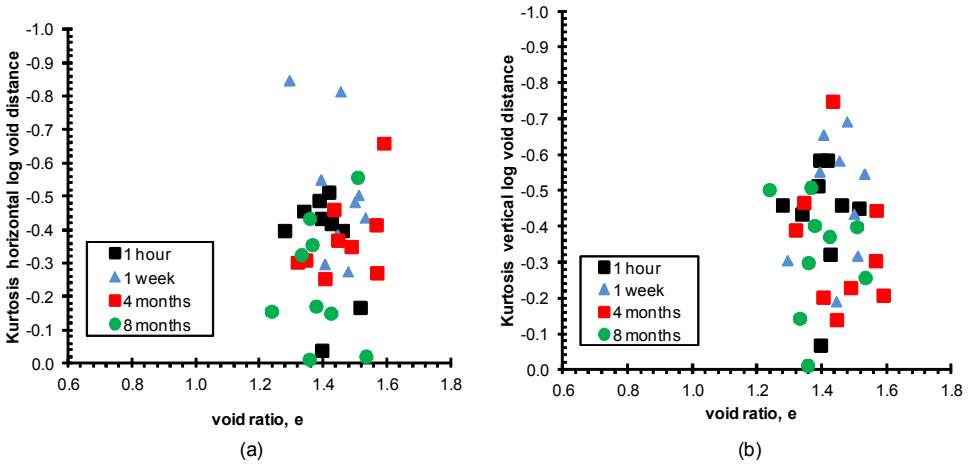

Figure 6-35 Kurtosis log void distance (sand) for loose moist tamped samples at σ'_v=57kPa i.e. 40301H, 40301W, 40304M and 40308M

Figure 6-36 shows plots of variance to mean of log void distance with void ratio (all particles) for loose samples. It appears that vertically, variance to mean ratio decreases with time (from 0.222 at 2 hour and 0.213 at 4 months), and then increases again at 8 months. Horizontally it appears that variance to mean ratios are nearly the same e.g. 0.222 at 1 hour to 0.226 at 4 months and 0.228 at 4 months. Figure 6-37 shows that variance to mean ratio for sand particle tend to change over time, suggesting some microstructural changes. Table 6-5 shows a consistent trend in vertical direction where variance to mean ratio decrease with time (e.g. 0.205 at one hour and 0.187 at 8 months). In horizontal direction, a tendency of lower variance to mean ratio was also observed (e.g. 0.193 at one hour and 0.189 and 0.183 at 4 months and 8 months respectively).

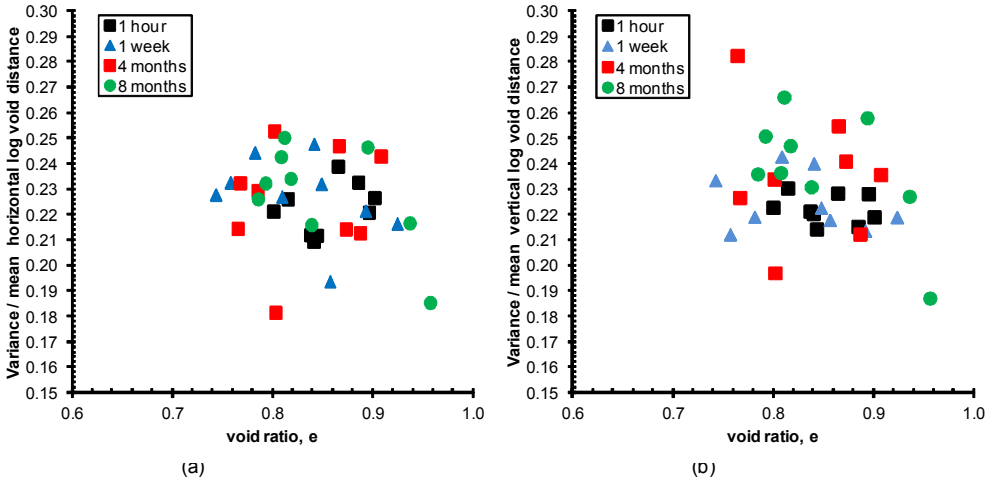

Figure 6-36 Variance/mean log void distance (all) for loose moist tamped samples at σ'_v=57kPa i.e. 40301H, 40301W, 40304M and 40308M

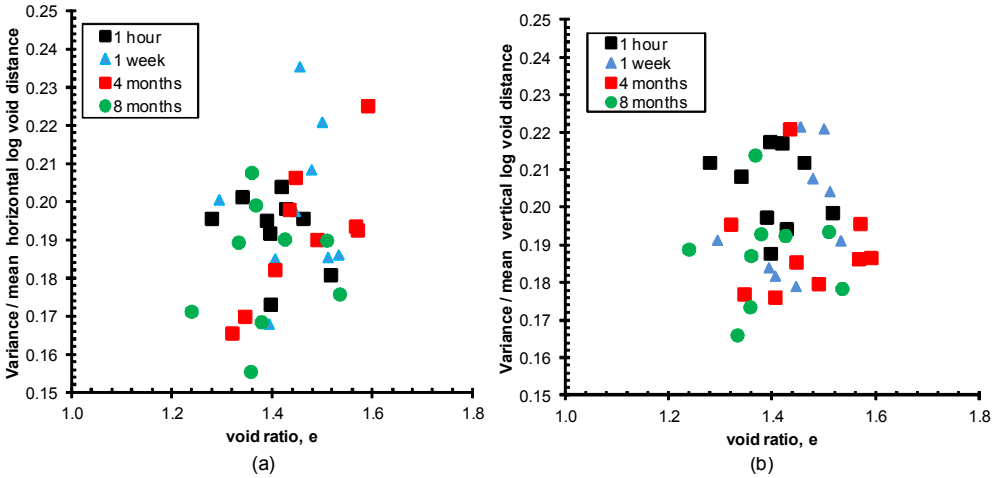

Figure 6-37 Variance/mean log void distance (sand) for loose moist tamped samples at σ'_v=57kPa i.e. 40301H, 40301W, 40304M and 40308M

b) 4060 samples

Figure 6-38 and Figure 6-39 show plot of void ratio and mean log void distance of loose moist tamped samples at vertical stress of 125 kPa for all and sand particles respectively. For all particles, Table 6-5 shows that mean log - distance decreases with time both vertically (from 1.136 to 1.054) and horizontally (from 1.138 to 1.047) over one week (see Table 6-5). This is in accordance with the DEM observation from Kang (2012) that during creep, a loose sample tend to

contract. Similar contraction trend was observed from the same table for sand particles in both directions.

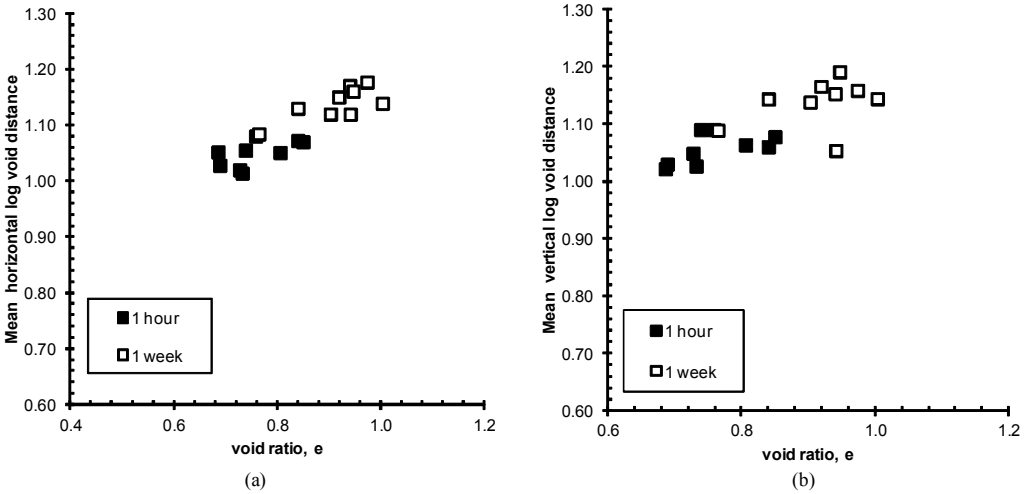

Figure 6-38 Mean log void distance (all) for loose moist tamped samples at σ'_v=125 kPa i.e. 40601H & 40601W

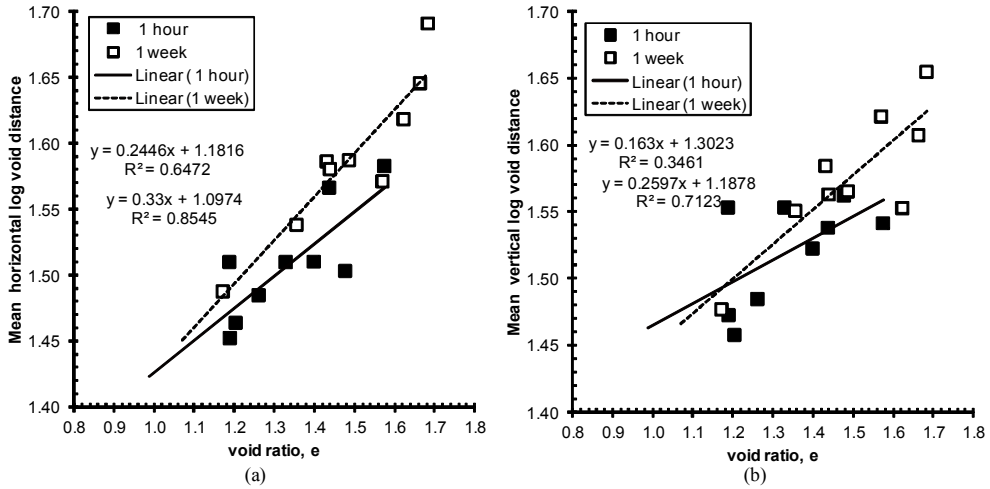

Figure 6-39 Mean log void distance (sand) for loose moist tamped samples at σ'_v=125 kPa i.e. 40601H & 40601W

Plot of variance versus void ratio is presented by Figure 6-40 (all particles) and Figure 6-41 (sand particles). For all particles, the variance tends to decrease with time (see Table 6-5). In the vertical direction the variance declines from 0.259 to 0.232 whilst in horizontal direction it decreases from 0.257 to 0.232. Whilst for sand particles, variance appears to be the same in vertical direction (i.e. about 0.31

and tend to increase in horizontal direction (i.e. from 0.288 at one hour and to 0.301 at one week).

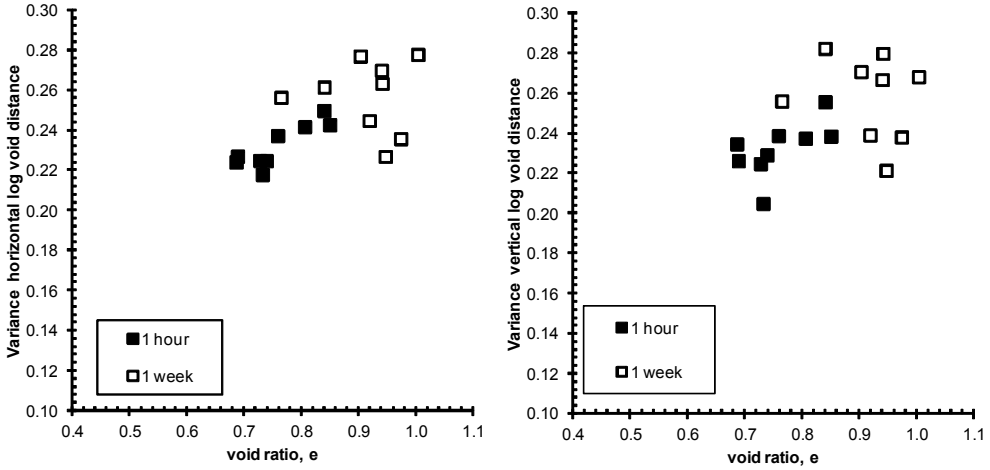

Figure 6-40 Variance log void distance (all) for loose moist tamped samples at σ'_v=125 kPa i.e. 40601H & 40601W

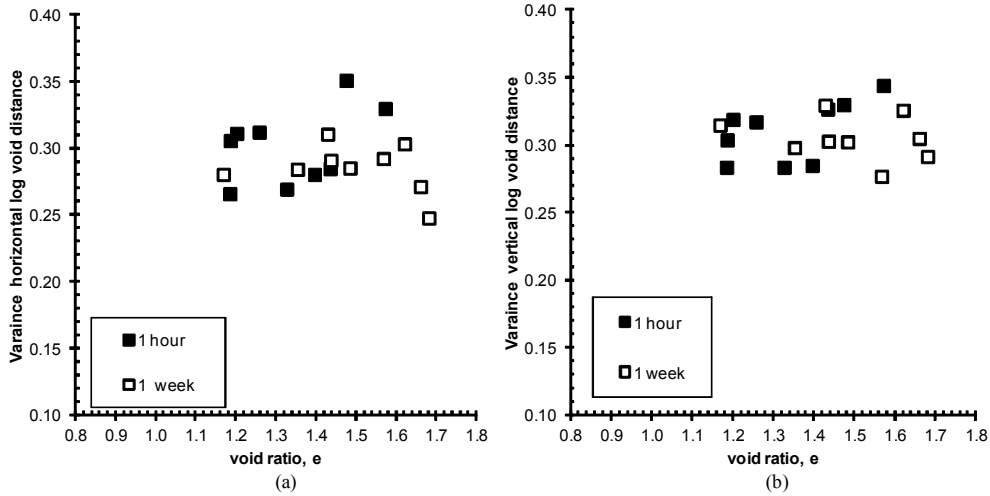

Figure 6-41 Variance log void distance (sand) for loose moist tamped samples at σ'_v=125 kPa i.e. 40601H & 40601W

Plots of kurtosis versus void ratio for all and sand particles are shown by Figure 6-42and Figure 6-43 respectively. For all particles, in the vertical direction kurtosis tends to increase with time i.e. from -0.959 to -0.924, whilst in the horizontal direction the kurtosis value becomes lower, -0.897 to -0.919 (see Table 6-5). For sand particles, kurtoses also decrease with time.

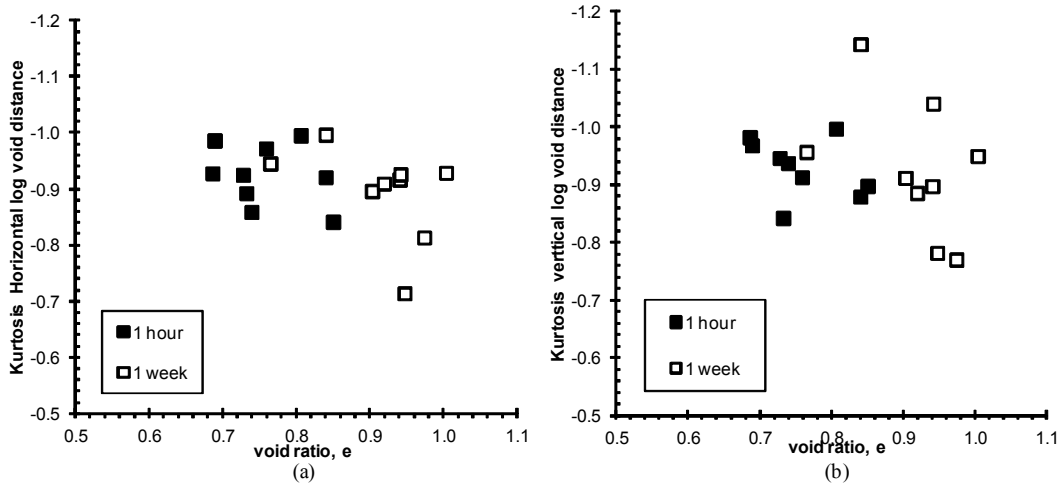

Figure 6-42 Kurtosis log void distance (all) for loose moist tamped samples at σ'_v=125 kPa i.e. 40601H & 40601W

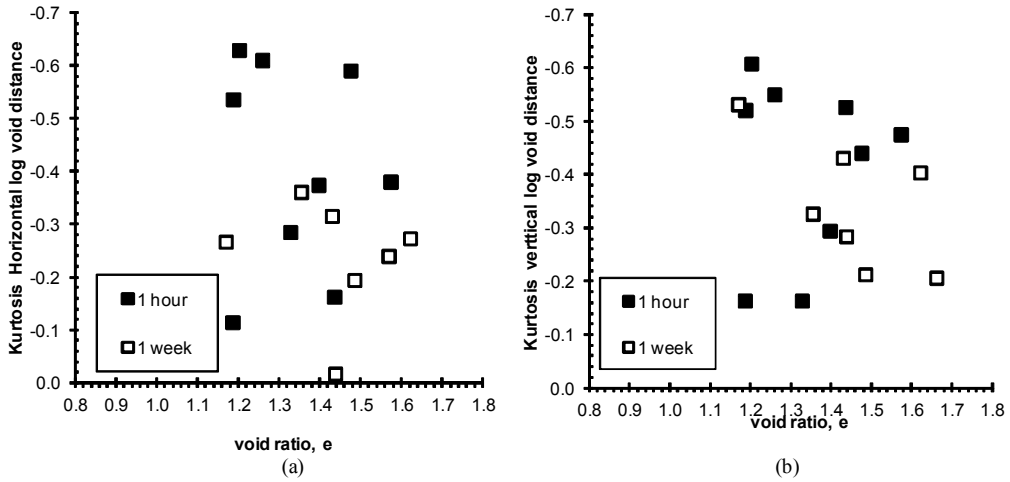

Figure 6-43 Kurtosis log void distance (sand) for loose moist tamped samples at σ'_v=125 kPa i.e. 40601H & 40601W

Figure 6-44 and Figure 6-45 present variance to mean ratio versus void ratio for all and sand particles respectively. Table 6-5 show that for all particles, variance to mean ratio tends to be lower with time. Whilst for sand particle the value tend to increase with time.

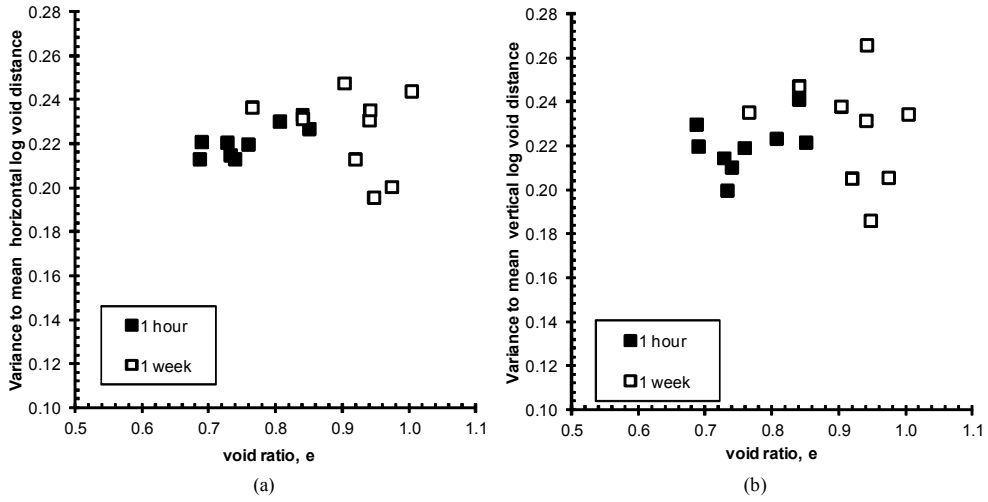

Figure 6-44 Variance to mean ratio of log void distance (all) for loose moist tamped samples at σ'_v=125 kPa i.e. 40601H & 40601W

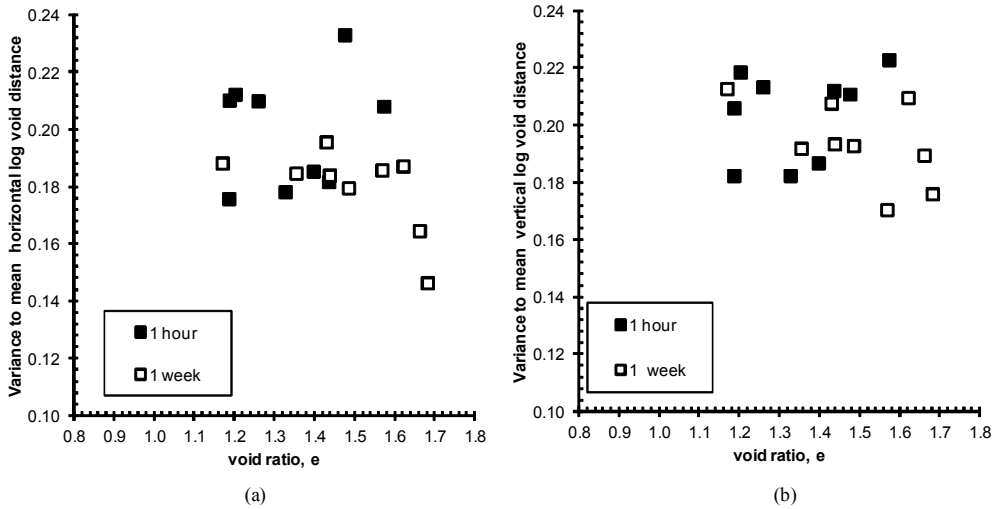

Figure 6-45 Variance to mean ratio of log void distance (sand) for loose moist tamped samples at σ'_v=125 kPa i.e. 40601H & 40601W

6.4.2.4 Loose dry pluviated sample

For loose dry pluviated samples, a plot of mean log-distance versus void ratio is shown by Figure 6-46. It can be seen from the figure that changes occur vertically and horizontally. Table 6-5 shows that vertical mean log void distance tends to be lower with time (1.064 at 1 hour and 1.054 at one week). Horizontal means log void distance are nearly the same for 1 hour sample (i.e. 1.079) and 1 week sample (i.e.1.088).

For sand particles (see Figure 6-47) mean log void distance tends to decrease with time (i.e. from 1.492 to 1.480 vertically and from 1.55 to 1.523 horizontally). A plot of variance versus void ratio is presented by Figure 6-48. The figure in general demonstrates a slight change in variance with time. Table 6-5 shows that variance tends to increase only slightly with time. Vertically the variance increases from 0.191 at 1 hour to 0.196 at 1 week. Whilst horizontally, the value increases from 0.187 to 0.189. For sand particles only, vertically, variance increases from 0.261 to 0.267, whilst horizontally it increases from 0.264 to 0.281. Similarly variance to mean ratio tends to increase slightly with time (Figure 6-50) i.e. 0.179 to 0.186 vertically and 0.173 to 0.174 horizontally. Figure 6-51 shows that for sand-sized particles variance to mean ratio become larger with time i.e. 0.175 to 0181 vertically and 0.176 to 0.184 horizontally.

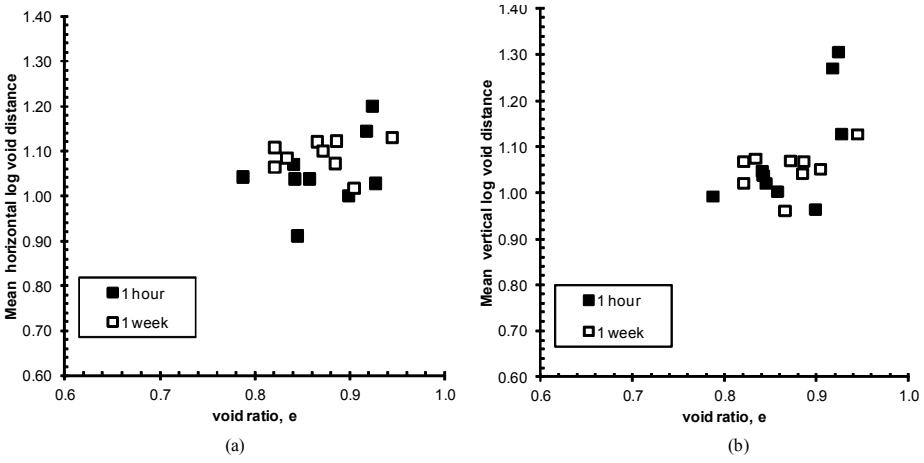

Figure 6-46 Mean log void distance for loose dry pluviated samples (all) at σ'_v =125kPa co i.e. 40601H_DD&40601W_DD: (a) horizontal (b) vertical

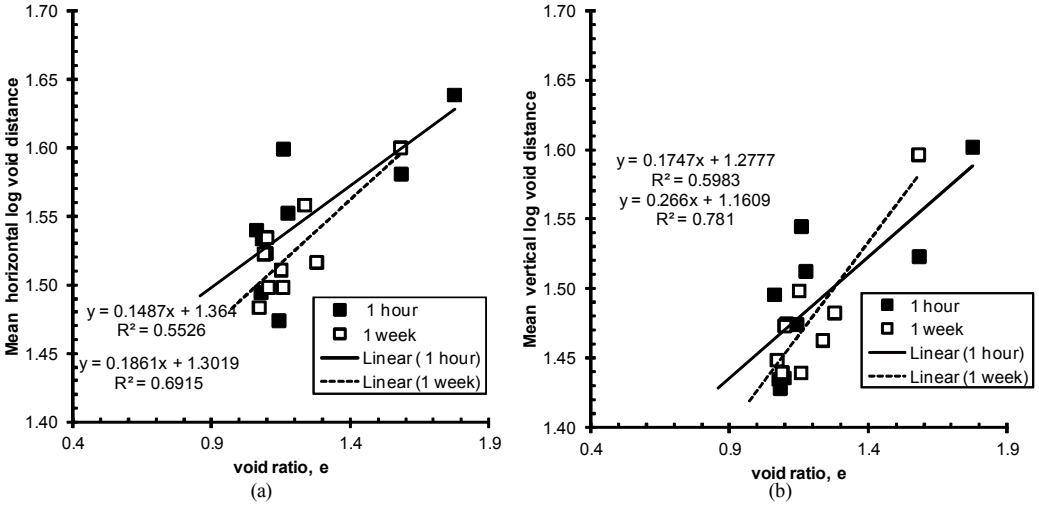

Figure 6-47 Mean log void distance for loose dry pluviated samples (sand) at σ'_v =125kPa co i.e. 40601H_DD&40601W_DD: (a) horizontal (b) vertical

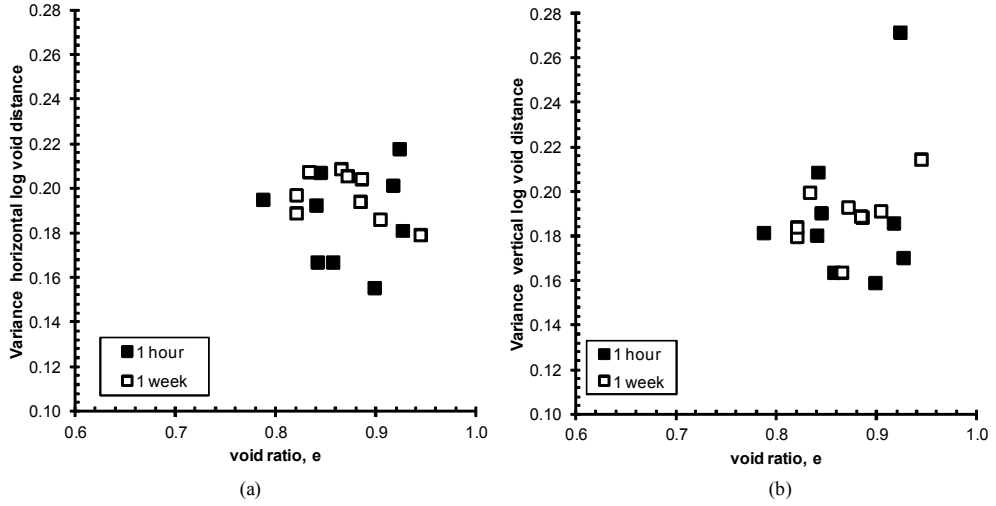

Figure 6-48 Variance log void distance for loose dry pluviated samples (all) at σ'_v =125kPa co i.e. 40601H_DD&40601W_DD: (a) horizontal (b) vertical

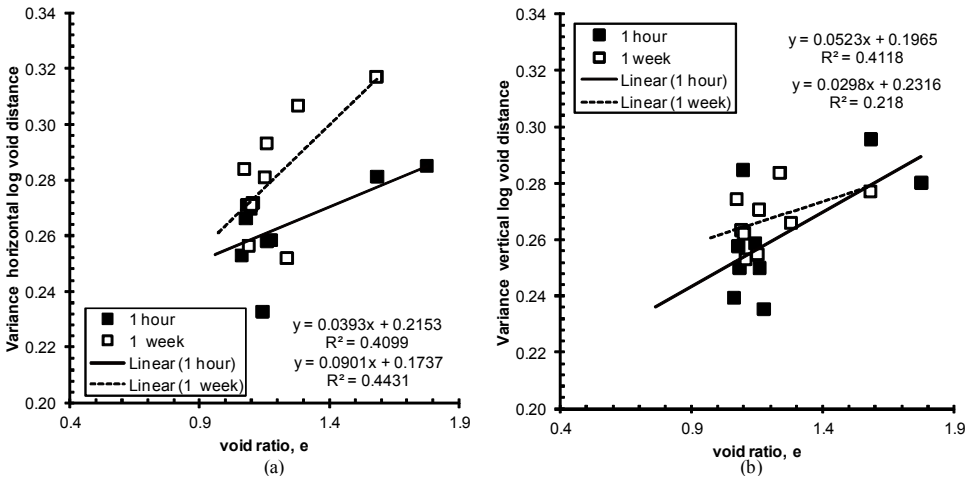

Figure 6-49 Variance log void distance for loose dry pluviated samples (sand) at σ'_v =125kPa co i.e. 40601H_DD&40601W_DD: (a) horizontal (b) vertical

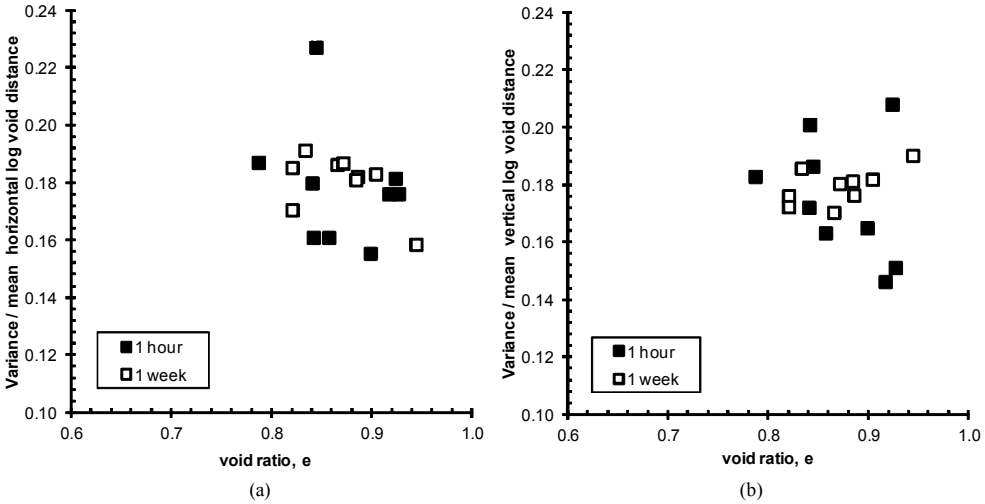

Figure 6-50 Index of dispersion log void distance for loose dry pluviated samples (all) at σ'_v =125kPa co i.e. 40601H_DD&40601W_DD: (a) horizontal (b) vertical

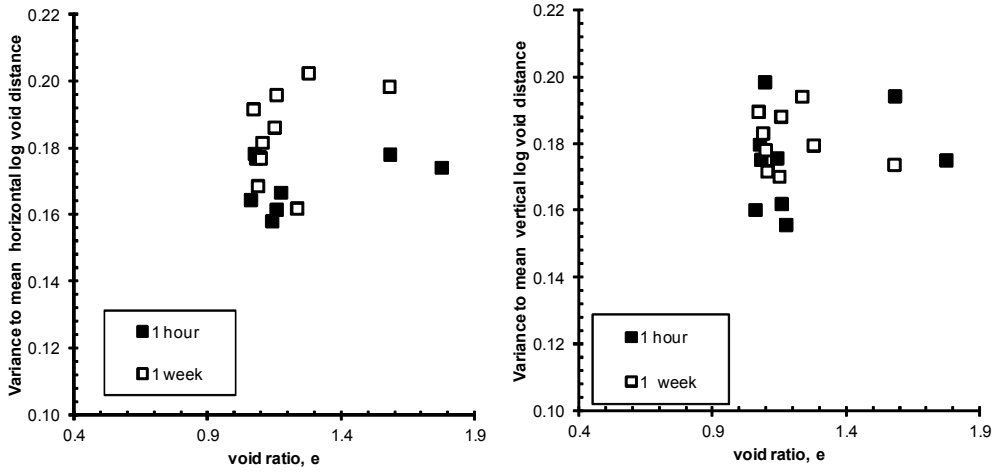

Figure 6-51 Index of dispersion log void distance for loose dry pluviated samples (sand) at σ'_v =125kPa co i.e. 40601H_DD&40601W_DD: (a) horizontal (b) vertical

The relationship between kurtosis and void ratio is illustrated by Figure 6-52. Kurtosis tends to decrease with time vertically i.e. from -0.745 to 0.787. Likewise in the horizontal direction kurtosis also becomes greater i.e. from -0.770 to -0.699. For sand (Figure 6-53), vertically the kurtosis is getting lower slightly with time (from -0.321 to -0.331) whilst horizontally it changes from -0.202 to -0.276.

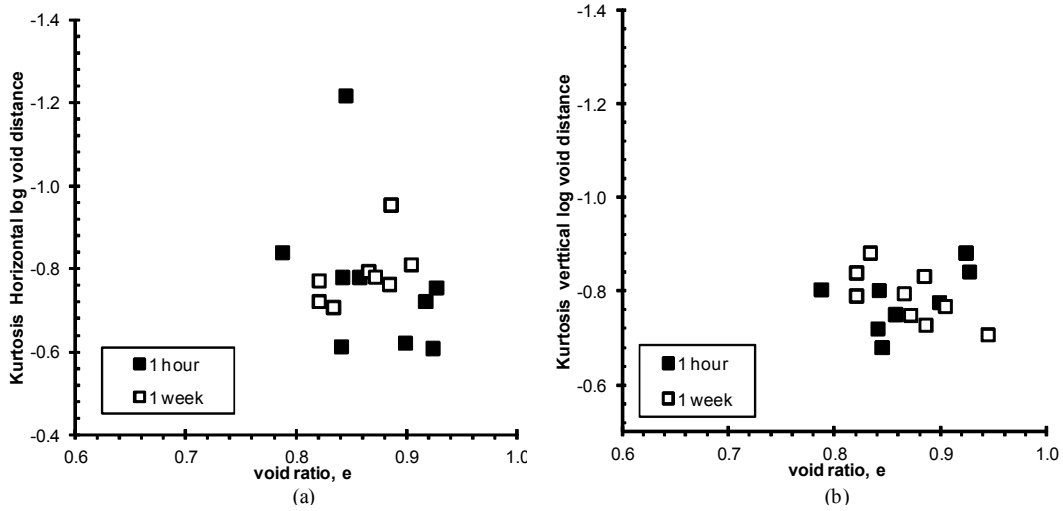

Figure 6-52 Kurtosis log void distance for loose dry pluviated samples (all) at σ'_v =125kPa co i.e. 40601H_DD&40601W_DD: (a) horizontal (b) vertical

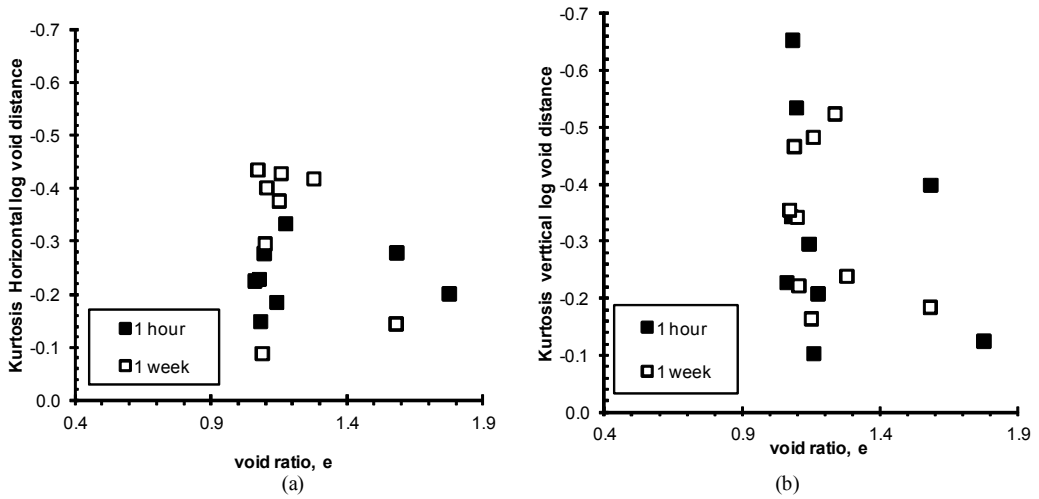

Figure 6-53 Kurtosis log void distance for loose dry pluviated samples (sand) at σ'_v =125kPa co i.e. 40601H_DD&40601W_DD: (a) horizontal (b) vertical

6.5 Observation of Void distance Changes due to Creep Induced Aging from Numerical Modeling

6.5.1 General

To the author's knowledge there have been no studies of void distance changes due to creep induced aging from numerical modelling. (Kang *et al.*, 2012), as explained in Chapter 2, investigated microstructure changes during creep in terms of void orientation evolution and contact anisotropy. Their chief finding is that split and union of voids or pore spaces is the basic mechanism of creep and as creep progresses, voids elongate toward the direction of principal stress direction.

This sub-section re-visits and re-analyzes the discrete element modelling (DEM) of biaxial creep test from (Kang *et al.*, 2012) in terms of void distance change. The samples were prepared via radius expansion. In addition the particle shape is round thus the initial fabric tends to be isotropic (no inherent fabric anisotropy). Following isotropic consolidation at 400kPa confining pressure a biaxial sample was sheared at constant velocity and then paused at certain deviator stress for approximately 50min and 157min for dense (sample D) and loose sample (sample A), respectively. It should be noted that those times in the DEM simulation

is not comparable to real time experiments. A time step was used instead by choosing any number of viscosities of dashpots to fit a creep response of the material. Thus in DEM, the creep process is accelerated. In Kang's study (2012) the time step was chosen such that the creep response (volumetric strain) of dense material is contraction followed by dilation (Kang, 2014) and contraction for the loose sample. In addition, while it is realized that the material properties (e.g. shape, gradation, span size) and stress conditions at the initial creep stage are different from those used in this study, it was thought the trend in void distance change may be similar as volumetric creep trends are similar. One major difference that should be considered is the boundary condition. In the real one dimensional fabric test used in this study, the soil cannot expand laterally (K_0 condition). Whereas in the DEM model the soil can expand laterally, that will allow particle contact separation. This probably in turn reduces the effect of aging.

Table 6-6 Comparison of material properties and stress condition of Kang's DEM (sample A for Loose and sample D for dense) and real fabric tests

Parameter	DEM	This study	Note
D_{max} (mm)	0.775	0.3	maximum diameter
D_{min}(mm)	0.225	0.032	minimum diameter
shape	circular	sub-angular	
s*	0.55	0.81	span size
e (dense)	0.18	0.656	void ratio
e (loose)	0.35	0.809	void ratio
R_A	1.43	1.87-2.14	creep stress ratio
R_D	2.46	2.21-2.55	creep stress ratio
σ'_3 (kPa)	400	30-120	confining pressure
BC	allow lateral expansion	K_0 condition	

*s=(Dmax-Dmin)/(Dmax-Dmin); BC=Boundary condition

Output data from the modelling about the position of each particle in each creep stage were provided through courtesy of Kang, D.H. (personal communication). A small program was written in Matlab to take some snapshot images for the initial creep condition (stage 0), middle (stage 8) and end of creep (stage 20). Nine images of the same region of interest (left, middle, right, bottom

and top) were taken from each stage of the dense and loose condition, as illustrated in Figure 6-54. Each image consists of approximately 280 particles.

Void distance distributions from nine images for initial condition, before creep starts are shown in Figure 6-55. As can be seen from the figure, the shape of distribution is similar to that of the reconstituted moist tamped sample (see Figure 6-8). The result of the statistical analysis of void distance is presented in Table 6-7. As dense test involved creep rupture, three stages of the dense sample (D0, D8 and D20) were captured. D20 (t_{creep}≈157min) is at the end of dilation (creep rupture) whilst D8 (t_{creep}≈18min) is during dilation before creep rupture ($t_{rupture}$≈26min). For the loose sample test only two stages (D0 and D20) were taken, as the sample contracted all the way and no creep rupture occurred. The letter and the number in the sample column represent dense (D), loose (A) and creep stage number (0 and 20).

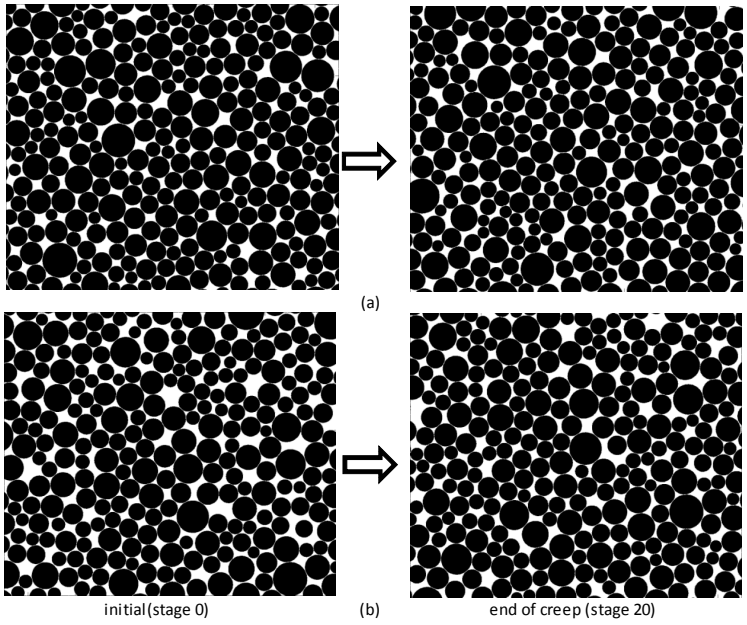

Figure 6-54 Example of DEM snapshot during creep stage (a) dense (b) loose (courtesy of Kang, D.H)

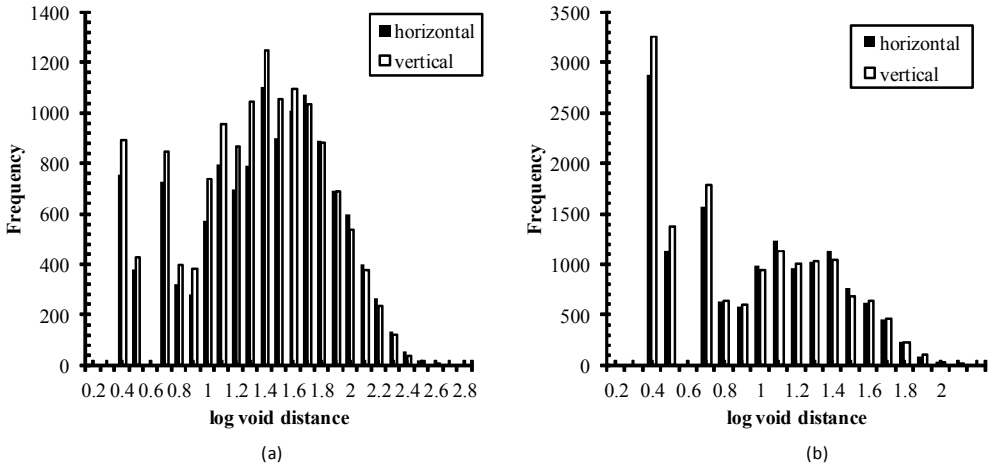

Figure 6-55 Void distance distribution from DEM at stage 0 (a) dense: D0 (b) loose: A20

Table 6-7 Changes in void distance from DEM

Sample	Void ratio	Mean		Variance		Kurtosis		Varian / Mean	
		V	H	V	H	V	H	V	H
D0	0.21	0.829	0.849	0.182	0.185	-1.101	-1.124	0.220	0.218
D8	0.22	0.835	0.883	0.189	0.175	-1.084	-1.091	0.226	0.198
D20	0.23	0.844	0.906	0.200	0.179	-1.065	-1.139	0.237	0.197
A0	0.27	0.919	0.930	0.206	0.211	-1.143	-1.095	0.225	0.197
A20	0.24	0.874	0.903	0.199	0.196	-1.110	-1.124	0.228	0.203

6.5.2 Results

Table 6-7 shows that generally the loose sample has higher mean log spacing than the dense sample e.g. for A0 mean log spacing are 0.919(V) and 0.930(H) compared to D0 with mean log spacing of 0.829(V) and 0.849(H). This is due the greater void ratio of the loose sample compared to the dense sample. Based on 27 images each of dense and 18 images of loose samples (before creep starts), a strong linear correlation was found between void ratio and void distance, as illustrated in

Figure 6-56. The values of coefficient of correlation, r^3, which is equal to square root of R^2, for the dense sample in the horizontal and vertical direction, are 0.91 and 0.84, respectively. Loose samples have r values of 0.91 horizontally and 0.95 vertically. The figure reveals that for both dense and loose sample, horizontal void spacing is generally larger than vertical ones, suggesting a strong influence of loading induced anisotropy (considering the initial condition tends to be isotropic).

Plots of mean log spacing and void ratio for each stage are shown in Figure 6-57. As creep progress, the mean void ratio of the dense sample tends to increase slightly (0.21 for D0; 0.22 for D8 and 0.23 for D20) whereas for the loose sample it tends to decrease slightly (0.27 for A0 and 0.24 for A20 20). This suggests that during creep, the dense sample eventually dilates (at least until D8 before rupture at D20) whereas the loose sample contracts. There is no creep rupture observed in triaxial creep of this study (see Chapter 4) thus only D8 is considered for the dense sample discussion. As the number of data points in Figure 6-57 becomes less i.e. 9 points, the coefficient of correlation also decreases. In the horizontal direction, r values of the dense sample for stage 0, 8 and 20 are 0.78, 0.52 and 0.66, respectively. In the vertical direction they are 0.42, 0.76 and 0.66. For the loose sample, r values in the horizontal direction for stage 0 and stage 20 are 0.76 and 0.77. Vertically they are 0.89 and 0.76, respectively. Despite the lower correlation value, generally the model shows a significant linear relationship between mean log spacing and void ratio.

Based on mean log spacing in Table 6-7 generally the model shows that as creep progresses, the mean void distance for the dense sample is increasing horizontally (from 0.849 of D0 to 0.883 of D8) and vertically (from 0.829 of D0 to 0.835 of D8). This is a quantitative evidence of the observation of Kang *et al* (2012) that for a dense sample small voids merged forming a larger void. This also indicates expansion in the void due to the dilative nature of the dense sample. For the loose sample the mean void distance tends to decrease throughout, both in the

[3] It should be noted that for a random data sets of 9, 18 and 27 points, the critical r values corresponding to 95% confidence interval are 0.602, 0.468 and 0.367. Values higher than critical r are considered significant.

horizontal and vertical direction. Again this is a quantitative evidence of the observation of Kang et al (2012) who believed void splitting is the basis for the creep mechanism in loose samples. This shows that during creep, the loose sample exhibits contraction.

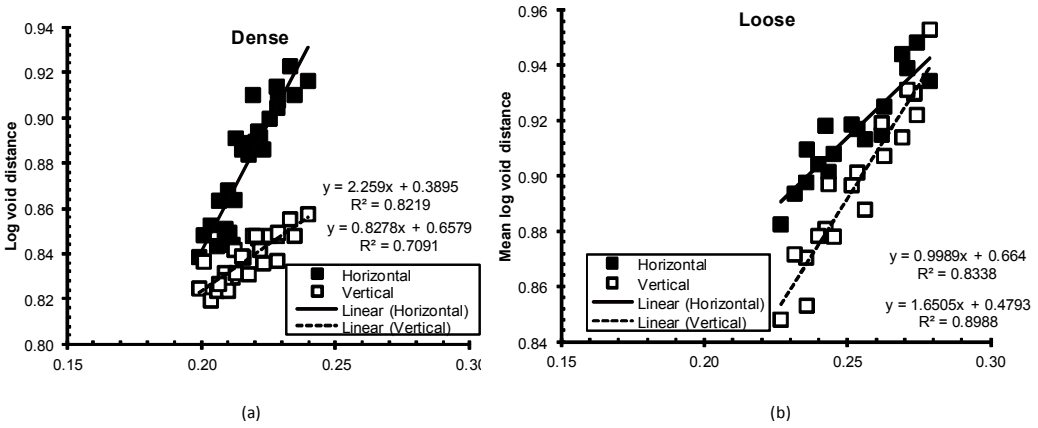

Figure 6-56 Log void distance vs. void ratio i.e. combined data in each direction from stage 0, 8 and 20 of (a) dense and stage 0 and 20 of (b) loose

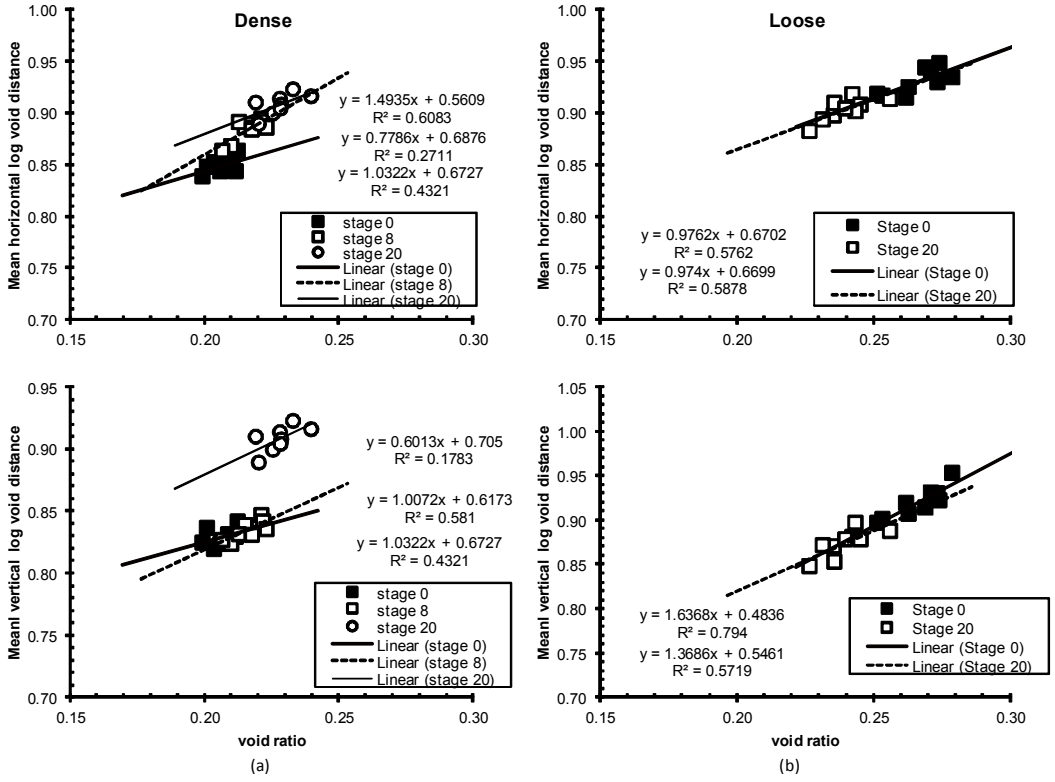

Figure 6-57 Log void distance vs. void ratio for each stage (a) dense (b) loose

In terms of mean variance, initially the dense sample has lower variance than the loose sample (see Table 6-7).This is in accordance with the observation by Jang and Frost (1998) that looser samples have more variability in local void ratio. It can be seen also that at the initial stage the difference between horizontal and vertical variance is very small, i.e. 0.002 and 0.005 for the dense and loose sample, respectively. Therefore although in the vertical direction the mean log-void distance is lower than that in the horizontal direction, as in dry pluviated samples (see section 6.3.2.3 and 6.4.2.4), generally based on the small difference in variance both vertically and horizontally, it can be said that generally initial fabric of the model is near isotropic as in moist tamped sample.

As creep progresses, the dense sample tends to develop a greater mean variance in the vertical direction (from 0.182 for D0 to 0.189 for D8) whereas horizontally it tends to decrease (from 0.185 for D0 to 0.175 for D8). This suggests more strong void structure is formed in the vertical direction whereas weak horizontal void structure collapses. Combining data from stage 0, 8 and 20, variance for the dense sample has strong linear relationship with void ratio (r=0.94) in the vertical direction, as shown in Figure 6-58(a). Likewise when analyzed for each stage the relation is still strong with r value greater than 0.72 (see Figure 6-59a). However in the horizontal direction when data from each stage are combined no linear correlation was found at an r value of -0.07. However when examined for each stage, the variance in the horizontal direction shows an increase in the linear relationship as creep progress, with r values equal to 0.31, 0.53 and 0.88, for stages 0, 8 and 20, respectively. Basically Figure 6-59(a) shows that initially there is no real correlation between variance and void ratio in the horizontal direction whereas in the vertical direction there is. This likely as the sample is numerically pluviated there will be particle contact in the direction of gravity. There will be large gaps between them when the scan line misses them so the variances increase with overall void ratio. As time goes by during creep, horizontal variances start to be better correlated which suggests some organization of particles in this direction.

For the loose sample, as the sample creeps with time, variances tend to decrease with time both horizontally (0.211 at stage 0 to 0.196 at stage 20) and vertically (0.206 at stage 0 to 0.199 at stage 20). This is likely due to local structure collapse thus the voids tend to become smaller i.e. larger voids split and more small voids are formed. As the voids became smaller the variance gets smaller. Variance and void ratio has a strong linear relationship in both horizontal and vertical directions with r values of 0.94 and 0.83, respectively, as shown in Figure 6-58(b). Likewise, a strong linear relationship between variance and void ratio were observed for each stage with an r value of at least 0.78.

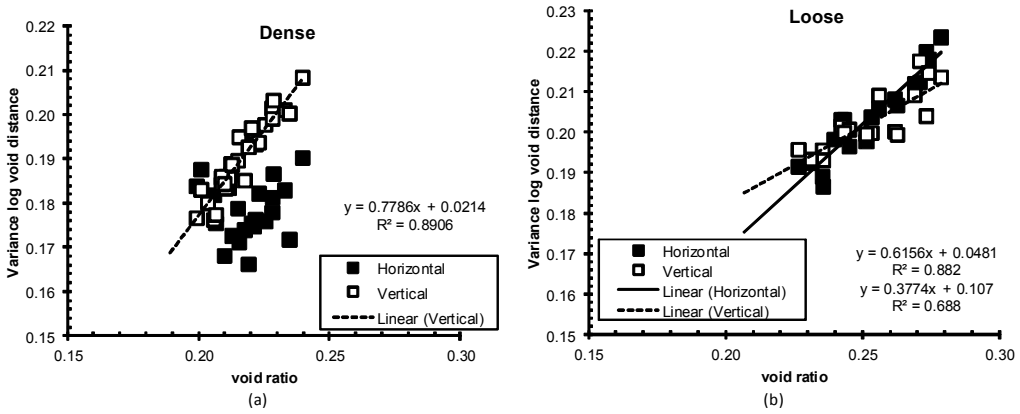

Figure 6-58 Variance log void distance vs. void ratio (a) dense (b) loose

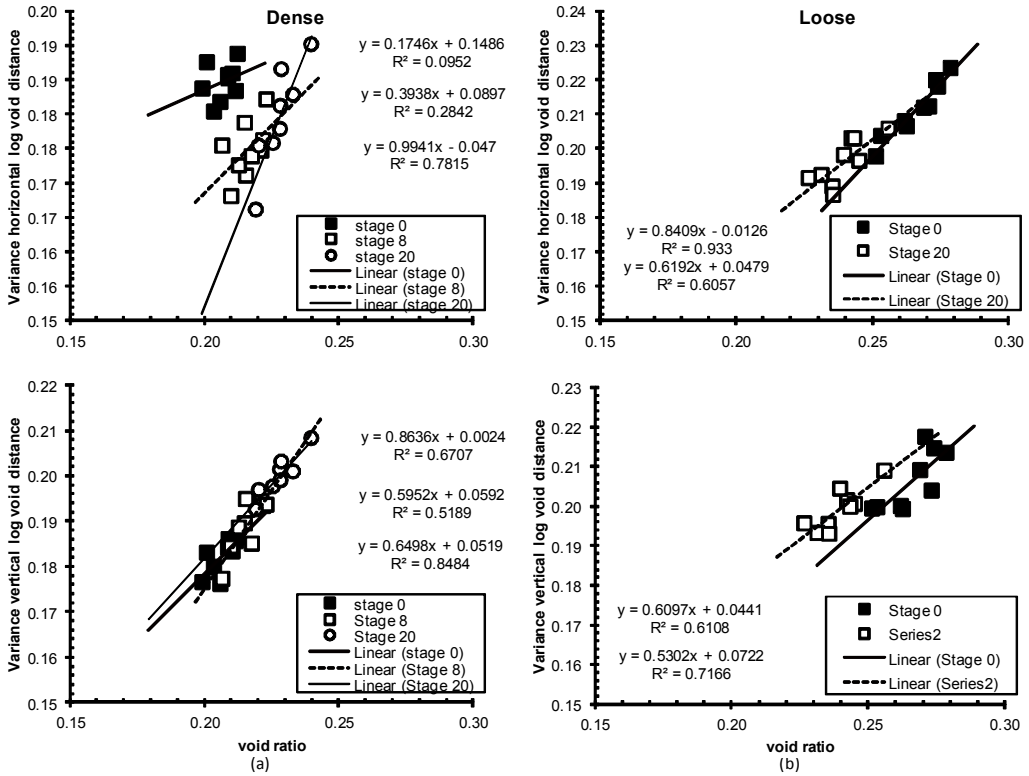

Figure 6-59 Variance log void distance vs. void ratio (a) dense (b) loose

Figure 6-60 shows a plot of variance to mean ratio against void ratio when data from each stage 0, 8 and 20 are combined. Figure 6-61(a) presents plot of variance to mean ratio per stage of creep for the dense sample. Generally as the sample creeps with time, the means index of dispersion of the dense sample (see Table 6-7) tends to increase vertically (from 0.22 at stage 0 to 0.226 at stage 8) and decrease horizontally (from 0.218 at stage 0 to 0.198 at stage 8). Figure 6-61(a) shows that a generally significant linear relationship exists in the vertical direction for each stage with a minimum r value of 0.7. In the horizontal direction a strong linear relationship is only found in stage 20 (r=+0.75), whereas stage 0 and 8 show no significant relationship. The loose sample as presented in Figure 6-60(b), on the other hand, has strong a linear relationship in the horizontal direction with r=+0.82 and no relationship in the vertical direction with r=+0.06. Furthermore, Figure 6-61(b) illustrates plots of the index of dispersion per stage of creep for the loose sample. As the loose sample creeps with time, the mean index of dispersion tends to increase vertically from 0.225 at stage 0 to 0.235 at stage 20. Horizontally mean index of dispersion increases from 0.198 at stage 0 to 0.203 at stage 20. The

tendency of increasing index of dispersion for the loose sample indicates particles cluster together over time. This would increase aging as particles are increasing in contacts. Generally the index of dispersion for the loose sample shows a relatively stronger linear relationship compared to the dense one. In the horizontal direction, stage 0 and stage 20 have r=+0.86 and r=+0.59, respectively, whilst in vertical direction, r=+0.43 for stage 0 and r=+0.46 for stage 20.

Figure 6-62 shows a plot of kurtosis versus void ratio when the data from stages 0, 8 and 20 (dense) and stage 0 and 20 (loose) in each direction are combined. For the dense sample, there is no correlation in the horizontal direction as the r value is -0.1. However there appears to be a very weak linear relation in the vertical direction with an r value of 0.349 (r critical=0.367). The coefficient of correlation values of each stage for the dense sample (Figure 6-63a) show slightly larger r values compared to the combined data, but still not a significant relationship. No significant relationship was also observed for the loose sample either for the combined data or at each stage (Figure 6-63b) with an r value of 0.23 (horizontal) and 0.35 (vertical).

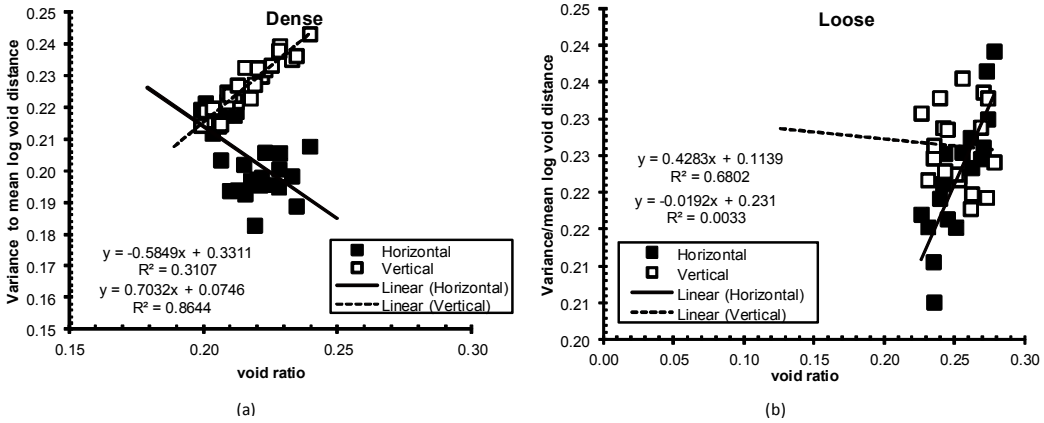

Figure 6-60 Variance/mean log void distance vs. void ratio (a) dense (b) loose

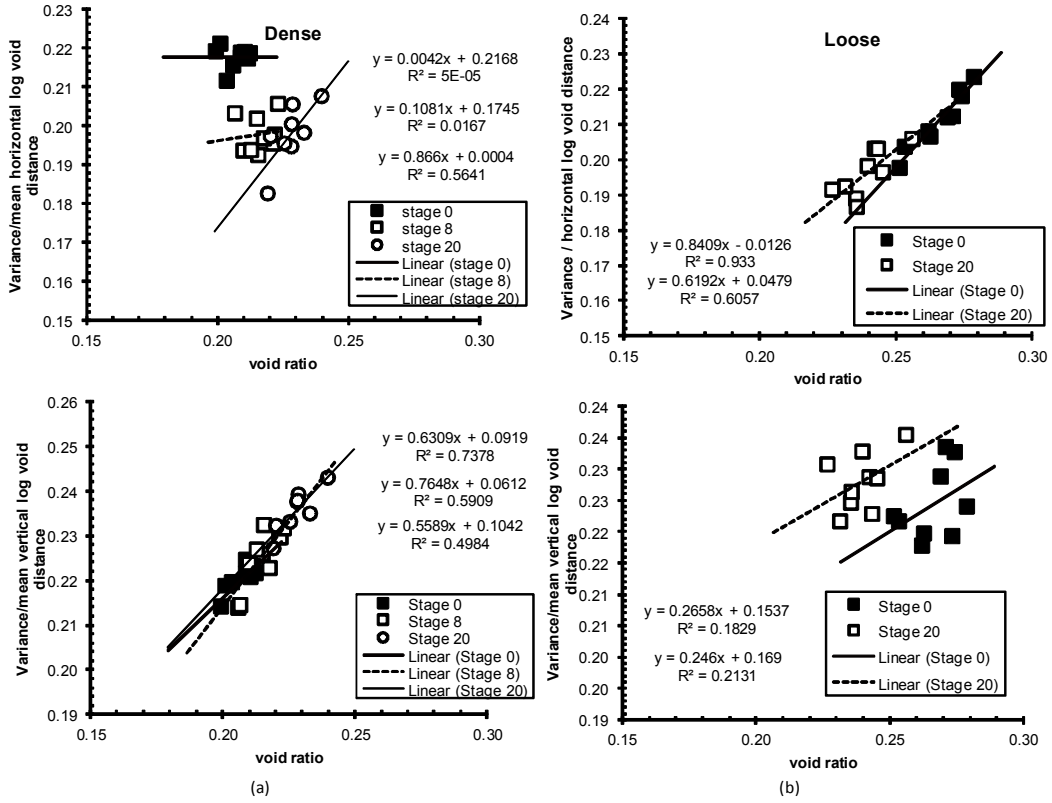

Figure 6-61 Variance/mean per stages log void distance vs. void ratio (a) dense (b) loose

For the dense sample, at the initial condition, the kurtosis is lower in the horizontal direction than in the vertical direction, indicating a flatter shape around the mean (larger variance in the horizontal direction compared to the vertical direction). This indicates more gaps in the horizontal direction compared to the vertical direction. The opposite trend was found for the initial condition of the loose sample i.e. kurtosis in the vertical direction is lower than in the horizontal direction; indicating that there is a greater number of relatively larger gaps in the vertical direction than in the horizontal direction. Accepting a linear relationship exists, it can be seen that as the dense sample creeps with time the kurtosis tends to be higher in the vertical direction (-1.101 at stage 0 to -1.065 at stage 20) and lower in the horizontal direction (-1.124 at stage 0 to -1.139 at stage 20). This indicates that with time more voids with larger gaps form horizontally whilst the number closely spaced in the vertical direction reduce. A similar tendency also was for the loose samples i.e. increase in the vertical direction from -1.143 at stage 0 to -1.110 at

stage 20 and decrease horizontally from -1.095 at stage 0 to -1.124 at stage 20. This suggests similar things occur for both dense and loose samples by which more uniform void orientation develops with time toward the vertical (major principal stress) direction as illustrated by Kang et al (2012) in Chapter 2.

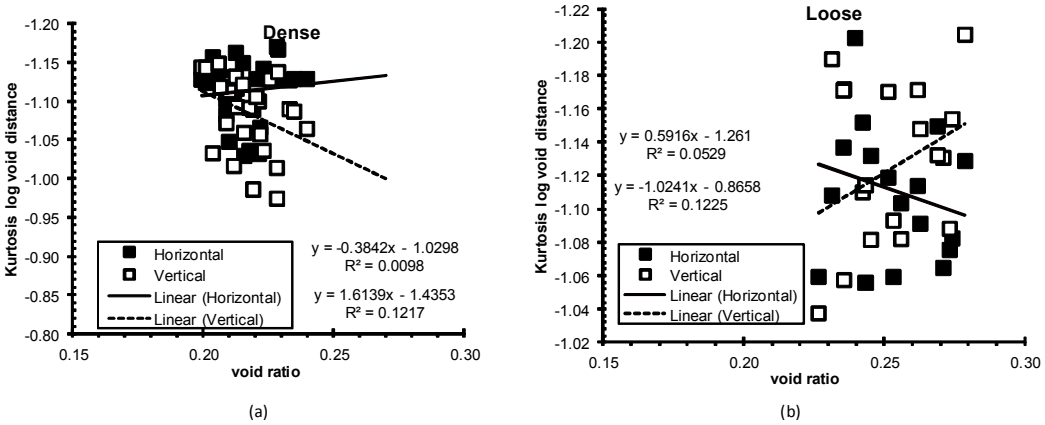

Figure 6-62 Combined kurtosis log void distance vs. void ratio (a) dense (b) loose

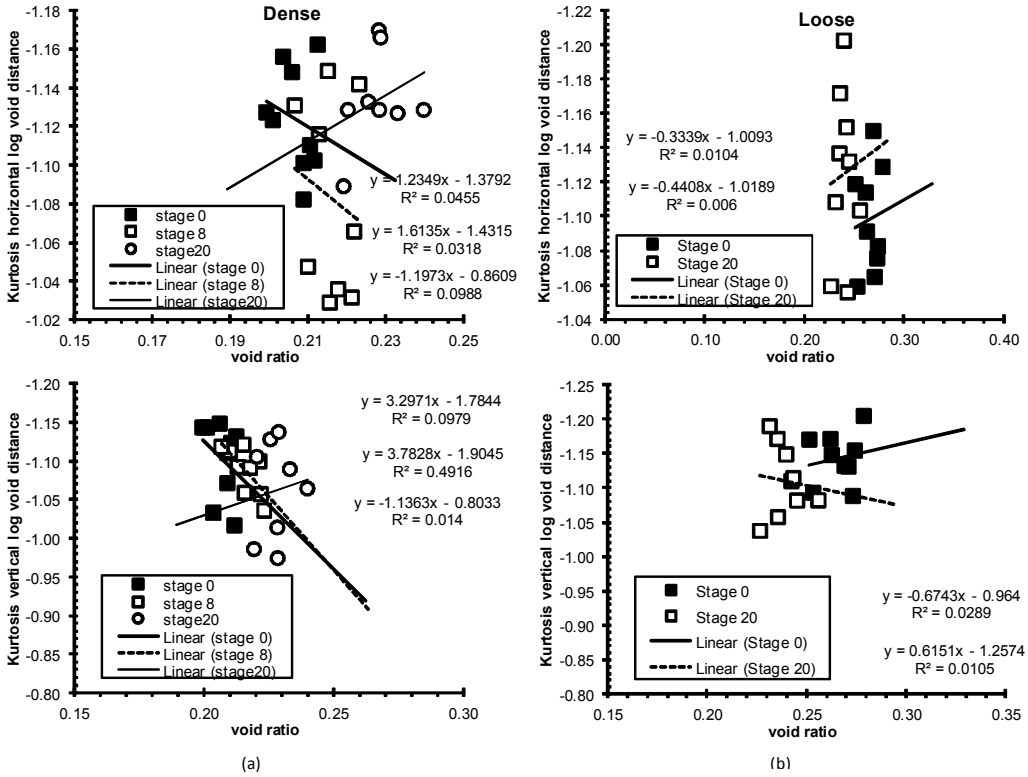

Figure 6-63 Kurtosis log void distance vs. void ratio of each stage (a) dense (b) loose

6.6 Discussion

6.6.1 Initial fabric

Moist tamping and dry pluviation produce different initial fabric both in terms particle orientation and spatial void distance distribution. Upon the application of load the particle orientation of moist tamped soil tends to be near random with a slight bias towards vertical (see Figure 6-7 left and Figure 6-26 left) whilst dry pluviated soil tends to produce particles which are horizontally orientated or perpendicular to loading direction (Figure 6-6 left and Figure 6-28 left). Dry pluviated samples, both dense and loose, are more orientated than moist tamped samples as indicated by higher r and κ values (Table 6-2 and Table 6-4). In term of degree of orientation also, 'fines' of moist tamped soil are less orientated than that of dry pluviated sample.

In terms of spatial void distance distribution moist tamped samples are more isotropic than dry pluviated samples as shown by less absolute difference of mean log spacing in the horizontal and vertical direction (see Table 6-3 and Table 6-5). Moist tamped samples have higher variances and variance to mean ratio than dry pluviated samples (see Table 6-3 and Table 6-5). This indicates that particles in moist tamped soil are initially more clustered or clumped than in dry pluviated soil. Moist tamped samples also tend to have lower kurtosis values than dry pluviated samples (see Table 6-3 and Table 6-5) which suggest that moist tamped soil is more structured.

Revisited Kang's DEM results, absolute differences between mean log void distance, [$\Delta\mu$], between vertical and horizontal directions, at the initial condition, are relatively small i.e. 0.019 (dense) and 0.011 (loose). These values are similar to those values from moist tamped samples i.e. 0.003-0.011(dense) and 0.002-0.019 (loose). This suggests that initially void fabric of DEM which is prepared by radius expansion method and moist tamped samples used in this study is similar i.e. near isotropic. For dry pluviated samples, dense samples are more anisotropic than loose

samples. The difference in mean log void distance of dense dry pluviated samples is 0.042, larger than dense moist tamped samples (0.003-0.011). This indicates dense dry pluviated soil is more anisotropic than dense moist tamped soil.

6.6.2 Density and relative number of grain contacts

The relative number of grain contacts in dense and loose silty sand can be approached by observing the change in the degree of particle orientation as illustrated by test 40601H_DD, 40601W_DD, 70601H_DD and 70601W_DD. Table 6-2 shows that the degrees of orientation for 70601H_DD (κ=0.36) and 70601W_DD (κ=0.46) tends to increase with time while Table 6-4 shows that the degrees of orientation of 40601H_DD (κ=0.42) and 40601W_DD (κ=0.4) are relatively similar with time. This implies that dense samples tend to have larger numbers of grain contacts than loose samples. This is in accordance with results from numerical modelling where dense samples tend to have larger average coordination number than loose samples (Alim *et al.*, 2006).

6.6.3 Density and role of fines

Table 6-2 shows that absolute difference of r and κ and values of 'fines' of 70601H_DD and 70601W_DD are 0.0231 and 0.04 respectively, while from Table 6-4, the difference for 40601H_DD and 40601W_DD are 0.09 and 0.06. This means that the changes are greater in dense samples than in loose samples. This implies that 'fines' in dense samples have more contact with each other compared to those in loose samples. Lade and Yamamuro (1997) reported that increasing density at particular fines content force fines to be displaced from their deposited location into void spaces, as illustrated in Figure 6-1 (b). Relatively smaller change in r and κ values for loose samples also implies that there are more floating fines particles in loose samples than in dense samples, as indicated by DEM results (Imole *et al.*, 2013; Kumar *et al.*, 2014). These floating particles might consist of S-V or S-S-V grain contacts. This is in also accordance with Thevanayagam and Mohan's postulation (2000).

6.6.4 Effect of aging time

Real fabric tests under K_0 condition show that there are changes with time both for dense and loose samples in term of particle orientation and spatial void distance distribution. The changes suggest that under constant load, there is some structuration over time. As aging progresses, particles rotate in space as shown by the right side of Figure 6-6, Figure 6-7, Figure 6-26 and Figure 6-28. As the initial fabrics of moist tamped and dry pluviated soils are different, effects of loading with time are also different.

Dense dry pluviated tests 70601H_DD and 70601W_DD show that the degree of orientation increases with time e.g. κ=0.36 at one hour of aging to κ=0.42 at one week (r=0.18 to r=0.2). This indicates reducing anisotropy of particle orientation, or in another words, particle orientation fabric becoming more isotropic with time. In addition much of the change in of degree of orientation appears to occur in 'fines' with r and κ values of sand becoming practically the same over time. On the other hand, dense moist tamped tests 70301H and 70301W show that κ values remain the same κ=0.11 with r value increasing over time (r=0.54 at one hour to r=0.57 at one week). Additionally, changes in degree of orientation for dense dry pluviated sample tend to be contributed from 'fines' whilst for dense moist tamped samples tends to be contributed from sand particles. This is likely because 'fines' particles in moist tamped soil is less orientated than those in dry pluviated soil as indicated by lower r and κ values of moist tamped samples. This suggests more contacts between 'fines' in dry pluviated samples than those in moist tamped samples. For loose moist tamped samples (40301H and 40301W) there is a slight change in degree of orientation up to one week. The degree of orientation starts to change significantly after four months (κ=0.1 at one week; κ=0.27 at 4 months; κ=0.25 at 8 months). Overall, regardless of the methods of deposition and density, particles tend to rotate with time.

Over time, real fabric tests and Kang's DEM which was revisited show that mean log-void distance tends to grow in dense samples (e.g. Table 6-3, Table 6-7 and Figure 6-10) and contract in loose samples (e.g. Table 6-5, Figure 6-29 and Figure 6-46) . The trends generally are in accordance with observations from DEM by Kang *et al.* (2012). In terms of grain contact evolution, Kang *et al.* (2012) shows that average coordination number during creep is decreasing in dense samples (contact separation due to dilation) and is increasing in loose samples due to pore collapse (contact creation). Dense dry pluviated samples show that the difference of mean log void distance in horizontal and vertical direction [$\Delta\mu$] is decreasing with time i.e. from 0.042 to 0.032 for all particles and 0.047 to 0.038 for sand particles. This is a similar trend as Bowman (2002) on dense air pluviated clean sand. This is likely due to similar initial anisotropic void fabric. This trend, on the other hand, is in contrast with DEM and dense moist tamped samples which initially are near isotropic. Variances to mean ratio values for moist tamped samples tend to decrease whereas those of dry pluviated samples tend to increase with time. Increase in variance and variance to mean ratio of dry pluviated sample (and DEM sample) indicates that particles are more clustered together with time. Whilst a slight decrease in variance to mean ratio of moist tamped sample suggests less clustered. In addition, kurtosis tends to be lower with time, which suggests more structured fabric. It appears that the decrease in kurtosis for sand particles only is different in direction between moist tamped and dry pluviated samples. For moist tamped samples, the decrease in kurtosis was larger in the vertical direction i.e. from -0.409 to -0.768 (Δ=0.36), indicating greater structuration in sand vertically, whilst horizontally, the kurtosis value actually increased slightly from -0.448 to -0.405 (Δ=0.04). On the other hand, dry pluviated samples show greater structuration in the horizontal direction over time with kurtosis value decreasing significantly from -0.168 to -0.378 (Δ=0.21), whilst vertically, kurtosis value decreased from-0.267 to -0.325 (Δ=0.06). The difference in direction of microstructure changes in terms of kurtosis is likely due to different in initial grain orientation of the particles and initial contact normal orientation. Moist tamped soil tends to produce random but slightly toward-vertical grain orientation. On the other hand, dry pluviated sample

tends to produce fabric with horizontally orientated grain fabric (Jang & Frost, 1998; Yusa & Bowman, 2013). Contact normal orientation in dry pluviated samples tends to be less concentrated in vertical direction than that of moist tamped sample (Yimsiri & Soga, 2010). In short moist tamped samples start already structured and clustered/clumped then there is less room to move than for dry pluviated samples (see section 6.3.2.2). Again this emphasizes that initial fabric plays a significant role during aging.

Overall it can be said that some structuration occurs during aging, however different trends in microstructures between dense and loose soil were observed, likewise between moist tamped and dry pluviated samples. This suggests microstructure changes in terms of particle orientation and spatial void distances alone may not be adequate to explain increase in stiffness due to aging. Change in contact normal forces or redistribution of contact forces, as suggested by DEM (see section 6.6.5), may help to shed more light on aging in silty sand.

6.6.5 Force chain change over time from DEM

The change of force chain network over time is not possible to observe in these fabric tests. However some observation from relatively current DEM results from other researchers can be borrowed and explained below.

Radjai *et al.* (1996), using numerical simulation of biaxial loading, showed that under loading, a granular assembly consists of a strong force and weak force network. A force network with higher normal force compare to sliding force is defined as strong, whilst the weak network carries very low normal contact force and high sliding force. This weak network acts as a prop to the strong network.

Wang *et al.* (Wang *et al.*, 2008) and Gao *et.al* (2010), using numerical simulation of granular assembly revealed that during aging, redistribution of normal contacts occurs. Normal contact forces become more homogenized with time. Strong force chains decrease and weak force chains increase which results in a more

stable structure. In addition Kang *et al.* (2012) show that void orientation becomes more homogenized with time i.e. elongated toward the principal stress direction.

Wang *et al.* (2014), based on an instrumented oedometer (via tactile sensor) and DEM, shows during secondary compression of sand loaded under K_0 condition, there are some changes that occur. Firstly, the percentage of weak force chains decreases. These weak force chains play a dominant role in small-strain deformation therefore the corresponding shear modulus. As the percentages of weak forces decrease, the associated weak force chain becomes stronger due to increasing normal contact force thus increasing shear modulus. Secondly, deviator fabric tends to decrease with time which suggests a gradual reduction in tendency of particle buckling. Therefore the material becomes stiffer.

6.7 Microstructure of Natural Sand from 'Gel-Push Sampling'

6.7.1 General

This section describes microstructural observation of granular soils from undisturbed samples via gel-push sampling. As microstructure study of granular soils from undisturbed sampless is relatively rare, it is deemed useful to fully make use of any available sample. The natural sands used here were obtained towards the end of the study, as left-over samples from another project on liquefaction assessment of Christchurch's soil (Cubrinovski, 2013; Jang & Frost, 1998; Taylor *et al.*, 2013). Gel push sampling was first developed in 1999 in Japan to obtained samples of sandy, gravelly soil and fractured rock. The method then progressively has been developed and modified by Kiso-Jiban Consultants under the guidance of Prof. Ishihara. The method utilizes high density polymer solution at very low velocity without circulation (preventing loss of fines particles) to reduce the friction between the Gel Push and the sample tube. The polymer coated on the sample is gelated and semi hardens the surface to protect the sample. Detail of the technique can be found in the paper by Taylor *et al.* (Taylor *et al.*, 2012). Following the Christchurch Earthquake 2010-2011, the method was brought to New Zealand as

part of University of Canterbury Research Project on liquefaction assessment of Christchurch (Taylor *et al.*, 2012).

6.7.2 Material properties

As the materials are from leftover samples, the amounts were limited. The sample dimensions were approximately 50mm in diameter and 40mm in height. They were collected from two sites around Christchurch City Centre i.e. Kilmore Street (gp-A) and Madras Street (gp-B) that were badly affected by the February Earthquake in 2011 (Cubrinovski, 2013; Cubrinovski *et al.*, 2012; Taylor *et al.*, 2013). Gel Push samples A and B were taken approximately from 6m depth and 4m depth, respectively. Ground water table for gp-A and gp-B were 2m and 3m below the ground surface. As the sample size was limited, the particle size distribution was obtained by laser particle sizer. The results are shown by Figure 6-47. It was found that gp-A is clean sand with 4 % of fines particles, whilst gp-B is silty sand with 30% of fines. The mean diameter of gp-A and gp-B are 235 micron and 95 micron, respectively.

6.7.3 Captured and processed images

Figure 6-65 (a) and Figure 6-65 (b) present examples of captured and processed images from gp-A and gp-B. A typical number of particles in one image are approximately 200 and 2000 for gp-A and gp-B, respectively, i.e. the number of particles of gp-B is approximately 10 times that of gp-A due to the increase in the fines content. Typically nine images were taken from each sample section i.e. left, middle and right side. Thus statistical analysis involved approximately 1800 and 18000 particles for gp-A and gp-B, respectively.

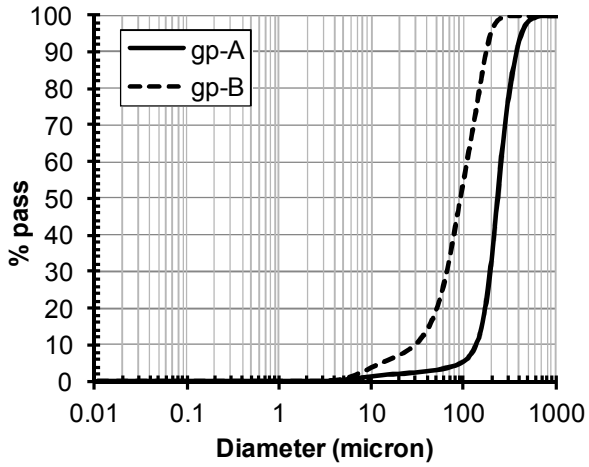

Figure 6-64 Grain size distribution from gel-push sampling

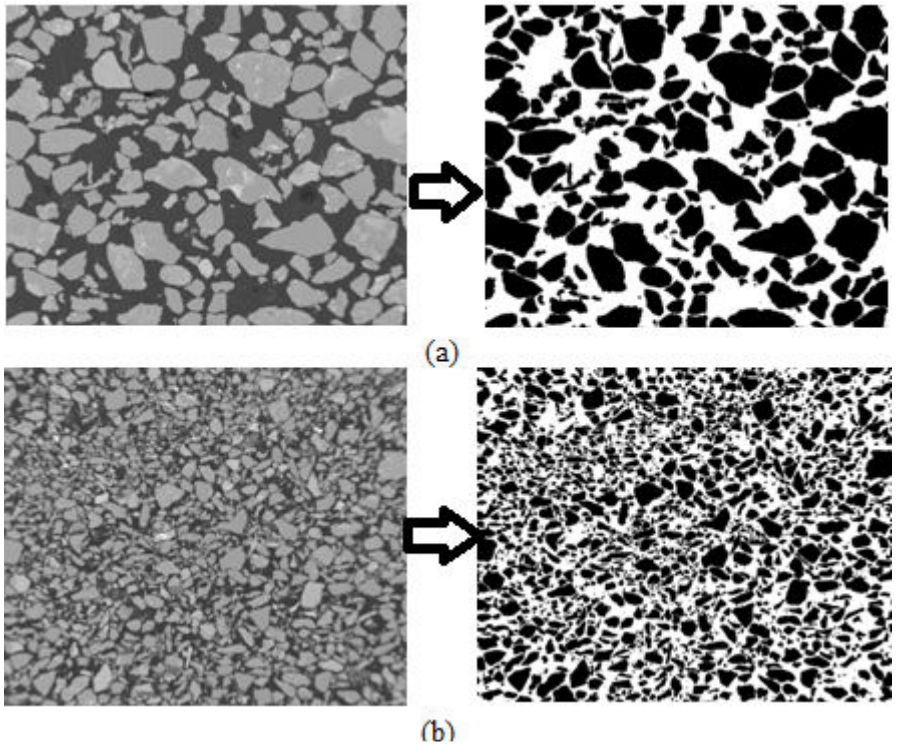

Figure 6-65 Typical captured and processed image from gel-push sampling

6.7.4 Orientation measure

The few published direct microstructure studies (Jang, 1997), based on expensive ground freezing, suggest qualitatively that sands under natural deposition have a preferred orientation with a tendency towards horizontal. However the

quantitative study of grain orientation and its anisotropy, particularly for silty sand under natural deposition, are still rare. This study attempts to provide some insight.

One factor that influences the final orientation of particles settling under gravity is moment inertia (Willmarth *et al.*, 1964). Moment inertia is closely related to particle elongation. Elongated particles which are deposited under gravity tend to be positioned at their long axes. Aspect ratio is probably the most related particle descriptor to elongation. Particle aspect ratio (AR) is defined as the ratio of the particle's long axis, dL, to short axis, dS (Equation 6-8). Aspect ratio that is higher than 1 indicates an elongated particle. A higher number for aspect ratio means a more elongated particle.

$$AR = \frac{dL}{ds} \qquad \textbf{Eq. 6-8}$$

A frequency distribution histogram of aspect ratio is shown in Figure 6-66. The calculations did not include particles touching the perimeter of the image because that would introduce errors into the results. It can be seen that most particles (approximately 70%) for both gp-A and gp-B have aspect ratio between 1.5 and 2, indicating many particles are elongated thus probably having a preferred orientation.

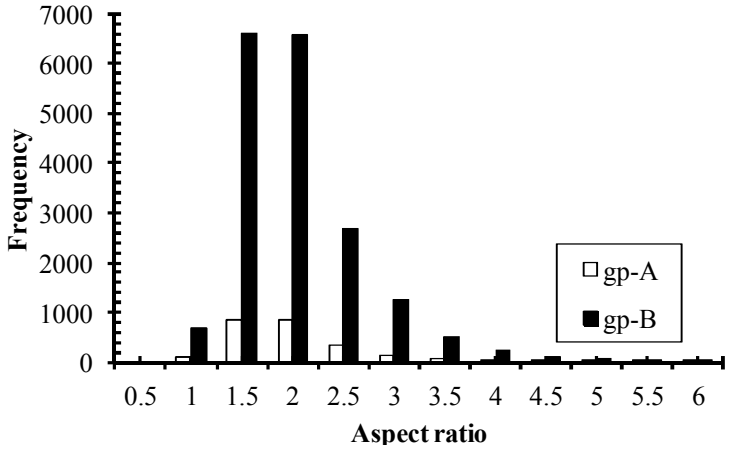

Figure 6-66 Aspect ratio distribution for gp-A and gp-B

Results of Fischer statistical analyses for orientation measurements of gp-A and gp-B are presented in Table 6-8. It can be seen from the table that the overall natural fabric has a preferred apparent orientation to the horizontal with mean angle 2.2^0 and 0.9^0 to horizontal axes, respectively. It is found from Table 6-8 that in general, for natural sand fabric both larger particles and fines particles tend to be orientated in the same direction. It can be seen that overall both samples have approximately the same degree of orientation with κ values of 0.53 and 0.52, respectively. This is supported also by relatively similar value of r.

Table 6-8 Particle orientation measures for gp-A and gp-B

Sample		$\alpha_m(^\circ)$	κ	r
gp- A	All	$87.8^0 \pm 1.2^0$	0.53	0.257
	Sand size	$88.9^0 \pm 0.9^0$	0.60	0.267
	'Fines size'	$81.9^0 \pm 3.0^0$	0.33	0.165
gp- B		$89.1^0 \pm 0.7^0$	0.52	0.252
	Sand size	$87.3^0 \pm 0.9^0$	0.80	0.371
	'Fines size'	$89.1^0 \pm 0.6^0$	0.51	0.246

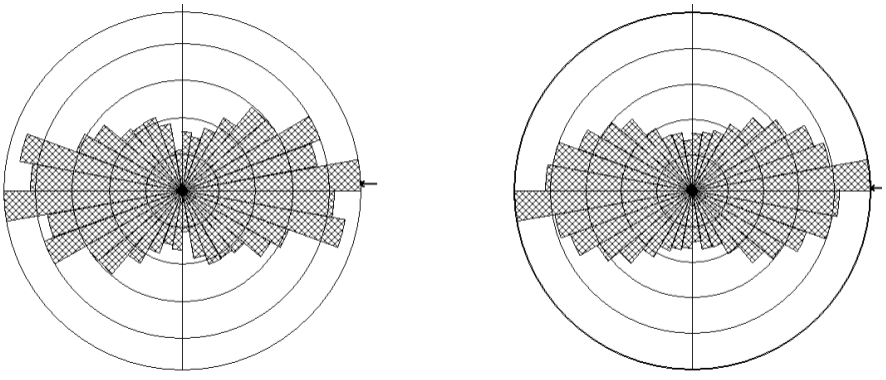

(a) (b)

Figure 6-67 Overall rose diagram for gp-A and gp-B

6.7.5 Void distance distribution

Figure 6-68 shows distribution of particle spacing on a histogram which gives a highly positive-skewed distribution, similar to those of reconstituted samples. This indicates that there are a large number of areas with closer void distance than areas with greater void distance.

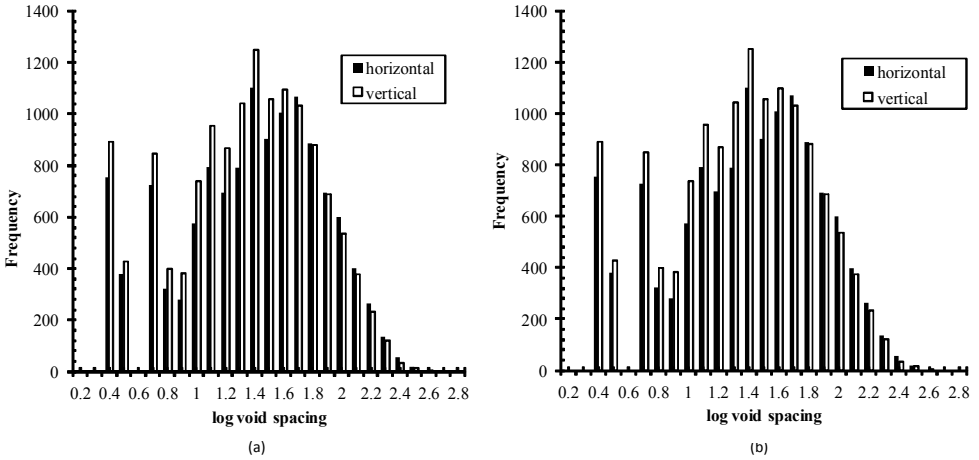

Figure 6-68 Void distance distribution of undisturbed samples i.e. (a) gp-A and (b) gp-B

The average spatial distribution results are shown in Table 6-9. Although direct comparison cannot be made with the reconstituted fabric test, due to different material properties, some general qualitative observations can be drawn.

Table 6-9 Void distance measures for gp-A and gp-B

Sample		e	Mean		Variance		Kurtosis		Var. / Mean	
			V	H	V	H	V	H	V	H
gp-A	All	0.733	1.281	1.325	0.044	0.238	0.249	-0.620	-0.585	0.185
	Sand	0.828	1.380	1.429	0.049	0.253	0.261	-0.534	-0.460	0.183
gp-B	All	0.726	0.958	1.015	0.057	0.147	0.163	-0.660	-0.695	0.154
	Sand	3.832	1.701	1.742	0.041	0.354	0.390	-0.437	-0.437	0.208
	Sand	0.733	1.281	1.325	0.044	0.238	0.249	-0.620	-0.585	0.185

Plots of mean log void distance versus void ratio for gp-A and gp-B are presented in Figure 6-69. It can be seen that means of log void distance of gp-A are generally larger than gp-B due to higher void ratio. The undisturbed samples were

taken from liquefied site, indicating a loose condition. Removing the 'fines' particles, it can be seen that Gp-B has significant increase in mean log void distance (approximately 70%) compare to gp-A (approximately 7%). This is because of the higher fines content of gp-B (30%) compared to gp-A (4%). Furthermore, mean log spacing in the vertical direction for both undisturbed samples are lower than that in horizontal direction indicating anisotropic condition. This relates to the result from orientation measurement that the fabric is horizontally orientated, such that a greater number of smaller vertical gaps exist. In short, similar fabric was found between undisturbed samples with dry pluviated sample.

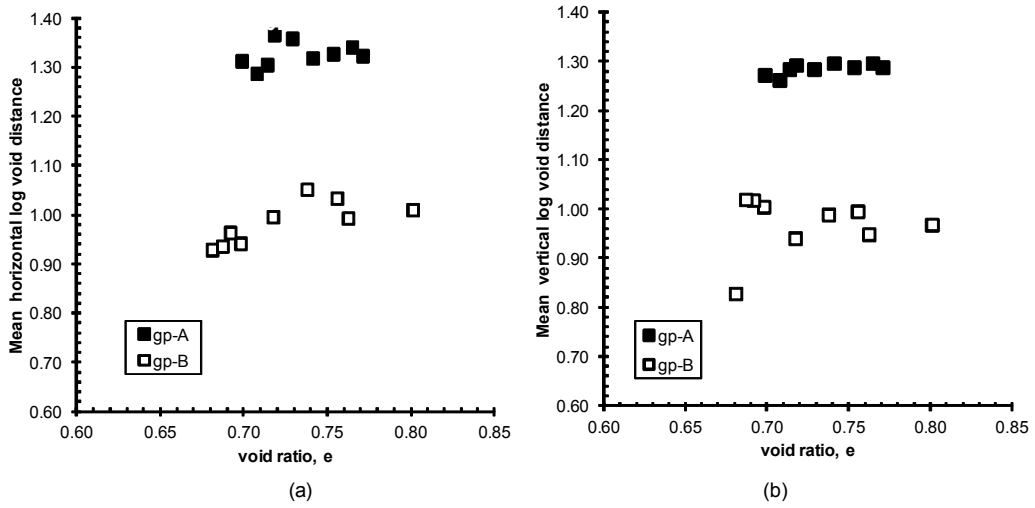

Figure 6-69 Mean log void distance versus void ratio, gp-A (a) and gp-B (b)

Variance of gp-A and gp-B versus void ratio are plotted in Figure 6-70 along with variance of loose dry pluviated sample i.e. 40601H_DD and 40601W_DD. Overall variance of undisturbed samples is slightly greater in the horizontal direction than in the vertical direction as for the dry pluviated sample. Gp-B has lower variance in both directions compared to gp-A, due to significant fines content. Removing the 'fines', the variance in gp-B increases almost 2.4 times compared to gp-B with fines, suggesting an important role of 30% fines. Whereas for gp-A the increase is only 1.05 times. Figure 6-71 shows variance to mean ratio versus void ratio. Figure 6-70 and Figure 6-71 show that gp-A generally has larger variance and variance to mean ratio than gp-B. This may be related to the fact that gp-A

experience higher vertical effective stress than gp-B. The figure also reveals that variance and variance to mean ratio of 40601W_DD samples tend to be above gp-B.

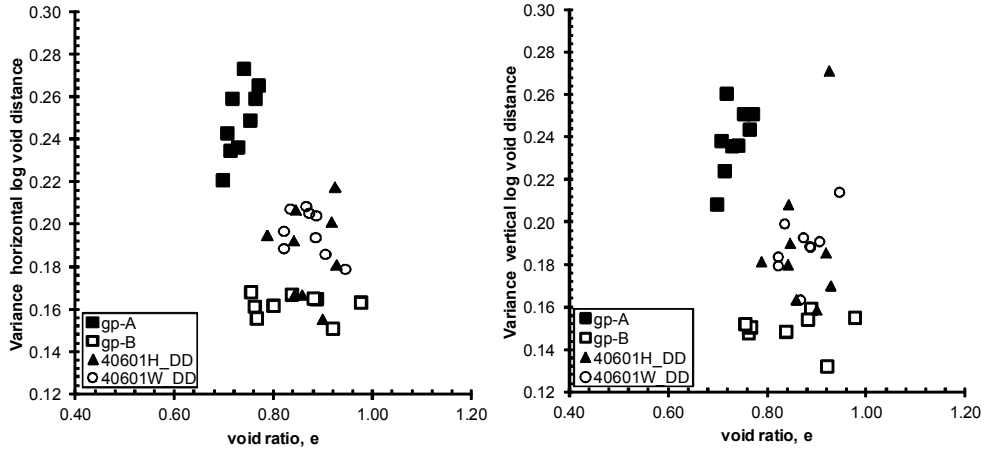

Figure 6-70 Variance log void distance versus void ratio for gp-A, gp-B, 40601H_DD and 40601W_DD (a) horizontal gp-B (b) vertical

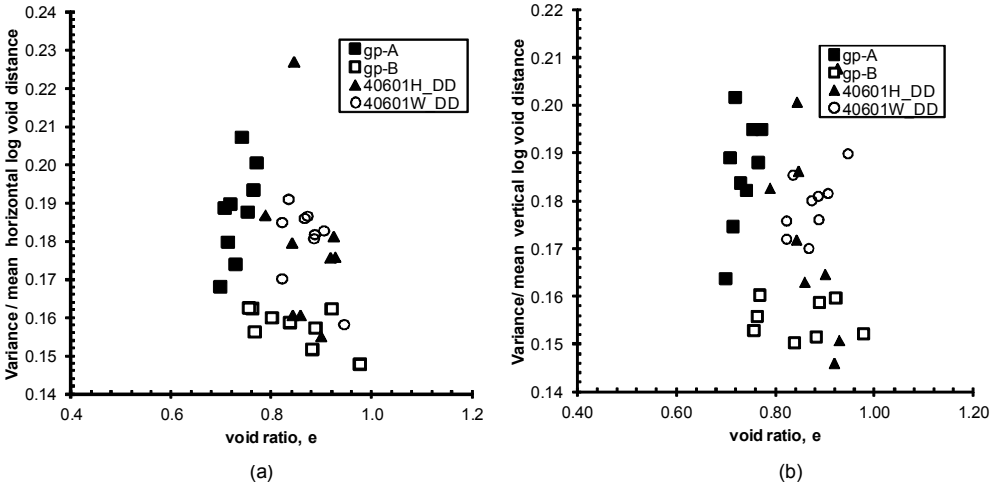

Figure 6-71 Variance to mean ratio log void distance versus void ratio ratio for gp-A, gp-B, 40601H_DD and 40601W_DD (a) horizontal gp-B (b) vertical

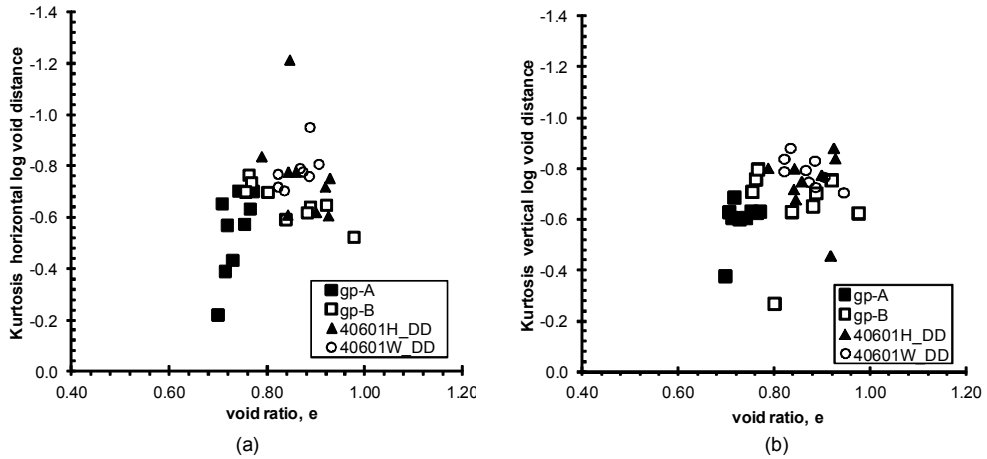

Figure 6-72 Kurtosis to mean ratio log void distance versus void ratio for gp-A, gp-B, 40601H_DD and 40601W_DD (a) horizontal gp-B (b) vertical

Figure 6-72 shows a plot of kurtosis versus void ratio. Generally the values of the kurtosis of undisturbed samples are relatively higher than those of loose dry pluviated samples. Relatively similar variance to mean ratio and kurtosis of undisturbed samples to loose reconstituted samples indicates the undisturbed samples are relatively 'very young' even in terms of engineering time scale. Disturbance due to liquefaction, on-going settlement, frequent aftershocks and groundwater flow may cause the soil to behave as young normally consolidated soil.

6.8 Summary

Microstructure of silty sand and effect of aging, in terms of particle orientation and spatial void distance distribution, can be summarized as follows:

6.8.1 Microstructure of silty sand

Moist tamping deposition on silty sand produces grain fabric which is randomly orientated with a slight bias towards vertical whereas dry pluviation produces fabric that tends to be horizontally orientated. Hence, in terms of grain orientation, moist tamping deposition of silty sand produces grain fabric which is more isotropic than dry pluviated tamped sample.

Undisturbed samples from gel-push sampling show similar anisotropic condition (in term of particle orientation) as dry pluviated samples. This suggests dry pluviated samples represent natural granular fabric more than moist tamped samples.

A general trend also can be observed that sand and 'fines' tend to have similar orientation. In silty sand, sand particles are more orientated than 'fines' both for moist tamped and dry pluviated samples. In addition, in term of degree of orientation, 'fines' of moist tamped samples are less orientated than 'fines' of dry pluviated samples, as r and κ values are close to zero.

Change in degree of orientation with time of 'fines' particles in dry pluviated samples (dense and loose) tends to be larger than for moist tamped samples. This may relate to the tendency that 'fines' in moist tamped samples are less orientated than in dry pluviated samples. This indicates dry pluviated samples tend to have more contacts between 'fines' compared to moist tamped samples. In another words, moist tamped samples have relatively more 'fines' that are just floating inside the voids compared to those in dry pluviated soil.

For 'fines' of dry pluviated silty sand, it appears that the change of r and κ values of dense sample with time (0.092 and 0.06 respectively) is larger than those of loose sample (0.02 and 0.04 respectively). This indicates that in dense silty sand, more 'fines' particles in the void are in contact with other particles (relative to loose samples). This is keeping in with DEM observation that denser polydisperse granular material has fewer floating particles compared to loose material, therefore

greater average coordination number (Kumar *et al.*, 2014). Those contacts where 'fines' are involved are hypothesized to be of the weak force chain, whereas in loose silty sand a relatively large number of fines are floating inside the voids without being in contact to each other.

Spatial void distance analysis shows that moist tamped soil is more isotropic than dry pluviated soil. In addition moist tamped samples have higher variances and variance to mean ratio than dry pluviated samples which indicates that moist tamped samples are initially more clustered than dry pluviated samples. Moist tamped samples also tend to have lower kurtosis values than dry pluviated samples which suggest that moist tamped samples are more structured.

6.8.2 Suggested creep induced aging mechanism of silty sand in this study

Taken all of the evidences from the fabric tests in this study, creep observation (Chapter 4) and observations from some DEM results of others researchers, a mechanism for creep induced aging in silty sand, for dense and loose sample, is hypothesized as follows.

Creep start at weak force chain because particles in this network carry relatively low normal force and higher sliding force compare to sliding resistance. The strong forces align continuously in the direction of principal stress (vertical in this study). Likewise, the weak force changes gradually from horizontal direction to vertical direction i.e. the percentage of weak forces in the horizontal direction is decreasing, although the major fabric orientation is still horizontal. It is likely that some fines particles (15% in this study) are part of weak force chain both in dense and loose samples of silty sand. Separate particle rotation analysis with time suggests that the weak force chains are different for dense and loose samples. In dense samples, relatively more fines are in contact with other grains (S-S and L-S-S-L) compared to loose samples (S-V or L-S-V). Any small disturbance on loading at contact points and time dependent change in strength can lead to particle rotation, sliding, yielding of asperities or local structure collapse. As particles in the network rotate (mainly fines particles in dense soil; sand particles in loose soil), the contact

normal force is more homogenized, the weak force chain gains more sliding resistance due to increase in normal contact force. Particle arching with voids elongated along the major principle stress direction can survive and prevail during creep induce aging so that all forces tend to align in the vertical direction. This particle arching gradually reduces the contact sliding ratios. Overall a more stable columnar structure develops.

7 Conclusions and Future Research

There have been relatively numerous previous laboratory studies on sand aging phenomenon. However the majority of them were conducted on relatively clean sand (fines content <5%) and were performed under isotropic condition. In nature, granular soils with fines content > 5% are not uncommon. Moreover, K_0 condition better reflects the field condition compared to isotropic condition. This study is an attempt to gain further insight on the mechanical aging of silty sand (fines content >12%) by linking change in macro-mechanical properties and change in microstructure (direct observation) during aging.

In terms of the material, as many factors (e.g. plasticity of fines, fines content, grain size composition, angularity and shape) affect silty sand behavior and not all those factors could be investigated during the study period, this study focused on aging of non-plastic silty sand with 15% fines content.

In order to achieve the aim a combination of triaxial tests and fabric tests were conducted. The majority of the triaxial tests were performed to observed creep following K_0 consolidation and its effect on small-strain undrained stiffness i.e. <0.1% shear strain (with few tests on aging effect on cyclic resistance under one way cyclic loading). Change in the microstructure was investigated by preserving the one dimensionally loaded specimens which were aged for different aging times using very low viscosity epoxy resin.

For the triaxial program, a total of 29 triaxial creep tests were performed on reconstituted silty sand. Two consolidation stress paths (K_0 and isotropic consolidation), densities (40% and 70%) and three creep times (one hour, 1 day and 1 week) have been applied to the specimens (moist tamped samples). A few tests were performed also on dry pluviated samples. The tests were conducted at low effective confining stress stresses i.e. σ'_3= 30 – 120 kPa as this is more relevant to most geotechnical aging problems (e.g. time effects on freshly deposited or

disturbed soils such as in the case of hydraulic fills, mine tailings, and post-liquefaction state of soil behavior following earthquakes).

For fabric testing, a total 14 tests were carried out with the same aging times and density as in the triaxial creep tests. The vertical effective stress applied for each fabric test was matched to the K_0 consolidation stage of the triaxial tests accordingly. Two undisturbed samples obtained by gel-push sampling were included to gain some knowledge about the undisturbed microstructure of silty sand. In addition to the fabric test, a spatial void distance analysis, based on Kang's *et al.* (2012) DEM model, was also conducted.

The material in this study is non-plastic, sub angular-angular in grains shape, silty sand with 15% fine content by weight. The mineral composition is mainly quartz or silica ($Si0_2$) with the percentage of element by atomic weight is mainly oxygen (49.6%) and silicon (37.9%). The mean grain size D_{50} is 0.175, coefficient of uniformity C_u of 4.1 and coefficient of curvature C_c of 1.4 and maximum and minimum void ratio e_{max} and e_{min} are 0.973 and 0.565, respectively. K_0 values for confining pressure range from 30-120kPa are 0.39-0.45 (dense) and 0.46-0.52(loose).

7.1 General Conclusions

The findings from this study indicate that creep following K_0 consolidation tends to be greater than creep of isotropically consolidated samples. Likewise K_0 consolidated samples gain more stiffness (at small-strain ranges) than isotropically consolidated samples. This implies that the beneficial time effect (in terms of small strain stiffness) in the field is relatively much larger than those obtained by laboratory studies which usually performed under isotropic condition. This suggested the importance of using of K_0 consolidation in laboratory, otherwise the gain in stiffness due time is underestimated. It was observed in this study that some microstructure changes occurred during aging where particles tended to rotate with time. Changes in the relationship between mean log-distance, variance, variance to mean ratio, and kurtosis with void ratio were observed, which suggested some

structuration with time. Generally the results show that there was a relation, to some degree, between changes in the microstructure over time and changes in macro mechanical properties of non-plastic silty sand. A detailed summary of the results from this experimental study is given below.

7.2 Creep Observations

Creep following K_0 consolidation indicated that the axial strains are in compression. This indicated that in the field condition i.e. K_0, freshly deposited or disturbed soil tends settle with time even though the magnitude is very small to be detected. Creep following K_0 consolidation showed that radial strain tend to expand over time, resulting in a tendency of increasing horizontal stress with time even at low stress used in this study. Volumetrically, creep tends to follow the fundamental behavior of soils when sheared in which dense soils initially contract and then dilate, while loose soil contracts.

Density was found to have significant effect on creep following K_0 condition. This was indicated, for example, by larger axial strain of loose soils compared to dense one (despite lower stress ration and mean effective stress). In addition, higher confining pressure caused greater volumetric and shear creep for both dense and loose samples. This suggests that deeper soils tend to creep and aged more, although later on it was found it is not always the case (see section 7.3), as density plays important role.

One significant finding is that dense dry pluviated sample developed more creep than dense moist tamped sample. This suggests that soil fabric also play significant role in time effects.

7.3 Aging Effects on Undrained Small –Strain Stiffness

Regardless the density, fabric and consolidation stress path this study showed that creep induced aging increased undrained small-strain stiffness, only gain in stiffness which is different.

An interesting finding is that there is a trade off between density and magnitude of confining pressure during K_0 consolidation. Generally higher confining stress increase creep tendency thus enhancing aging, however there is a certain confining pressure where the aging effects become less due to local structure collapse. In this study it was found that loose K_0 consolidated soil at 30kPa confining pressure gained more increase stiffness with time compared to dense soil, whilst at 60kPa and 120kPa, dense soil gains more in stiffness than loose soil.

This study revealed that dry pluviated sample exhibit larger increase of undrained small-strain stiffness compared to moist tamped samples. In addition, this study showed that the number of cycles to trigger cyclic softening and liquefaction for one way cyclic loading increases with the aging duration with the tendency that the aging effect is more pronounced at lower cyclic stress ratios.

7.4 Silty Sand Microstructure and Its Changes during Aging

7.4.1 Initial fabric

This study has provided a quantitave evidence of some silty sand microstructure characteristics, based on reconstituted and undisturbed samples from gel-push.

In terms of particle orientation this study showed that initially moist tamped samples (both dense and loose) are isotropically orientated, as indicated by low r and κ values, whereas dry pluviated samples are anistropically oriented. Undisturbed samples from gel-push sampling show similar anisotropic condition in terms of particle orientation as for dry pluviated samples. Sand particles are more

orientated than 'fines' (particles having minimum feret diameter smaller than 75μm) both in moist tamped and dry pluviated samples.

Overall moist tamped samples, in term of spatial void distance, are initially more clustered and structured than dry pluviated samples. This study also revealed that dense dry pluviated soil is more anisotropic in terms of spatial void distance than dense moist tamped sample. Lastly, loose dry pluviated sample is more isotropic in terms of spatial void distance than dense dry pluviated sample.

7.4.2 Effect of sustained loading with time

Statistical analysis showed that microstructures changes in term of particle orientation and spatial void distance did occurred during aging.

(a) Change in particle orientation

For dense dry pluviated soil (all particles), with respect to particle orientation, κ value increases which indicate reducing anisotropy of particle orientation (more isotropic with time). For dense moist tamped soil (all particles), the κ values tend to be the same. In addition, much of the change in κ values of dense dry pluviated sample appears to occur in the 'fines' whilst for dense moist tamped sample tend to be contributed from sand particles. This is likely because 'fines' particles in moist tamped is less orientated than those in dry pluviated sample. This suggests more contact between 'fines' in dry pluviated sample than those in moist tamped sample.

Long term fabric tests on loose moist tamped samples showed that relative significant change in the κ values were found after 4 months of aging. However 8 months sample no significant changes in κ values compared to 4 months sample.

(b) Change in spatial void distance

Over time, the mean log void distance of dense samples tends to grow whereas for loose sample it reduces. A similar behavior was observed from revisiting the DEM simulations of Kang (2012). This indicates that average

coordination number during creep is decreasing in dense samples (contact separation due to dilation) and is increasing in loose samples due to pore collapse (contact creation) as demonstrated by Kang (2012).

Dense dry pluviated samples show that differences in mean log void distance in the horizontal and vertical directions are decreasing with time. This trend is in contrast with the numerical DEM simulations of Kang (2012) (which were prepared by radius expansion and hence produced isotropic fabric as moist tamped sample).

Variances to mean ratio of void distance for moist tamped samples tend to decrease whereas those of dry pluviated samples tend to increase with time. Increase in variance and variance to mean ratio of dry pluviated samples (and Kang's et al DEM samples) indicates that particles are more clustered together with time. This is because moist tamped samples start already clustered in comparison to dry pluviated samples.

For all particles, kurtosis of void distance tends to be lower with time, which suggests more structured fabric. Direction of structuration, particularly for sand particles, appears to be different between moist tamped and dry pluviated samples. Moist tamped soil tends to experience greater structuration in the vertical direction whereas dry pluviated sample tends to become more structured in the horizontal direction. Revisited Kang et al. DEM sample also showed that kurtosis tends to increase in the vertical direction and decrease in the horizontal direction.

Spatial void distance qualitatively indicated that generally the undisturbed samples are relatively 'very young', even in term of engineering time scale, as indicated by relatively similar variance to mean ratio and kurtosis values of reconstituted sample aged for one hour and one week. Disturbance due to liquefaction, on-going settlement, frequent aftershocks and groundwater flow may cause the soil to behave as young normally consolidated soil.

7.5 Future Research

The current research has provided additional understanding of the mechanical aging mechanisms on silty sand under low stress ratio, which is relevant to such soils aging after disturbance at shallow depth. However there are numbers of areas that need further research to be carried out in terms of experimental and theoretical aspects in order to gain better understanding. The following points outline areas in which future research could be carried out:

7.5.1 Experimental aspect

It would be interesting to investigate triaxial creep and microstructural change of sand with different fines content and different shape of sand and fines. Triaxial creep following liquefaction in triaxial apparatus may also be useful to investigate the time effect on liquefied soil.

Combination with other non destructive methods of examining fabric change such high resolution of X-ray computed tomography may be useful. Use of the photo-elastic method with a mixture of glass rod/beads size to simulate sand and silt mixtures may be used to investigate the change in force distribution over time.

7.5.2 Theoretical aspect

Discrete numerical methods have shown that it is possible to model creep of relatively similar size (Charlie *et al.*, 1992b; Kang *et al.*, 2012; Suarez *et al.*, 2009a; Wang *et al.*, 2014; Wang *et al.*, 2008). In addition discrete numerical methods also have been used to model polydisperse granular material behavior when sheared (Kumar *et al.*, 2014; Madadi *et al.*, 2012; Voivret *et al.*, 2009). Therefore it should be possible to combine these two in order to simulate the behavior of silty sand material during creep. This type of study may continue to shed light on the change in force chain distribution and role of fines during aging.

References

Afifi, S. S., & Woods, R. D. (1971). Long-term Pressure Effects on Shear Modulus of Soils. *Journal of Soil and Foundation Engineering, 97*, 1445-1460.

AGRA. (1995). Draft report on results of blast densification SM-3 site, Quebec. Quebec: AGRA Earth & Environmental, Ltd.

Al-Sanad, H., & Ismael, N. (1996). Effects of Aging on Freshly Deposited or Densified Calcareous Sands. *Transportation Research Record: Journal of the Transportation Research Board, 1547*(-1), 76-81. doi: 10.3141/1547-11

Alim, M. A., Suzuki, K., & Iwashita, K. (2006). *Effect of confining pressure on the strength behavior of granular material simulated by the discrete element method.* Paper presented at the Proceedings of the 10th IAEG International Congress, IAEG2006, Nottingham.

Alshibli, K. A., & El-Saidany, H. A. (2001). Quantifying Void Ratio in Granular Materials Using Voronoi Tessellation. *Journal of Computing in Civil Engineering, Vol. 15*(3), 232-238.

Alshibli, K. A., & Sture, S. (1999). Sand Shear Band Thickness Measurements by Digital Imaging Techniques. *Journal of Computing in Civil Engineering, 13*(2), 103-109.

Anderson, D. G., & Stokoe, K. H. (1978). Shear modulus: a time-dependent soil property *ASTM Special Technical Publication*, 66-90.

Arangelovski, G., & Towhata, I. (2007). Accumulated Deformation of Sand in One-Way Cyclic Loading under Undrained Conditions. In H. Ling, L. Callisto, D. Leshchinsky & J. Koseki (Eds.), *Soil Stress-Strain Behavior: Measurement, Modeling and Analysis* (Vol. 146, pp. 653-662): Springer Netherlands.

Ashford, S. A., Rollins, K. M., & Lane, J. D. (2004). Blast-induced liquefaction for full-scale foundation testing. *Journal of Geotechnical and Geoenvironmental Engineering, 130*(8), 798-806. doi: 10.1061/(asce)1090-0241(2004)130:8(798)

Astedt, B., Weiner, L., & Holm, G. (1992). *Increase in bearing capacity with time for friction piles in silt and sand.* Paper presented at the Nordic Geotech, Meeting.

Atkinson, J., & Sallfors, G. (1991). *Experimental determination of soil properties.* Paper presented at the Proceeding 10th Europena Condeference on Soil Mechanic and Foundation Engineering, Florence, Italy.

Augustesen, A., Liingaard, M., & Lade, P. V. (2004). Evaluation of time-dependent behavior of soils. *International Journal of Geomechanics, 4*(3), 137-156.

Axelsson, G. (2000). *Long-term set-up of driven piles in sand.* Dr.Tech. C806264, Kungliga Tekniska Hogskolan (Sweden), Sweden. Retrieved from http://search.proquest.com.ezproxy.canterbury.ac.nz/docview/304670647?accountid=14499 ProQuest Dissertations & Theses A&I database.

Bahadori, H., Ghalandarzadeh, A., & Towhata, I. (2008). Effect of non plastic silt on the anisotropic behavior of sand. *Soils and Foundations, 48*(4), 531-545.

Barton, M. E. (1993). *Cohesive Sands: The Natural Transition from Sands to Sandstones.* Paper presented at the Proceedings of An International Symposium of the International Society for Soil Mechanics and Foundations (ISSMFE), Geotechnical Engineering of Hard Soils – Soft Rocks, Rotterdam.

Baxter, C. D. P. (1999). *An Experimental Study on the Aging of Sands.* Phd Thesis, Virginia Tech, Blacksburg, VA.

Baxter, C. D. P., & Mitchell, J. K. (2004). Experimental study on the aging of sands. *Journal of Geotechnical and Geoenvironmental Engineering, 130*(10), 1051-1062. doi: 10.1061/(asce)1090-0241(2004)130:10(1051)

Bishop, A. W., and Henkel, D.J. (1962). *The Measurement of Soil Properties in the Triaxial Test*. London: Edward Arnold Ltd.

Bowman, E. T. (2002). *The Aging and Creep of Dense Granular Materials.* PhD Thesis, University of Cambridge, Cambridge, UK.

Bowman, E. T., & Soga, K. (2003). Creep, aging and microstructural change in dense granular materials. *Soils and Foundations, 43*(4), 107-117.

Brown, D. F. (1989). *Evaluation of Tri Star Vibrocompaction Probe.* MAScThesis, The University of British Columbia.

Bullock, P. J., Schmertmann, J. H., McVay, M. C., & Townsend, F. C. (2005). Side shear setup. II: Results from Florida test piles. *Journal of Geotechnical and Geoenvironmental Engineering, 131*(3), 301-310.

Burland, J. B. (1989). "Ninth Laurits Bjerrum Memorial Lecture: "Small is Beautiful" - the stiffness of soils at small strains". *Canadian Geotechnical Journal 26*, 499-516.

Canterbury, E. (2012). Review of liquefction hazard information in eastern Canterbury, including Christchurch City and part of Selwyn, Waimakairi and Hurunui District: Institute of Geological and Nuclear Sciences Limited.

Carraro, J. A. H., & Salgado, R. (2004). Mechanical Behaiour of non-textbook soil. Indiana: Purdue University.

Charlie, W. A., Rwebyogo, M. F., & Doehring, D. O. (1992a). Time-Dependent Cone Penetration Reisitance Due to Blasting. *Journal Geotechnical Engineering, 118*(8), 1200-1215.

Charlie, W. A., Rwebyogo, M. F. J., & Doehring, D. O. (1992b). Time-Dependent Cone Penetration Resistance due to Blasting. *Journal of Geotechnical Engineering, 118*(8), 1200-1215. doi: 10.1061/(asce)0733-9410(1992)118:8(1200)

Chatfield, C. (1983). *Statistic for Technology* (Third ed.). London: Chapman and Hall.

Cho, G., Dodds, J., & Santamarina, J. (2006). Particle Shape Effects on Packing Density, Stiffness, and Strength: Natural and Crushed Sands. *Journal of Geotechnical and Geoenvironmental Engineering, 132*(5), 591-602. doi: doi:10.1061/(ASCE)1090-0241(2006)132:5(591)

Cubrinovski, M. (2013, 29 April-4 May). *Liquefaction-Induced Damage in 2010-2011 Christchurch (New Zealand) Earthquakes.* Paper presented at the 7th International Conference on Case Histories in Geotechnical Engineering, Chicago, Illnois-USA.

Cubrinovski, M., Henderson, D., & Bradley, B. A. (2012). *Liquefaction impact in residentail areas in the 2010-2011 Christchurch earthquakes.* Paper presented at the International Symposium on Enginerring Lessons Learned from Giant earthquake, Tokyo, Japan.

Daramola, O. (1980). Effect of consolidation age on stiffness of sand. *Geotechnique, 30*(2), 213-216.

De Boer, R. B. (1977). On the thermodynamics of Pressure Solution – Interaction

between Chemical and Mechanical Forces. *Geochemica et Cosmochimica Acta, Vol. 41*, 249-256.

De Gennaro, V., Canou, J., Dupla, J. C., & Benahmed, N. (2004). Influence of loading path on the undrained behavior of a medium loose sand. *Canadian Geotechnical Journal, 41*(1), 166-180.

Debats, J.-M., & Sims, M. (1997). *Vibroflotation in Reclamations in Hong Kong.* Paper presented at the Proceedings of the ICE - Ground Improvement.

Dejong, J. T., Fritzges, M. B., & Nusslein, K. (2006). Microbially Induced Cementation to Control Sand Response to Undrained Shear. *Journal of Geotechnical and Geoenvironmental Engineering, 132*(11), 381-1392.

Denisov, N. Y., Dudler, I. V., Durante, V. A., & Khazanov, M. I. (1963). *Studies of changes of strength an compressibility of hydraulically sands in time.* Paper presented at the European Conference on SOil Mechanic and Foundation Engineering, Weisbaden.

di Prisco, C., & Imposimato, S. (1996). Time dependent mechanical behavior of loose sands. *Mechanics of Cohesive-frictional Materials, 1*(1), 45-73. doi: 10.1002/(sici)1099-1484(199601)1:1<45::aid-cfm3>3.0.co;2-o

Dittes, M., & Labuz, J. F. (2002). Field and Laboratory Testing of St. Peter Sandstone. *Journal of Geotechnical and Geoenvironmental Engineering, 128*(5), 372-380.

Dowding, C. H., & Hryciw, R. D. (1986). A Laboratory Study of Blast Densification of Saturated Sand. *Journal of Geotechnical Engineering, 112*(2), 187-199.

Dumas, J. C., & Beaton, N. F. (1988). Discussion of 'Practical prob-lems from surprising soil behavior,' by J. K. Mitchell. *Journal Geotechnical Engineering, 114*(3), 367-368.

Evans, T. M. (2005). *Microscale physical and numerical investigations of shear banding in granular soils.* Ph.D. 3198533, Georgia Institute of Technology, United States -- Georgia. Retrieved from http://search.proquest.com.ezproxy.canterbury.ac.nz/docview/305000175?accountid=14499 ProQuest Dissertations & Theses A&I database.

Fisher, N. I. (1993). *Statistical Analysis of Circular Data*: Cambridge University Press.

Fourie, A. B., & Tshabalala, L. (2005). Initiation of static liquefaction and the role of K0 consolidation. *Canadian Geotechnical Journal, 42*(3), 892-906. doi: 10.1139/t05-026

Frost, J. D., & Park, J. Y. (2003). A Critical Assessment of the Moist Tamping Technique. *Geotechnical Testing Journal, 26*(1).

Fukushima, S., & Tatsuoka, F. (1984). Strength and deformation characteristic of saturated sand at extremely low pressures. *Soils and Foundations, 24*(4), 30-48. doi: 10.3208/sandf1972.24.4_30

Gao, Y., Yeung, C., & Wang, Y. (2011). Aging effects on the stiffness anisotropy in sands. In J. e. al. (Ed.), Geomechanics and Geotechnics: From Micro to Macro. London: Taylor & Francis Group.

Garrison, R. E., Luternauer, J. L., Grill, E. V., Macdonald, R. D., & Murray, J. W. (1969). Early diagenetic Cementation of Recent Sands, Fraser River Delt, British Columbia. *Sedimentology, 12*, 27-46.

GDS. (2000). *GDS Advanced Digital Controller*.

Ghionna, V. N., & Porcino, D. (2006). Liquefaction resistance of undisturbed and reconstituted samples of a natural coarse sand from undrained cyclic triaxial tests. *Journal of Geotechnical and Geoenvironmental Engineering, 132*(2), 194-202.

Gohl, W. B., Howie, J. A., Hawson, H. H., & Diggle, D. (1994). *Field Experience with Blast Densification in an Urban Setting*. Paper presented at the Proceeding 5th U.S. National Conference on Earthquake Engineering, Chicago.

Gu, X., Huang, M., & Qian, J. (2014). DEM investigation on the evolution of microstructure in granular soils under shearing. *Granular Matter, 16*(1), 91-106. doi: 10.1007/s10035-013-0467-z

Gu, X., Yang, J., & Huang, M. (2013). DEM simulations of the small strain stiffness of granular soils: effect of stress ratio. *Granular Matter, 15*(3), 287-298. doi: 10.1007/s10035-013-0407-y

Handford, G. T. (1988). *Densification of an Existing Dam with Explosives*. Paper presented at the Proceeding of Hydraulic Fill Structures Specialty Conference, Fort Collins, Colorado.

Hanzawa, H. (1980). Undrained strength and stability analysis for a quick sand. *Soils and Foundations, 20*(2), 17-29.

Holzer, T. L., & Youd, T. L. (2007). Liquefaction, Ground Oscilation and Soil Deformation at The Wildlife Array,California. *Bulletin of the Seismological Society of America, 97*(3), 961-976.

Howie, J., Shozen, T., & Vaid, Y. (2002). Effect of aging on stiffness of very loose sand. *Canadian Geotechnical Journal, 39*(1), 149-156.

Howie, J. A., & Amini, A. (2004). *Effect of Aging on Shear Wave Velocity by Seismic Cone*. Paper presented at the Proceedings ISC-2 on Geotechnical and Geophysical Site Characterization, Rotterdam.

Hryciw, R. D. (1986). *A Study of the Physical and Chemical Aspects of Blast Densification of Sand*. Ph.D. Thesis, Northwestern University, Evanston.

Human, C. A. (1992). *Time Dependent Property Changes of Freshly Deposited or Densified Sand*. Phd Thesis, University of California.

Ibrahim, A. A., & Kagawa, T. (1991a). Microscopic measurement of sand fabric from cyclic tests causing liquefaction. *Geotechnical Testing Journal, 14*(4), 371-382.

Ibrahim, A. A., & Kagawa, T. (1991b). Microscopic measurement of sand fabric from cyclic tests causing liquefaction. *Geotechnical Testing Journal 14*(4), 371-382.

Ibraim, E., Di Benedetto, H., & Doanh, T. (2009). Time-Dependent Behavior and Static Liquefaction Phenomenon of Sand. *Geotechnical and Geological Engineering, 27*(1), 181-191. doi: 10.1007/s10706-008-9217-0

Imole, O. I., Kumar, N., Magnanimo, V., & Luding, S. (2013). Hydrostatic and Shear Behavior of Frictionless Granular Assemblies under Different Deformation Conditions[dagger]. *Kona, 30*, 84.

Ishihara, K. (1985). *Stability of Natural Deposit during Earthquakes.* Paper presented at the Proceeding 11th of International Conference on Soil Mechanic and Foundation Engineering, Sanfransico, California.

Ishihara, K. (1993). Liquefaction and Flow Failure during Earthquakes. *Geotechnique, Vol. 63*, 351 - 415.

Iwashita, K., & Oda, M. (2000). Micro-deformation mechanism of shear banding process based on modified distinct element method. *Powder Technology, 109*(1–3), 192-205. doi: http://dx.doi.org/10.1016/S0032-5910(99)00236-3

Jang, D. J. (1997). *Quantification of sand structure and its evolution during shear using image analysis.* Phd Thesis, Georgia Insitute of Technology.

Jang, D. J., & Frost, J. D. (1998). *Sand Structres Differences resulting from Specimen Preparation procedures.* Paper presented at the ASCE Specialty Conference on Geotechnical Eartquake Engineering and Soil Dynamic, Seattle.

Jardine, R. J. (1992). Some observations on the kinematic nature of soil stiffness. *Soils and Foundations, 32*(2), 111-124.

Jardine, R. J., Standing, J. R., & Chow, F. C. (2006). Some observations of the effects of time on the capacity of piles driven in sand. *Geotechnique, 56*(4), 227-244. doi: 10.1680/geot.2006.56.4.227

JGS. (2000). *Standards of Japanese Geotechnical Society for Laboratory Shear Test (English Version)*.

Jirathanathaworn, T. (2009). *Development of photoelastic methods towards study of mechanical aging of 2-dimensional granular assemblies.* Ph.D. 3392814, University of Michigan, United States -- Michigan. Retrieved from http://search.proquest.com.ezproxy.canterbury.ac.nz/docview/304627499?accountid=14499 ProQuest Dissertations & Theses A&I database.

Joshi, R. C., Achari, G., Kaniraj, S. R., & Wijeweera, H. (1995). Effect of aging on the penetration resistance of sands. *Canadian Geotechnical Journal, 32*(5), 767-782.

Kang, D. H. (2014, December). [personal communication].

Kang, D. H., Yun, T. S., Lau, Y. M., & Wang, Y. H. (2012). DEM simulation on soil creep and associated evolution of pore characteristics. *Computers and Geotechnics, 39*(0), 98-106. doi: 10.1016/j.compgeo.2011.09.003

Krumbein, W. C. (1941). Measurement and geological significance of shape and roundness of sedimentary particles. *Journal of Sedimentary Petrology, 11*, 64-72.

Kumar, N., Imole, O. I., Magnanimo, V., & Luding, S. (2014). Effects of polydispersity on the micro–macro behavior of granular assemblies under different deformation paths. *Particuology, 12*(0), 64-79. doi: http://dx.doi.org/10.1016/j.partic.2013.07.011

Kuo, C. Y., Frost, J.D., and Chameau, J.-L.A. (1998). Image analysis determination of stereology based fabric tensors. *Geotechnique, 48*(4), 515-525.

Ladd, R. (1978). Preparing Test Specimens Using Undercompaction. *ASTM Geotechnical Testing Journal, Vol. 1*(1), 16-23.

Lade, P. V., & Liu, C. T. (1998). Experimental study of drained creep behavior of sand. *Journal of Engineering Mechanics, 124*(8), 912-920.

Lade, P. V., & Yamamuro, J. A. (1997). Effects of nonplastic fines on static liquefaction of sands. *Canadian Geotechnical Journal/Revue Canadienne de Geotechnique, 34*(6), 918-928. doi: http://dx.doi.org/10.1605/01.301-0005134524.2009

Lade, P. V., Yamamuro, J. A., & Bopp, P. A. (1997). Influence of Time Effects on Instability of Granular Materials. *Computers and Geotechnics, 20*(3-4), 179-193.

Lade, P. V., Yamamuro, J. A., & Liggio Jr, C. D. (2009). *Effects of fines on compressibility and static liquefaction of granular materials.* Paper presented at the 1st International Symposium on Computational Geomechanics, COMGEO I, April 29, 2009 - May 1, 2009, Juan-les-Pins, France.

Lam, C. K. K. (2003). *Effects of Aging Duration, Stress Ratio during Aging and Stress Path on Stress-Strain Behavior of Loose Fraser River Sand.* MASc, Univeristy of British Coulombia.

Leclerc, M. A. (2008). *Evaluation of Gas Dissipation as a Mechanism for Aging of Sands.* Master theses, University of Rhode Island, Kingston, Rhode Island.

Lee, K. M. (2001). Influence of placement method on the cone penetration resistance of hydraulically placed sand fills. *Canadian Geotechnical Journal, 38*(3), 592-607. doi: 10.1139/t01-012

Lloyd, G. (1987). Atomic number and chrystallographic contrast images with the SEM: a review of backscattered electron techniques. *Mineralogical Magazine, 51,* 3-19.

Lupogo, K. (2009). *Effects of fines on the mechanical behavior of sandy soils.* Master, TU Delf.

Madadi, M., Shaebani, M. R., Luding, S., & Wolf, D. E. (2012). Influence of polydispersity on micromechanics of granular materials. *Physical Review E: Statistical, 85*(1 Pt 1), 011301. doi: 10.1103/PhysRevE.85.011301

Mair, R. J. (1993). Developments in geotechnical engineering research: application to tunnels and deep excavations. *Proceedings of the ICE - Civil Engineering, 97*, 27-41. Retrieved from http://www.icevirtuallibrary.com/content/article/10.1680/icien.1993.22378

Masad, E. (1998). *Permeability simulation of reconstructed anisotropic soil medium.* Phd, Washington State University.

McGeary, R. K. (1961). Mechanical Packing of Spherical Particles. *Journal of the American Ceramic Society, 44*(10), 513–522.

Mejia, C. A., Vaid, Y. P., & Negussey, D. (1988, 12-16 September). *Time dependent behavior of sand.* Paper presented at the Proceedings of the International Conference on Rheology and Soil Mechanics, Coventry.

Mesri, G., Feng, T. W., & Benak, J. M. (1990). Postdensification penetration resistance of clean sands. *Journal of Geotechnical Engineering, 116*(7), 1095-1115.

Mesri, G., & Vardhanabhuti, B. (2009). Compression of granular materials. *Canadian Geotechnical Journal, 46*(4), 369-392. doi: 10.1139/T08-123

Miller, H. J. (1994). *Development of instrumentation to study the effects of aging on the small strain behavior of sands.* Phd Thesis, University of New Hampshire.

Mitchell, J. K. (1986). Practical Problems from Surprising Soil Behavior. *Journal of Geotechnical Engineering, 112*(3), 255-289.

Mitchell, J. K. (2008). *Aging of Sand- A Continuing Enigma?* Paper presented at the 6th Int. Conf. on Case Histories in Geotechnical Engineering, Arlington, VA.

Mitchell, J. K., & Soga, K. (2005). *Fundamentals of soil behavior* (3rd ed.): John Wiley& Sons.

Mitchell, J. K., & Solymar, Z. V. (1984). Time-Dependent Strength Gain in Freshly Deposited or Densified Sand. *Journal of Geotechnical Engineering, 110*(11), 1559-1576.

Murashev, A. K. (1997). *Effect of Age-strengthening on Initial Stiffness and Settlements of Soils.* Paper presented at the Proceedings of the Fourteenth International Conference on Soil Mechanics and Foundation Engineering, Hamburg.

Murayama, S., Michihiro, K., & Sakagami, T. (1984). Creep characteristic of sands *Soils and Foundations, 24*(2), 1-15. doi: 10.3208/sandf1972.24.2_1

Narsilio, G. A., Santamarina, J. C., Hebeler, T., & Bachus, R. (2009). Blast densification: Multi-instrumented case history. *Journal of Geotechnical and Geoenvironmental Engineering, 135*(6), 723-734. doi: 10.1061/(asce)gt.1943-5606.0000023

Negussey, D. (1984). *An Experimental Studi of Small Strain Response of Sand.* Phd, University ofBritish Coloumbia

British Coloumbia.

Ng, N., Berner, P., & Covil, C. (1996). The Aging Effects of Sand. *Ground Engineering: AAHK Chek Lak Kok.*

Ng, W. K., Selamat, M. R., & Choong, K. K. (2010). Soil/pile set-up effects on driven pile in Malaysian soil. *Electronic Journal of Geotechnical Engineering, 15 A*, 1-12.

Oda, M. (1972). Deformation mechanism of sands in triaxial compression Tests. *Soils and Foundations, 12*(4), 45-63.

Oda, M. (1976). Fabrics and their effects on the deformation behavior of sand: Department of Foundation Engineering, Faculty of Engineering, Saitama University, Japan.

Okochi, Y., & Tatsuoka, F. (1984). Some factors affecting Ko-values of sand measured in triaxial cell. *Soils and Foundations, 24*(3), 52-68.

Park, J. Y. (1999). *A Critical Assessment of Moist Tamping and Its Effect on the Initial and Evolving Structure of Dilatant Triaxial Specimens.* Phd Thesis, Georgia Institute of Technology, Atlanta.

Petraborg, G. G. (1987). *A review of time-dependent changes in the strength characteristics of cohesionless soils.* MS Thesis, University of California.

Radjai, F., Jean, M., Moreau, J.-J., & Roux, S. (1996). Force Distributions in Dense Two-Dimensional Granular Systems. *Physical Review Letters, 77*(2), 274-277.

Rees, S. (2010). *Effect of fines on undrained behavior of Christchurch Soils.* Phd Thesis, University of Canterbury.

Rees, S. (n.d.). *Introduction to triaxial testing - Part 3.pdf.* Retrieved from http://www.gdsinstruments.com/__assets__/pagepdf/0000-1/Introduction to triaxial testing - Part 3.pdf

Richart, F. E., & Yu , P. (1984). Stress Ratio Effects on Shear Modulus of Dry Sands. *Journal of Geotechnical Engineering, 110*(3), 331-345.

Rogers, B. T., Graham, J. A., & Jefferies, M. G. (1990). *Compaction of Hydraulic Fill Sand in Molikpaq Core.* Paper presented at the Proceeding 43rd Conference Canadienne de Geotechnique.

Rollins, K. M., & Anderson, J. K. S. (2008). *Cone Penetration Resistance Variation with Time after Blast Liquefaction Testing.* Paper presented at the Geotechnical Earthquake Engineering and Soil Dynamics, GSP 181, (D. Zeng, M.T. Manzari, and D.R. Hiltunen, eds.).

Saftner, D. A. (2009). *Sand Aging: Time Dependent Strength Gain in Recently Disturbed Sand.* Paper presented at the Proceedings of the 4th International Young Geotechnical Engineer's Conference, Alexandria, Egypt.

Saftner, D. A. (2011a). *Time-Dependent Strength Gain in Recently Disturbed Granular Materials.* Ph.D. 3476755, University of Michigan, United States -- Michigan. ProQuest Dissertations & Theses A&I database.

Saftner, D. A. (2011b). *Time Dependent Change in Recently Disturebed Granular Materials.* Phd Theses, University of Michigan.

Salgado, R., Bandini, P., & Karim, A. (2000). Shear Strength and Stiffness of Silty Sand. *Journal of Geotechnical and Geoenvironmental Engineering, 126*(5), 451-462. doi: 10.1061/(asce)1090-0241(2000)126:5(451)

Sawada, S.-i. (2007). Effect of Loading Condition on Liqefaction Strength of Saturated Sand. In H. Ling, L. Callisto, D. Leshchinsky & J. Koseki (Eds.),

Soil Stress-Strain Behavior: Measurement, Modeling and Analysis (Vol. 146, pp. 637-644): Springer Netherlands.

Schmertmann, J. H. (1991). The Mechanical Aging of Soils. *Journal of Geotechnical Engineering, 117*(9), 1288-1330.

Schmertmann, J. H., Baker, F., Gupta, R., & Kessler, K. (1986a). CPT/DMT QC of Ground Modification at a Power Plant. *Geotechnical Special Publication 6*, 985-1001.

Schmertmann, J. H., Baker, W., Gupta, R., & Kessler, K. (1986b). *CPT/DMT QC of Ground Modification at a Power Plant.* Paper presented at the Use of In situ Tests in Geotechnical Engineering, ASTM STP No. 6.

Seed, H. B. (1979). Soil liquefaction and cyclic mobility evaluation for level ground during earthquakes. *Journal of the Geotechnical Engineering Division, 105(GT2)*, 201-255.

Seed, H. B., & Idriss, I. M. (1970). Soil moduli and damping factors for dynmic response analysis (Vol. Report 70-10). Berkeley,California: EERC.

Sheldon, H. A., & Wheeler, J. (2003). Influence of Pore Fluid Chemistry on the state of Stress in Sedimentary Basins. *Geological Society of America, Vol. 31*(1), 59-62.

Sheldon, H. A., Wheeler, J., Worden, R. H., & Cheadle, M. J. (2003). An Analysis of the Roles of Stress, Temperature, and pH in Chemical compaction of Sandstones. *Journal of Sedimentary Research, Vol. 73*(1), 64-71.

Shozen, T. (2001). *Deformation under the constant stress state and its effect on stress-strain behavior of Fraser River Sand.* Master of Applied Science, University of British Coloumbia.

Sitharam, T., & Dash, H. (2008). Effect of Non-Plastic Fines on Cyclic Behavior of Sandy Soils *GeoCongress 2008 : Geosustainability and Geohazard Mitigation* (pp. 319-326).

Soga, K., Bowman, E. T., & Drummond, W. (2001). Particle shape characterisation using Fourier descriptor analysis. *Géotechnique, 51*(6), 545-554. doi: 10.1680/geot.2001.51.6.545

Suarez, N. R., Brandon, L., & Mitchell, J. K. (2009a). Discrete Element Modeling of Aging in Granular Media. In H. I. Ling, A. Smyth & R. Betti (Eds.), Poro-Mechanics IV (pp. 335-340). Lancaster: DEStech Publications, Inc.

Suarez, N. R., Brandon, T. L., & Mitchell, J. K. (2009b). *Discrete Element Modeling of Aging in Granular Media*. Paper presented at the Poro-

Mechanics IV:Proceedings of the Fourth Biot Conference on Poromechanics, New York. <Go to ISI>://WOS:000270143600047

Sympatech GmBH. (2013) Retrieved from http://www.sympatec.com/EN/Science/Characterisation/05_ParticleShape.html

Tatsuoka, F., & Hoque, E. (2004). Effects of stress ratio on small-strain stiffness during triaxial shearing. *Géotechnique, 54*(7), 429-439. doi: 10.1680/geot.2004.54.7.429

Tatsuoka, F., Santucci de Magistris, F., Hayano, K., Momoya, Y., & Koseki, J. (2000). *Some new aspects of time effects on the stress–strain behavior of stiff geomaterials. The geotechnics of hard soils–soft rocks.* Paper presented at the Procceding of Second International Conference on Pre-Failure Deformation Characteristic, Napoli.

Taylor, M. L., Cubrinovski, M., Bradley, B. A., & Horikoshi, K. (2013, 20-23 Nov). *The undrained cyclic strength of undisturbed and reconstituted Christchurch sands.* Paper presented at the 19th New Zealand Geotechnical Society Symposium, Queenstown, New Zealand.

Taylor, M. L., Cubrinovski, M., & Haycock, I. (2012). *Application of new 'Gel-push' sampling procedure to obtain high quality laboratory test data for advanced geotechnical analyses*.

Terzaghi, K. (1934). Large Retaining Wall Test. *Engineering News Record*, 136-140.

Terzhagi, K. (1956). *Varieties of submarine slope failures.* Paper presented at the Proceeding of 8thTexas Conference on Soil Mechanic and Foundation Engineering.

Thevanayagam, S., & Mohan, S. (2000). Intergranular state variables and stress&strain behavior of silty sands. *Géotechnique, 50*, 1-23.

Thomann, T. G. (1990). *Stiffness and strength changes in cohesionless soils due to stress history and dynamic disturbance.* Phd Phd, University of Michigan.

Troncoso, J., Ishihara, K., & Verdugo, R. (1988, August 2-9). *Aging effect on cyclic shear strength of tailing materials.* Paper presented at the Proc. IX World Conference on Earthquake Engineering, Tokyo-Kyoto.

Vaid, Y. P., Sivathayalan, S., & Stedman, D. (1999). Influence of Specimen-Reconstituting Method on the Undrained Response of Sand. *Geotechnical Testing Journal, 22*(3), 187-195.

Vlahinić, I., Andò, E., Viggiani, G., & Andrade, J. (2014). Towards a more accurate characterization of granular media: extracting quantitative descriptors from tomographic images. *Granular Matter, 16*(1), 9-21. doi: 10.1007/s10035-013-0460-6

Voivret, C., Radjaï, F., Delenne, J. Y., & El Youssoufi, M. S. (2009). Multiscale Force Networks in Highly Polydisperse Granular Media. *Physical Review Letters, 102*(17), 178001.

Wadell, H. (1932). Volume, shape and roundness of rock particles. *Journal of Geology, 40*, 443-451.

Wanatowski, D., & Chu, J. (2008). Effect of specimen preparation method on the stress-strain behavior of sand in plane-strain compression tests. *Geotechnical Testing Journal, 31*(4), 308-320.

Wang, Y.-H., & Gao, Y. (2014). Examining the behavior and mechanisms of structuration in sand under the \hbox {K}_{0} condition. *Granular Matter, 16*(1), 55-68. doi: 10.1007/s10035-013-0457-1

Wang, Y.-H., Lau, Y., & Gao, Y. (2014). Examining the mechanisms of sand creep using DEM simulations. *Granular Matter, 16*(5), 733-750. doi: 10.1007/s10035-014-0514-4

Wang, Y.-H., & Tsui, K.-Y. (2009). Experimental Characterization of Dynamic Property Changes in Aged Sands. *Journal of Geotechnical and Geoenvironmental Engineering, 135*(2), 259-270. doi: 10.1061/(asce)1090-0241(2009)135:2(259)

Wang, Y. H., & Tsui, K. Y. (2008). *Density Effects on the Aging Behavior of Sands and the Anisotropy of Aging-induced Stiffness Increases*. Paper presented at the Proceedings of the Geotechnical Earthquake Engineering and Soil Dynamics(GEESD) IV Sacramento, C.A.

Wang, Y. H., Xu, D., & Tsui, K. Y. (2008). Discrete element modeling of contact creep and aging in sand. *Journal of Geotechnical and Geoenvironmental Engineering, 134*(9), 1407-1411. doi: 10.1061/(asce)1090-0241(2008)134:9(1407)

Weyl, P. K. (1959). Pressure Solution and the Force of Crystallization – A Phenomenological Theory. *Journal of Geophysical Research, Vol. 64,*(11), 2001-2025.

Wilding, L. P., Smeck, N. E., & Dress, L. R. (1977). Silica in Soils: Quartz, Cristobalite, tridymite, and Opal *in Minerals in Soil Environments* (pp. 471-552). Madison, Wisc: Soil Science Society of America.

Willmarth, W. W., Hawk, N. E., & Harvey, R. L. (1964). Steady and Unsteady Motions and Wakes of Freely Falling Disks. *The Physic of Fluid, 7*(2).

Witchman, T. (2005). *Explicit accumulation model for noncohesive soils under cyclic loading.* Phd Thesis, Ruhr-University Bochum.

Wood, F. M., Yamamuro, J. A., & Lade, P. V. (2008). Effect of depositional method on the undrained response of silty sand.(Technical report). *Canadian Geotechnical Journal, 45*(11), 1525(1513).

Yamamuro, J. A., & Covert, K. M. (2001). Monotonic and cyclic liquefaction of very loose sands with high silt content. *Journal of Geotechnical and Geoenvironmental, Vol. 127*, 3124-3324.

Yamamuro, J. A., & Lade, P. V. (1997). Static liquefaction of very loose sands. *Canadian Geotechnical Journal/Revue Canadienne de Geotechnique, 34*(6), 905-917. doi: http://dx.doi.org/10.1139/cgj-34-6-905

Yamamuro, J. A., & Lade, P. V. (2011). Evaluation of static liquefaction potential of silty sand slopes. *Canadian Geotechnical Journal, 48*(2), 247-264. doi: 10.1139/T10-063

Yamamuro, J. A., & Wood, F. M. (2004). Effect of depositional method on the undrained behavior and microstructure of sand with silt. *Soil Dynamics and Earthquake Engineering, 24*(9-10), 751-760. doi: 10.1016/j.soildyn.2004.06.004

Yamamuro, J. A., Wood, F. M., & Lade, P. V. (2008). Effect of depositional method on the microstructure of silty sand. *Canadian Geotechnical Journal, 45*(11), 1538-1555. doi: 10.1139/t08-080

Yan, G., Chunkit, Y., & Yuhsing, W. (2010). Aging effects on the stiffness anisotropy in sands *Geomechanics and Geotechnics* (pp. 519-523): CRC Press.

Yang, J., & Wei, L. M. (2012). Collapse of loose sand with the addition of fines: the role of particle shape. [Article]. *Geotechnique, 62*(12), 1111-1125.

Yang, S. (2004). *Characterization of properties of sand-silty mixture.* Norwegian University of Science and Technology

Yimsiri, S., & Soga, K. (2010). Dem analysis of soil fabric effects on behavior of sand. *Geotechnique, 60*(6), 483-495.

Yusa, M., & Bowman, E. T. (2013). *Quantification of time-dependent microstructural change of a silty sand under load.* Paper presented at the Powder and Grain 2013, Sydney.

Zhang, Y., Xue, Y. Q., Wue, J. C., & Shi, X. Q. (2006). Creep model of saturated sands in oedometer tests. *Geotechnical Special Publication, 150*, 328-335.

APPENDIX A
Silica 100g Technical Data

FEATURES

LANG LANG, VICTORIA

Sibelco's Silica Flour 100G is produced from chemically treated and water washed high purity silica sand. The milling process ensures minimal contamination, resulting in high purity silica flour. Silica 100G is an inherently inert white product, with low moisture.

Silica 100G is tested and controlled to rigorous standards which ensure consistent chemical and physical properties resulting in predictable and repeatable performance. Sibelco Australia actively manages a Quality Management System certified to ISO9001:2008.

Sibelco's comprehensive range of Silica flour is used in a wide range of industrial applications. Silica 100G typically finds use in applications such as adhesives, frits, and flooring. The following typical properties may help you to determine the suitability of the product to best suit your application.

CHEMICAL AND ANALYTICAL DATA

Mean Values. These Do Not Represent A Specification

Mean Percent by Weight		(UAL 8.5)	
Silica	(SiO_2)		**99.8**
Alumina	(Al_2O_3)		**0.09**
Ferric Oxide	(Fe_2O_3)		**0.02**
Titania	(TiO_2)		**0.02**
Lime	(CaO)		**<0.1**
Loss on Ignition	(1000°C)		**0.1**
Oil Absorption	(mls/100g)	UAL2.9(d)	**22**
Specific Gravity		UAL2.13(b)	**2.66**
pH	(20% Slurry)	UAL2.11	**6.4**
Bulk Density (compacted)	(g/cm^3)	UAL2.10(a)	**1.8**
Surface Area	(m^2/g)	UAL2.8(c)	**0.5**
Powder Brightness	(R457nm)	UAL2.1(d)	**72**
Powder CIE Color	L*	UAL2.1(e)	**90.38**
	a*		**+0.97**
	b*		**+4.33**

PARTICLE SIZE ANALYSIS

Mean Values. These Do Not Represent A Specification

	MICRONS	
% Finer	212	**96.6**
	150	**95.2**
	90	**83.7**
	75	**78.1**
	53	**66.9**
	45	**61.7**
	20	**24.6**
	10	**19.1**
	2	**5.5**
	1	**3.5**

ORDERING INFORMATION

Shipping Point: Lang Lang, Victoria
Availability: 25 kg Multi-Wall Paper Bags / Bulk Bags/ Bulk Tanker

DISCLAIMER: Ranges and values of trial sample testing or on a Technical Information Sheet are typical or expected ranges and are not guaranteed ranges. You must satisfy yourself that the product is suitable for the purpose for which you intend to use it. Sibelco makes no representations as to suitability, fitness or merchantability.

HAZARD WARNING: Prolonged inhalation can cause delayed lung injury including silicosis, a progressive, disabling and sometimes fatal lung disease. In accordance with the National Occupational Health and Safety Commission's "Approved Criteria for Classifying Hazardous Substances", Free Crystalline Silica (Quartz) has been classified as a Hazardous Substance. This product contains Free Crystalline Silica (Quartz). The International Agency for Research on Cancer has determined that Free Crystalline Silica inhaled from occupational sources can cause cancer in humans. Risk of injury is dependent on the duration and level of exposure. The risk of lung disease is increased if smoking is combined with silica respiration.
Avoid creating dust when handling, using or storing the product. Use only with adequate ventilation to keep exposure low. Do not use as a dry abrasive blasting agent. Undertake health and safety risk assessments on safe methods of handling and use appropriate to your workplace.
To prevent inhalation of airborne dust, wear respiratory protection in accordance with Australian Standard AS1715 and AS1716. To prevent potential irritation to eyes, wear eye protection in accordance with Australian Standard AS1337.
Please refer to the relevant Sibelco Australia Limited Material Safety Data Sheet (MSDS) for health hazard information before opening or using this product and take care when disposing of the empty bag/container (as it may contain product residue). If you do not have an MSDS, please ring the following ACOHS 24 hour emergency phone number: 1800 638 556 and you will be sent one

FOR PRODUCT INFORMATION AND CUSTOMER SERVICE

AUST: Adelaide +61 8 8240 8200 Brisbane +61 7 3909 4500 Melbourne +61 3 9586 5400
Sydney +61 2 9637 7066 Perth +61 8 9362 1411 Newcastle +61 2 4028 9300
NZ Auckland +64 9 914 7010 Visit our website www.sibelco.com.au

SIBELCO AUSTRALIA

ACN 000 971 844

APPENDIX B

Potential errors for triaxial test and preliminary local measurement performance and repeatability

B.1 Potential strains and stresses error for triaxial test

Transducer	Resolution	Accuracy	Potential error	
Load cell (2kN)	0.2 N	2 N	2 N	0.1 %
Cell pressure(2000kPa)	0.2 kPa	2 kPa	2 kPa	0.1 %
Back pressure(2000kPa)	0.2 kPa	2 kPa	2 kPa	0.1 %
Pore presssure(2000kPa	0.2 kPa	2 kPa	2 kPa	0.1 %

Measurement	Strain	Resolution	Accuracy	Potential error=accuracy+resolution	
Local	ε_a	0.0006 mm	0.001 mm	0.002 mm	0.004 %
	ε_r	0.0006 mm	0.001 mm	0.002 mm	0.006 %
	ε_s				0.010 %
	ε_v				0.02 %
External	ε_{ae}	0.01 mm	0.1 mm	0.1 mm	0.1 %
	ε_{re}				0.06 %
	ε_{se}				0.1 %
	ε_{ve}	1 mm^3	0.1%ΔV+20mm^3		0.01 %

Note
local axial strain is realtive to 65mm gauge length
local radail strain is realtive to 50mm sample diameter
External axial strain is relative to 100m sample height
External volumetric strain is relative to volume of 100m sample height and 50 in diameter
ΔV= volume change

B.2 Local performance

Examples of measured local axial and radial strain during creep of a K_0 consolidated dense sample are demonstrated in Figure B-1. Overview one hour creep is taken as an example, as it gives clearer pictures about the variation in measurements compared to a longer time. As can be seen from Figure B-1 (a), both local and external axial strains show the same trend i.e. in compression. The axial strain measured externally is ≈57% greater than the axial strain measured locally. This is likely due to sample bedding error. Bowman (2002) found the same trend for dense clean sand and reported that typically external measurement is 25% to

50% greater than local measurement during creep. Larger differences between external and local in this study compared to Bowman's findings may be due to different material (silty sand compared to clean sand). Local and external radial strain show that during one hour creep the change in diameter of the sample is very small i.e. less than 0.01%. Interestingly, a different trend was found for local and external radial strains, as shown in Figure 1 (b). External radial strain indicates that the sample is already expanding across the whole cylindrical body of the sample. Local strain, on the other hand shows that there is no clear indication yet of the direction of radial strain because there is no significant change in the diameter of the sample ($\varepsilon_r \approx 0$). It should be noted that local radial LVDT measure strain at discrete point only i.e. middle height. Therefore some localized factors such as variation in local void ratio (e.g. Frost and Jang, 2000) may have more pronounced effects.

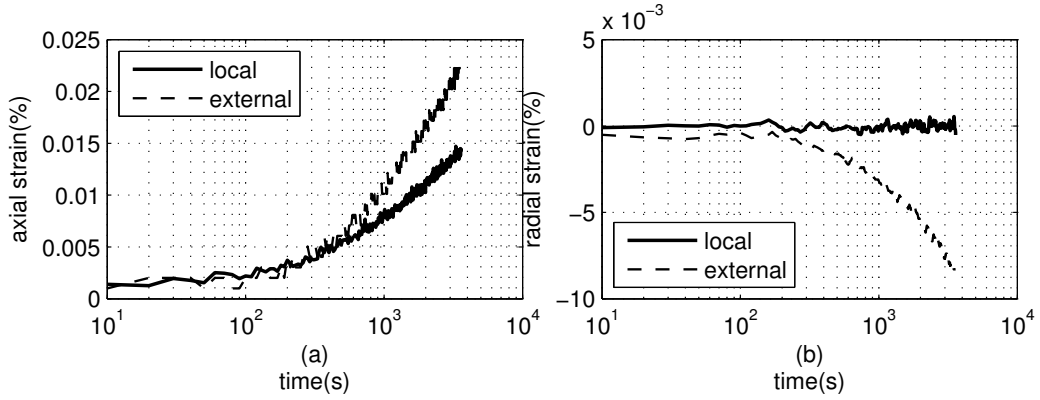

Figure 1 Initial overview of local measurements during creep

Example stress-strain relationships during undrained shear obtained from external and local LVDT are presented in Figure B-2. As can be seen generally, the local system results in a stiffer response, which is expected because it measures the response at the middle of the sample which is relatively free from the sample bedding effect. In the small strain range (less than 0.1% strain), measured local strains are about 20% greater than externally measured ones. This number is smaller than previous studies e.g. Sharma and Fahey (2003), who reported that local strains are up to 2-3 times higher external one (isotropic consolidated sample). One

possible explanation is because the sample in the figure was K_0 consolidated hence seating and bedding errors are less likely here than for isotropically consolidated samples.

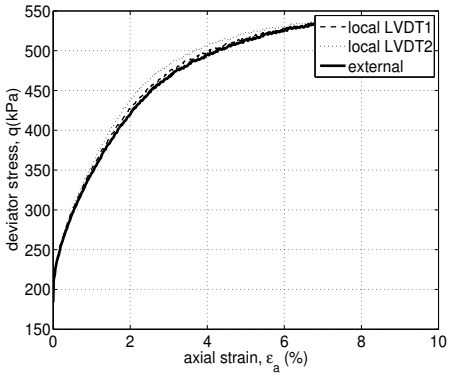

Figure B-2 Initial overview of local measurement during shear

B.3 Repeatability

As the final consolidation pressure cannot be controlled during K_0 consolidation, in order to compare specimens for different aging time, it is necessary that final consolidation pressures between the samples are comparable. Therefore the K_0 consolidation stage can be used as a repeatability check of the sample preparation. Considering the resolution of the transducers, for this study the variation of mean consolidation pressure of ± 2kPa and K_0 ± 0.05 are considered to be adequate.

Figure B-3 presents an example of the relationship between K_0 and final effective consolidation pressure for different aging time. The final consolidation pressure for one hour, one day and one week on the figure are 180.0, 179.9 and 180.8kPa respectively whilst K_0 values are 0.39, 0.39 and 0.39 respectively. Those numbers indicate that sample preparation and stress path were relatively repeatable.

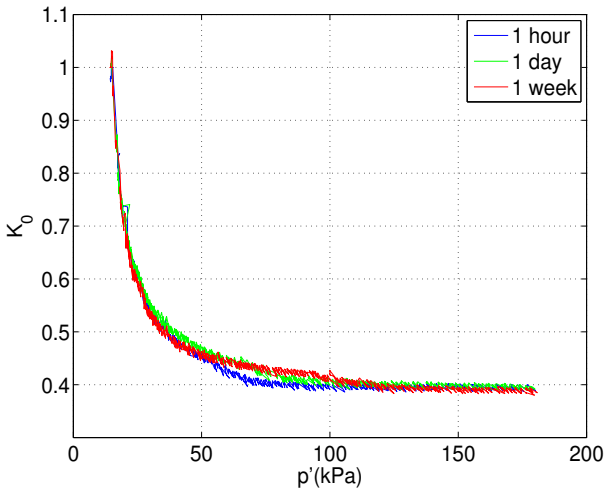

Figure B-3 K_0 consolidation as repeatability check

APPENDIX C
Stability of stress during creep

Figure C-1 presents an example of the stability of the measurement of cell pressure, pore pressure and deviator stress for one week creep time for a dense sample used in this study. Pore pressure, back pressure and cell pressure tend to vary more than deviator stress. This is likely because GDS controllers use water to measure stress. Water inside the controller and their tubes is more likely to be sensitive to temperature variation compared to the load cell. Overall the stresses variations, up to one week, are still acceptable and within the 'dead band' of the GDS controller i.e. 2kPa (Rees, personal communication, 2011).

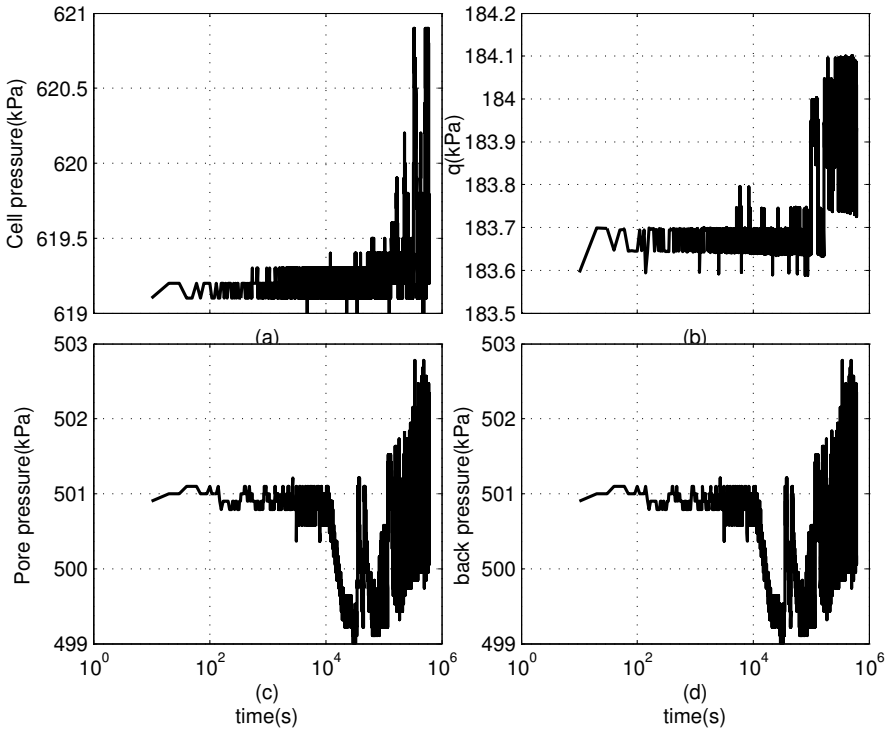

Figure C-1 Stresses stability during creep

APPENDIX D
Triaxial creep test (Dense K_0 consolidated)

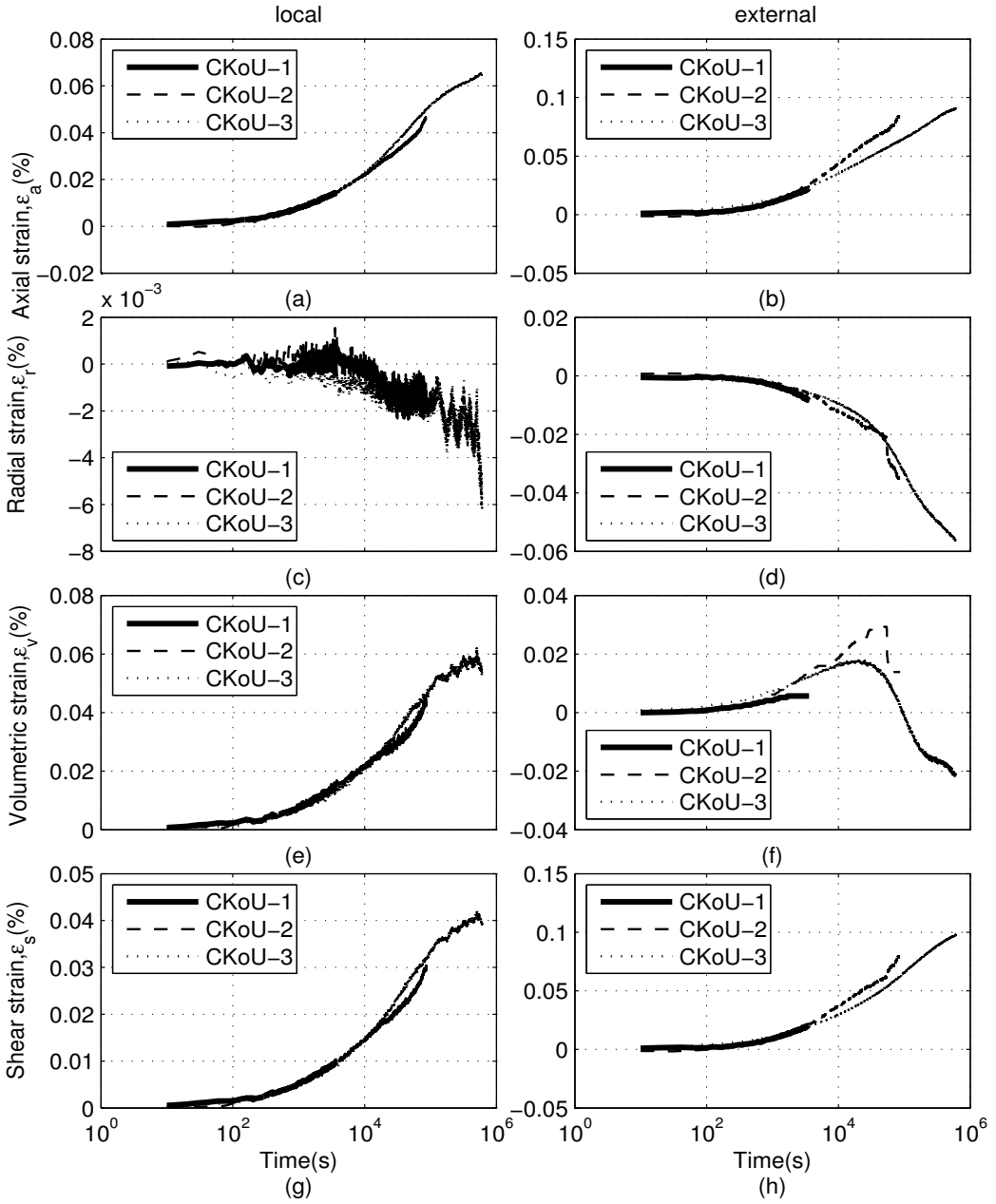

Figure D-1 strains development during creep of dense samples at 120 kPa confining pressure (CKoU-1, CKoU-2 and CKoU-3) for 1 hour, 1 day and 1 week of creep time, respectively

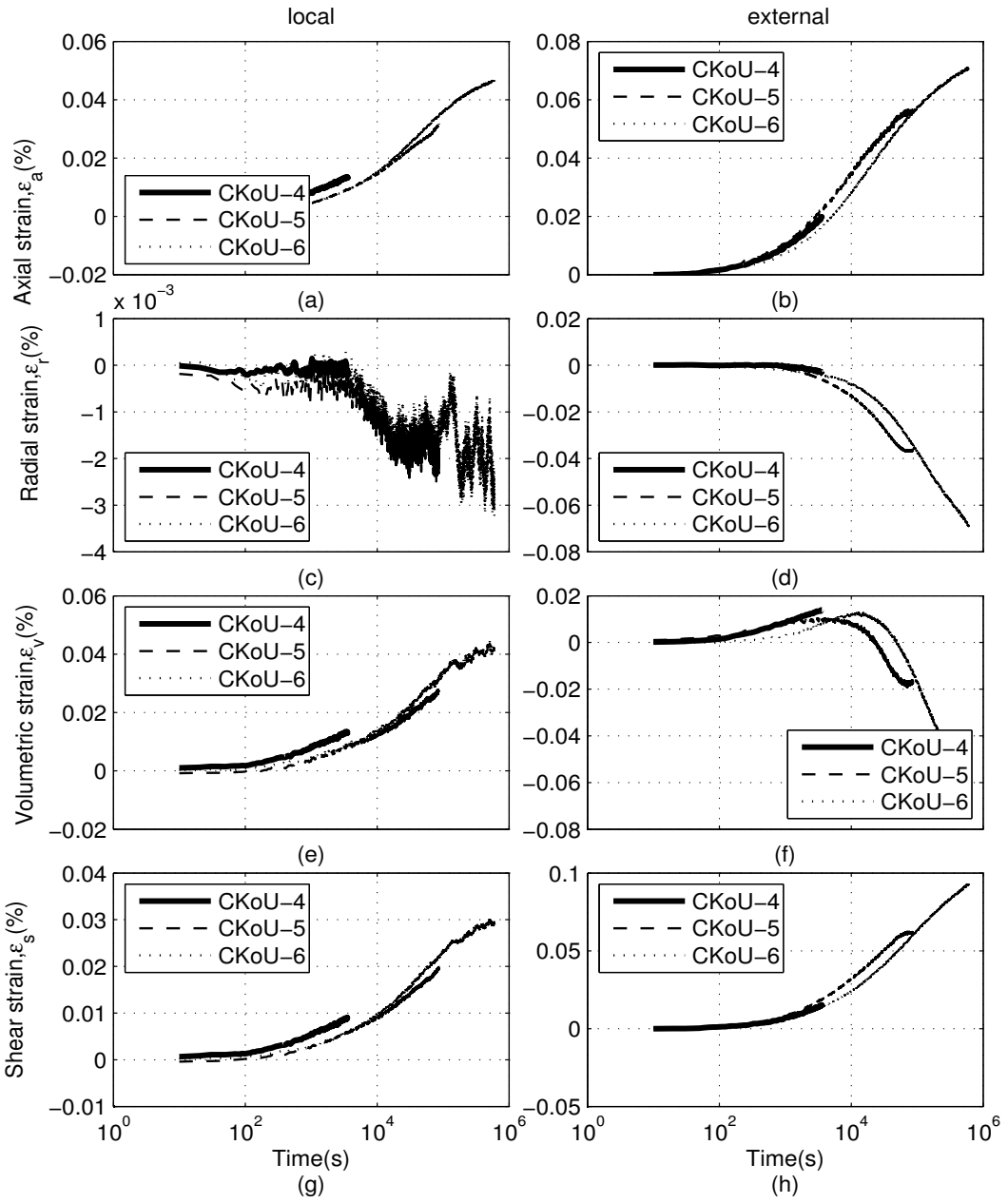

Figure D-2 strains development during creep of dense samples at 60 kPa confining pressure (CKoU-4, CKoU-5 and CKoU-6) for 1 hour, 1 day and 1 week of creep time, respectively

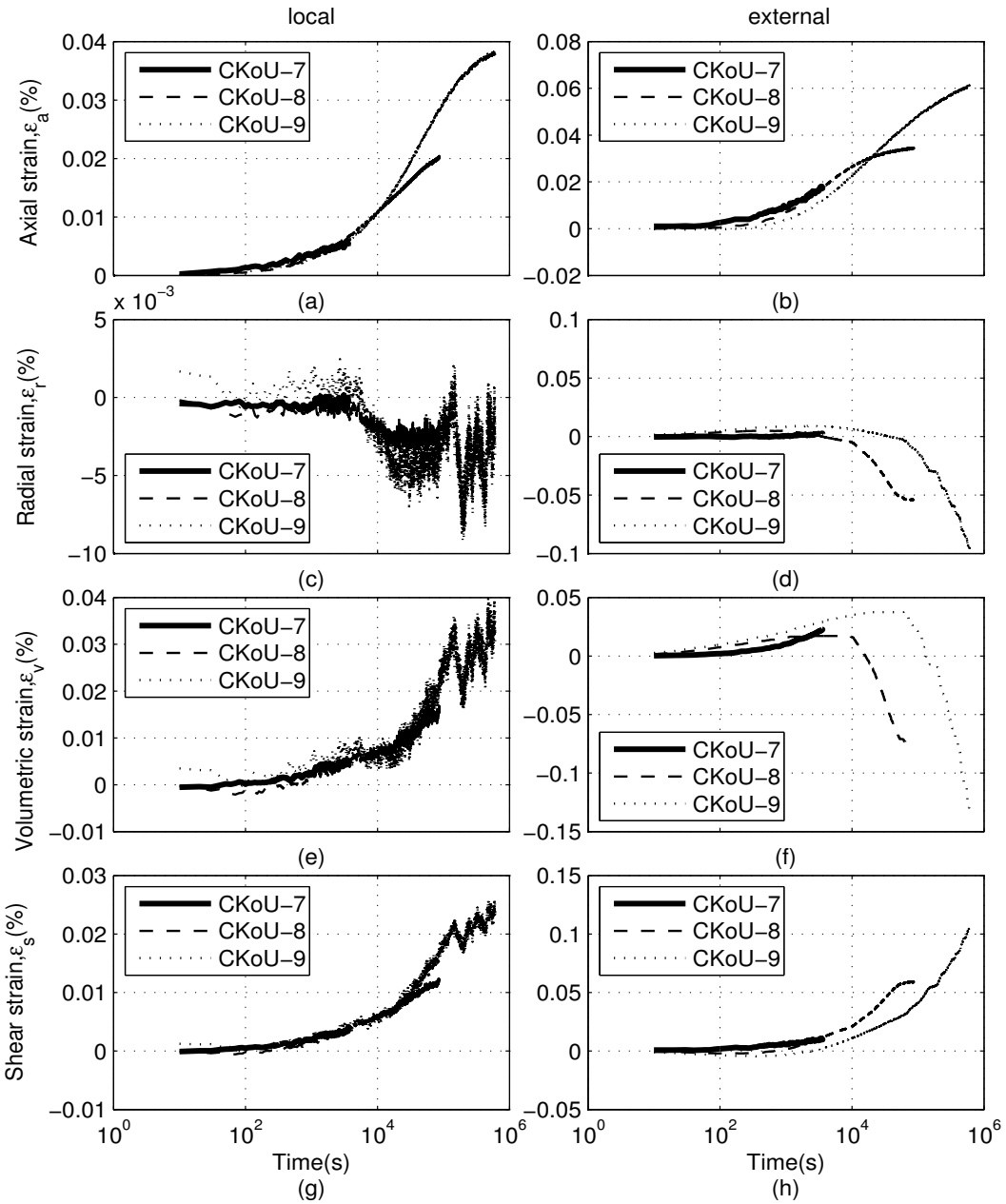

Figure D-3 strains development during creep of dense samples at 30 kPa confining pressure (CKoU-7, CKoU-8 and CKoU-9) for 1 hour, 1 day and 1 week of creep time, respectively

APPENDIX E
Triaxial creep test (Loose K_0 consolidated)

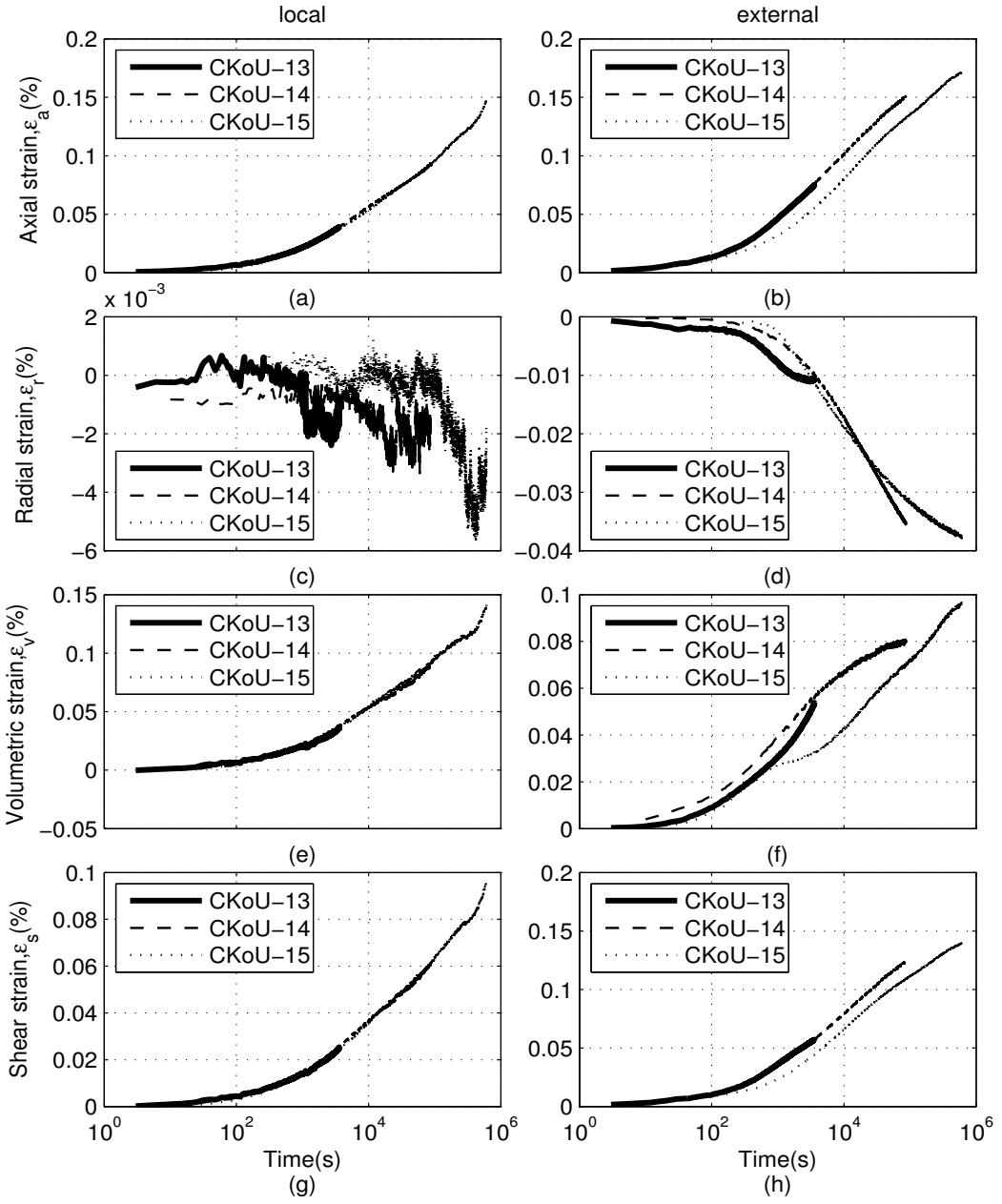

Figure E-1 strains development during creep of loose samples at 120 kPa confining pressure (CKoU-13, CKoU-14 and CKoU-15) for 1 hour, 1 day and 1 week of creep time, respectively

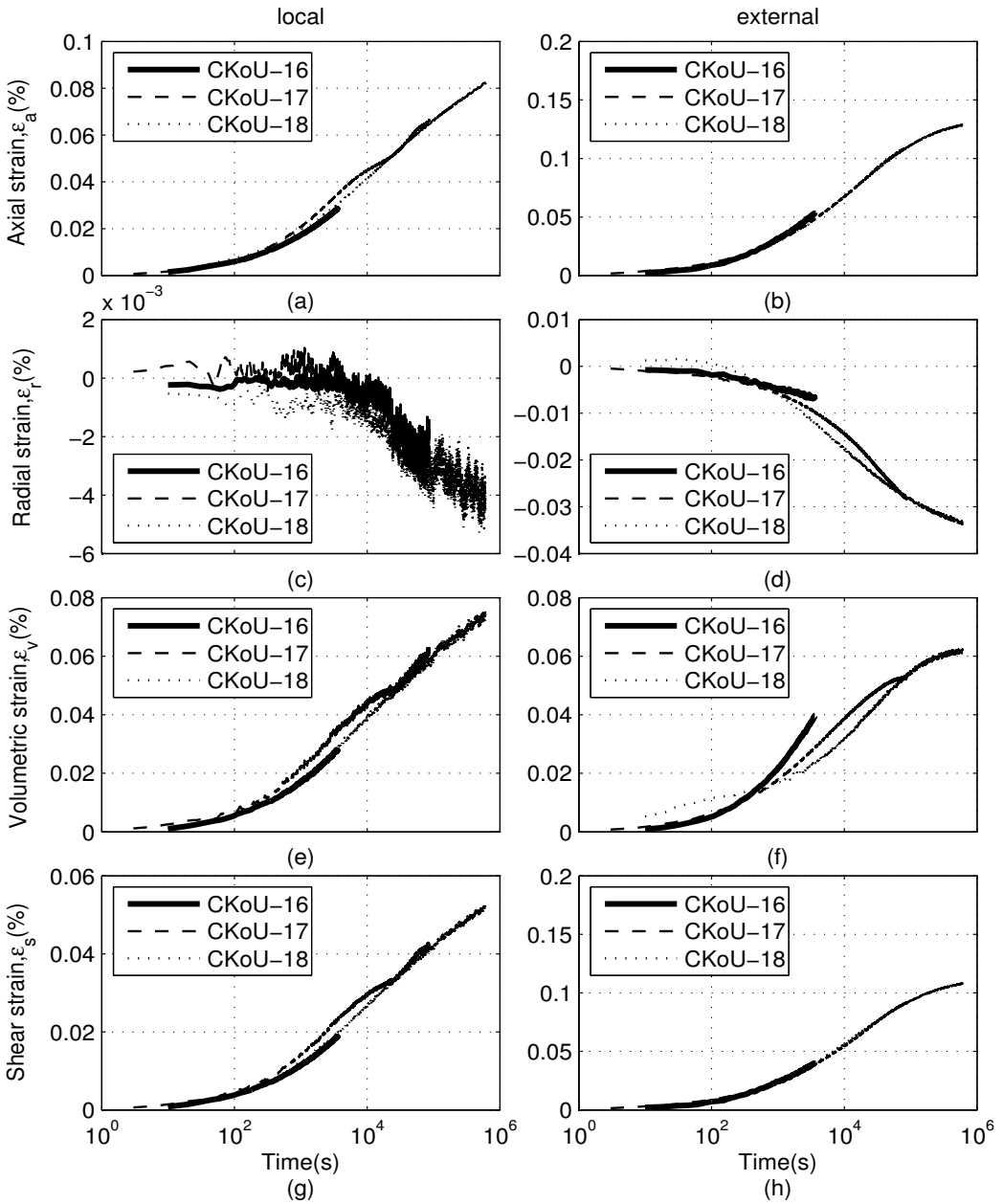

Figure E-2 strains development during creep of loose samples at 60 kPa confining pressure (CKoU-16, CKoU-17 and CKoU-18) for 1 hour, 1 day and 1 week of creep time, respectively

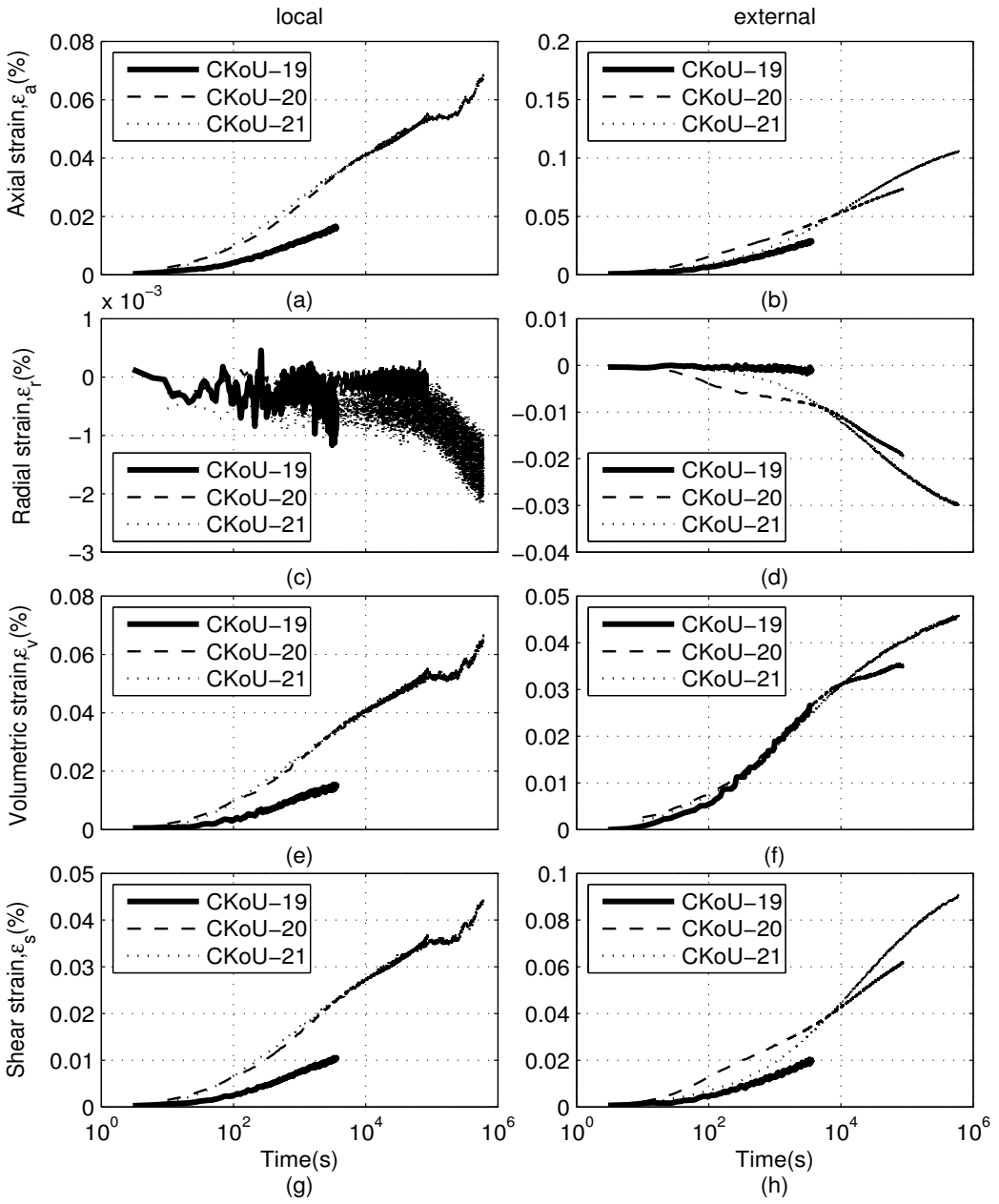

Figure E-3 strains development during creep of loose samples at 30 kPa confining pressure (CKoU-19, CKoU-20 and CKoU-21) for 1 hour, 1 day and 1 week of creep time, respectively

APPENDIX F
Example SEM images

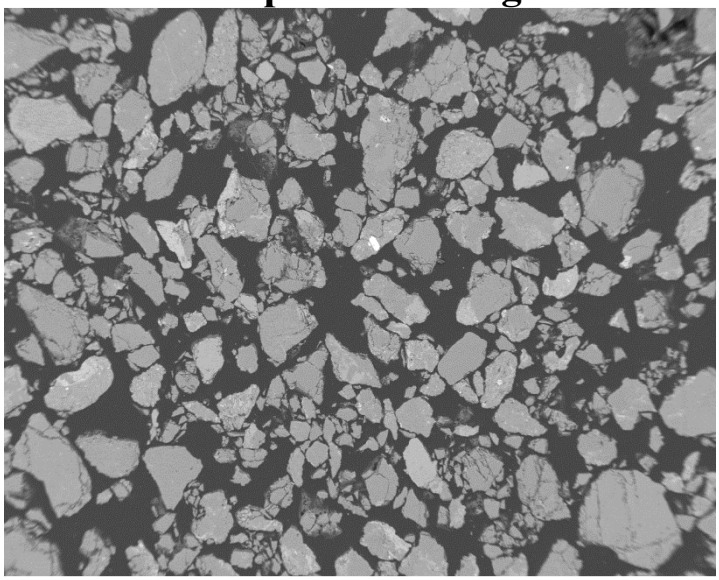

(a) 40301H

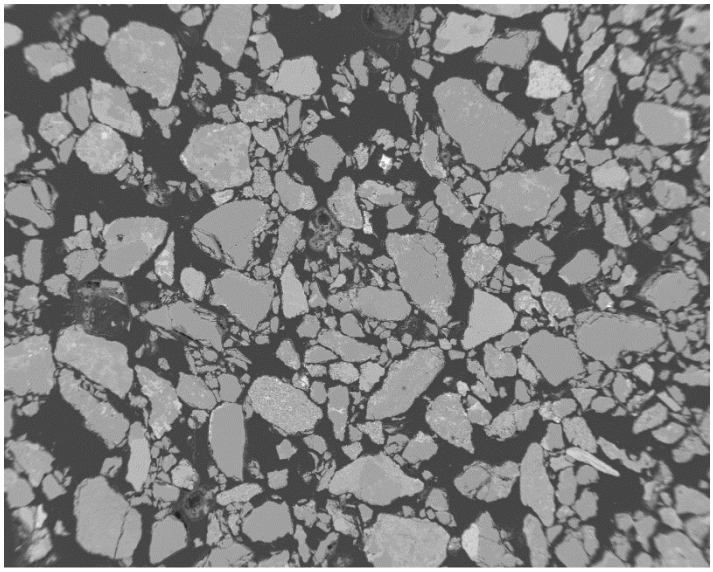

(b) 40301W

Figure F-1 SEM images for loose moist tamped sample at vertical stress, σ'_v=57 kPa for (a) 1 hour (b) 1 week of aging time

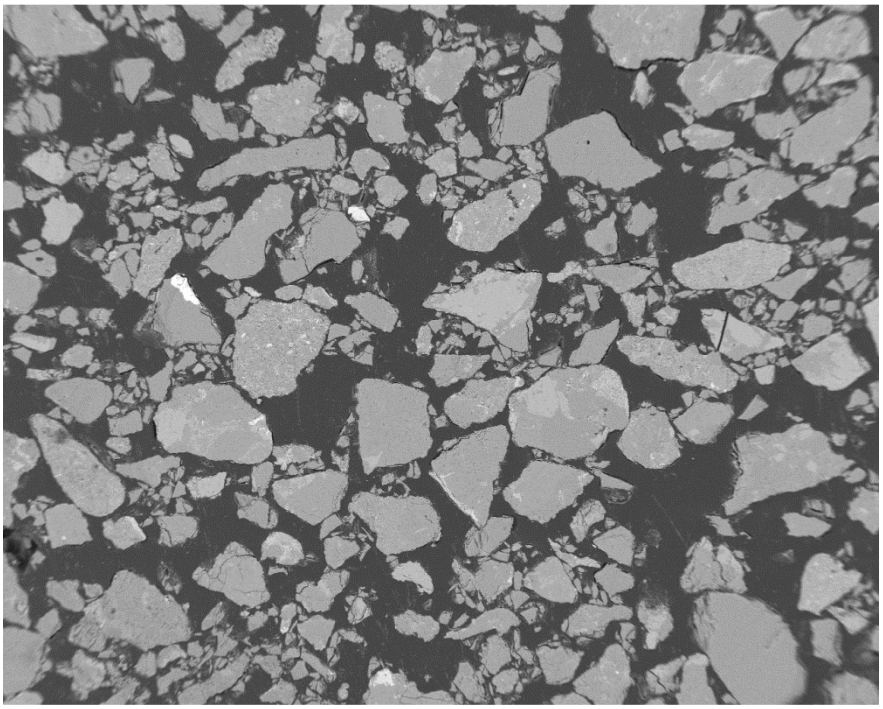

(a) 40304M

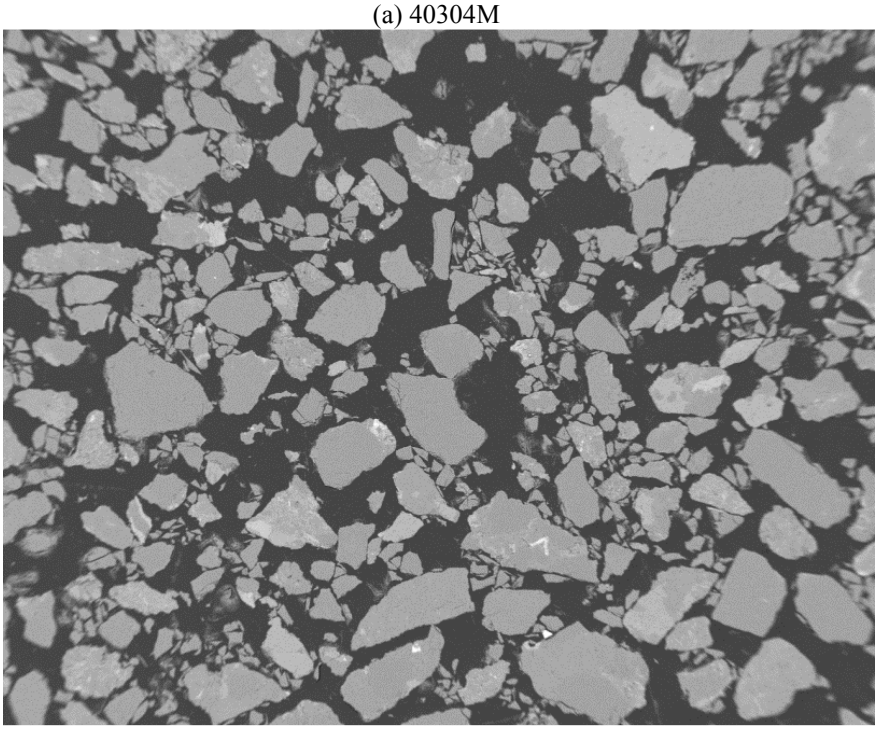

(b) 40308M

Figure F-2 SEM images for loose moist tamped sample at vertical stress, σ'_v=57 kPa (a) 4 month (b) 8 week of aging time

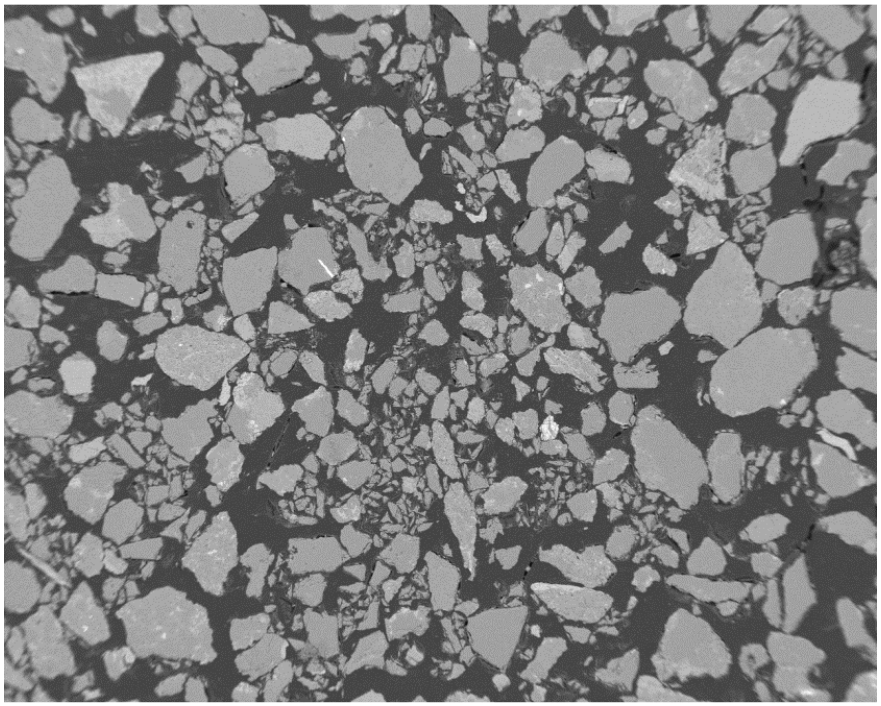

(a) 40601H

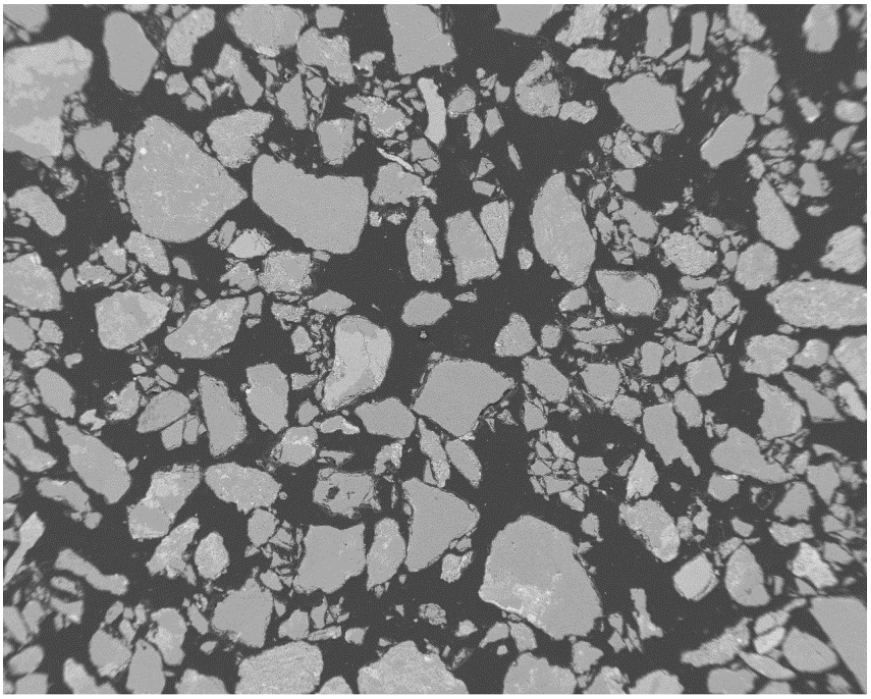

(b) 40601W

Figure F-3 SEM images for loose moist tamped sample at vertical stress, σ'_v=125 kPa for (a) 1 hour (b) 1 week of aging time

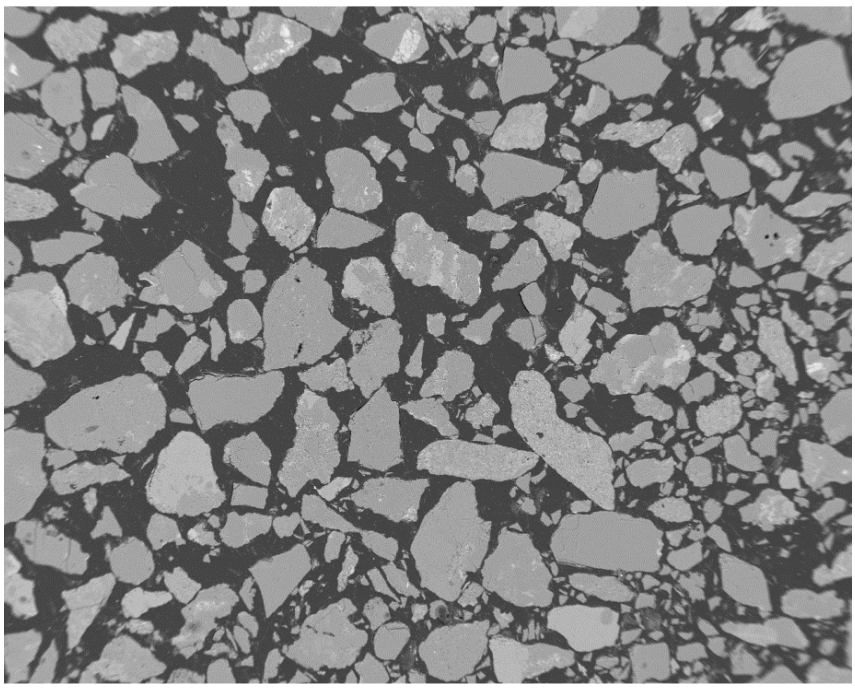

(a) 40601H_DD

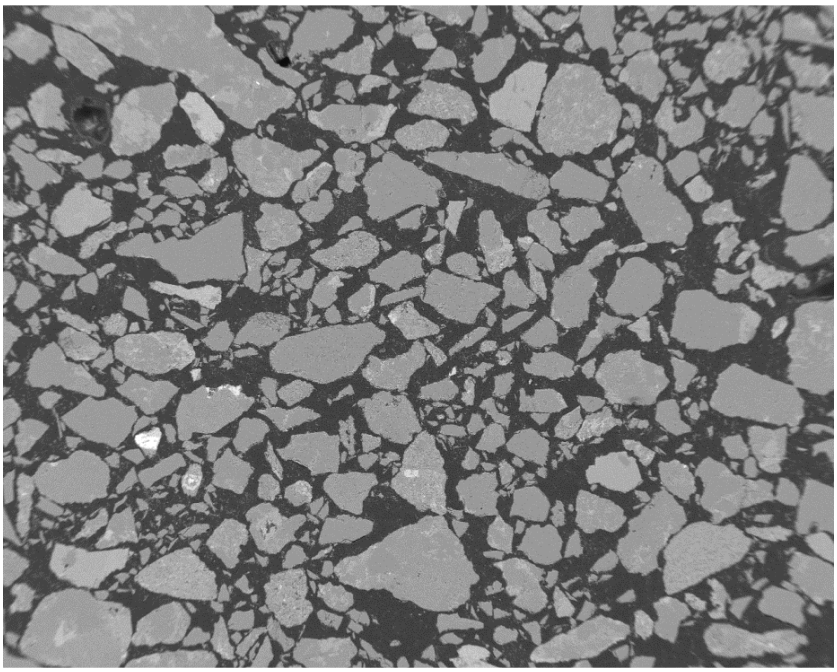

(b) 40601W_DD

Figure F-4 SEM images for loose dry pluviated tamped sample at vertical stress, σ'_v=125 kPa for (a) 1 hour (b) 1 week of aging time

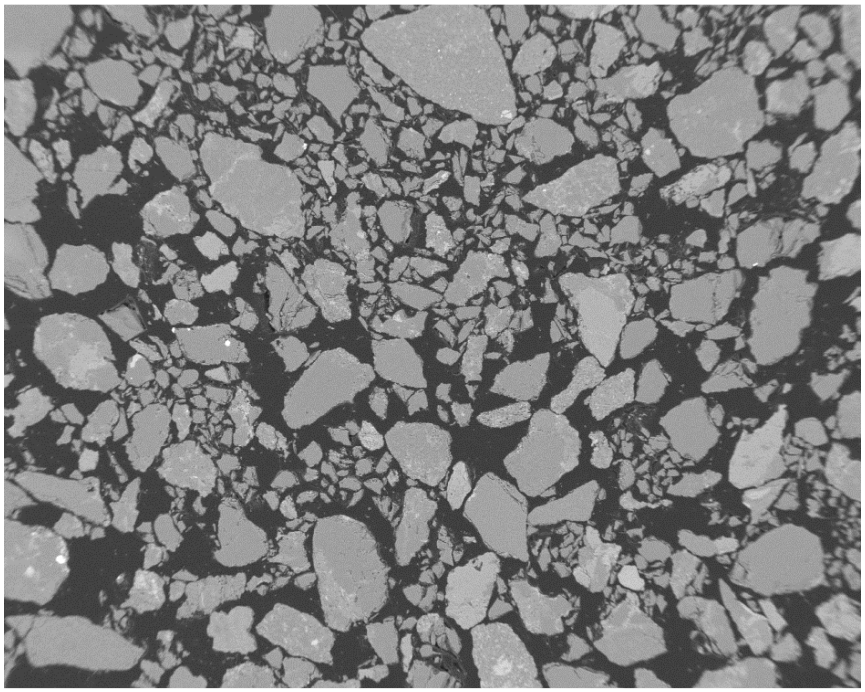

(a) 70301H

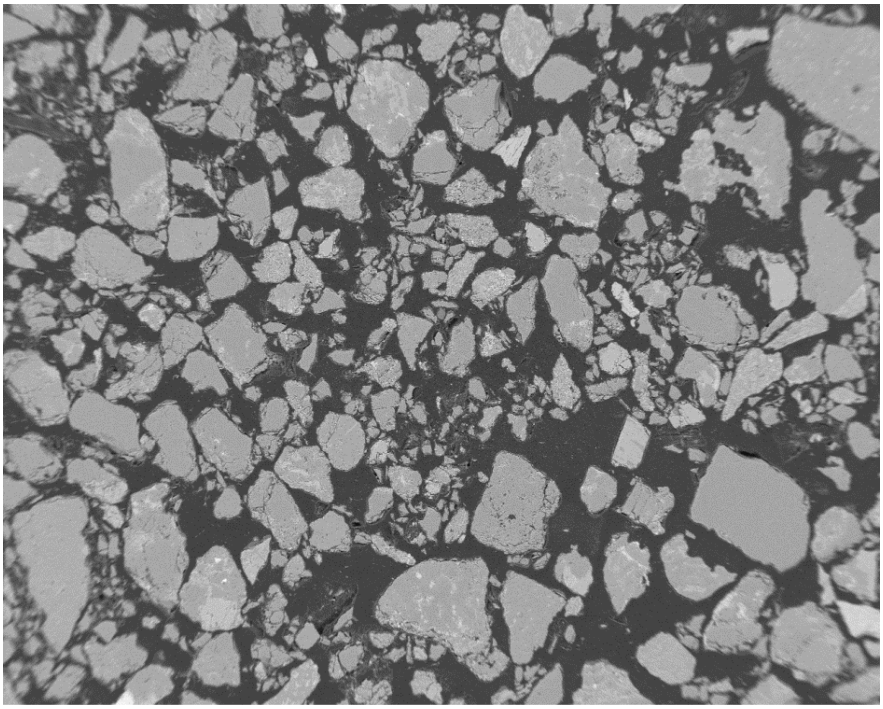

(b) 70301W

Figure F-5 SEM images for dense moist tamped sample at vertical stress, σ'_v=67 kPa for (a) 1 hour (b) 1 week of aging time

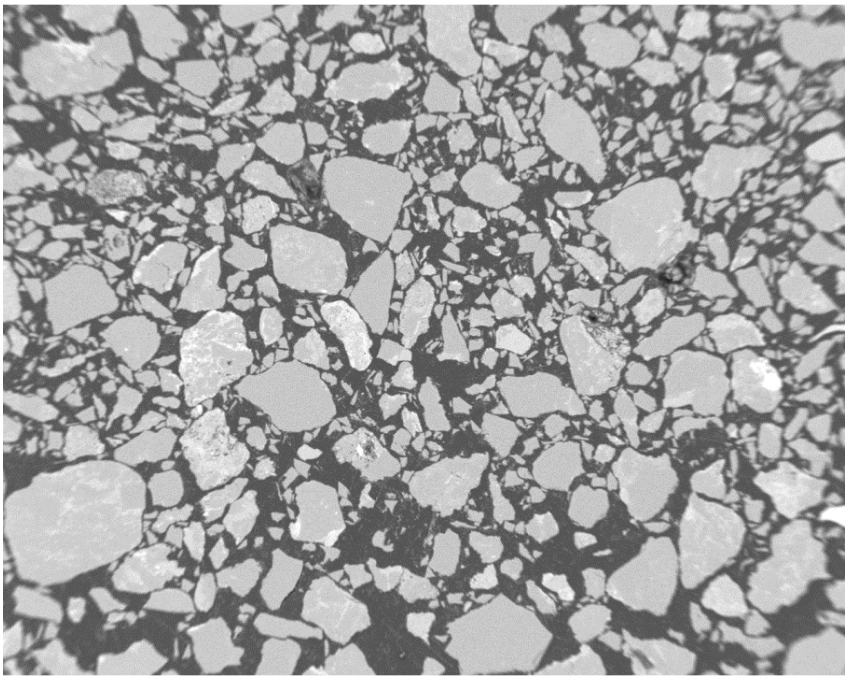

(a) 70601H_DD

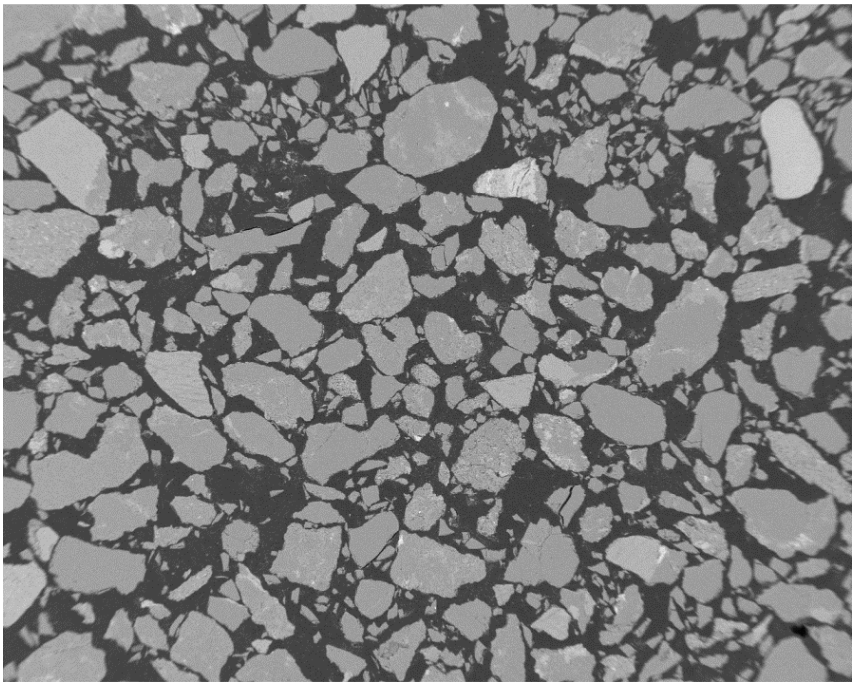

(b) 70601W_DD

Figure F-6 SEM images for dense dry pluviated sample at vertical stress, σ'_v=113 kPa for (a) 1 hour (b) 1 week of aging time

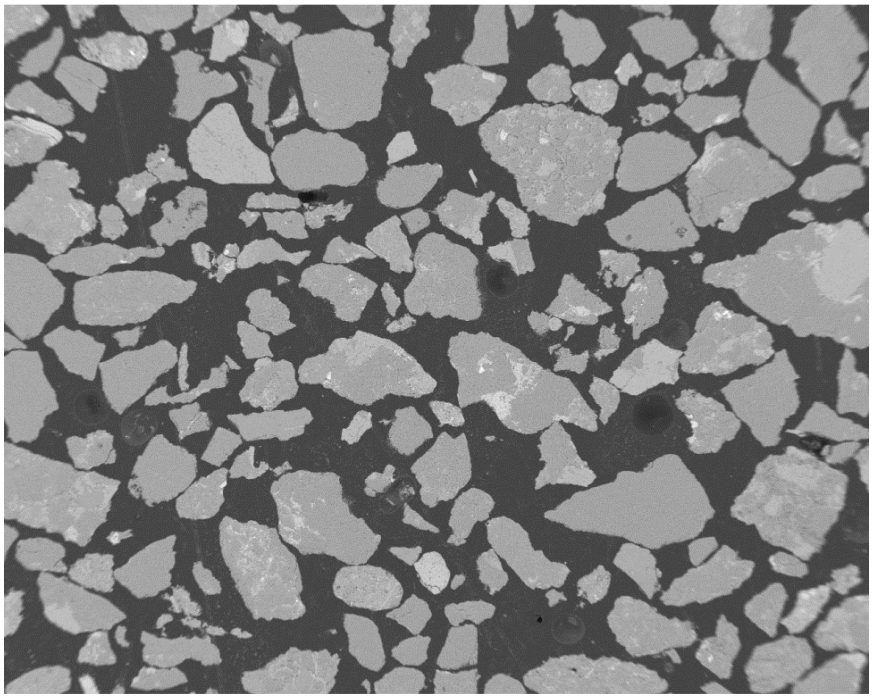

(a) gp-A

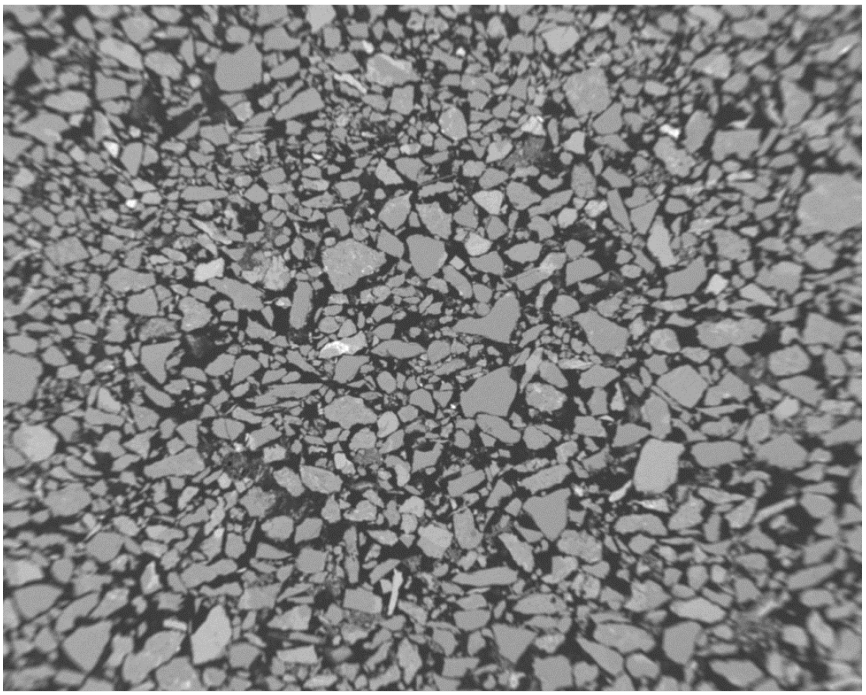

(b) gp-B

Figure F-7 SEM images for undisturbed sample from gel push (a) gp-A (b) gp-B at at vertical stress, σ'_v=80 kPa and σ'_v=50 kPa respectively

APPENDIX G
Example of not-weighted and weighted(by area) rose diagram

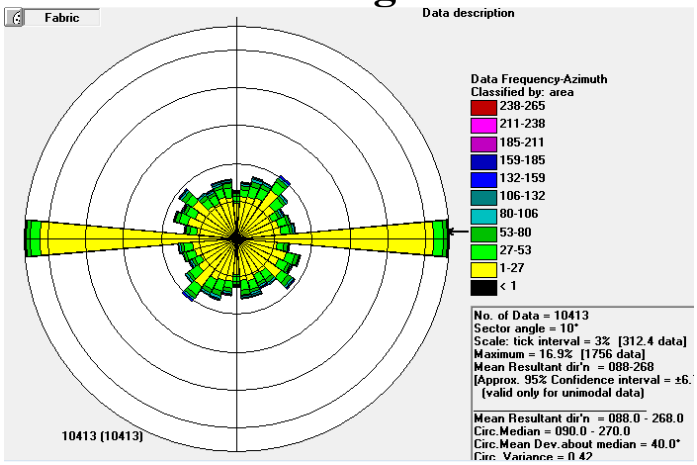

(a) Rose diagram 70301W not weighted

Figure G (a) shows the very large number of grains in the 80-90 bin, and frequency classifying shows that the major contribution are the very small grain areas

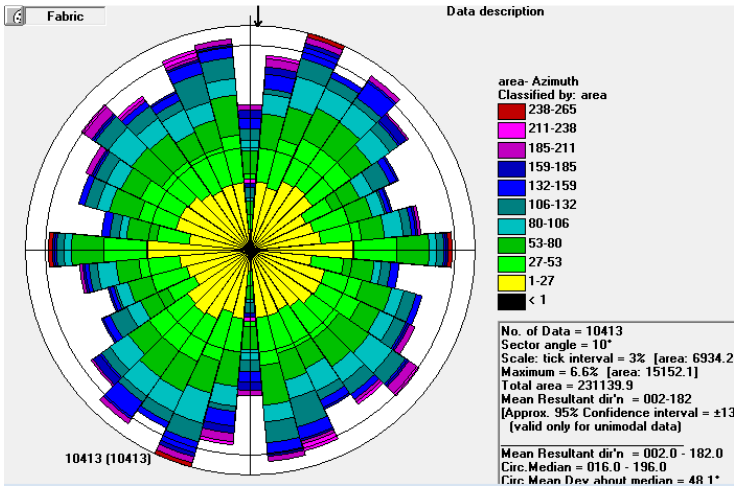

(b) Rose diagram 70301W weighted

In Figure G(b), the **total** grain area is included in each of the orientation sectors. In this plot the significance of the large number of grains with an azimuth of 90 is reduced because the total grain area of those grains is moderately small.

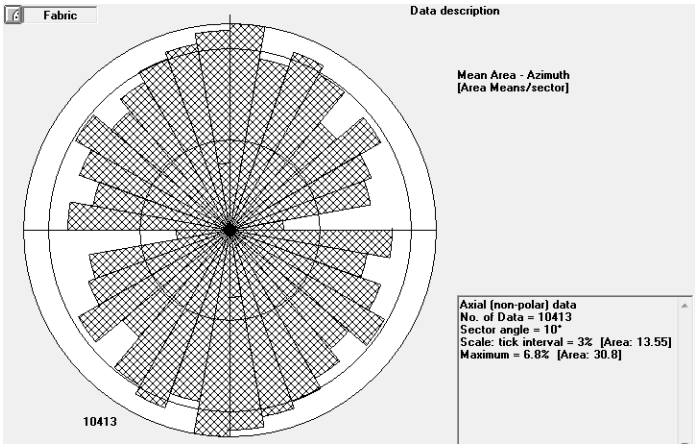

(c) Mean grain area per orientation70301W

Figure G (c) is the mean grain area per orientation azimuth. This plot shows that the 005-010 sectors contain the largest mean grains. It also shows that the mean grain area of the 085-095 sectors is negligible.

APPENDIX H

Calculation example of sand fraction in impregnation chamber based on weight-volume relationship

For loose sample

Void ratio, e= 0.8098

Diameter of impregnation chamber=49.56mm

Sample height=39.99

Volume total sample in impregnation chamber, Vt=77164mm^3

Volume of sand, Vsand=37099mm^3

Volume of fine, Vfine= 5537.16mm^3

Vsand/Vt=37099/77164*100=48%

For dense sample

Void ratio, e= 0.8098

Volume total sample in impregnation chamber, Vt=77164mm^3

Volume of sand, Vsand=39790.7mm^3

Volume of fine, Vfine= 5938mm^3

Vsand/Vt=39790/77164*100=52%